

Data Report for a Wave Characterization Study at the Ohmsett Wave Basin

January 2005

*William Asher
Applied Physics Laboratory
University of Washington
Seattle, Washington*

Summary of Major Findings

1. In the case of paddle conditions that generate waves that do not break, the distribution of wave heights is constant as a function of time and lateral position across the tank (i.e., perpendicular to the direction wave propagation) but wave height varies significantly in the longitudinally direction along the tank (i.e., parallel with the direction of wave propagation).
2. In the case of paddle conditions that generate waves that are breaking, the instantaneous distribution of wave heights varies with time and lateral and longitudinal position in the wave tank, but the long-term average of significant wave height is fairly constant as a function of position.
3. There does not appear to be a single location in the tank where a wave-height gauge located at that location would provide a reliable measurement of average wave conditions over the entire tank surface.
4. Longitudinal seiche modes are present in the tank for the non-breaking wave fields.
5. Breaking waves suppress the excitation of the longitudinal seiche modes but excite other low-frequency processes such as lateral seiche modes.
6. Wave breaking removes harmonics of the dominant wave frequency.
7. There is evidence that mean currents exist in the wave basin but it is unclear what role, if any, these currents have on modulating the wave field.

Overview and Motivation

Surface waves exist at all scales nearly continually on natural bodies of water and these waves will affect the performance of oil recovery equipment, containment devices, and dispersants. The Ohmsett wave basin was designed to provide a method for testing skimmers, booms, chemical dispersants, and other oil-spill related technology using a controlled reproducible wave field. One of the critical parameters in relating the usability, performance, and efficiency of oil spill remediation technologies in the Ohmsett facility to the performance of these same devices on natural bodies of water is detailed knowledge of the properties of the mechanically-generated wave field in the wave basin.

The period and wavelength of waves produced by the hinged-flap type wave paddle at the Ohmsett wave basin are determined by the stroke amplitude and the oscillation frequency of the wave flap. However, there exists the possibility of substantial variations in wave amplitude over the tank surface because a paddle-type wave generator excites harmonics of the dominant wave frequency [Dean and Dalrymple, 1991]. The net effect of combining different wave frequencies will be a pattern of constructive and destructive interferences that can increase or reduce wave amplitudes over the tank surface. An additional complication arises if the wavemaker excites lower order oscillation modes in the tank, such as seiching (i.e., the first slosh mode of the tank). These basin-scale oscillations can interact nonlinearly with the wavemaker and the wave field to induce variability wave height as a function time and position in the tank.

Accurate knowledge of the wave field in the wave basin is critical both in assessing the performance of booms, skimmers, dispersants and emulsifiers relative to their behavior during testing, and in relating the test results to real-world conditions. This is especially true since wind-generated waves exist over a continuum of frequencies and amplitudes depending on fetch, wind speed, wind duration, and wave-current interactions [Kinsman, 1984]. It is also clear that in order to relate the waves in the tank to field conditions using only a bulk estimation such as significant wave height, $H_{1/3}$, (defined here as the average height of the 1/3 largest amplitude waves) it is necessary to understand both the spatial variability and temporal evolution of the wave field in the tank. Once the temporal and spatial scales of the variability are quantified, it will be possible to relate a point measurement of $H_{1/3}$ in the Ohmsett facility to conditions expected in the natural environment.

The wave characterization study described here was conducted in December, 2004 and measured the tank averaged $H_{1/3}$, the spatial and temporal variability in $H_{1/3}$, and the spatial variability in the near-surface water currents. Data were recorded for regular waves (RW) generated using 10 different combinations of stroke length, L_S , and stroke frequency, F_S , of the wave paddle and for harbor chop waves (HC) generated using 8 combinations of L_S and F_S . These conditions were chosen to span the range of most commonly used settings and are listed in Table 1. The range of frequencies were chosen so that the lowest frequency measured at a particular stroke length was below the critical drive frequency for wave breaking and the highest frequency was above the breaking threshold.

Instrumentation and Experimental Setup

An array of seven precision pressure transducers (six: PX-439-002GI, one: PX-438-005GI, Omega Engineering Inc., Stamford Connecticut), two capacitance-type wave-wire gauges (WG-30, RBR Ltd., Ottawa, Ontario), and an acoustic height gauge (PSA-900A, Datasonics, Cataumet, Massachusetts) were used to measure water surface elevations. The seven pressure transducers and two wave-wire height gauges were mounted on the “vac” bridge at 2-m intervals across the width of the wave basin as shown in Figure 1 and described in Table 2. The acoustic height gauge was mounted several meters behind the main array at a lateral location of approximately 6 m. Subsurface currents were measured at a depth of 0.5 m at two locations using acoustic Doppler velocimeters (LabADV, Sontek Instruments, San Diego, California) mounted to the vac bridge (see Figure 1 and Table 2). The instrument array was traversed along the tank in 20 m intervals with the northernmost station located 40 m south of the northern end of the wave tank and southernmost station 20 m north of the southern end of the tank. This spacing gave a total of eight sampling stations located along the tank and were numbered as listed in Table 2 with station 1 located at the northern end of the tank. A data set for a specific set of wave paddle parameters consisted of sampling all eight stations. The stations were sampled sequentially for each wave paddle condition, starting at either station 1 or station 8 depending on whether station 1 or 8 was the final station in the previous data set.

The analog data from the wave probes were collected using a computer-controlled, analog-to-digital converter, and custom data acquisition software. The data acquisition rate for the wave probes 100 Hz, giving a Nyquist frequency that was a factor of 50 larger than the highest measurable wave frequencies. Data from the ADVs was collected at 25 Hz using LabADV software provided by the manufacturer.

Each wave height sensor in the main array was calibrated by measuring its output voltage for a known water surface elevation. The calibration curves for the pressure sensors and wave height gauges used to process the data are shown in Figure 2. The sensor response was verified by comparing the depth calculated from the sensor response curve using voltages measured for calm water with the known depth of the sensor. No significant deviations in the response of the sensors was identified by this procedure.

The water velocities measured by the ADV were validated by comparing the measured velocities with water velocities calculated based on the wave properties determined from the wave-wire data. Specifically, the along-tank horizontal velocity, v_x , and the vertical velocity, v_z , from the ADV's were compared to velocities calculated from

$$v_x = -\frac{H\omega \cosh(k(h-z))}{2 \sinh(kh)} \quad (1)$$

$$v_z = -\frac{H\omega \sinh(k(h-z))}{2 \sinh(kh)} \quad (2)$$

where H is the wave height (cm), ω is the dominant wave frequency (Hz), k is the wave number

of the dominant wave (cm^{-1}), h is the water depth (cm), and z is the depth of the sensor below the mean water level (cm) [Dean and Dalrymple, 1991]. The wave number is defined as $2\pi/L$ where L is the dominant wavelength. In turn, L is calculated by solving the dispersion relation given by

$$L = \frac{g}{2\pi} T^2 \tanh\left(\frac{2\pi h}{L}\right) \quad (3)$$

where g is the acceleration of gravity and T is the dominant wave period ($=1/\omega$) [Dean and Dalrymple, 1991]. The dominant wave period, or frequency, is readily estimated from power spectra of the pressure record time series. These comparisons indicated that the ADVs were operating correctly and producing reasonable water velocities.

Water surface video images were collected using two Uniq UM-400 ½”-format RS-170 CCD cameras (Uniq Vision, Santa Clara, California) each equipped with a 6-75 mm telephoto lens. The field of view for each lens was set to be 37°. The cameras were connected to a computer based video acquisition system controlled by custom software. One camera was mounted to the observation tower on the main bridge and looked at the water surface southwards towards the wavemaker. The second camera looked at the water surface northwards. Video frames were digitized at the rate of 1 frame per second and the raw binary files were converted to JPEG images.

Wind speed/direction, air and water temperature, barometric pressure, and relative humidity were logged at one-minute intervals using a Davis WeatherMonitor II (Davis Instruments, Hayward, California) and the Davis WeatherLink software package. The resulting data set was then filtered to yield 15-minute average values of relevant meteorological conditions during the measurements.

Measurement Procedure and Data Analysis

$H_{1/3}$ was measured as a function of position in the tank at the eight stations of the vac bridge listed in Table 4. Wave heights were measured with the 10-probe array for 360 s at a station, at which point the bridge was traversed to the next position and a new 360-s data record was collected from the probes. Therefore, it took approximately 90 minutes of time to traverse the tank and collect wave data for each setting of the wave paddle. In addition to the profiles of wave height made by traversing the instrument array through the tank, the time it took the wave basin to reach a steady-state wave field was determined by measuring wave and current properties at either Station 1 (north end of wave basin, farthest station from wave paddle) or Station 8 (south end of wave basin, closest station to wave paddle) for the first 10 to 20 minutes of operation of the wave paddle.

Water surface currents were measured simultaneously with wave heights. Time synchronization between the two data records was provided by initializing the system clock on each computer to the time reference signal provided by a GPS receiver. Average water velocities in the vertical along-tank horizontal, and cross-tank horizontal directions were estimated directly from the velocities provided by the Sontek data processing program GETVEL.EXE. Average net

horizontal velocities (i.e., the vector sum of the along-tank and cross-tank velocity) and total velocity (vector sum of all three velocity components) were calculated as

$$V_H = \frac{1}{N} \sum_{i=1}^N \sqrt{V_{AT}^2(i) + V_{CT}^2(i)} \quad V_T = \frac{1}{N} \sum_{i=1}^N \sqrt{V_{AT}^2(i) + V_{CT}^2(i) + V_Z^2(i)} \quad (4)$$

where N is the number of velocity records in the average (equal to 25 times the sampling period) V_H is the net horizontal velocity, V_T is the total velocity, V_{AT} is the along-tank horizontal velocity, V_{CT} is the cross-tank horizontal velocity, and V_Z is the vertical velocity.

The raw time series from the wave wires and pressure transducers were digitally filtered using a sixth-order Chebyshev filter with a 20 dB point of 20 Hz. The stop band for the filter was chose to be an order of magnitude larger than the highest frequency waves that could be measured by the wave probes. Water surface elevations and wave energy power spectra were then calculated from the filtered time series. All time series calculations were performed in Matlab V11.1 (The Mathworks, Natick, Massachusetts) using the Matlab Signal Processing Toolbox and the Matlab m-files listed in Appendix 1.

Time series of water surface elevation from both wave-wire gauges were calculated directly using the calibration curves in Figure 2. However, the data records from the pressure transducers required correcting for the effects of the dynamic pressure of the propagating waves as discussed in Dean and Dalrymple [1991]. Specifically, this involved calculating the pressure response factor, K_p , for each transducer using the relation

$$K_p = \frac{\cosh(k(h-z))}{\cosh(kh)} \quad (5)$$

where k is estimated from Eqs. 3 and the spectral estimates of the dominant wave frequency. Average power spectra at each station for each wave probe were calculated by segmenting each 36,000-point time series into sub-records that were 40.96 s long and overlapped each other by 5 s, calculating the power spectrum for each sub-record, and then averaging the nine individual spectra. The dominant wave frequency was then taken as the frequency at the maximum power in the averaged spectrum. The time series of corrected water surface elevation, $\eta(t)$, could then be computed from the pressure record as

$$\eta(t) = \frac{p(t) - \rho g z}{\rho g K_p} \quad (6)$$

where ρ is the density of seawater and z is the depth of the pressure sensor below the mean water level.

Significant wave height is defined as the average height of the third largest waves. For deep water waves $H_{1/3}$ can be estimated as four times the standard deviation of the surface elevation time series. The waves in the wave basin behaved approximately like deep-water waves and therefore this relationship was used to estimate $H_{1/3}$ for each probe at each station as an average value over the 360 s of data from each time series for $\eta(t)$ as

$$H_{1/3}(S,P) = \sqrt{\frac{N_S \sum_{i=1}^{N_S} \eta(t_i)^2 - \left(\sum_{i=1}^{N_S} \eta(t_i) \right)^2}{N_S(N_S - 1)}} \quad (7)$$

where $H_{1/3}(S,P)$ is the significant wave height for probe P at station S, N_S is the total number of samples in the 360 s time series of $\eta(t)$ (equal to 36,000 for a sampling rate of 100 Hz), and t_i stands for the i 'th sample in the time series. $H_{1/3}$ was also calculated as a 20-s running average over the data record so that the temporal evolution of wave height could be determined. In this case, $H_{1/3}(S,P)$ was defined with the limits of the summation in Eq. 7 being separated by 2000 points, or 20 s at a sampling rate of 100 Hz.

Results

Figure 3 shows the 15-minute averages of wind speed, wind direction, air temperature, water temperature, relative humidity, and barometric pressure during the wave characterization experiment. Measurements were made over the period December 5-9, starting at approximately 0700 EST and continuing until approximately 2300 EST. Although no rainfall data were collected, the period of high relative humidity on December 7 was caused by a rainstorm passing over the East Coast of the continental United States. There was no observed effect of local meteorological conditions on the large-scale features of the wave field. However, it should be noted that small-scale roughness features or near-surface drift currents such as might be caused by wind stress were not observable using the instruments deployed during these measurements.

Table 3 shows ω , T, L, $H_{1/3}$ computed as average values over the entire tank where the averaging is over the 72 individual measurements of each parameter (i.e., nine total wave probes times eight total sampling stations). Also listed in Table 3 are the standard deviations in the tank-averaged $H_{1/3}$ values, $\sigma_{H_{1/3}}$. With the exception of RW generated using a stroke length of 1.5 inches, $H_{1/3}$ is seen to increase with paddle frequency for the paddle frequencies that are below the breaking threshold at that stroke amplitude.

Figures 4-21 show power spectra calculated as described above for pressure transducer P1 (i.e., the tank centerline) at each of the eight sampling stations along the wave basin. The power spectra show that the spectral composition of the waves is uniform throughout the tank regardless of paddle condition or wave type and that the dominant wave frequency is found at the drive frequency of the wave paddle for both the RW and HC wave patterns. Additionally, for a given stroke length and wave pattern, it is seen that the wave fields generated by the lower frequency wave paddle settings contain wave energy at the harmonic frequencies of the paddle frequency. In contrast, the wave fields generated by higher paddle frequencies display a continuum of wave frequencies with little evidence for the presence of harmonics of the paddle frequencies. This is clearly seen by comparing the power spectra for RW04 (3" stroke @ 21 cpm paddle frequency) in Fig. 7 with the power spectra for RW07 (3" stroke @ 35 cpm paddle frequency) in Fig. 10.

Table 4 shows $H_{1/3}$ for each wave paddle condition in Table 3 where $H_{1/3}$ was computed as an

average of the nine wave probes at each station along the tank. These values can be used to observe gross uniformity of wave height in the tank as a function of wave paddle setting. Figures 22-39 show contour maps of $H_{1/3}$ calculated from $\eta(t)$ for each probe at each station for a particular wave paddle condition. These contour plots show the net spatial variability of the wave field in the wave basin.

In order to study the temporal variability of the wave field, 20-s moving averages of $H_{1/3}$ were calculated as described in the previous section. Figures 40-57 show time series of the moving average values of $H_{1/3}$ for each set of wave paddle conditions for wave data taken along the centerline of the tank at each of the eight stations. Figures 58-75 show time series of the moving averages of 20-s running mean average values for $H_{1/3}$ except that instead of plotting data from the centerline of the tank for all eight stations, all nine probes across the tank at station 1 (north end of tank) have been plotted for each wave paddle setting. Similarly, Figures 76-93 show all nine probes at station 4 (middle of tank) and Figures 94-111 show all nine probes at station 8 (south end of tank). Figures 112-129 are plots of 20-s running mean averages of $H_{1/3}$ for data taken during initiation of the wave paddle. These “start-up” time series were recorded at either Station 1 (north end of the tank) or Station 8 (south end of the tank), depending on location of the instrument array at the start of the data set.

Video data records for the wave characterization data are incomplete due to some wave data being recorded at times when it was too dark to obtain a usable video image and during periods of heavy rain when droplets formed on the wind of the camera housings. A larger problem with quantitative analysis of these video images is the problems associated in trying to image wave fields in a shallow tank with a homogenous bottom. Because of the low contrast between the crest and troughs of the waves, it is difficult to see details of the wave field in many of the images. Figures 130 and 131 show typical video images of waves in the wave basin taken looking southward from station 4 for conditions RW06 and RW07.

Figures 132-149 show time series of 20-s averages of the net horizontal water velocity calculated using Eq. 4 from the two ADV's in the main array. The ADV data show there were significant mean currents in the wave tank. Furthermore, in some cases these currents were not stationary with respect to time and showed significant lateral variability between the two velocimeters. However, in other cases the 20-s averaged surface velocities were almost constant with essentially zero difference between the two probes. There was no clear correlation between wave type and behavior of the near-surface currents.

Discussion

The dominant wave characteristics data shown in Table 3 is reassuring in that for a given paddle stroke length, the dominant wavelength decreases with increasing paddle frequency. Additionally, at a given paddle frequency, wavelength increases with increasing stroke length. Although these findings are obvious, they provide support that the wave probe array was accurately characterizing the wave field in the tank.

Figure 150 is a plot of the tank-averaged values for $H_{1/3}$ as a function of paddle frequency from the data in Table 3. This figure shows that in general $H_{1/3}$ increases with drive frequency at a fixed stroke although there is no clear systematic variation, especially for the higher paddle frequencies. In particular, for several strokes studies $H_{1/3}$ actually decreases at the highest paddle frequency. It is not clear why average wave amplitude decreases, but a possible explanation is that in all cases there was significant wave breaking at the maximum paddle frequency used. Wave breaking extracts energy from the wave field and converts it into turbulent kinetic energy. As the breaking frequency increases with paddle frequency, relatively higher amounts of energy are taken from the wave field by the breaking process. Support for this hypothesis can be seen in both the power spectra in Figures 4-21 and in the contour plots of $H_{1/3}$ over the wave basin shown in Figures 22-39.

The power spectra for the 3" HC paddle conditions are shown in Figures 15-18. At the lowest paddle frequency, the power spectrum shows significant components at the harmonic frequencies of the dominant wave frequency. However, as the paddle frequency increases, the wave energy at these harmonics of the dominant wave energy are suppressed, presumably because the breaking process removes the shorter wavelength components. The contour maps of $H_{1/3}$ for these same four data sets also show variations that are consistent with energy extraction by wave breaking. The contour plot in Figure 33 for HC04 (3" stroke, 20 cpm) shows a uniform wave field in the sense there is little across-tank variability in $H_{1/3}$. However, as the paddle frequency increases for the data shown in Figures 34-36, the wave field becomes more variable in the transverse direction. Furthermore, at the highest frequency, there is a noticeable decrease in $H_{1/3}$ in the center of the tank at the northern end (i.e., farthest from the wave paddle). This decrease in wave amplitude is also indicative of energy being extracted from the wave field by the breaking process.

The onset of breaking also has significant impacts on the spatial variability of the wave field. Using the series RW04-RW07 as an example, at the lower wave paddle frequencies where waves were not observed to be breaking, the contour plots for the lowest frequencies (Figures 25 and 26) show that $H_{1/3}$ is fairly consistent in the transverse direction (i.e., across the tank) at a given longitudinal (i.e., along the tank) position. However, there is a very large longitudinal variation in $H_{1/3}$ with wave heights being much larger in the center of the wave basin than at either end. In contrast, the wave height data at the higher paddle frequencies shown in Figures 27 and 28 has less longitudinal variability in $H_{1/3}$ but greater variability in the transverse direction. Similar patterns in the distribution of $H_{1/3}$ can be seen in the series HC04-HC07 (harbor chop, 3" stroke) in Figures 33-36, in the series RW08-RW10 (regular wave, 4.5" stroke) in Figures 29-31, and in the series HC08-HC10 (harbor chop, 4.5" stroke) in Figures 37-39. Another way to see this change in variability from longitudinal to transverse is by comparing plots of the running mean averages of $H_{1/3}$ as a function of tank location at the same wave paddle condition. For example, in the case of nonbreaking waves the data from all probes at station 1, 4, or 8 for RW08 (4.5" stroke, 15 cpm), Figures 65, 83, and 101, respectively, lie nearly on top of each other. However, Figure 47 shows that when data from these stations is superimposed, there is a factor of 5 difference in $H_{1/3}$ along the tank. In contrast, for a breaking case there is significant variability

among all nine probes at stations 1, 4, and 8 for RW10 (4.5" stroke, 25 cpm) Figures 67, 85, and 103, respectively. Figure 49 shows that there is only a factor of 2 difference on average in $H_{1/3}$ among these stations. The net result of these changes in wave field spatial characteristics is that the breaking process makes $H_{1/3}$ more uniform as a long-term average over the length of the tank. This is seen in the data in Table 3, where $\sigma_{H_{1/3}}$ is smaller for the higher paddle frequencies given a constant stroke length.

One of the more striking features of the time series showing 20-s moving averages of $H_{1/3}$ shown in Figures 40-111 are the oscillations in $H_{1/3}$ with periods of approximately 80 s that appear in some, but not all, of the time series (see the time series for HC08, station 4 in Figure 91 for a good example of these oscillations). It should be stressed that these oscillations are not waves in the wave field, but changes in the wave field itself over the course of 80 s. The most likely explanation for these features is the presence of seiche modes, or basin-scale oscillations in the water.

The natural seiche frequencies of the Ohmsett wave tank can be calculated using the expression

$$T_s = \frac{2 L_T}{n \sqrt{g h}} \quad (8)$$

where L_T is the length of the wave basin, n is the seiche mode order, g is the acceleration of gravity, and h is the depth of the water. Taking $n = 1$ for the lowest order mode (i.e., a sloshing motion of the water back and forth), the fundamental seiche period of the tank is shown to be 81 s (freq. = 0.0124 Hz), nearly identical to the period observed in the time series data for many of the paddle conditions. The prevalence of these low-frequency oscillations was studied by computing tank-averaged wave power spectra calculated using power spectra calculated from all nine wave probes at all eight sampling stations. However, in contrast to the power spectra shown in Figures 4-21, these power spectra were calculated using 32,000 data points so that the frequency resolution was 0.00156 Hz. Figures 151 and 152 show tank-averaged power spectra for wave paddle settings that lead to non-breaking and breaking wave fields, respectively. In the case of the non-breaking conditions, the power spectra all clearly show the presence of the fundamental seiche mode and its overtones at 0.012 Hz and multiples thereof. In contrast, the breaking cases show no obvious low-frequency peaks in the power spectra. The implication is that for reasons that are not understood at present, the breaking process suppresses the excitation of the longitudinal seiche modes in the wave basin.

In some of the breaking cases (e.g., RW06, station 4, Fig. 81) oscillations in $H_{1/3}$ with periods on the order of 15 s are visible. It is likely these are transverse seiche modes of the tank, as application of Eq. 7 using the tank width instead of length gives a timescale of 8.2 s, corresponding to a frequency of 0.12 Hz. Several of the power spectra, mainly for conditions where the waves were breaking, display peaks in this region of frequencies, suggesting that the effect of breaking waves shifts the bulk tank oscillations from mainly end-to-end to side-to-side. However, this interpretation is somewhat suspect in that unlike the lower frequency motions seen in Figure 151 which all occur at the same frequency, in some cases the frequency at which these higher frequency oscillations occur is as high as 0.17 Hz and as low as 0.07 Hz. Therefore, the

possibility exists that these oscillations are not lateral seiche modes but related to some other physical process.

In terms of general features of the wave height fields, these data suggest that in the case of a regular wave pattern for the two longer stroke lengths where the waves are not spontaneously breaking, the tank is characterized by increased wave height in the middle of the tank (in the longitudinal sense) and decreased wave height at the ends. It is not possible to extend this to a general conclusion concerning the regular wave pattern since this pattern of larger waves at mid-tank was not observed for the low-frequency wave fields at a stroke amplitude of 1.5 inches. Interestingly, there is some evidence suggesting that the pattern of large waves in the center of the tank is associated with the presence of the seiche modes. In the case of the low paddle frequency wave fields for a stroke length of 1.5", there was no evidence of seiching in the power spectra. Based on this it is possible there is a critical threshold input wave energy required to excite the seiche modes in the tank.

These seiche motions are also visible in the ADV current records as the 80-s oscillations in the mean currents measured in the surface of the tank. It is somewhat tempting to explain the increase in the mid-tank wave height seen for non-breaking wave patterns to wave-current interactions due to the seiching. However, the contour plot of $H_{1/3}$ for HC04 (Fig. 33) shows a minimum in $H_{1/3}$ at mid-tank, yet the ADV data for HC04 at mid-tank (Fig. 142) shows significant currents. It is difficult to rationalize how wave-current interactions would suppress average wave height for HC04 yet increase wave height in other cases. Furthermore, there was no obvious correlation of the directional information of the mean currents with peaks in the significant wave height time series, suggesting that the currents generated by seiching were not interacting with the wave field. The ADV velocity records also show coherence, or similar trends and cycles between the average velocities measured on either side of the tank. This suggests that mean currents were present under some conditions. However, the data is too sparse in a spatial sense to permit generation of maps of flow patterns in the tank. It is likely that detailed analysis of the currents in the wave tank will require a dedicated study using an array of current probes mounted at a range of depths in the wave basin.

Two main problems were encountered in the analysis of the data from the DataSonics PSA-900A acoustic height gauge, one related to calibration and one related to the presence of large noise spikes. Because of the combination of these problems, the second of which was the most serious, it was not possible to compare wave heights calculated from the PSA-900A with those derived from the pressure transducers and wave-wire gauges. However, based on the data it is possible to comment briefly on the performance of the PSA-900A. As shown in Figure 153, the noise spikes mentioned above were not single-point transients that could easily be removed by digital filtering. Instead, they were large peaks in the output voltage where the peak itself lasted several tenths of a second, and then slowly decayed back to the time varying mean signal with a time constant of several seconds. An example of this behavior is shown in Figure 153 where it is important to note that the data in Fig. 153 have already been digitally filtered using the sixth-order 20 dB Chebyshev filter. Development of an algorithm capable of removing these transients

was beyond the scope of this project and detailed data analysis on the Datasonics probe records was not possible.

It is likely that the transients observed in the PSA-900A were caused by critical wave slope phenomena or breaking waves, where the local surface slope reflected the acoustic signal from the probe outside the acceptance cone of the detector. This is supported by the observation that the transients observed in the PSA-900A were more prevalent at the higher wave paddle frequencies. Figure 154 shows time series of water surface elevation taken at station 4 from the non-breaking case RW08. Aside from the already-mentioned issue with calibration, the PSA-900A time series is consistent with data from both the wave-wire gauge and the pressure transducer. If it is a critical wave slope issue that causes the data spikes it should not be assumed that the probe will be accurate under all non-breaking wave conditions. The presence of wind-generated ripples on the water surface may present similar critical events to the probe. However, it is not possible to test this hypothesis using the present data set.

In attempting to resolve the problems with the Datasonics probe, the engineering support staff at Datasonics in Cataumet, Massachusetts was contacted via telephone and electronic mail. The results of these conversations were the discovery that the manufacturer no longer supports the PSA-900A for air-side measurements because it was found to be inherently unstable, failing in the precise manner encountered in the data set. This suggests although the PSA-900A functions well at low wave amplitudes where there is no breaking (at least in terms of there being no large spikes in the output voltage), because of the problems with signal loss due to the spiking behavior it should be replaced as the primary wave measurement probe at Ohmsett.

The measurements made here rely on the assumption that the wave field is stationary in the statistical sense with respect to time (stationarity in the temporal sense should not be confused with spatial homogeneity). Mathematically, this means that mean values measured over a suitable time period are not dependent on the particular time period chosen for the measurements. Operationally it implies that the sampling intervals were long enough to span many cycles of any periodic phenomena in the wave basin. Typically these timescales are determined by the lowest order seiche mode, which in this case sets the timescale at approximately 80 s. Given that, there is no a priori reason to suppose the data interval of 360 s was too short to assume the wave field in the tank was statistically stationary. However, in some cases, particularly for low paddle drive frequencies, there are some indications that the wave tank may take a fairly long time (on the order of 10-15 minutes) to achieve stationarity. This can be seen in the startup time series where the values for $H_{1/3}$ along the tank centerline are seen to be highly variable (RW01, RW04, HC04, and HC08, Figs. 112, 115, 123, and 127, respectively, are good examples of this behavior).

In terms of tank homogeneity, or spatial variability, it should also be noted that the possibility exists that some of the spatial variability observed in the contour plots is actually temporal variability. In other words, because it was not possible to simultaneously sample the tank longitudinally, longitudinal temporal variations in wave height with time scales longer than the

sampling interval of 360 s would appear to be spatial inhomogeneities. In other words, in the time it takes to sample the waves in the tank at one station and move to the next station, the waves that would have been at the next station when the first station were sampled are different from the waves that are there when the second sample is actually measured. Although this would be a serious problem, it is deemed to be an unlikely complication since the spatial variations observed (e.g., the larger wave heights mid-tank for some of the non-breaking cases) are consistent between different wave paddle conditions. Furthermore, the changes in spatial homogeneity from laterally uniform to variable also appear to be highly correlated with changes in a fundamental wave-related process (i.e., wave breaking), suggesting that the spatial variations measured were true spatial variabilities and not aliased slow temporal changes.

General Conclusions

The main conclusions from these measurements are that the wave facility produces wave fields that are stable in the sense that the overall spatial and long-term temporal mean values are constant, but can be highly variable over small spatial and temporal scales. The onset of breaking likely represents a critical transition in the pattern of wave height in the tank with wave height changing from being laterally constant but longitudinally variable for non-breaking cases to a higher degree of cross-tank variability but relatively more uniform average wave heights along the length of the tank for breaking cases. In addition to this transition in spatial variability, the temporal variability changes from either nearly constant values of $H_{1/3}$ or values of $H_{1/3}$ that change very slowly to relatively rapid fluctuations in $H_{1/3}$ that are possible related to changes in the seiche modes of the tank.

Because of these spatial and temporal transitions in the character of the wave field, there does not appear to be a systematic dependence of tank-averaged $H_{1/3}$ on wave paddle frequency at a constant stroke length. The data indicate that $H_{1/3}$ increases with increasing paddle frequency up to the breaking threshold, at which point increases in breaking remove energy from the field so that $H_{1/3}$ remains constant or decreases. Furthermore, the data show that it cannot be generally assumed that non-breaking wave fields in the facility are any less variable in terms of wave height than breaking wave fields. The key point is that the spatial distribution of this variability is different for breaking and non-breaking wave fields. Unfortunately, in both cases there does not appear to be any one location where a single point measurement of the significant wave height would adequately characterize the spatial or temporal variability over the entire tank.

These results do show that depending on the type of test to be conducted, the wave field selected makes a difference. For example, if temporal stability of the wave field at a particular location in the wave tank is important, non-breaking wave fields would be preferable to breaking wave fields. However, if a constant average value of $H_{1/3}$ over a large area of the tank is important, breaking wave fields are to be preferred (with the understanding that there may be changes in wave amplitude over short timescales but over longer time periods the average significant wave height is relatively constant regardless of tank position). Examples of these two extremes would be provided by testing of a device that is not towed through the water and a device that is meant

to be towed. In the former case a non-breaking wave field might be preferred in that the wave height where the device is tested will be relatively constant throughout the test. In the latter case, although wave height varies with time, the variability is uniform throughout the tank so that the device will experience the same conditions during the test (provided the test duration is longer than the frequency of fluctuations in waveheight in the tank).

The startup time series indicate that in general 5 minutes is adequate time for the wave field to become statistically stationary. However, wave paddle settings producing relatively low amplitude waves, it is recommended that the startup equilibration time be increased to at least 10 minutes. This data set was not able to resolve issues related to reproducibility of a particular wave pattern for a given set of paddle conditions. Similarly, the dependence of the distribution of $H_{1/3}$ on initial conditions in the tank when the wave paddle is started remains unmeasured.

It is likely that there exists a substantial body of literature that would address some of the unresolved questions regarding the behavior of a wave tank such as the Ohmsett facility. Preliminary searches in the Science Citation Index (SCI) database were unable to find any relevant papers, but this could be due to the fact that SCI does not index articles published before the early 1980's. It is also possible that the information has been published in the form of data reports in the so-called gray literature which are not indexed in SCI. In either case, a more comprehensive search might be useful in understanding the behavior of the wave basin.

Finally, the overall recommendation from this report would be to adopt a wave height measurement technology that could be deployed at several locations across the tank. As shown in the contour plots of $H_{1/3}$ measured by each probe (Figs. 22-39), any lateral location across the tank could sit in a local maximum or minimum of the wave field. Sampling the wave field across the tank might give a more representative view of the wave field and its variability for all conditions. The power spectra demonstrate that nearly all of the wave energy is contained in frequencies below a few Hertz, suggesting relatively low-cost acoustic height gauges designed to work in air (e.g., Siemens Airanger SPL series control electronics w/ an Echomax Ultrasonic Level Transducers, http://www.lesman.com/downloads/s07sp_level.pdf) might be a better alternative to the PSA-900A. The possibility also exists that the PSA-900A may merely need some “tender loving care” in terms of calibration and evaluation to ensure it is providing reliable wave height information, at least for non-breaking wave conditions.

References

Dean, R.G., and R.A. Dalrymple, *Water Wave Mechanics for Engineers and Scientists*, 353 pp., World Scientific Ltd., Singapore, 1991.

Kinsman, B., *Wind Waves: Their Generation and Propagation on the Ocean Surface*, 676 pp., Dover Publications, Mineola, 1984.

Table 1: Wavemaker Settings for Wave Characterization Test and Wave Paddle Frequency Relative to Breaking Threshold.

Wave Type	Code	Paddle Stroke (inches)	Paddle Frequency (cpm)	Breaking/Nonbreaking	Date Run Acquired	Time Run Acquired (EST)
Regular Wave	RW01	1.5	35	Nonbreaking	12/09/2004	07:30
Regular Wave	RW02	1.5	40	Breaking	12/09/2004	14:25
Regular Wave	RW03	1.5	45	Breaking	12/09/2004	17:15
Regular Wave	RW04	3	23	Nonbreaking	12/05/2004	15:50
Regular Wave	RW05	3	29	Nonbreaking	12/06/2004	08:45
Regular Wave	RW06	3	33	Breaking	12/06/2004	12:00
Regular Wave	RW07	3	35	Breaking	12/06/2004	14:55
Regular Wave	RW08	4.5	15	Nonbreaking	12/08/2004	16:45
Regular Wave	RW09	4.5	21	Breaking	12/08/2004	19:30
Regular Wave	RW10	4.5	27	Breaking	12/08/2004	21:40
Harbor Chop	HC03	1.5	40	Breaking	12/09/2004	22:30
Harbor Chop	HC04	3	20	Nonbreaking	12/07/2004	09:15
Harbor Chop	HC05	3	25	Nonbreaking	12/07/2004	13:00
Harbor Chop	HC06	3	30	Breaking	12/07/2004	16:15
Harbor Chop	HC07	3	35	Breaking	12/07/2004	19:10
Harbor Chop	HC08	4.5	20	Nonbreaking	12/07/2004- 12/08/2004	21:30 07:30
Harbor Chop	HC09	4.5	25	Breaking	12/08/2004	10:00
Harbor Chop	HC10	4.5	30	Breaking	12/08/2004	13:30

Table 2: Station Location and Locations of Wave and Current Probes in the Main Array

Station #	Distance (m) ¹	Distance from centerline of wave basin ² (m)										
		Probe Identity										
		P7 ³	P6 ³	P5 ³	A1 ³	WB ³	P1 ³	WA ³	A0 ³	P2 ³	P3 ³	P4 ³
1	40	8	6	4	3	2	0	-2	-3	-4	-6	-8
2	60	8	6	4	3	2	0	-2	-3	-4	-6	-8
3	80	8	6	4	3	2	0	-2	-3	-4	-6	-8
4	100	8	6	4	3	2	0	-2	-3	-4	-6	-8
5	120	8	6	4	3	2	0	-2	-3	-4	-6	-8
6	140	8	6	4	3	2	0	-2	-3	-4	-6	-8
7	160	8	6	4	3	2	0	-2	-3	-4	-6	-8
8	180	8	6	4	3	2	0	-2	-3	-4	-6	-8

¹Distance measured as positive from the north end of the pool towards the south

²Distance defined as positive to the west edge of the tank

³Identity of the probes is as follows: P1-PX438-005GI; P2 - PX439-002GI; P3 - PX439-002GI; P4 - PX439-002GI; P5 - PX439-002GI; P6 - PX439-002GI; P7 - PX439-002GI; WA - WG-30; WB - WG-30, A0 - ADV; A1 - ADV

Table 3: Wavemaker Settings for Wave Characterization Test and Associated Data for Dominant Wave Frequency, ω (Hz), Dominant Wave Period, T, Dominant Wavelength, L (m), Tank-Averaged Significant Wave Height, $H_{1/3}$ (cm), and Standard Deviation of the 72 Individual Measurements of $H_{1/3}$ Used to Computer the Tank-Averaged $H_{1/3}$, $\sigma_{H_{1/3}}$.

Wave Type	Code	Paddle Stroke (inches)	Paddle Frequency (cpm)	ω (Hz)	T (s)	L (m)	$H_{1/3}$ (cm)	$\sigma_{H_{1/3}}$ (cm)
Regular Wave	RW01	1.5	35	0.595	1.68	4.40	24.5	6.06
Regular Wave	RW02	1.5	40	0.635	1.58	3.87	23.5	2.84
Regular Wave	RW03	1.5	45	0.640	1.56	3.81	21.9	2.94
Regular Wave	RW04	3	23	0.385	2.60	9.67	30.2	11.5
Regular Wave	RW05	3	29	0.464	2.16	7.06	33.6	11.0
Regular Wave	RW06	3	33	0.535	1.87	5.40	40.6	3.67
Regular Wave	RW07	3	35	0.554	1.80	5.06	40.3	5.32
Regular Wave	RW08	4.5	15	0.244	4.10	18.0	30.0	11.1
Regular Wave	RW09	4.5	21	0.342	2.93	11.6	54.8	11.6
Regular Wave	RW10	4.5	27	0.439	2.28	7.77	47.9	15.6
Harbor Chop	HC03	1.5	40	0.598	1.67	4.36	29.3	2.92
Harbor Chop	HC04	3	20	0.320	3.12	12.7	24.5	13.2
Harbor Chop	HC05	3	25	0.415	2.41	8.56	41.4	16.3
Harbor Chop	HC06	3	30	0.488	2.05	6.44	48.4	7.00
Harbor Chop	HC07	3	35	0.526	1.90	5.58	47.9	4.87
Harbor Chop	HC08	4.5	20	0.333	3.01	12.0	49.8	17.3
Harbor Chop	HC09	4.5	25	0.410	2.44	8.72	54.8	14.7
Harbor Chop	HC10	4.5	30	0.481	2.08	6.59	57.6	6.91

Table 4: Average Significant Wave Height as a Function of Station and Wavemaker Condition

Station #	Distance (m)	RW01	RW02	RW03	RW04	RW05	RW06	RW07	RW08	RW09	RW10
1	40	22.2	21.9	20.5	26.7	35.7	38.1	36.7	12.4	32.7	43.2
2	60	22.7	22.5	21.0	26.3	40.9	36.8	35.6	27.1	50.7	59.6
3	80	25.7	24.5	21.1	21.6	31.1	40.5	37.7	39.2	33.6	43.2
4	100	25.4	24.2	23.0	43.0	22.9	40.5	41.4	47.6	66.9	45.2
5	120	23.4	24.0	21.8	42.3	42.6	42.6	40.7	40.4	47.6	49.8
6	140	25.6	23.5	22.2	26.5	31.8	41.1	42.1	21.1	54.7	47.3
7	160	25.3	23.4	22.3	28.1	23.9	42.7	44.2	25.5	50.0	45.5
8	180	25.8	24.2	23.2	27.0	40.1	42.9	44.2	26.4	41.4	49.8

Station #	Distance (m)	HC03	HC04	HC05	HC06	HC07	HC08	HC09	HC10
1	40	29.7	53.4	30.5	45.3	45.0	35.2	64.8	48.9
2	60	28.4	28.3	38.1	47.2	44.7	46.7	47.9	53.9
3	80	28.8	20.7	48.0	51.0	46.7	46.9	51.4	55.5
4	100	29.0	14.5	49.7	48.7	45.9	79.1	61.8	58.3
5	120	28.4	8.1	46.8	50.3	47.6	50.2	65.0	58.4
6	140	29.6	23.9	36.6	48.0	48.9	64.8	52.2	58.1
7	160	30.2	27.0	36.2	49.2	52.2	36.7	39.7	63.4
8	180	30.3	20.3	45.4	47.8	52.3	38.5	55.9	64.3

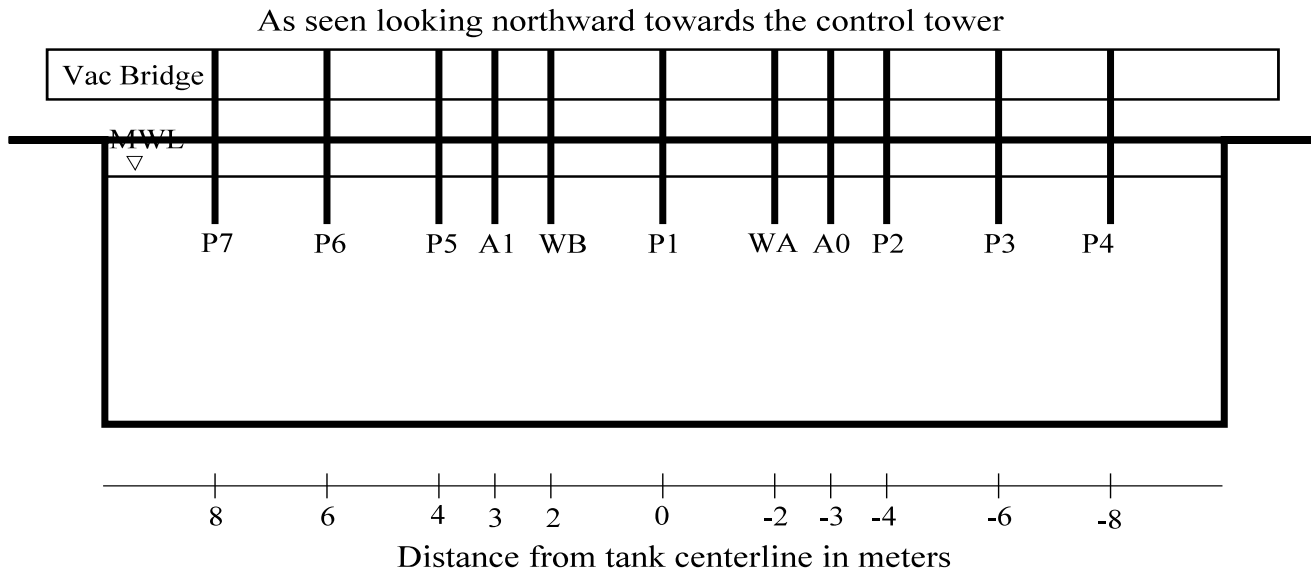


Figure 1: Schematic of instrument array mounted on vac bridge. Instrument codes are as follows: P1 - PX438-005GI pressure transducer; P2 - PX439-002GI pressure transducer; P2 - PX439-002GI pressure transducer; P3 - PX439-002GI pressure transducer; P4 - PX439-002GI pressure transducer; P5 - PX439-002GI pressure transducer; P6 - PX439-002GI pressure transducer; P7 - PX439-002GI pressure transducer; WA - WG-30 1.5 m capacitance wave gauge; WB - WG-30 1.5 m capacitance wave gauge; A0 - acoustic Doppler velocimeter; A1 - acoustic Doppler velocimeter. All instruments mounted at a mean depth of 50 cm.

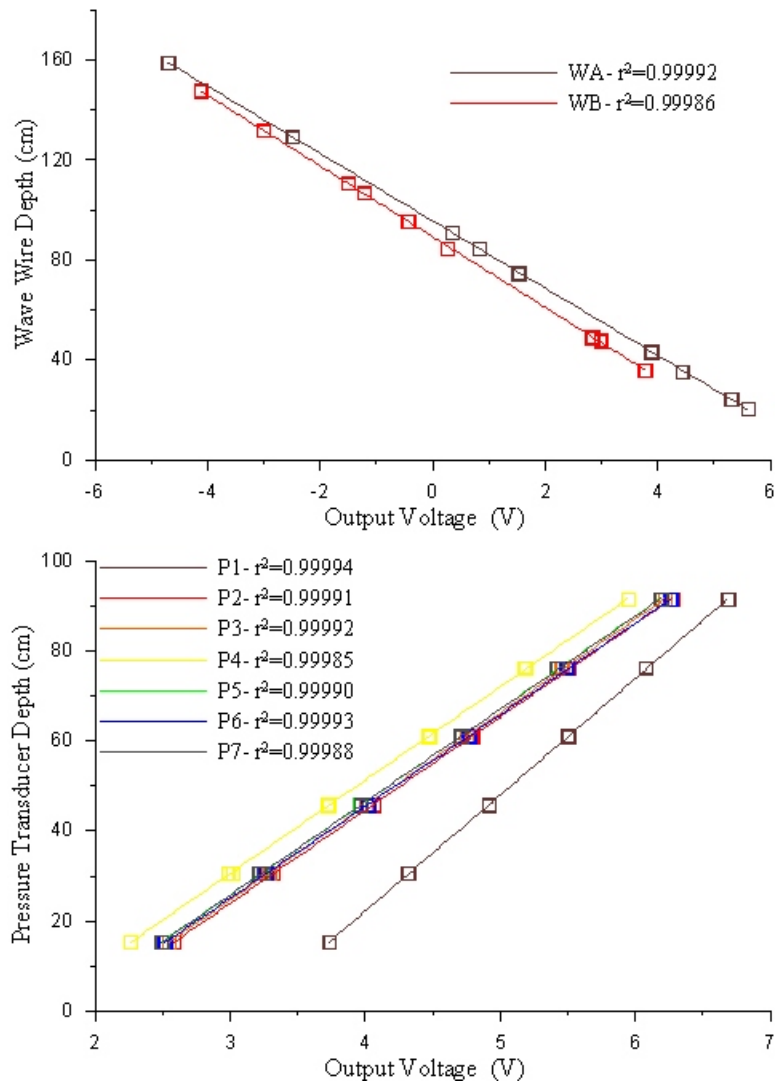


Figure 2: Calibration response curves for the pressure transducers and capacitance wire wave gages used during this study. The top panel shows the response of the wire wave gages where the identity of the probes are as follows: WA - WG-30, $y = -2$ m; WB - WG-30, $y = +2$ m. The bottom panel shows the response of the seven pressure transducers where the identity of the six probes are as follows: P1 - PX438-005GI, $y = 0$ m; P2 - PX439-002GI, $y = -2$ m; P3 - PX439-002GI, $y = -4$ m; P3 - PX439-002GI, $y = -8$ m; P5 - PX439-002GI, $y = 4$ m; P6 - PX439-002GI, $y = 6$ m; P7 - PX439-002GI, $y = 8$ m.

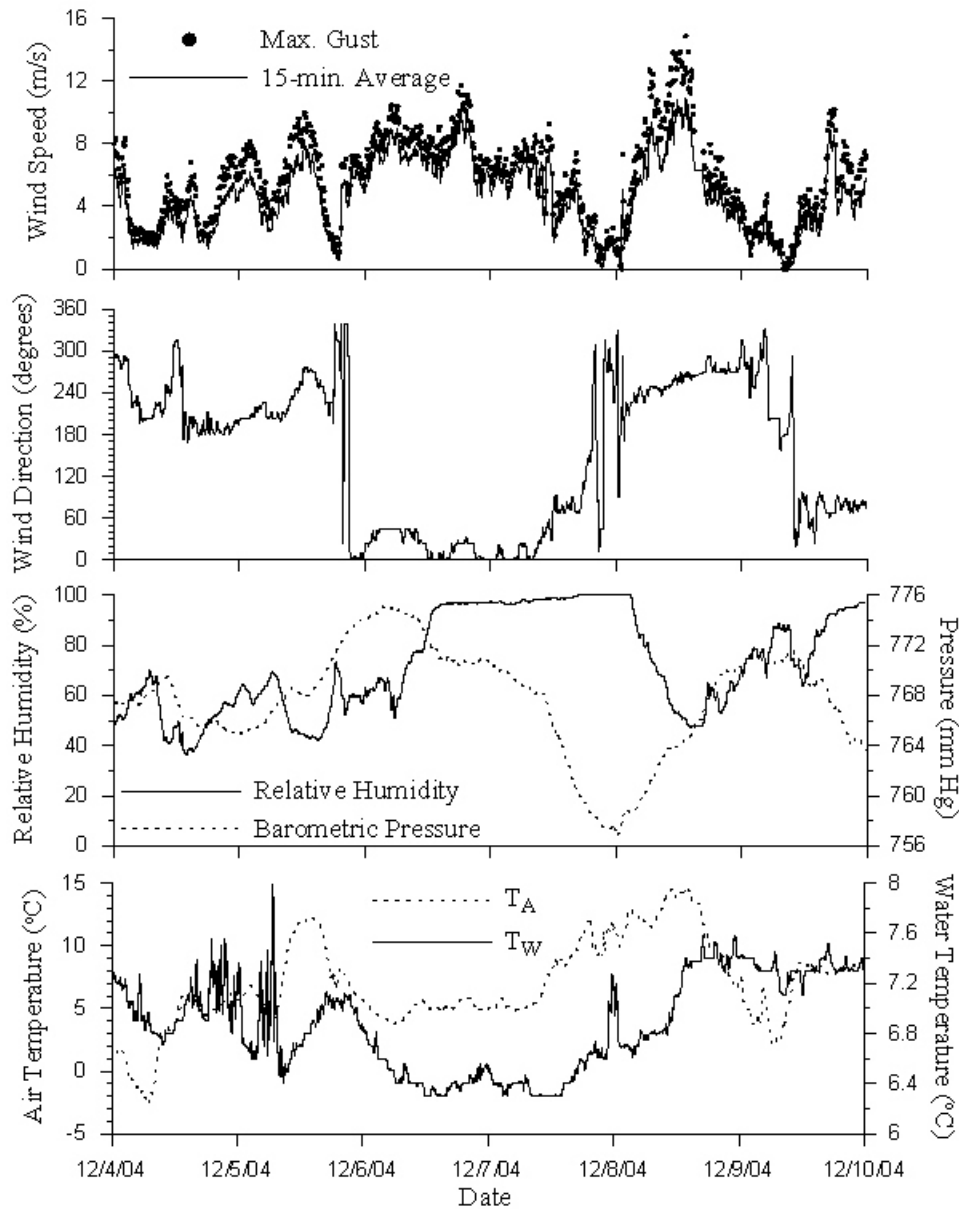


Figure 3: Meteorological conditions and tank water temperature measured during the wave characterization study. Data were recorded at 1-min intervals using a Davis Instruments WeatherMonitor II meteorological station modified to record tank water temperature using a Davis Instruments platinum RTD thermistor. The wind direction was measured relative to the axis of the tank with zero degrees pointing along the tank towards the control tower to the north. The data shown in the figure have been running-mean filtered to 15-minute averages.

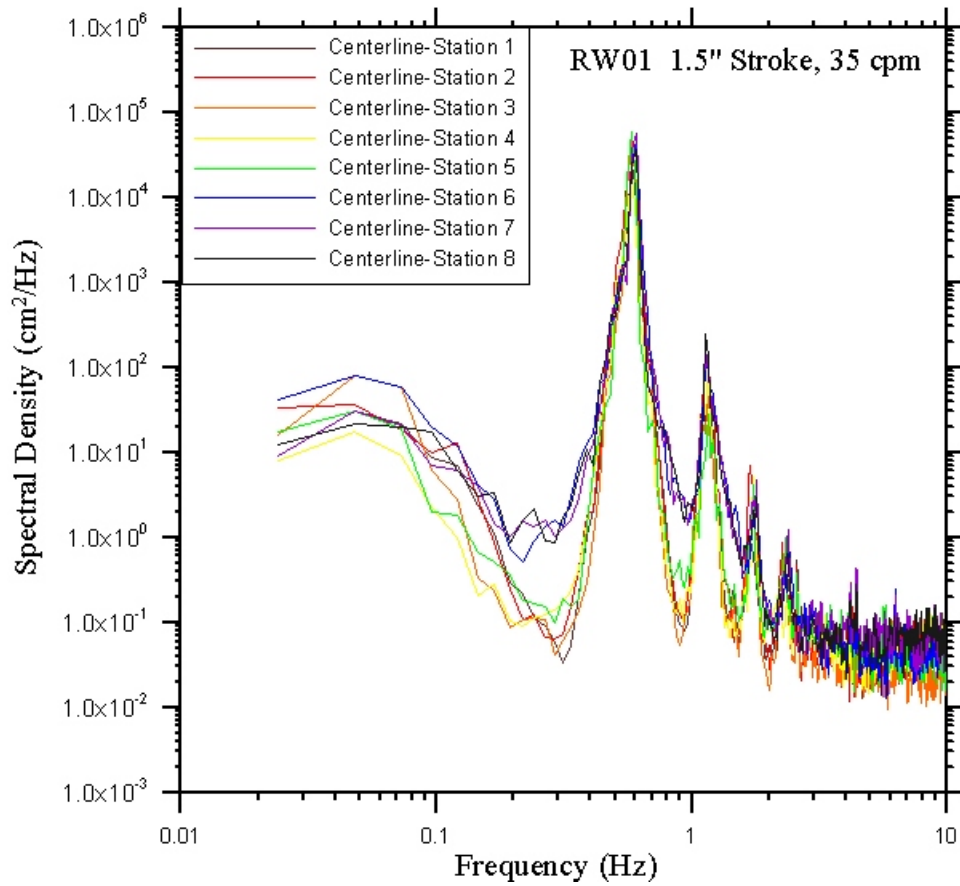


Figure 4: Power spectra of the water surface elevation time series shows plotted for pressure transducer P1 mounted on the tank centerline. Paddle conditions for this run correspond to RW01, 1.5" stroke, 35 cpm speed.

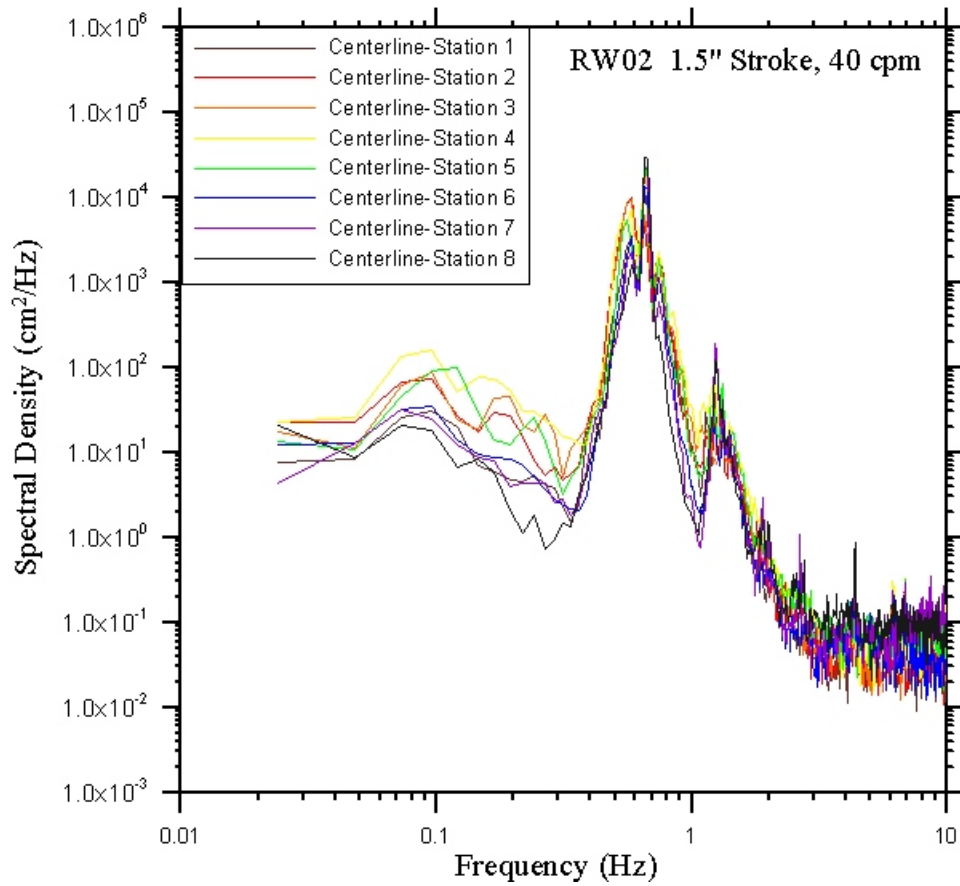


Figure 5: Power spectra of the water surface elevation time series shows plotted for pressure transducer P1 mounted on the tank centerline. Paddle conditions for this run correspond to RW02, 1.5" stroke, 40 cpm speed.

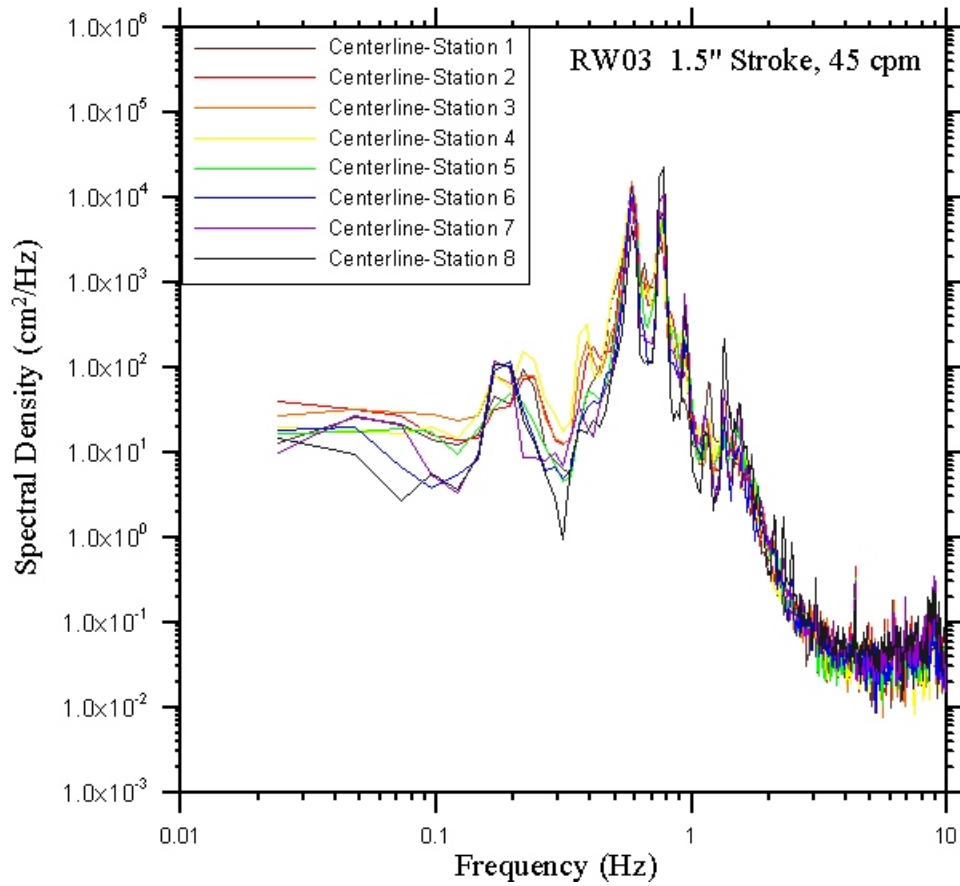


Figure 6: Power spectra of the water surface elevation time series shows plotted for pressure transducer P1 mounted on the tank centerline. Paddle conditions for this run correspond to RW03, 1.5" stroke, 45 cpm speed.

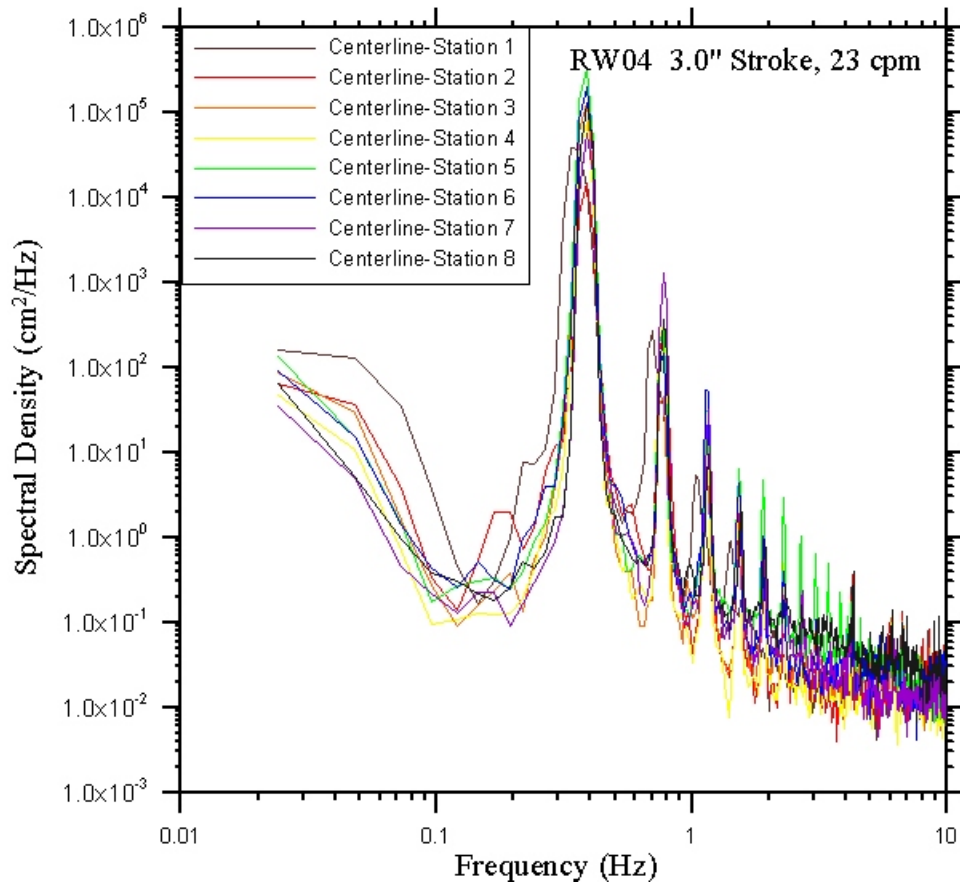


Figure 7: Power spectra of the water surface elevation time series shows plotted for pressure transducer P1 mounted on the tank centerline. Paddle conditions for this run correspond to RW04, 3.0" stroke, 21 cpm speed.

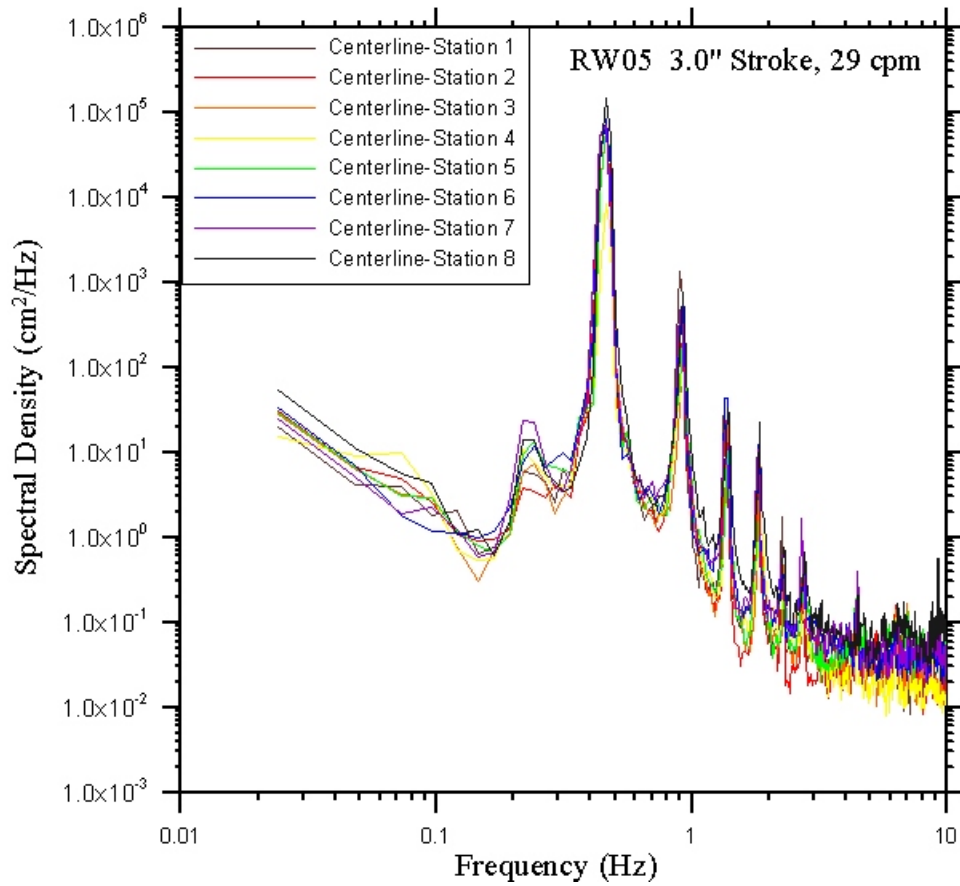


Figure 8: Power spectra of the water surface elevation time series shows plotted for pressure transducer P1 mounted on the tank centerline. Paddle conditions for this run correspond to RW05, 3.0" stroke, 37 cpm speed.

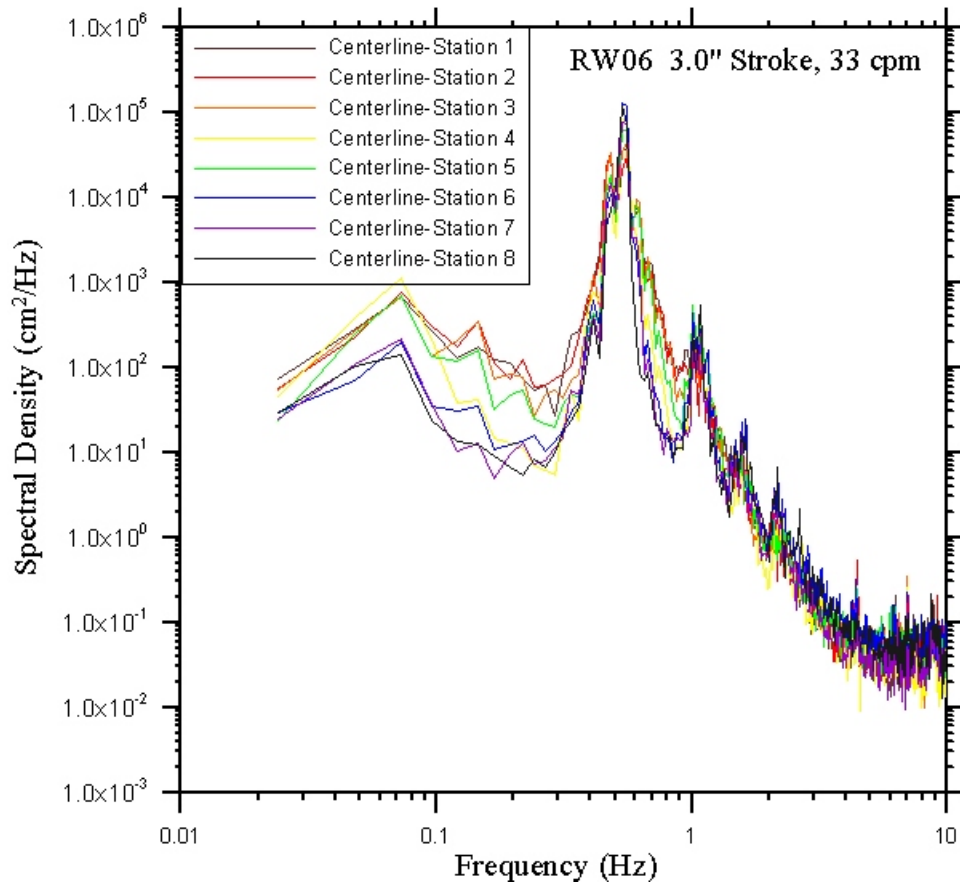


Figure 9: Power spectra of the water surface elevation time series shows plotted for pressure transducer P1 mounted on the tank centerline. Paddle conditions for this run correspond to RW06, 3.0" stroke, 33 cpm speed.

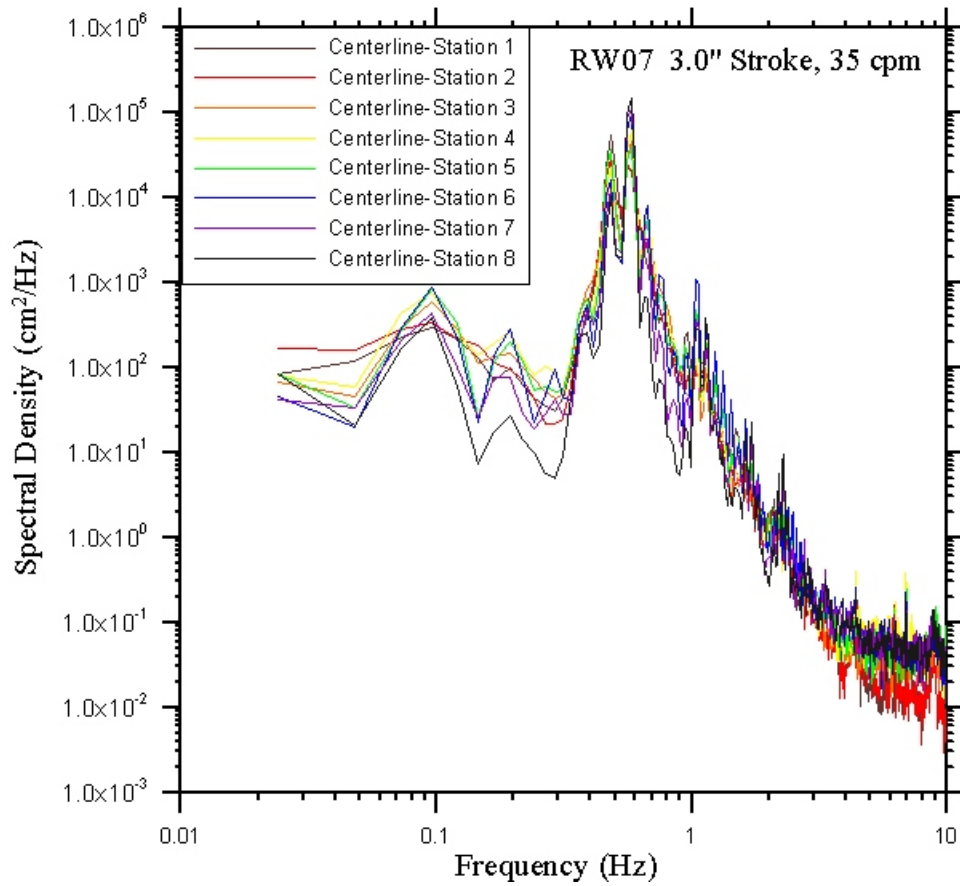


Figure 10: Power spectra of the water surface elevation time series shows plotted for pressure transducer P1 mounted on the tank centerline. Paddle conditions for this run correspond to RW07, 3.0" stroke, 35 cpm speed.

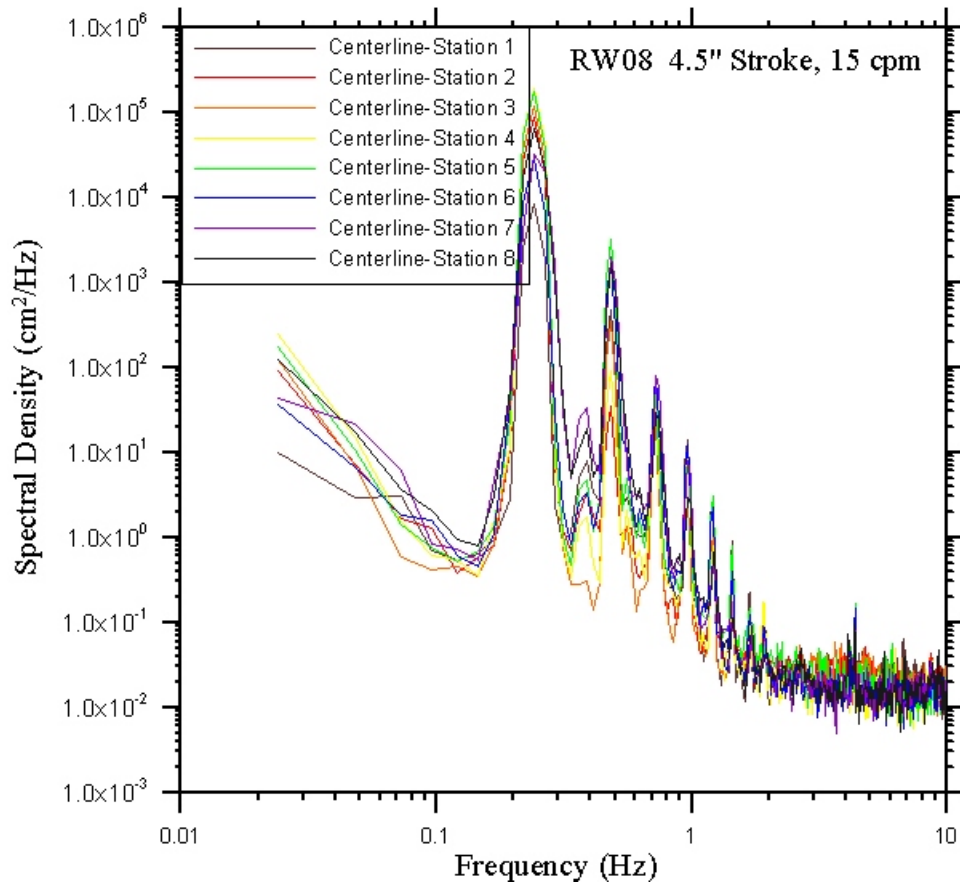


Figure 11: Power spectra of the water surface elevation time series shows plotted for pressure transducer P1 mounted on the tank centerline. Paddle conditions for this run correspond to RW08, 4.5" stroke, 15 cpm speed.

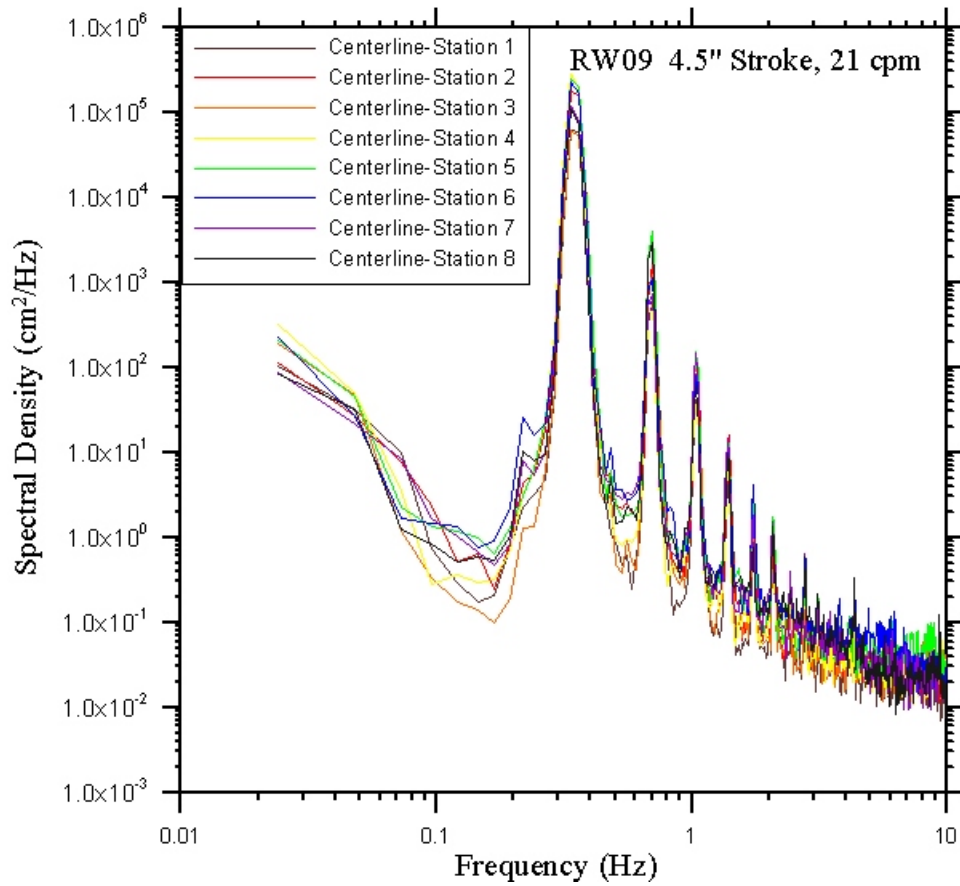


Figure 12: Power spectra of the water surface elevation time series shows plotted for pressure transducer P1 mounted on the tank centerline. Paddle conditions for this run correspond to RW09, 4.5" stroke, 21 cpm speed.

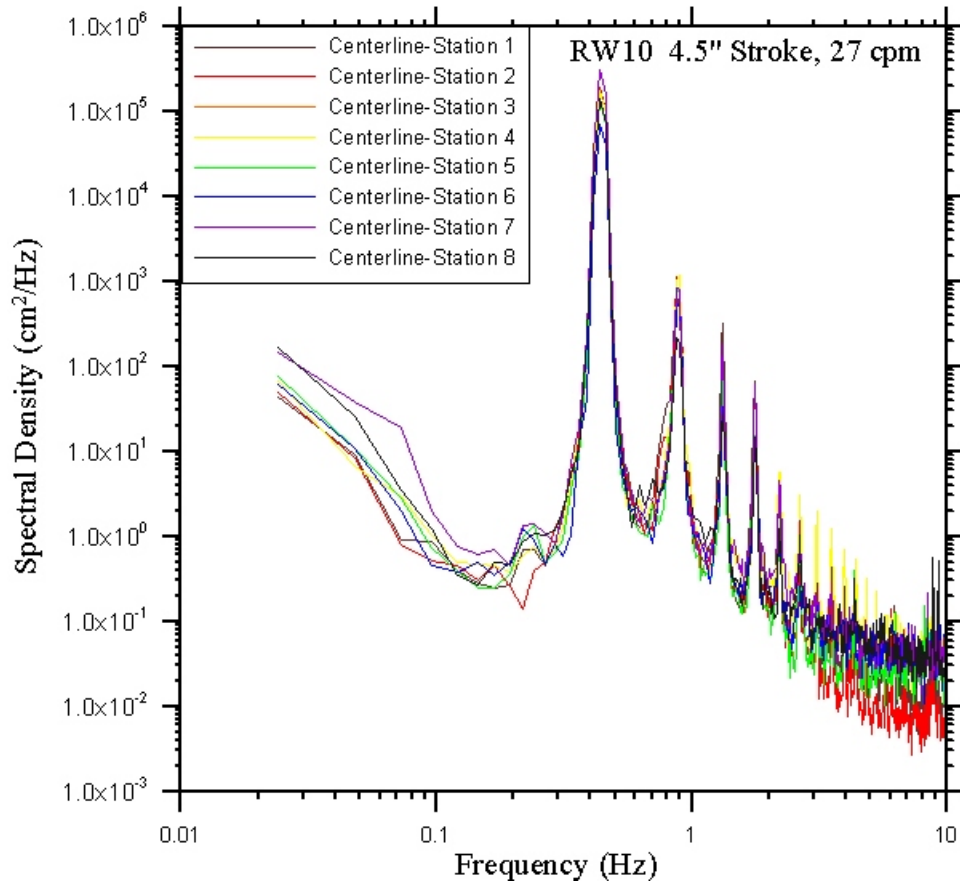


Figure 13: Power spectra of the water surface elevation time series shows plotted for pressure transducer P1 mounted on the tank centerline. Paddle conditions for this run correspond to RW10, 4.5" stroke, 27 cpm speed.

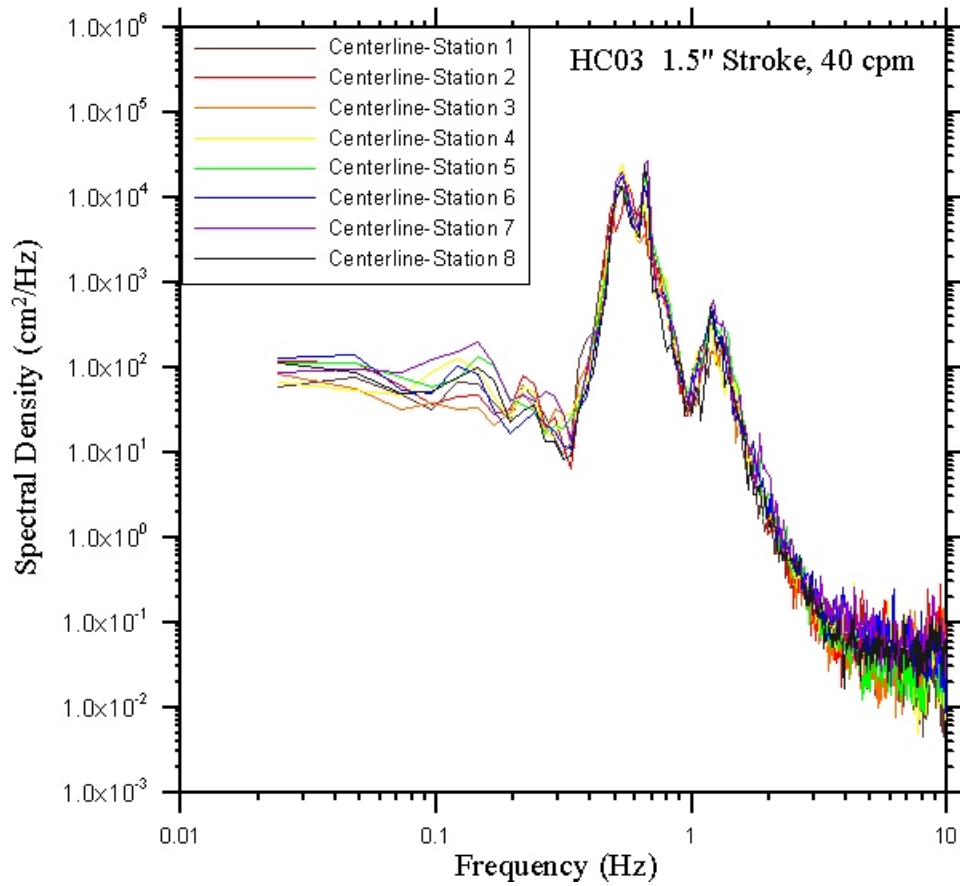


Figure 14: Power spectra of the water surface elevation time series shows plotted for pressure transducer P1 mounted on the tank centerline. Paddle conditions for this run correspond to HC03, 1.5" stroke, 40 cpm speed.

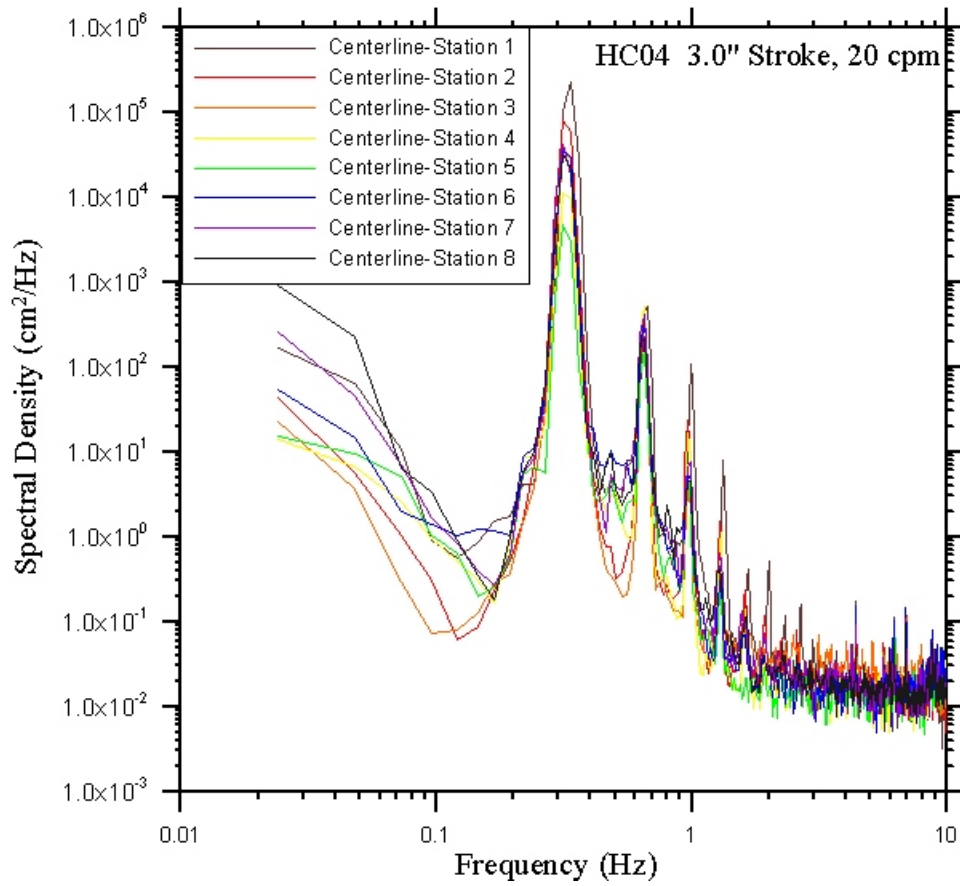


Figure 15: Power spectra of the water surface elevation time series shows plotted for pressure transducer P1 mounted on the tank centerline. Paddle conditions for this run correspond to HC04, 3.0" stroke, 20 cpm speed.

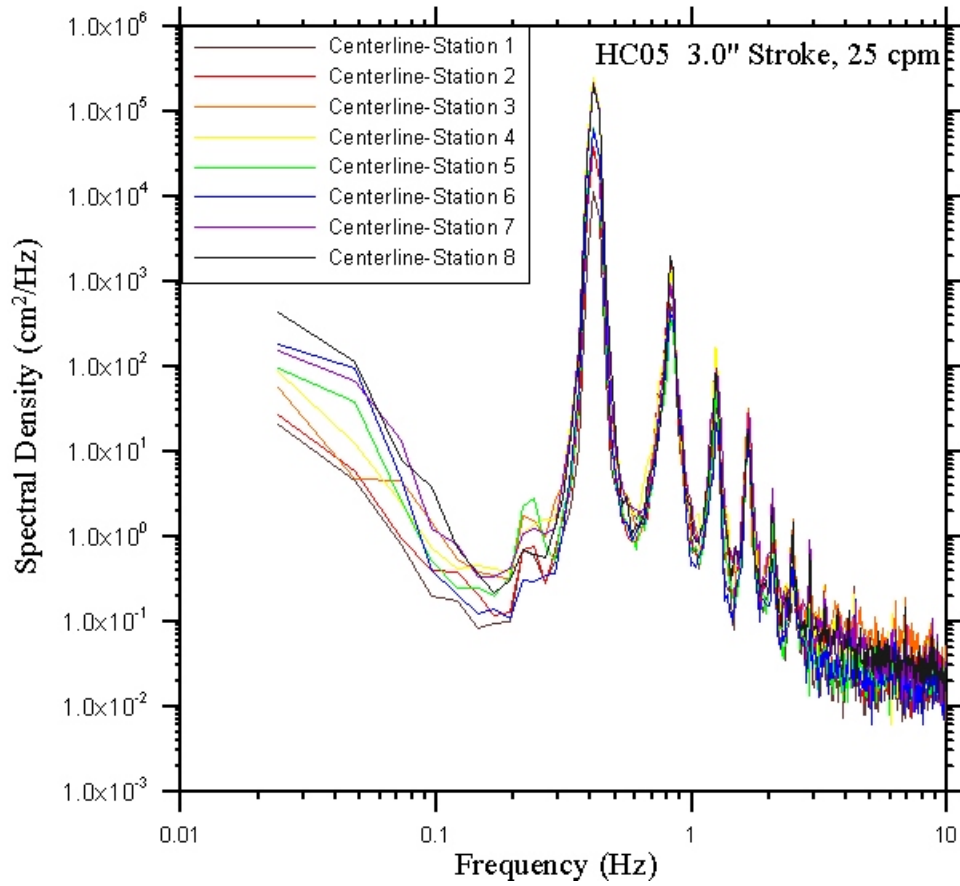


Figure 16: Power spectra of the water surface elevation time series shows plotted for pressure transducer P1 mounted on the tank centerline. Paddle conditions for this run correspond to HC05, 3.0" stroke, 25 cpm speed.

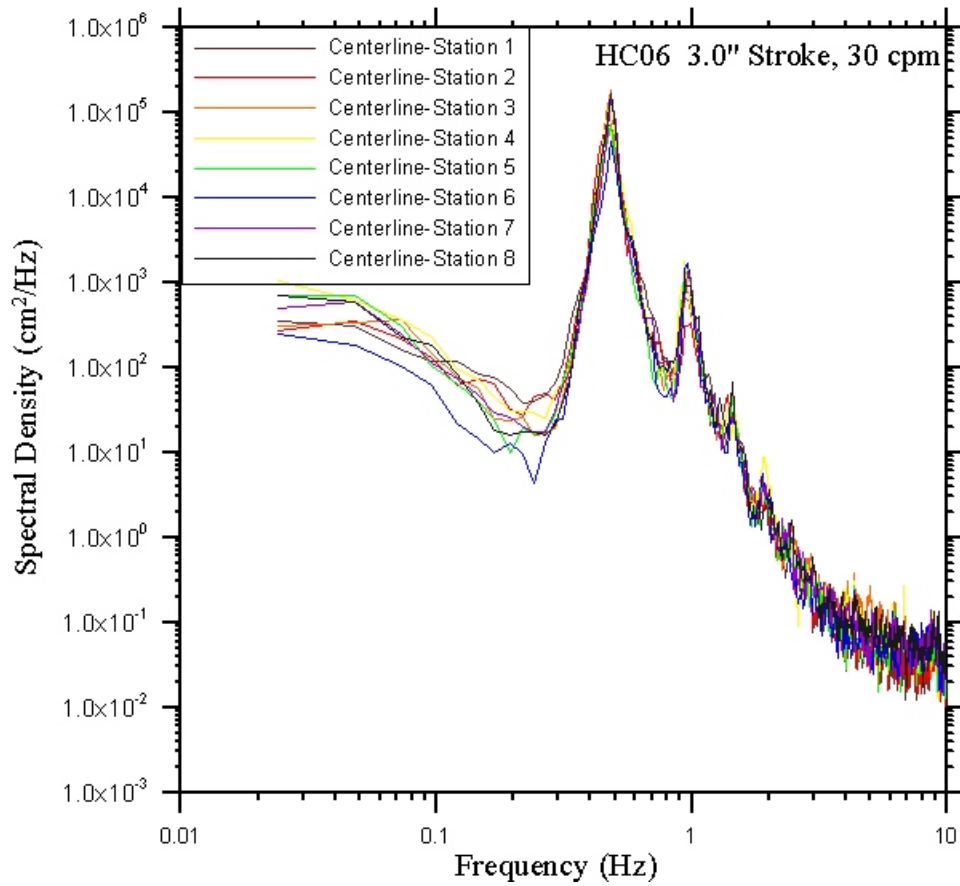


Figure 17: Power spectra of the water surface elevation time series shows plotted for pressure transducer P1 mounted on the tank centerline. Paddle conditions for this run correspond to HC06, 3.0" stroke, 30 cpm speed.

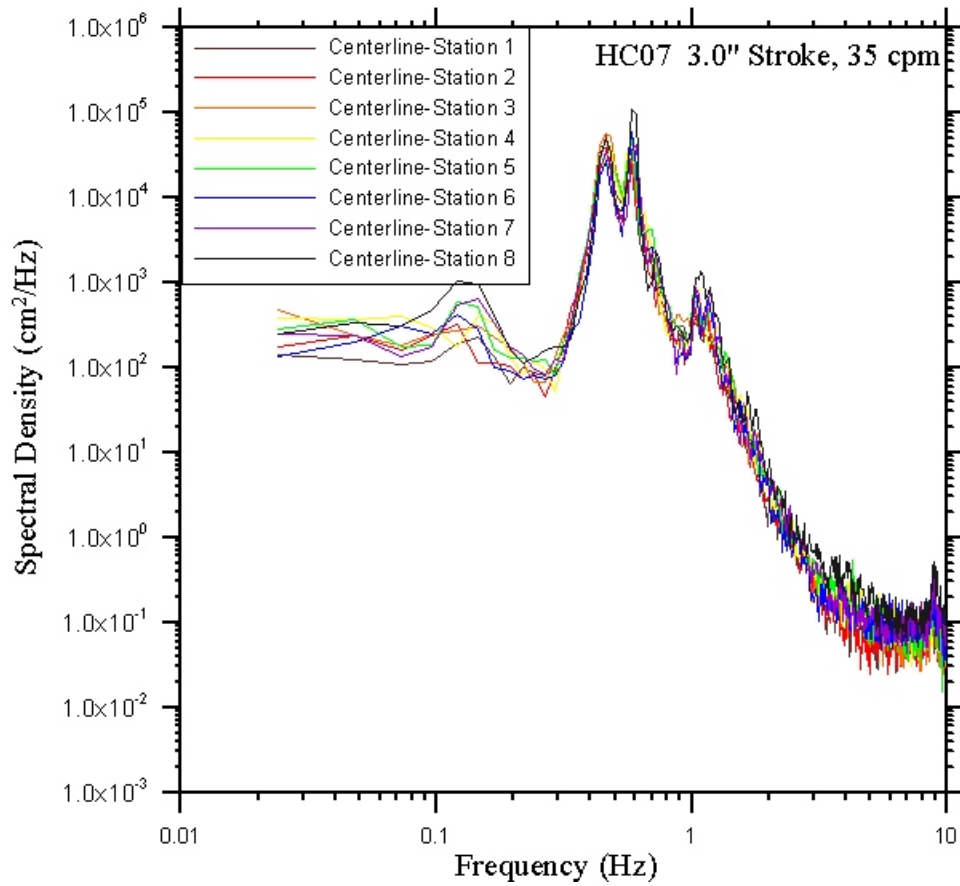


Figure 18: Power spectra of the water surface elevation time series shows plotted for pressure transducer P1 mounted on the tank centerline. Paddle conditions for this run correspond to HC07, 4.5" stroke, 35 cpm speed.

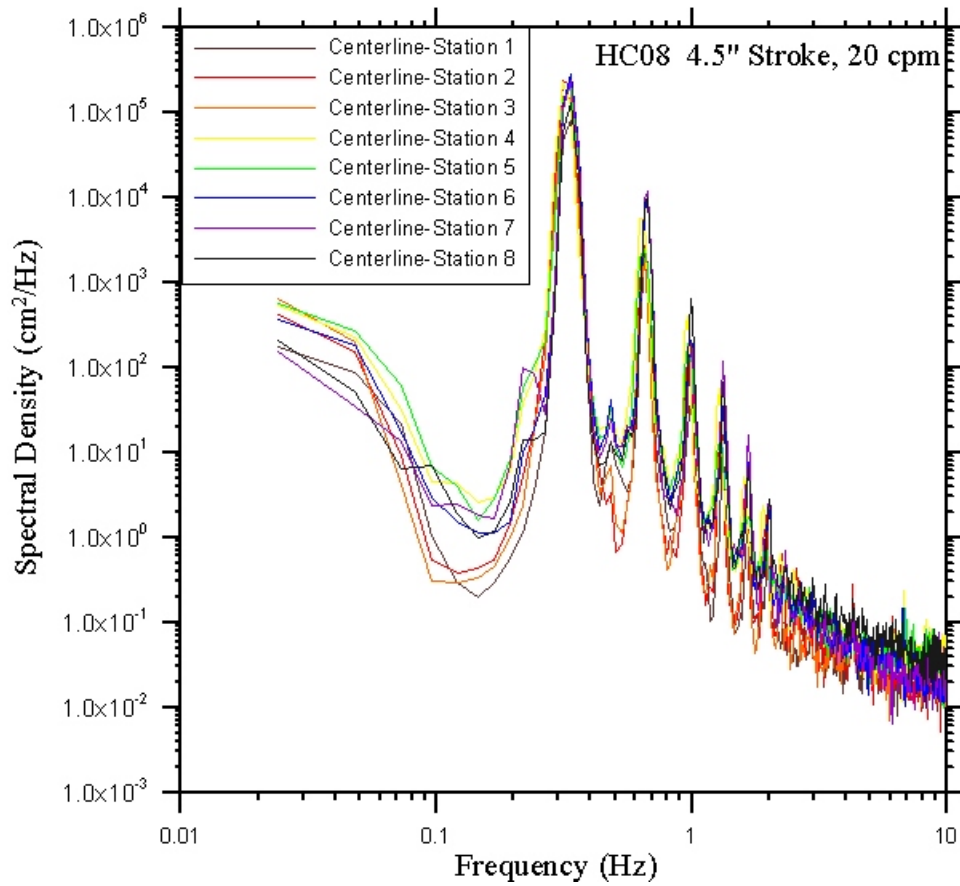


Figure 19: Power spectra of the water surface elevation time series shows plotted for pressure transducer P1 mounted on the tank centerline. Paddle conditions for this run correspond to HC08, 4.5" stroke, 20 cpm speed.

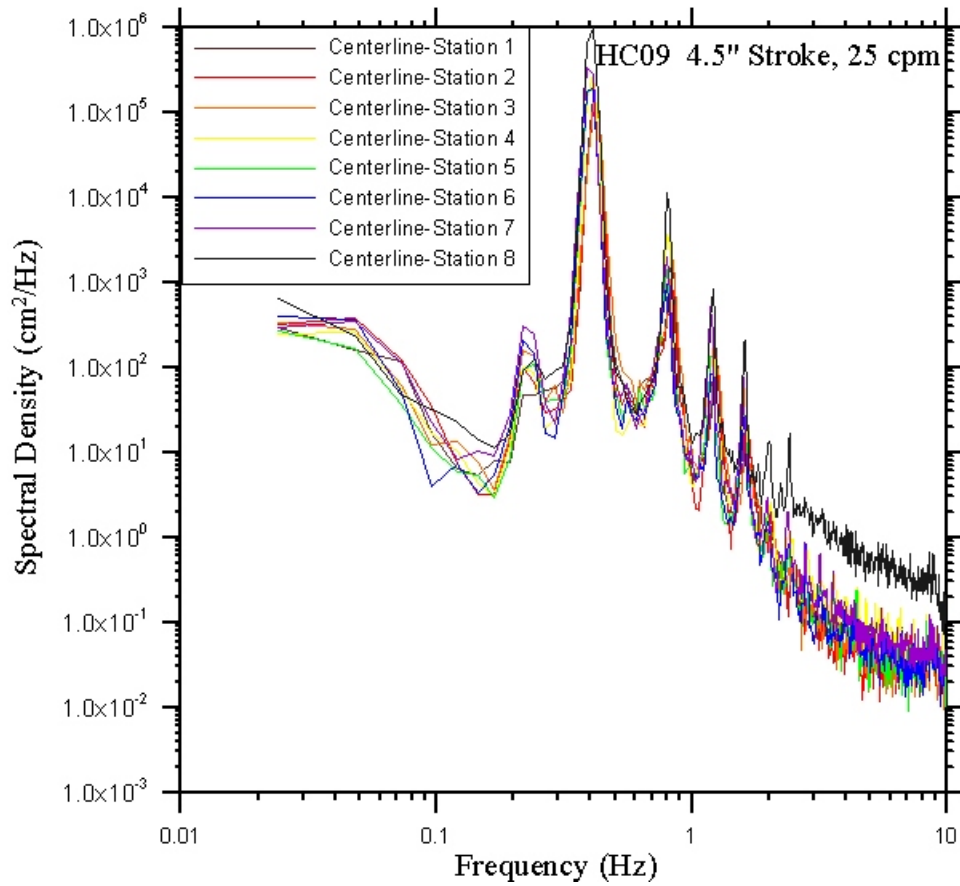


Figure 20: Power spectra of the water surface elevation time series shows plotted for pressure transducer P1 mounted on the tank centerline. Paddle conditions for this run correspond to HC09, 4.5" stroke, 25 cpm speed.

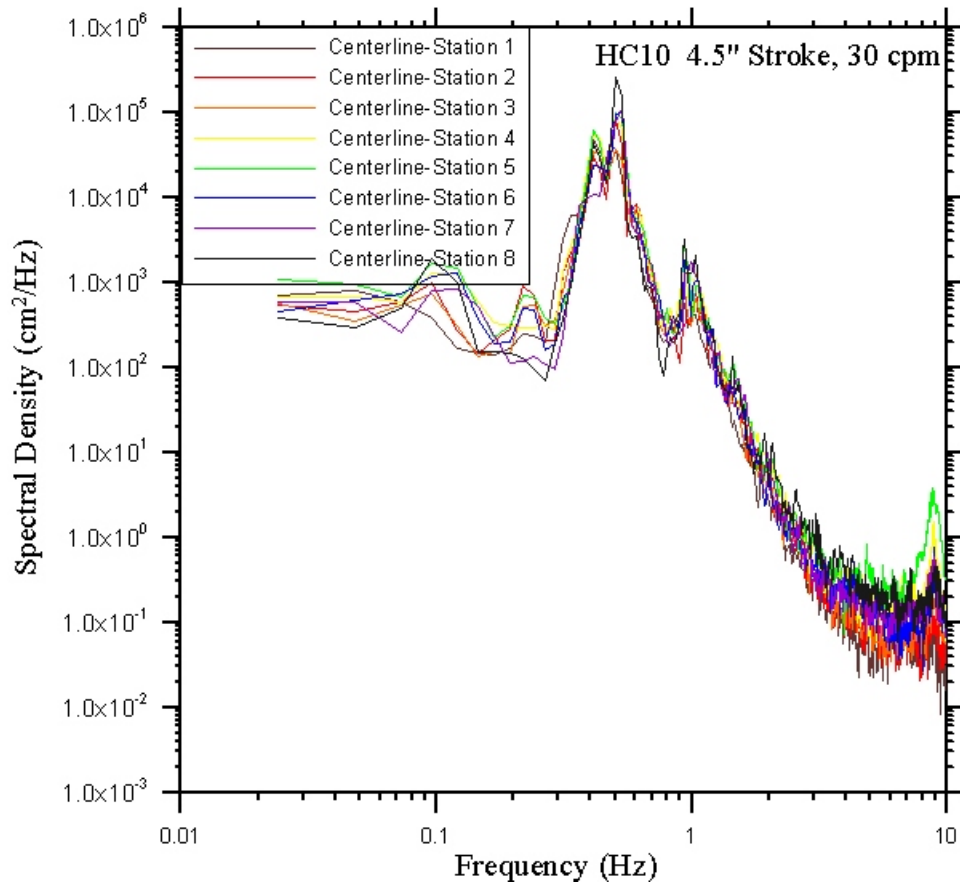


Figure 21: Power spectra of the water surface elevation time series shows plotted for pressure transducer P1 mounted on the tank centerline. Paddle conditions for this run correspond to HC10, 4.5" stroke, 30 cpm speed.

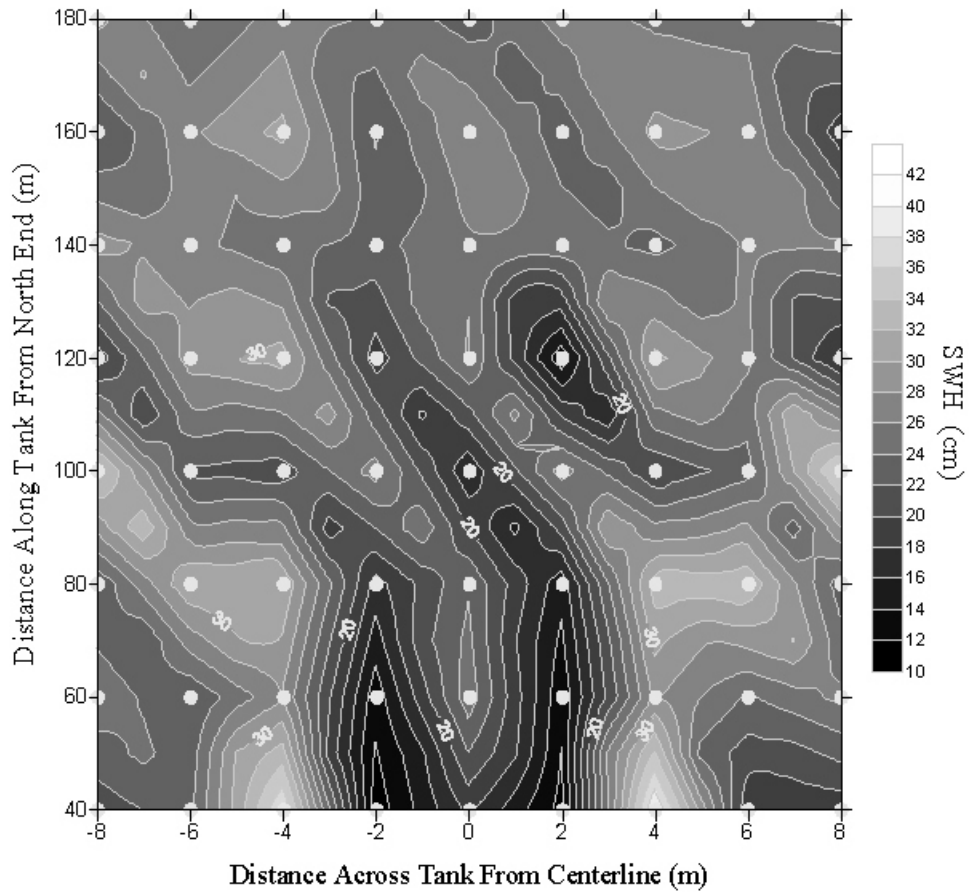


Figure 22: Contour plot of significant wave height, $H_{1/3}$ (cm), as a function of position in the Ohmsett wave basin. The grey circles show the locations of the wave probes used to record the wave height data. The individual values for $H_{1/3}$ were calculated as 360-s averages for each of the nine probes in the main array at each of the eight stations along the tank. Paddle conditions for this run correspond to RW01, 1.5" stroke, 35 cpm speed.

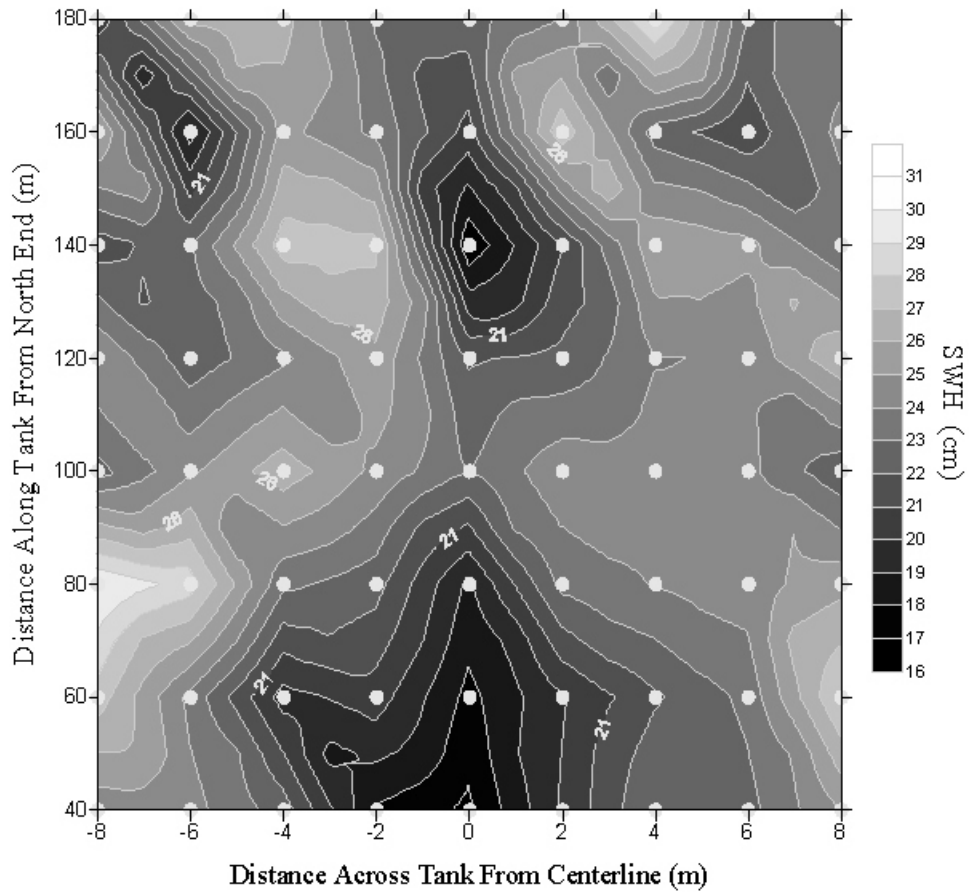


Figure 23: Contour plot of significant wave height, $H_{1/3}$ (cm), as a function of position in the Ohmsett wave basin. The grey circles show the locations of the wave probes used to record the wave height data. The individual values for $H_{1/3}$ were calculated as 360-s averages for each of the nine probes in the main array at each of the eight stations along the tank. Paddle conditions for this run correspond to RW02, 1.5" stroke, 40 cpm speed.

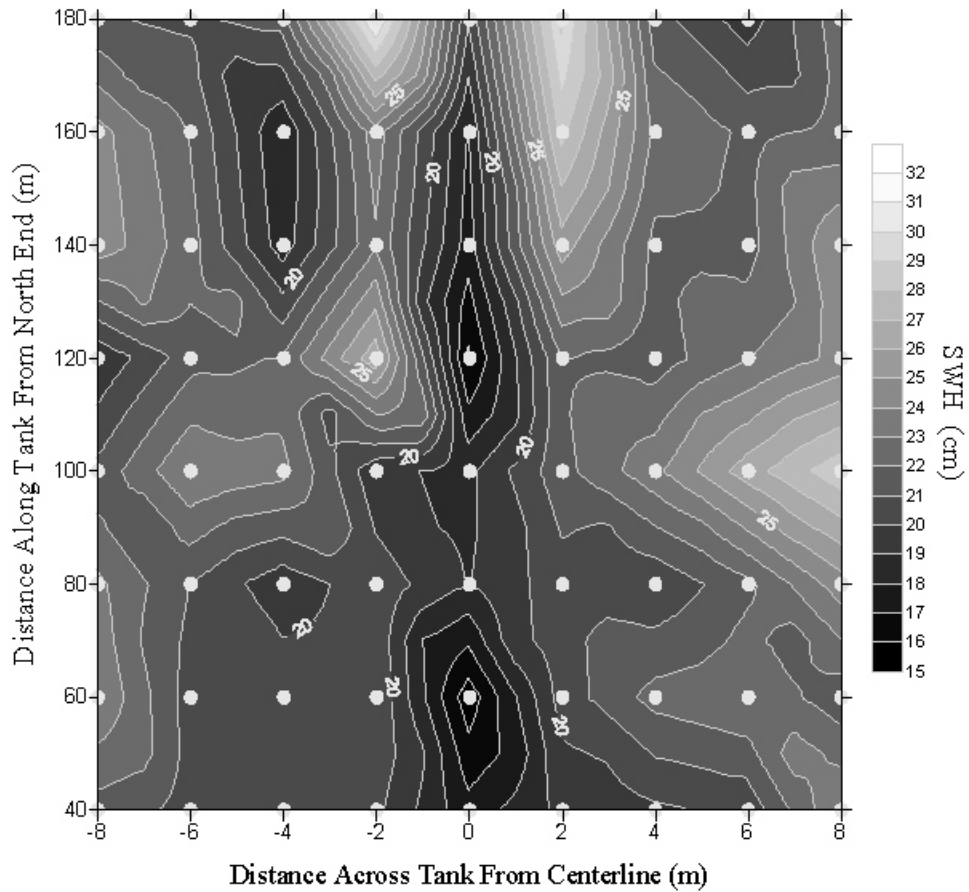


Figure 24: Contour plot of significant wave height, $H_{1/3}$ (cm), as a function of position in the Ohmsett wave basin. The grey circles show the locations of the wave probes used to record the wave height data. The individual values for $H_{1/3}$ were calculated as 360-s averages for each of the nine probes in the main array at each of the eight stations along the tank. Paddle conditions for this run correspond to RW03, 1.5" stroke, 45 cpm speed.

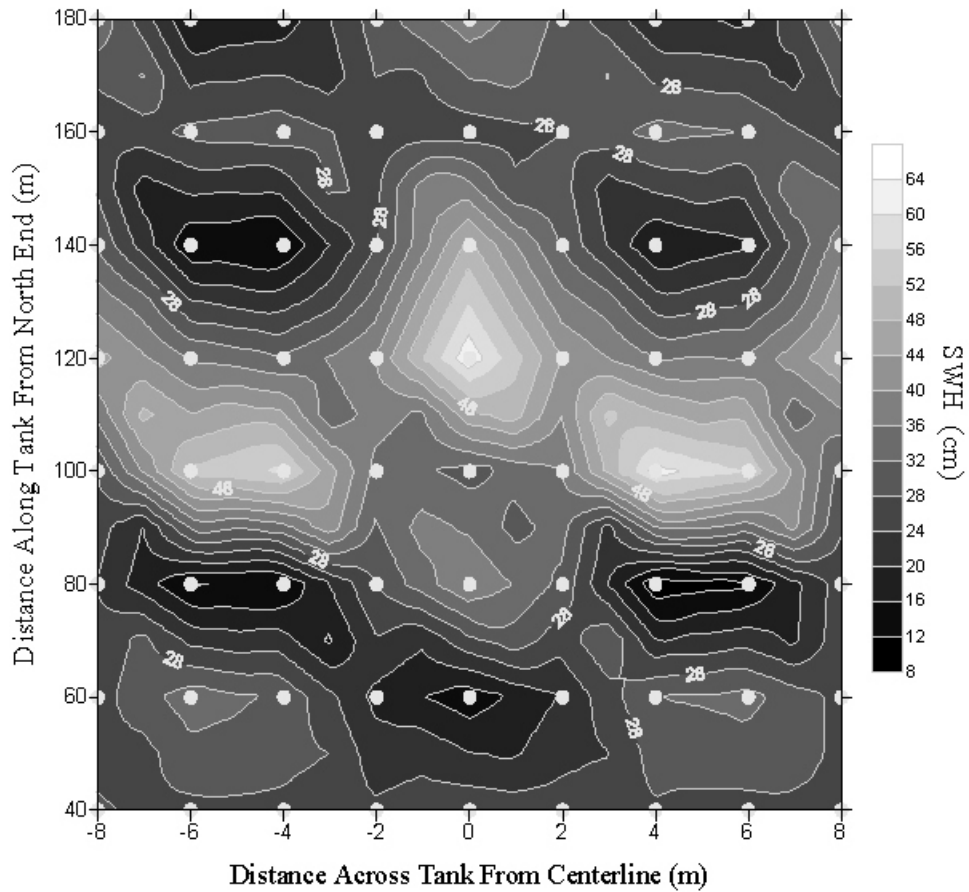


Figure 25: Contour plot of significant wave height, $H_{1/3}$ (cm), as a function of position in the Ohmsett wave basin. The grey circles show the locations of the wave probes used to record the wave height data. The individual values for $H_{1/3}$ were calculated as 360-s averages for each of the nine probes in the main array at each of the eight stations along the tank. Paddle conditions for this run correspond to RW04, 3.0" stroke, 21 cpm speed.

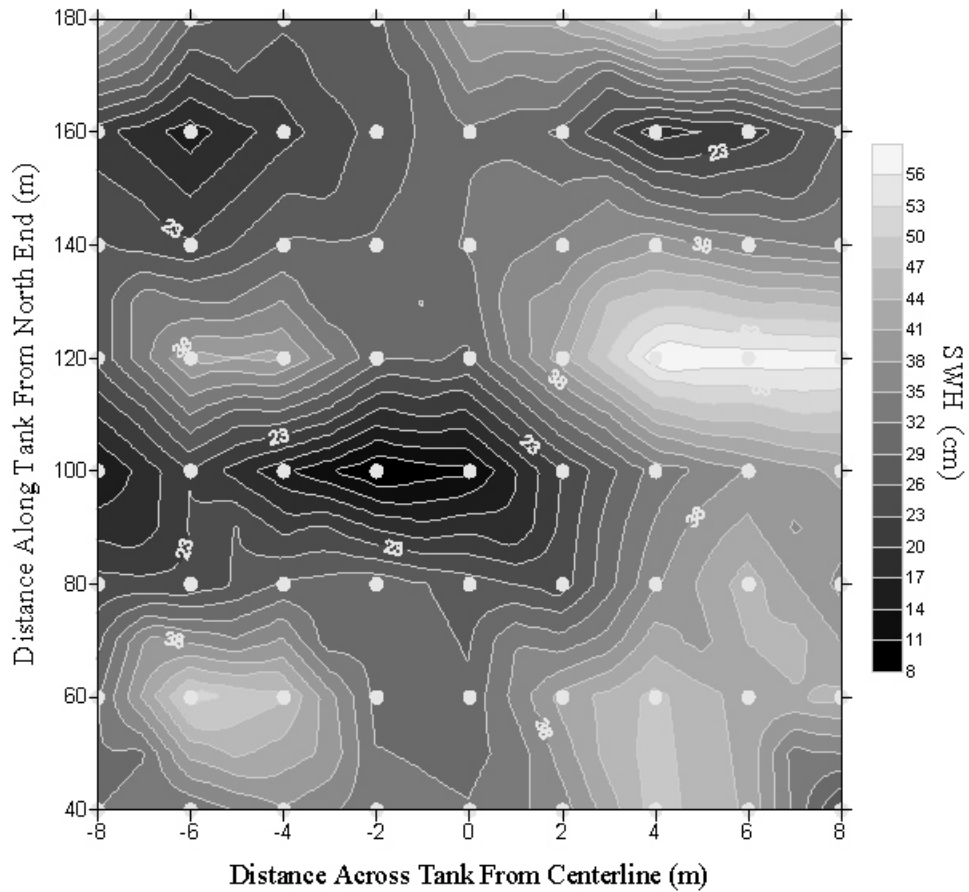


Figure 26: Contour plot of significant wave height, $H_{1/3}$ (cm), as a function of position in the Ohmsett wave basin. The grey circles show the locations of the wave probes used to record the wave height data. The individual values for $H_{1/3}$ were calculated as 360-s averages for each of the nine probes in the main array at each of the eight stations along the tank. Paddle conditions for this run correspond to RW05, 3.0" stroke, 37 cpm speed.

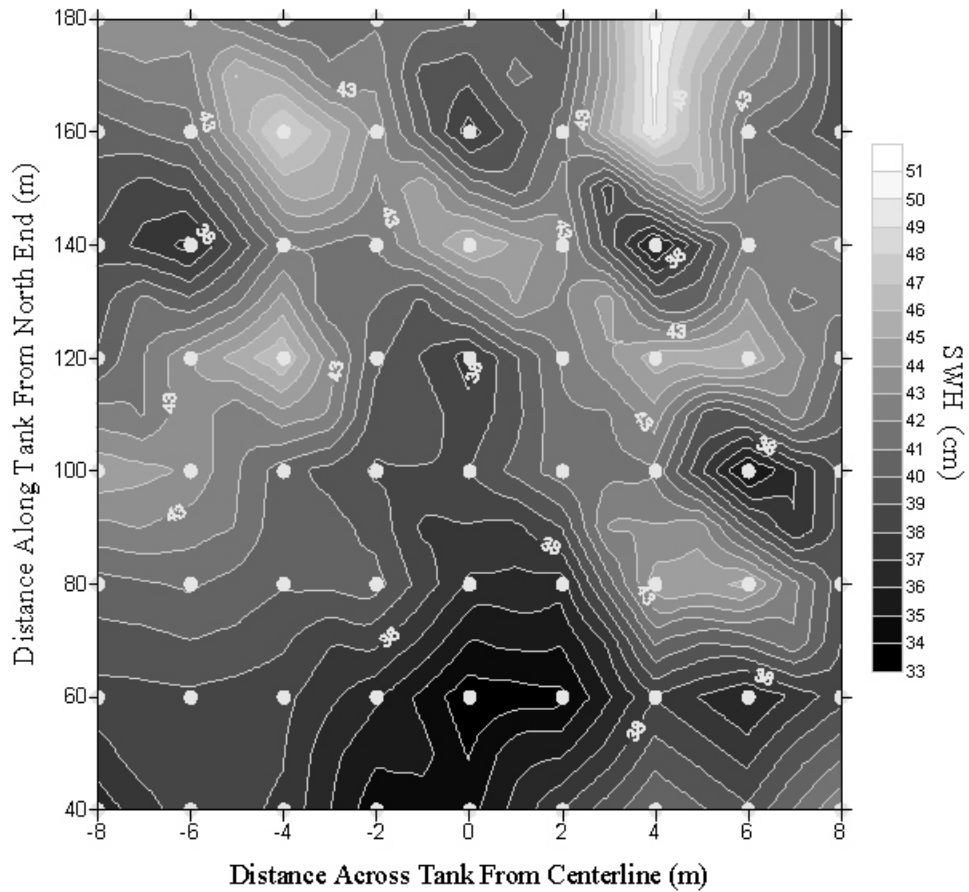


Figure 27: Contour plot of significant wave height, $H_{1/3}$ (cm), as a function of position in the Ohmsett wave basin. The grey circles show the locations of the wave probes used to record the wave height data. The individual values for $H_{1/3}$ were calculated as 360-s averages for each of the nine probes in the main array at each of the eight stations along the tank. Paddle conditions for this run correspond to RW06, 3.0" stroke, 33 cpm speed.

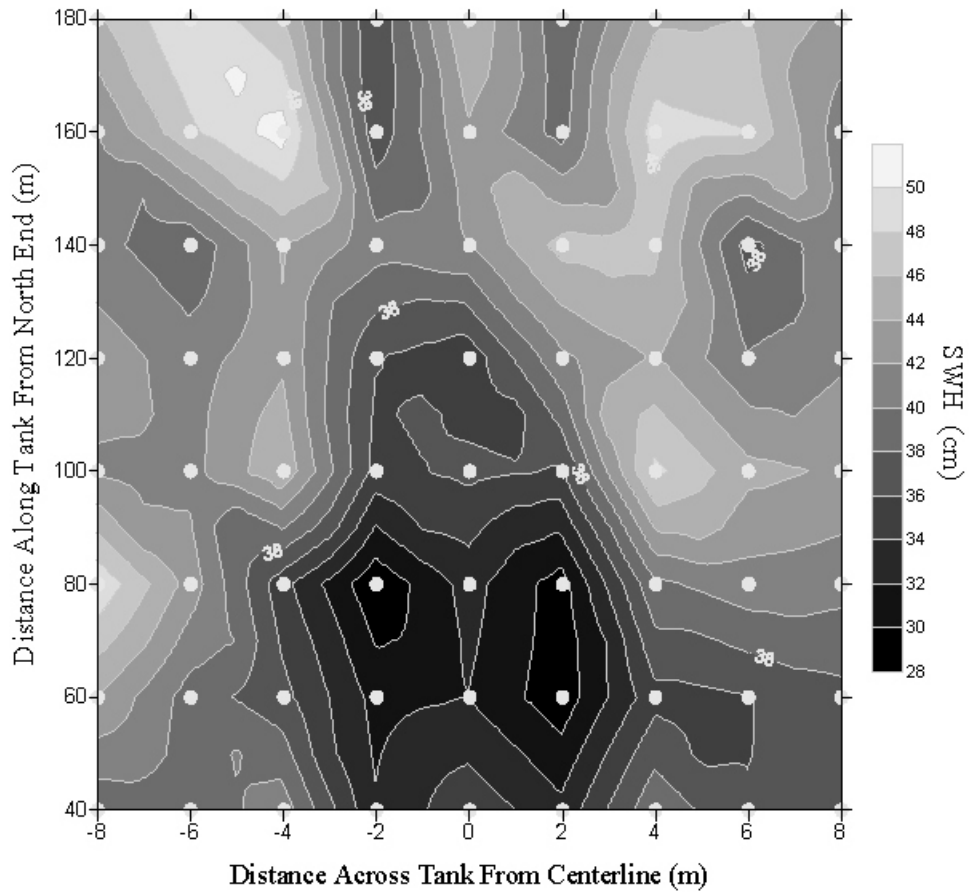


Figure 28: Contour plot of significant wave height, $H_{1/3}$ (cm), as a function of position in the Ohmsett wave basin. The grey circles show the locations of the wave probes used to record the wave height data. The individual values for $H_{1/3}$ were calculated as 360-s averages for each of the nine probes in the main array at each of the eight stations along the tank. Paddle conditions for this run correspond to RW07, 3.0" stroke, 35 cpm speed.

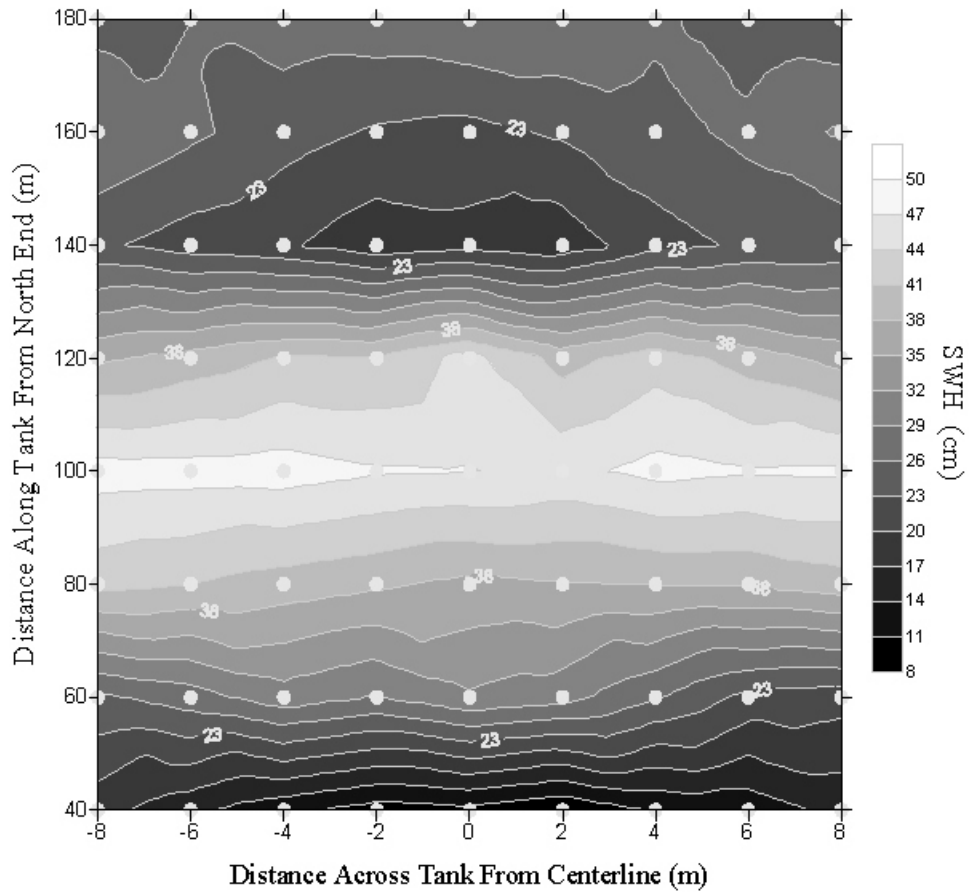


Figure 29: Contour plot of significant wave height, $H_{1/3}$ (cm), as a function of position in the Ohmsett wave basin. The grey circles show the locations of the wave probes used to record the wave height data. The individual values for $H_{1/3}$ were calculated as 360-s averages for each of the nine probes in the main array at each of the eight stations along the tank. Paddle conditions for this run correspond to RW08, 4.5" stroke, 15 cpm speed.

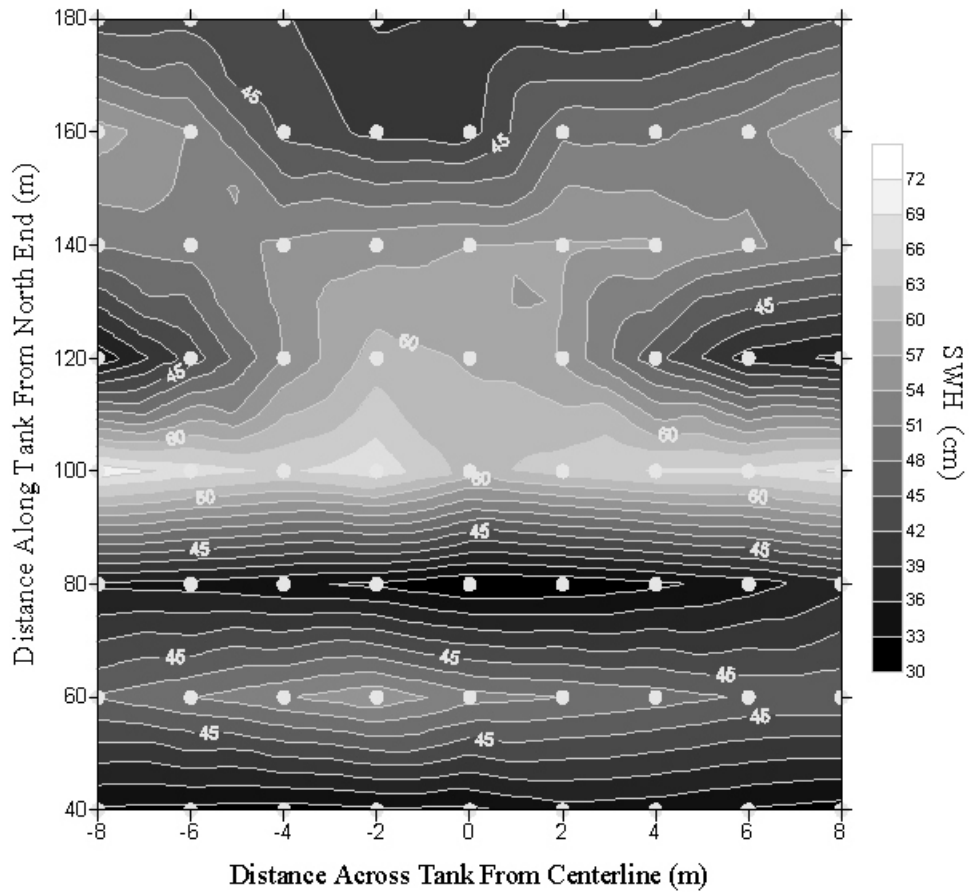


Figure 30: Contour plot of significant wave height, $H_{1/3}$ (cm), as a function of position in the Ohmsett wave basin. The grey circles show the locations of the wave probes used to record the wave height data. The individual values for $H_{1/3}$ were calculated as 360-s averages for each of the nine probes in the main array at each of the eight stations along the tank. Paddle conditions for this run correspond to RW09, 4.5" stroke, 21 cpm speed.

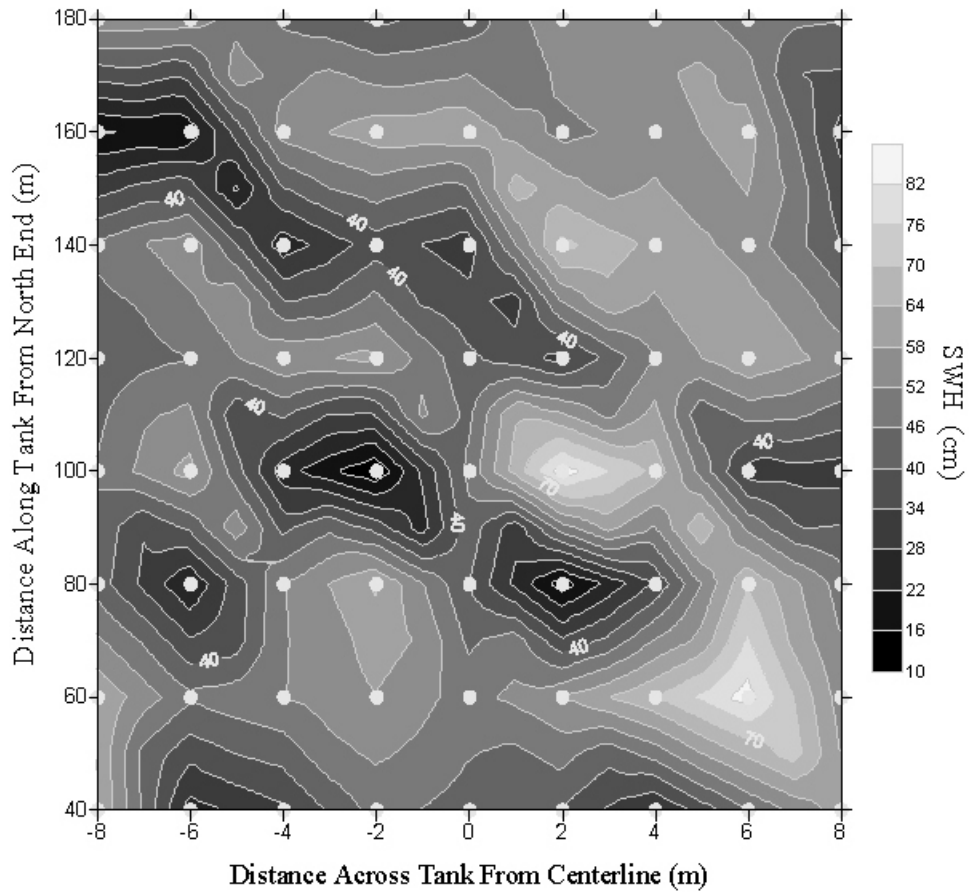


Figure 31: Contour plot of significant wave height, $H_{1/3}$ (cm), as a function of position in the Ohmsett wave basin. The grey circles show the locations of the wave probes used to record the wave height data. The individual values for $H_{1/3}$ were calculated as 360-s averages for each of the nine probes in the main array at each of the eight stations along the tank. Paddle conditions for this run correspond to RW10, 4.5" stroke, 27 cpm speed.

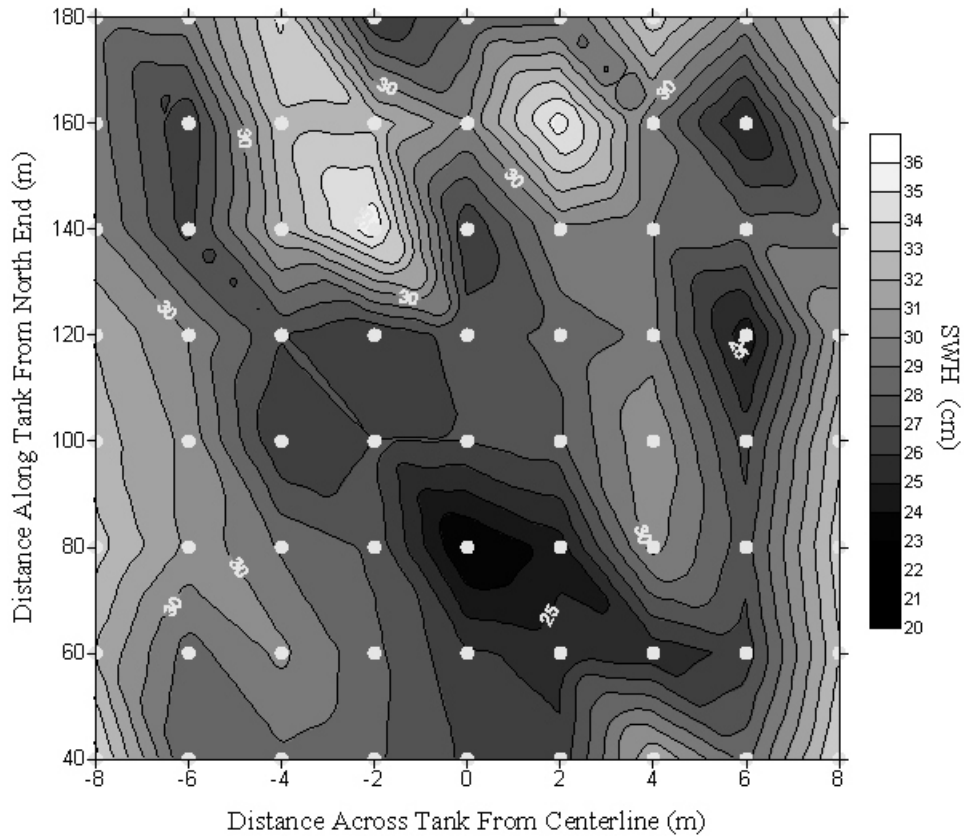


Figure 32: Contour plot of significant wave height, $H_{1/3}$ (cm), as a function of position in the Ohmsett wave basin. The grey circles show the locations of the wave probes used to record the wave height data. The individual values for $H_{1/3}$ were calculated as 360-s averages for each of the nine probes in the main array at each of the eight stations along the tank. Paddle conditions for this run correspond to HC03, 1.5" stroke, 40 cpm speed.

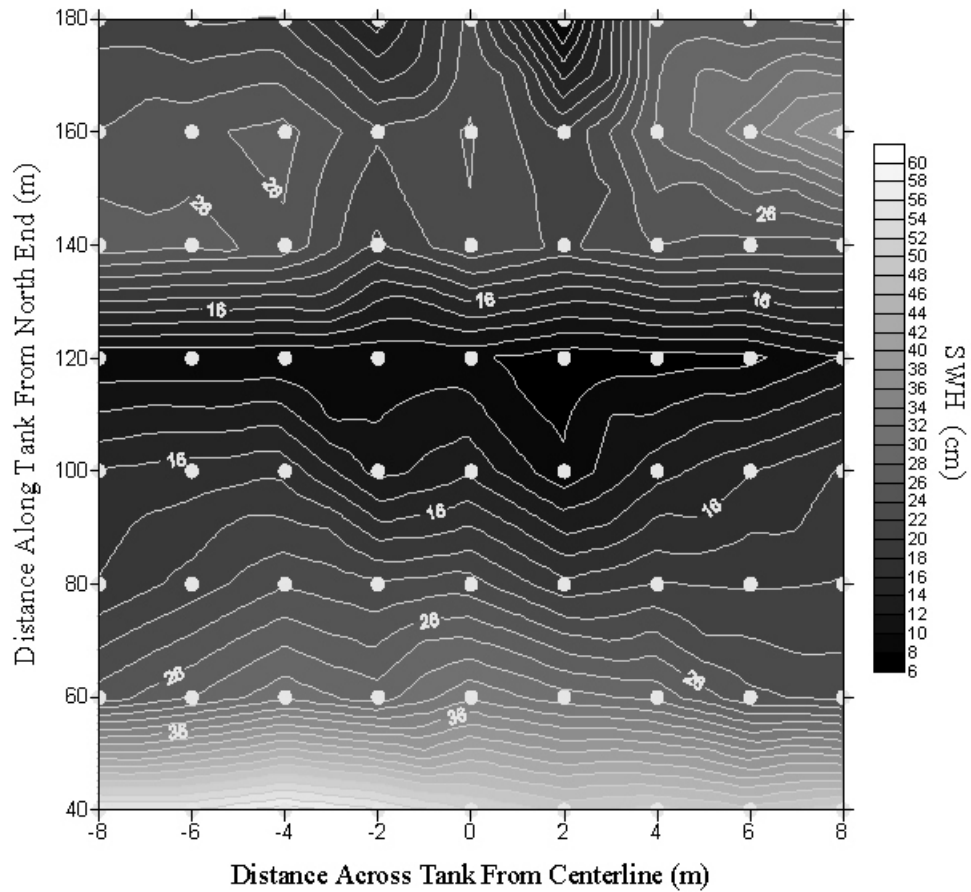


Figure 33: Contour plot of significant wave height, $H_{1/3}$ (cm), as a function of position in the Ohmsett wave basin. The grey circles show the locations of the wave probes used to record the wave height data. The individual values for $H_{1/3}$ were calculated as 360-s averages for each of the nine probes in the main array at each of the eight stations along the tank. Paddle conditions for this run correspond to HC04, 3.0" stroke, 20 cpm speed.

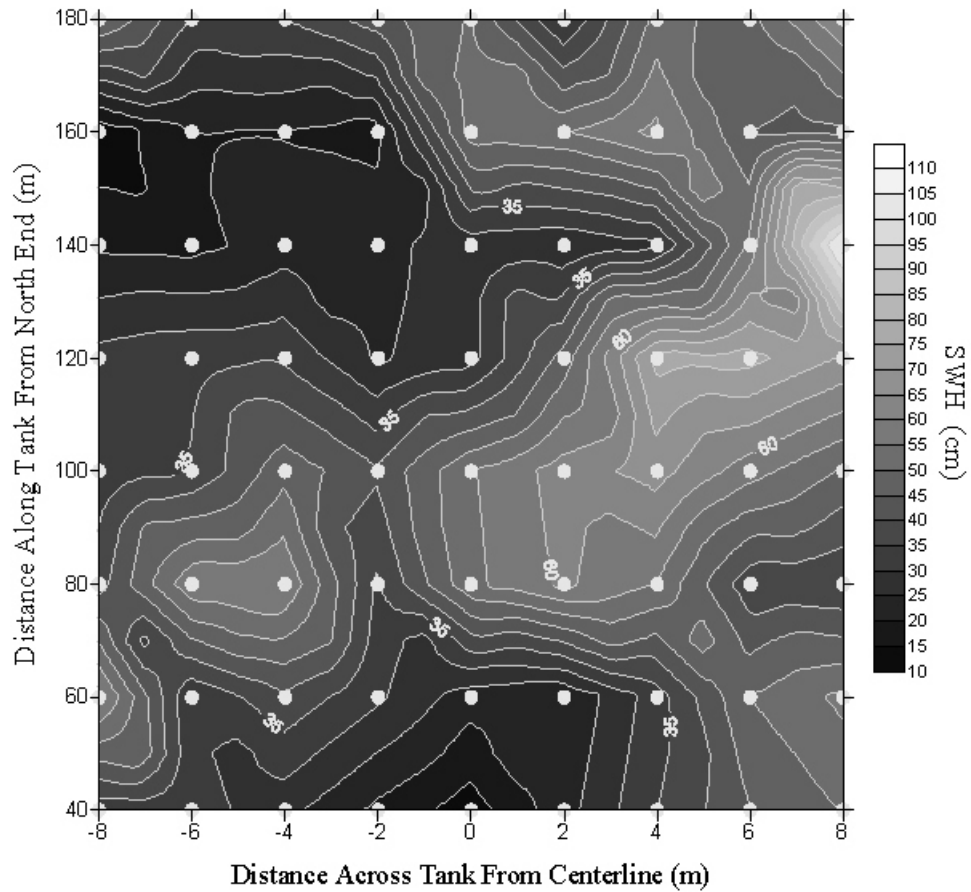


Figure 34: Contour plot of significant wave height, $H_{1/3}$ (cm), as a function of position in the Ohmsett wave basin. The grey circles show the locations of the wave probes used to record the wave height data. The individual values for $H_{1/3}$ were calculated as 360-s averages for each of the nine probes in the main array at each of the eight stations along the tank. Paddle conditions for this run correspond to HC05, 3.0" stroke, 25 cpm speed.

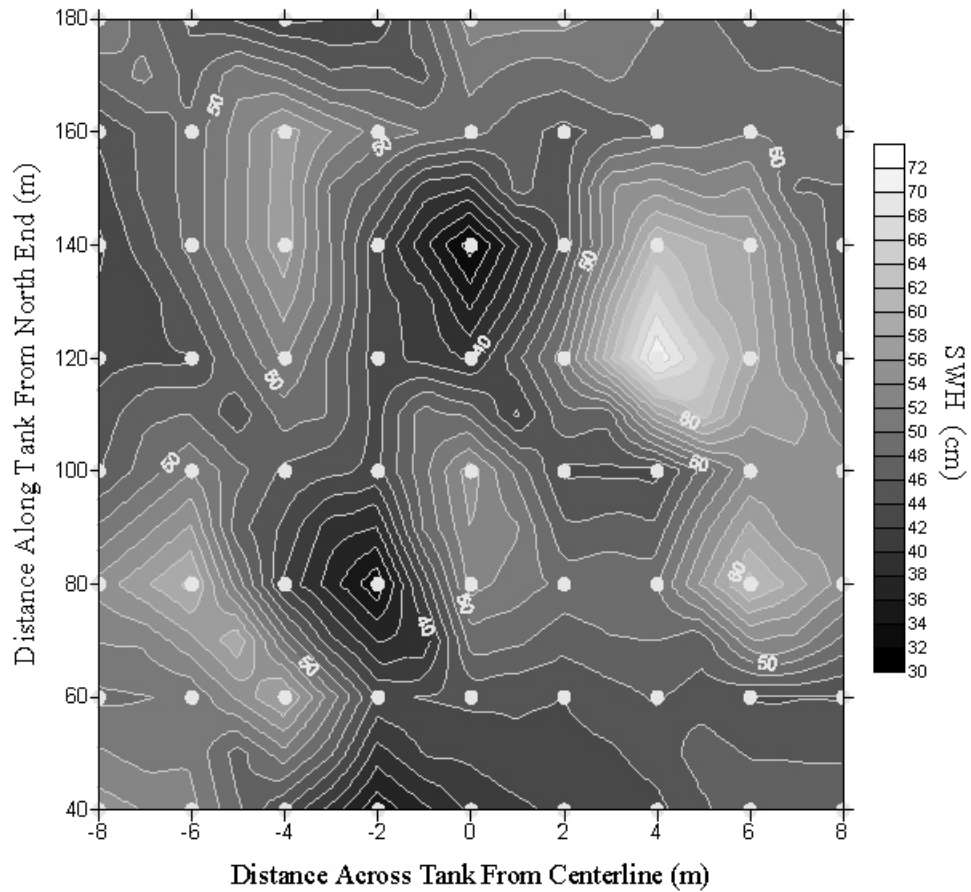


Figure 35: Contour plot of significant wave height, $H_{1/3}$ (cm), as a function of position in the Ohmsett wave basin. The grey circles show the locations of the wave probes used to record the wave height data. The individual values for $H_{1/3}$ were calculated as 360-s averages for each of the nine probes in the main array at each of the eight stations along the tank. Paddle conditions for this run correspond to HC06, 3.0" stroke, 30 cpm speed.

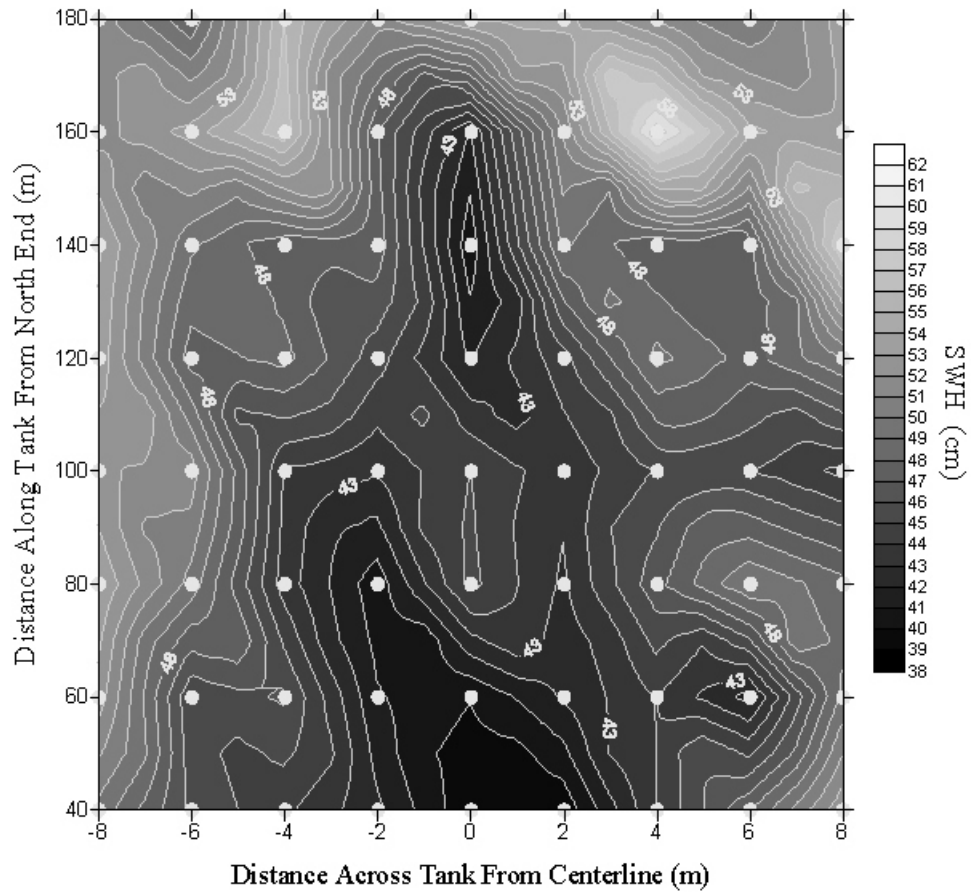


Figure 36: Contour plot of significant wave height, $H_{1/3}$ (cm), as a function of position in the Ohmsett wave basin. The grey circles show the locations of the wave probes used to record the wave height data. The individual values for $H_{1/3}$ were calculated as 360-s averages for each of the nine probes in the main array at each of the eight stations along the tank. Paddle conditions for this run correspond to HC07, 4.5" stroke, 35 cpm speed.

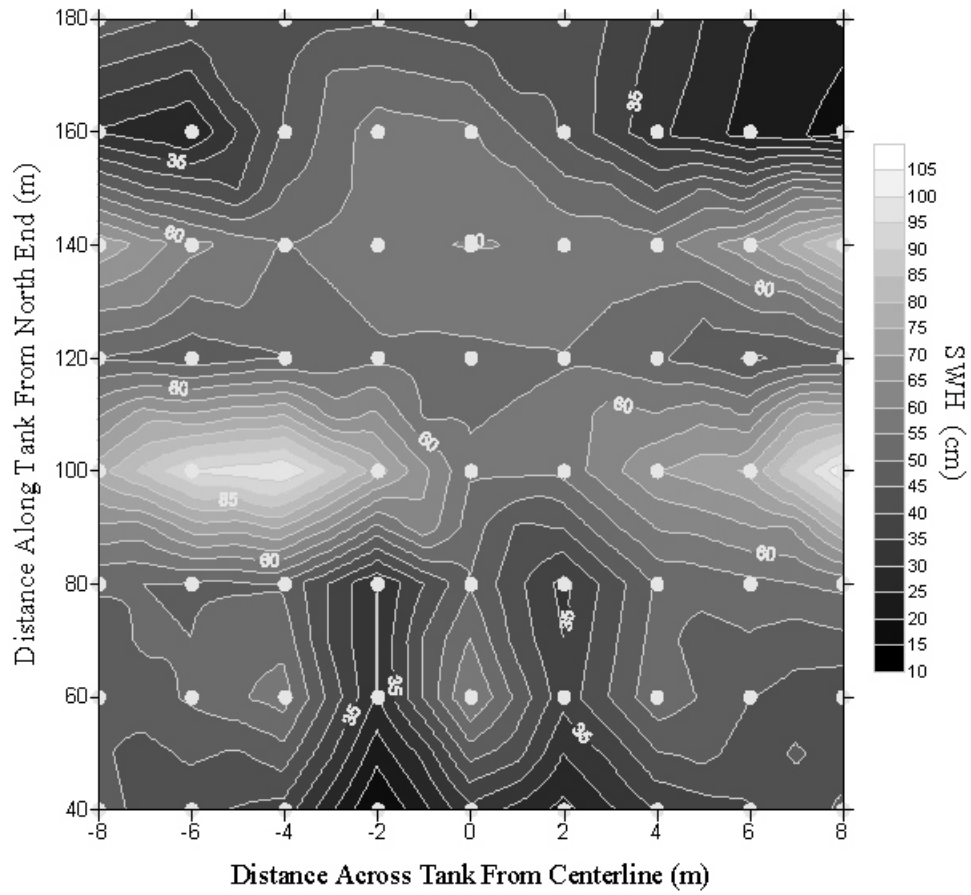


Figure 37: Contour plot of significant wave height, $H_{1/3}$ (cm), as a function of position in the Ohmsett wave basin. The grey circles show the locations of the wave probes used to record the wave height data. The individual values for $H_{1/3}$ were calculated as 360-s averages for each of the nine probes in the main array at each of the eight stations along the tank. Paddle conditions for this run correspond to HC08, 4.5" stroke, 20 cpm speed.

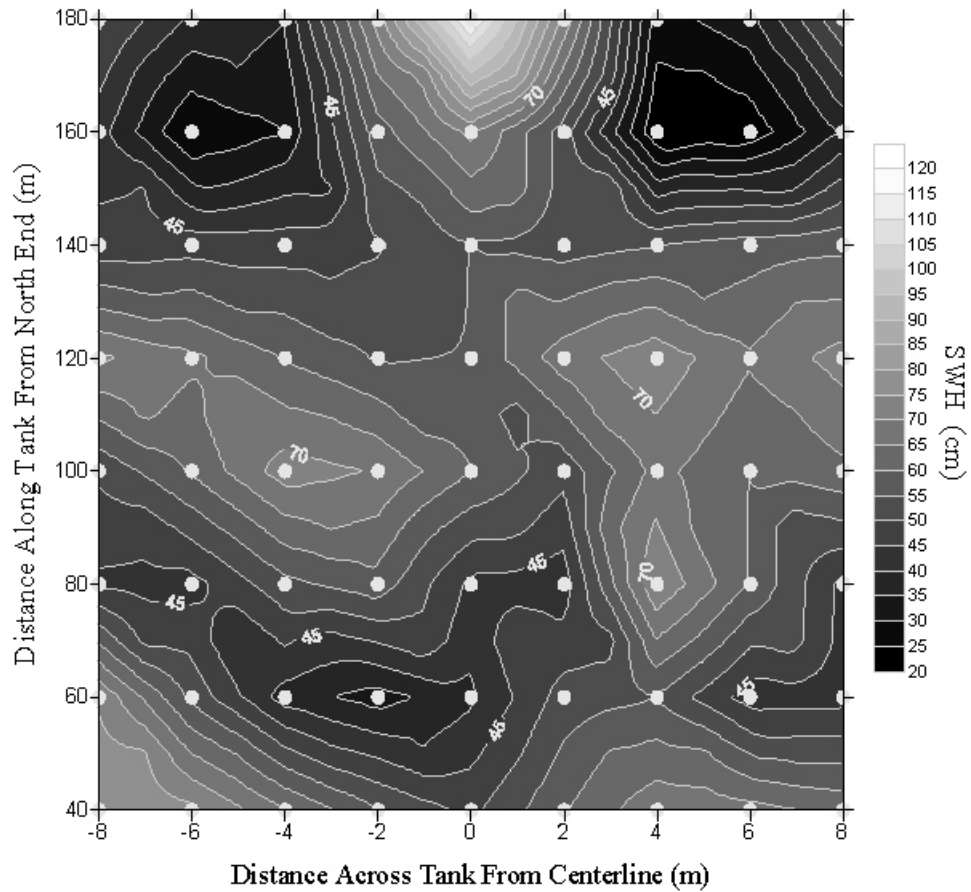


Figure 38: Contour plot of significant wave height, $H_{1/3}$ (cm), as a function of position in the Ohmsett wave basin. The grey circles show the locations of the wave probes used to record the wave height data. The individual values for $H_{1/3}$ were calculated as 360-s averages for each of the nine probes in the main array at each of the eight stations along the tank. Paddle conditions for this run correspond to HC09, 4.5" stroke, 25 cpm speed.

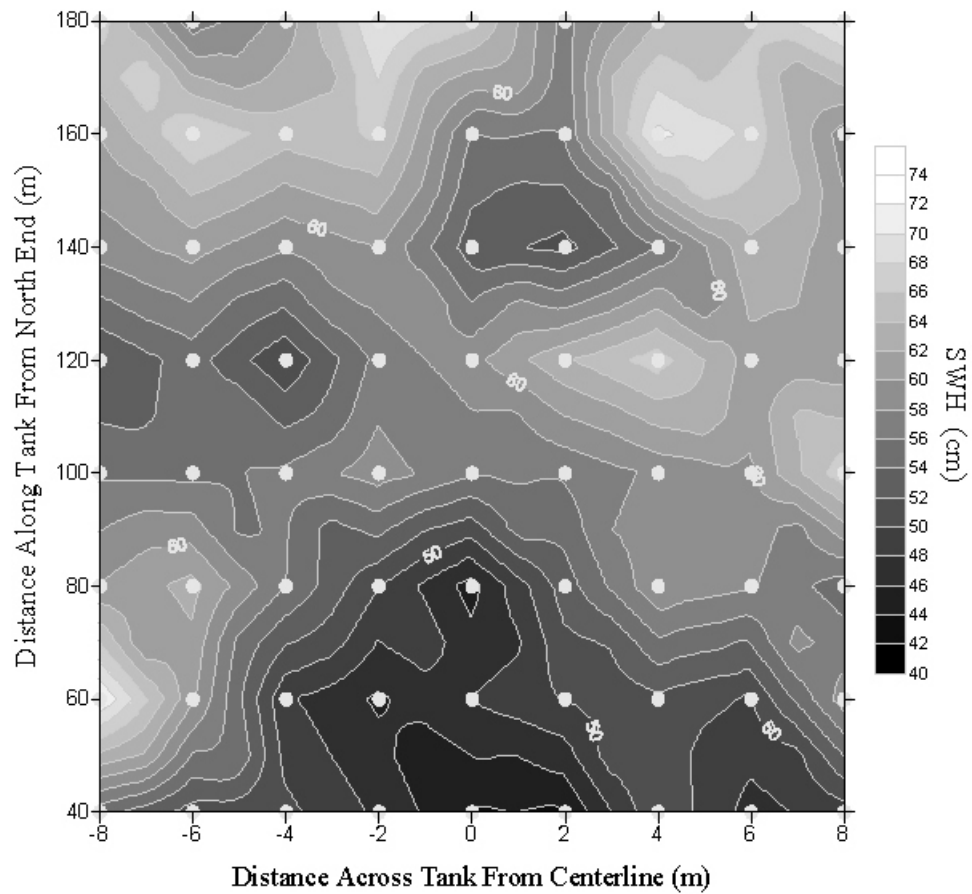


Figure 39: Contour plot of significant wave height, $H_{1/3}$ (cm), as a function of position in the Ohmsett wave basin. The grey circles show the locations of the wave probes used to record the wave height data. The individual values for $H_{1/3}$ were calculated as 360-s averages for each of the nine probes in the main array at each of the eight stations along the tank. Paddle conditions for this run correspond to HC10, 4.5" stroke, 30 cpm speed.

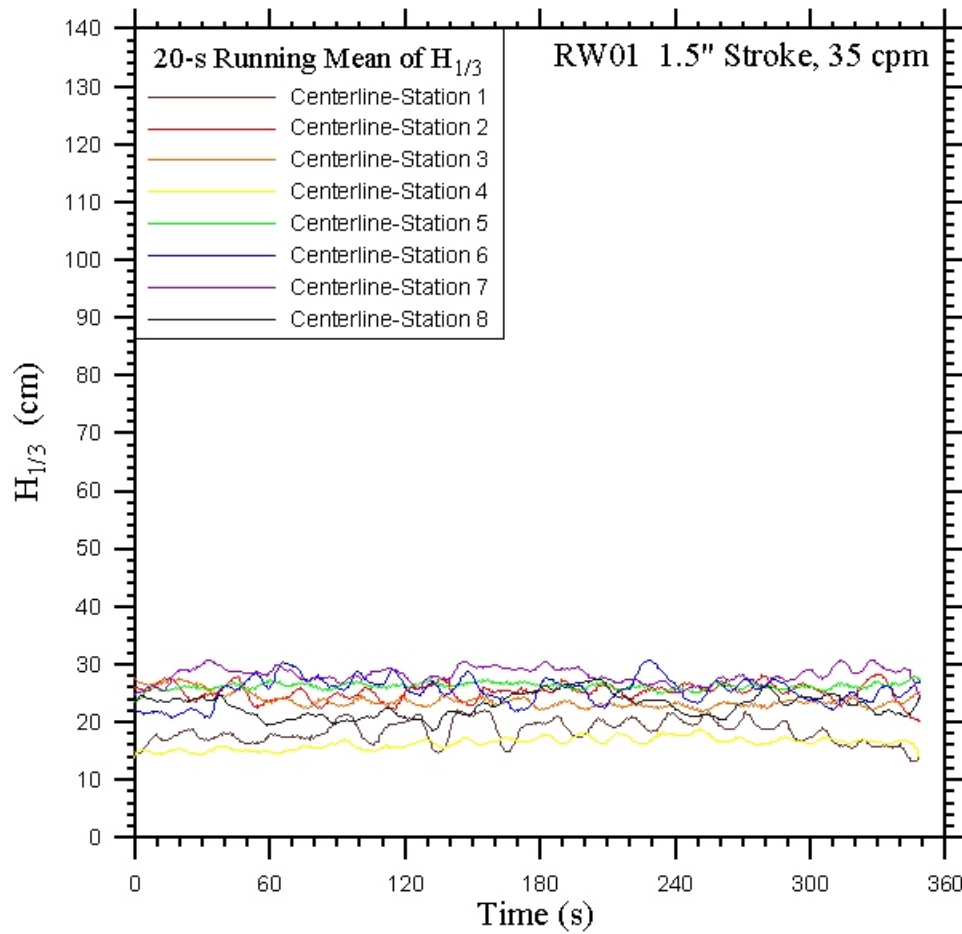


Figure 40: Significant wave height, $H_{1/3}$, calculated as a 20 s moving averaged along the centerline of the wave basin at the eight sampling stations plotted versus time. Paddle conditions for this run correspond to RW01, 1.5" stroke, 35 cpm speed.

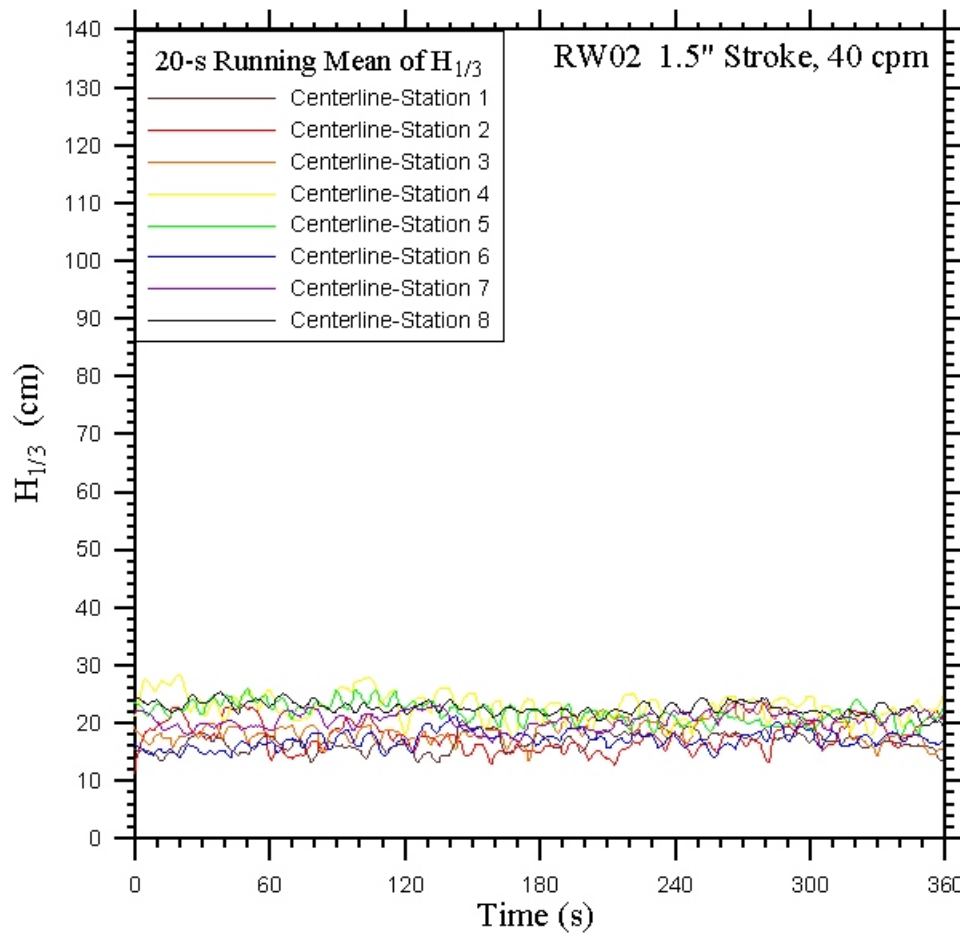


Figure 41: Significant wave height, $H_{1/3}$, calculated as a 20 s moving averaged along the centerline of the wave basin at the eight sampling stations plotted versus time. Paddle conditions for this run correspond to RW02, 1.5" stroke, 40 cpm speed.

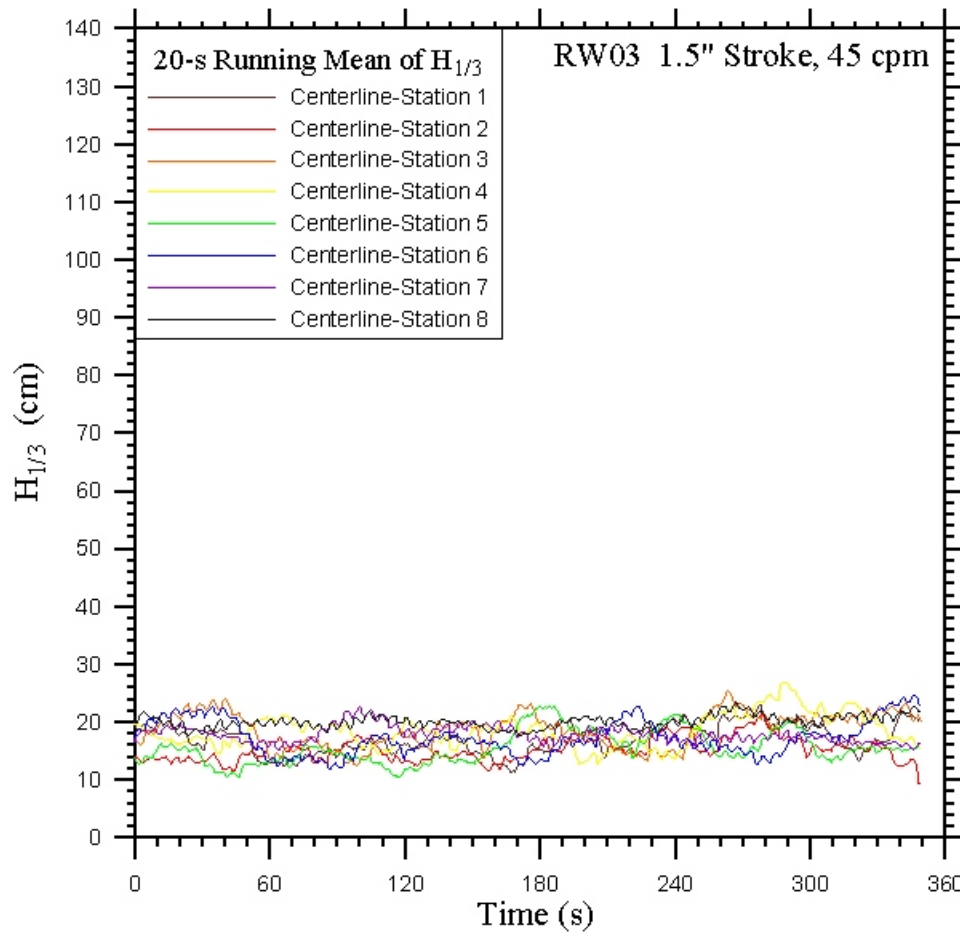


Figure 42: Significant wave height, $H_{1/3}$, calculated as a 20 s moving averaged along the centerline of the wave basin at the eight sampling stations plotted versus time. Paddle conditions for this run correspond to RW03, 1.5" stroke, 45 cpm speed.

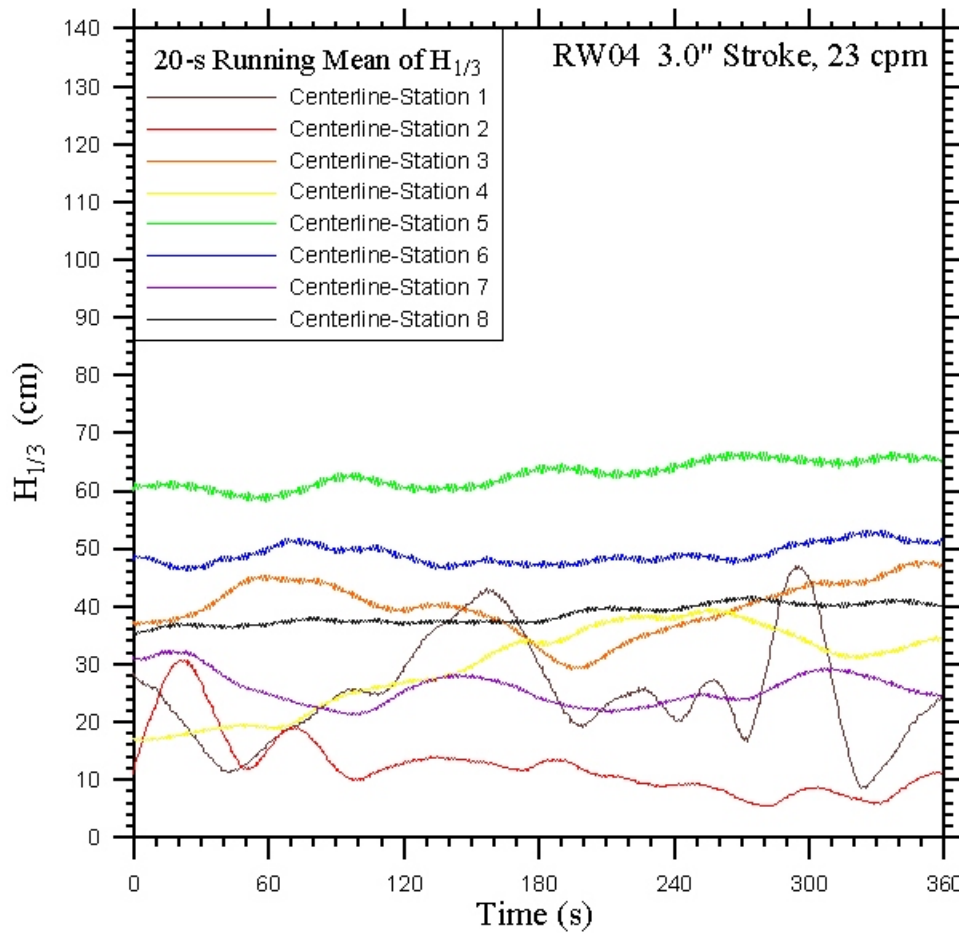


Figure 43: Significant wave height, $H_{1/3}$, calculated as a 20 s moving averaged along the centerline of the wave basin at the eight sampling stations plotted versus time. Paddle conditions for this run correspond to RW04, 3.0" stroke, 21 cpm speed.

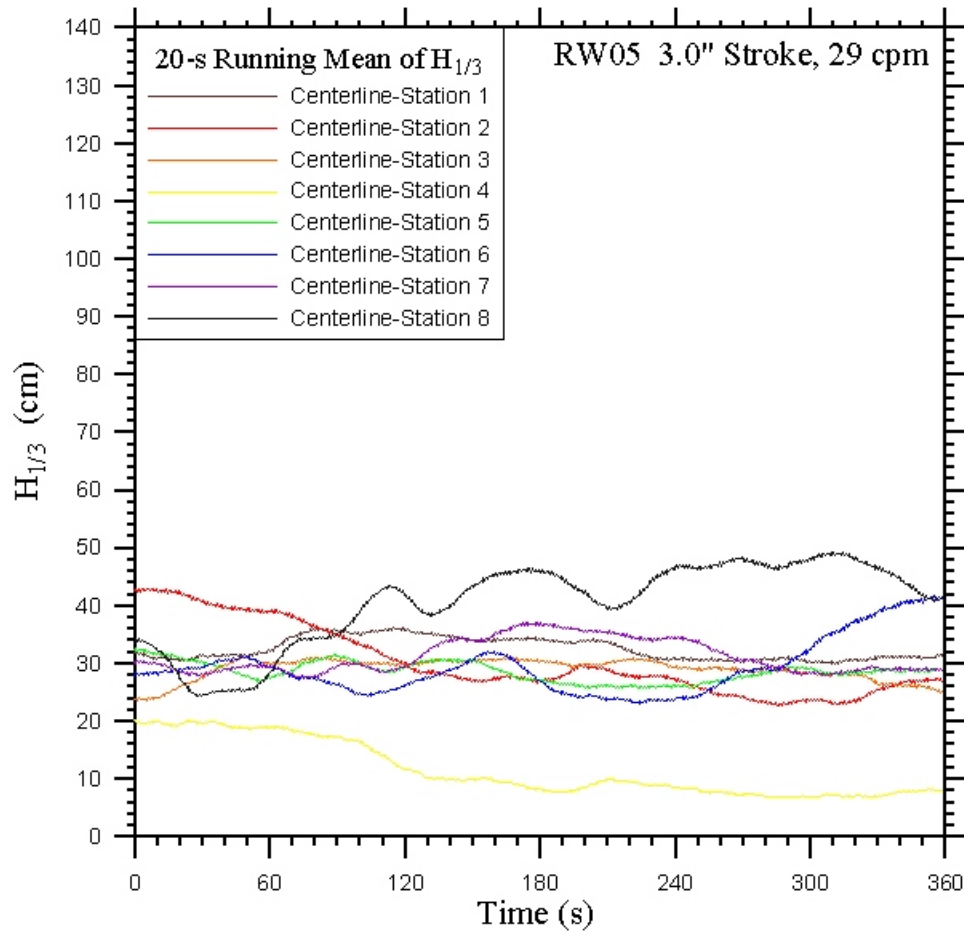


Figure 44: Significant wave height, $H_{1/3}$, calculated as a 20 s moving averaged along the centerline of the wave basin at the eight sampling stations plotted versus time. Paddle conditions for this run correspond to RW05, 3.0" stroke, 37 cpm speed.

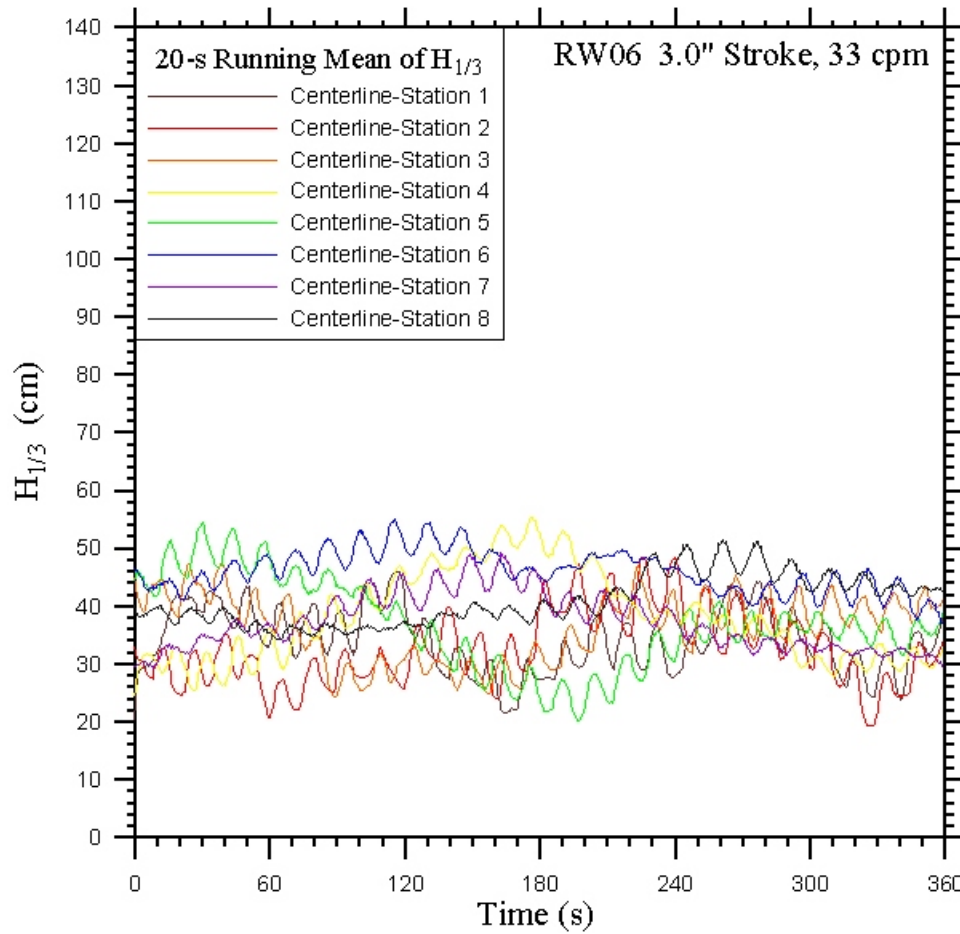


Figure 45: Significant wave height, $H_{1/3}$, calculated as a 20 s moving averaged along the centerline of the wave basin at the eight sampling stations plotted versus time. Paddle conditions for this run correspond to RW06, 3.0" stroke, 33 cpm speed.

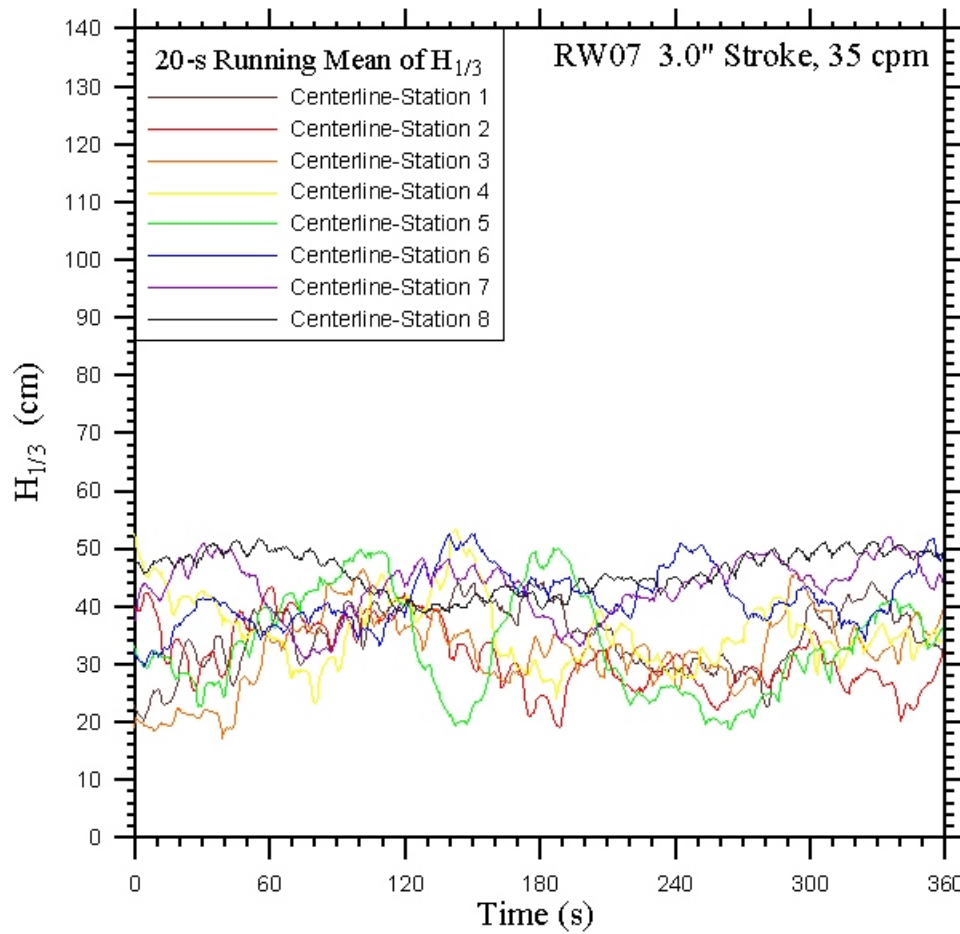


Figure 46: Significant wave height, $H_{1/3}$, calculated as a 20 s moving averaged along the centerline of the wave basin at the eight sampling stations plotted versus time. Paddle conditions for this run correspond to RW07, 3.0" stroke, 35 cpm speed.

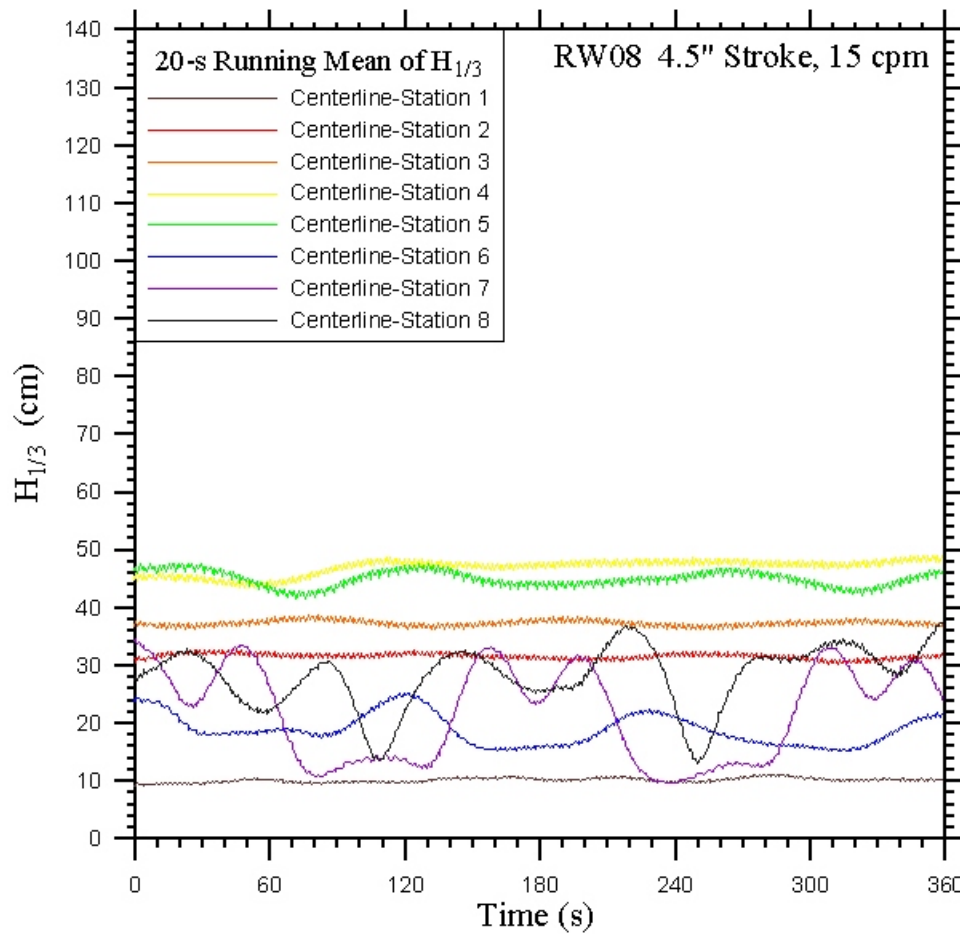


Figure 47: Significant wave height, $H_{1/3}$, calculated as a 20 s moving averaged along the centerline of the wave basin at the eight sampling stations plotted versus time. Paddle conditions for this run correspond to RW08, 4.5" stroke, 15 cpm speed.

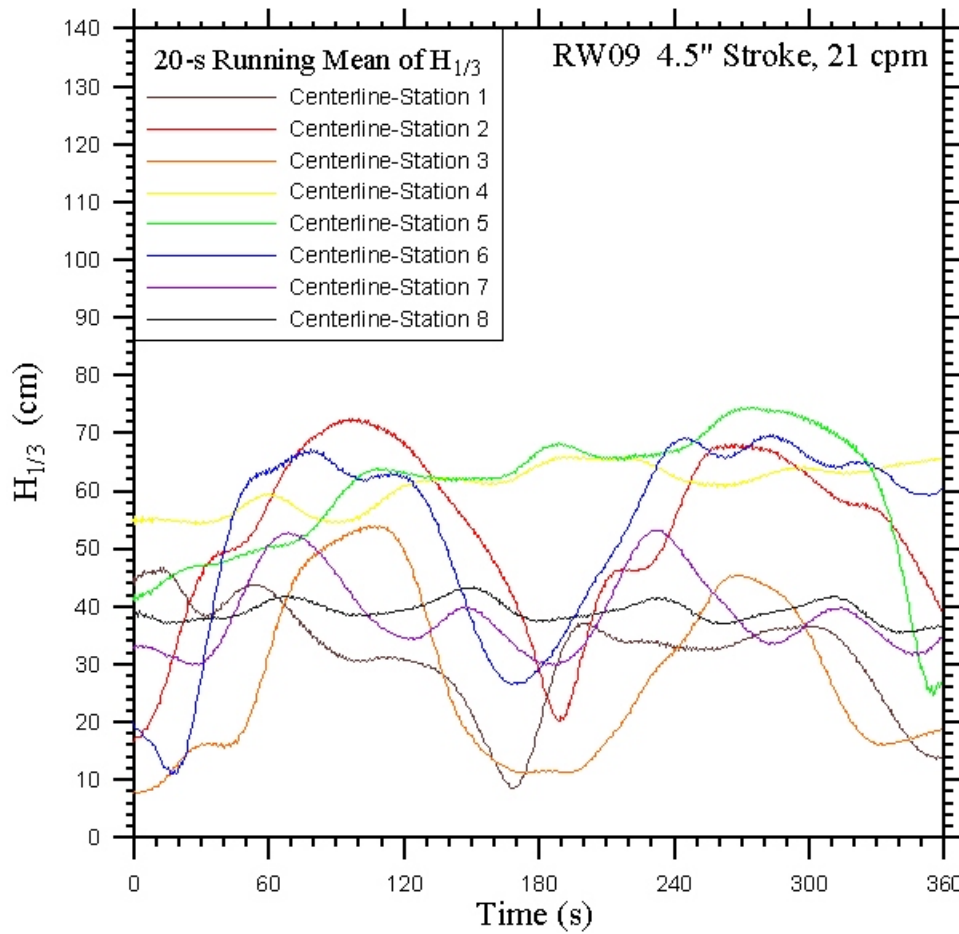


Figure 48: Significant wave height, $H_{1/3}$, calculated as a 20 s moving averaged along the centerline of the wave basin at the eight sampling stations plotted versus time. Paddle conditions for this run correspond to RW09, 4.5" stroke, 21 cpm speed.

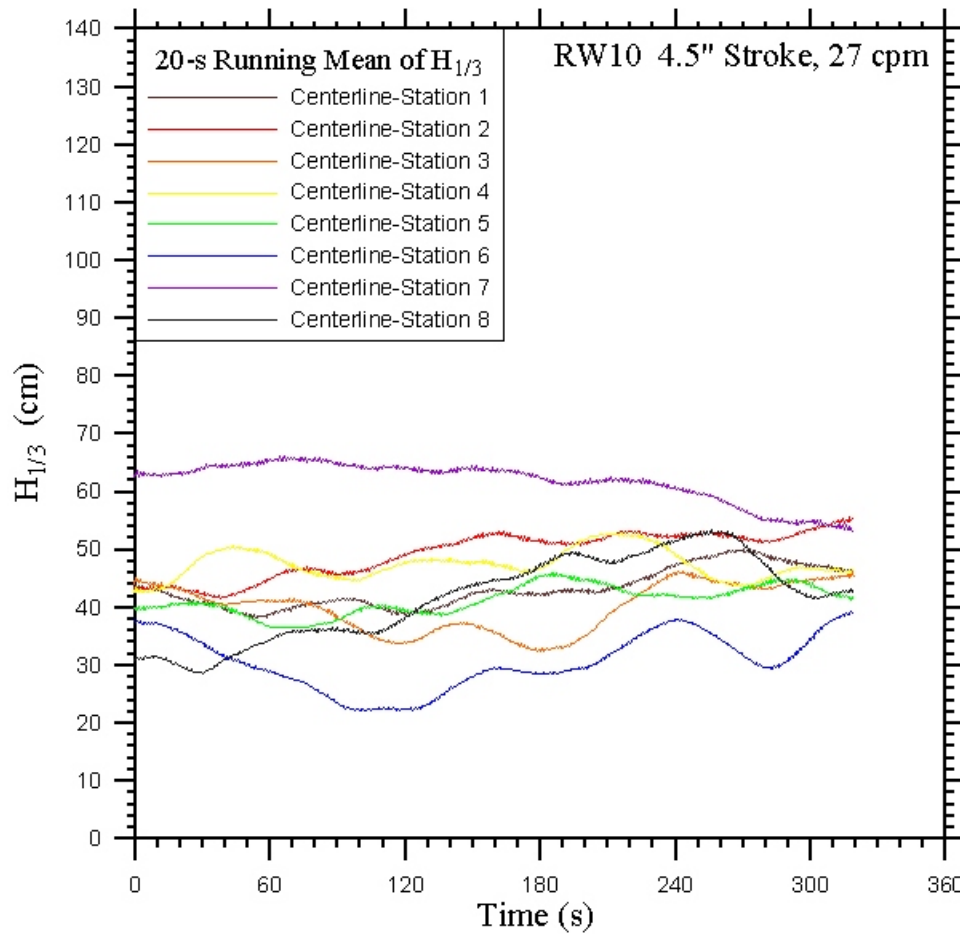


Figure 49: Significant wave height, $H_{1/3}$, calculated as a 20 s moving averaged along the centerline of the wave basin at the eight sampling stations plotted versus time. Paddle conditions for this run correspond to RW10, 4.5" stroke, 27 cpm speed.

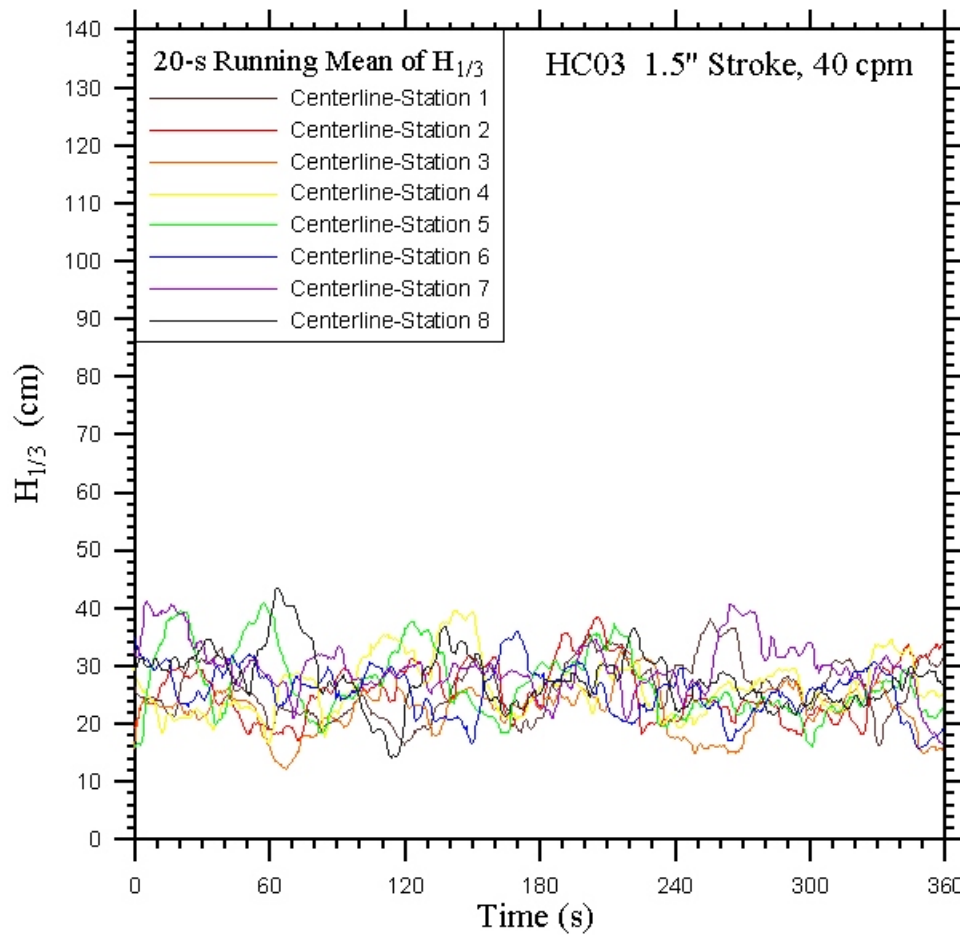


Figure 50: Significant wave height, $H_{1/3}$, calculated as a 20 s moving averaged along the centerline of the wave basin at the eight sampling stations plotted versus time. Paddle conditions for this run correspond to HC03, 1.5" stroke, 40 cpm speed.

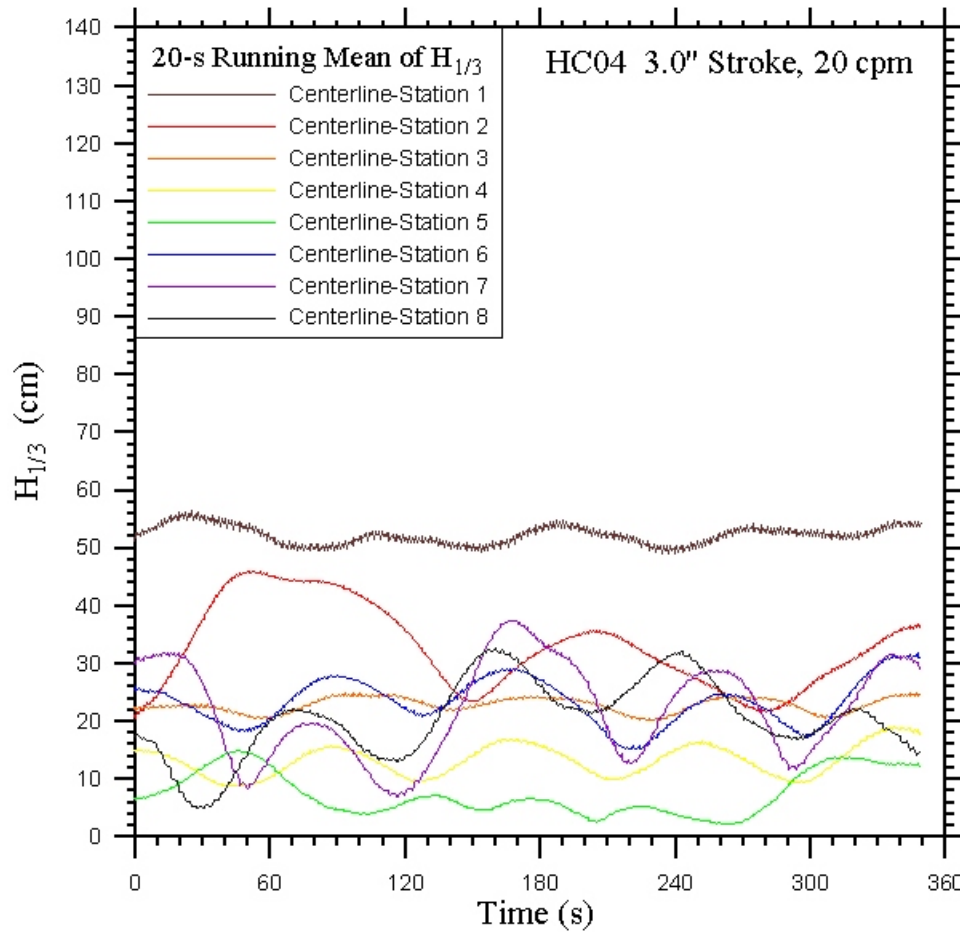


Figure 51: Significant wave height, $H_{1/3}$, calculated as a 20 s moving averaged along the centerline of the wave basin at the eight sampling stations plotted versus time. Paddle conditions for this run correspond to HC04, 3.0" stroke, 20 cpm speed.

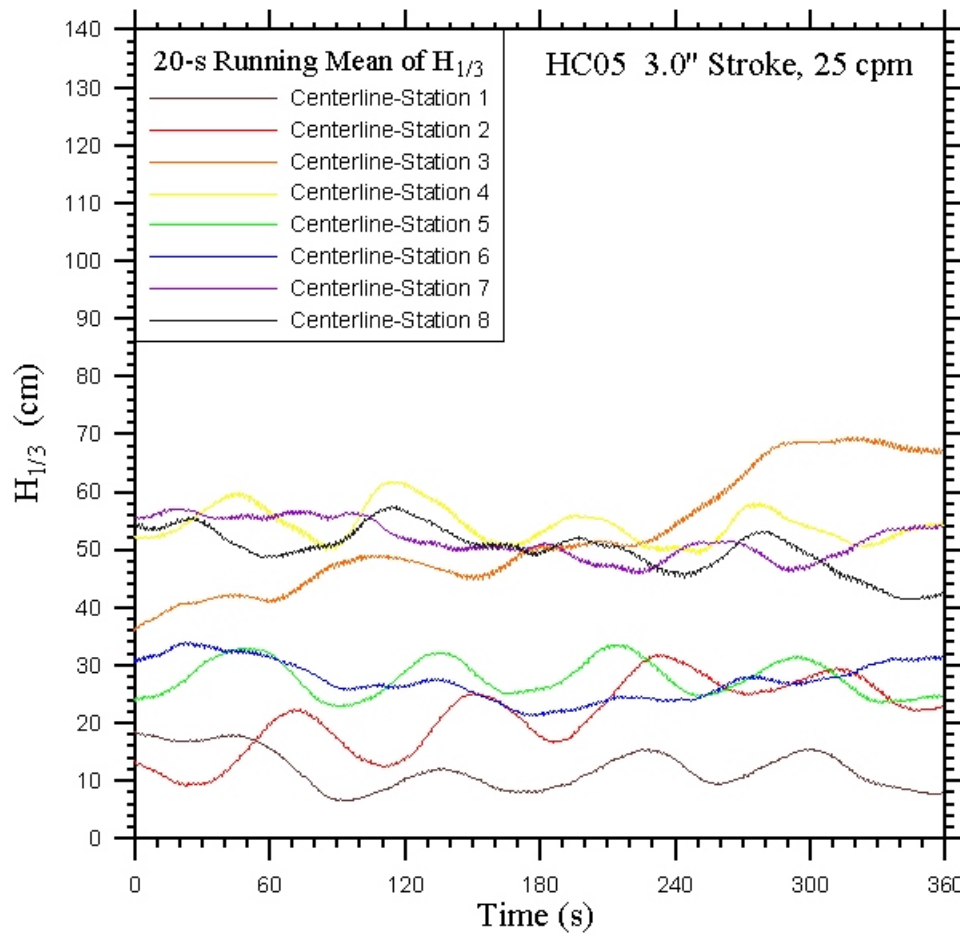


Figure 52: Significant wave height, $H_{1/3}$, calculated as a 20 s moving averaged along the centerline of the wave basin at the eight sampling stations plotted versus time. Paddle conditions for this run correspond to HC05, 3.0" stroke, 25 cpm speed.

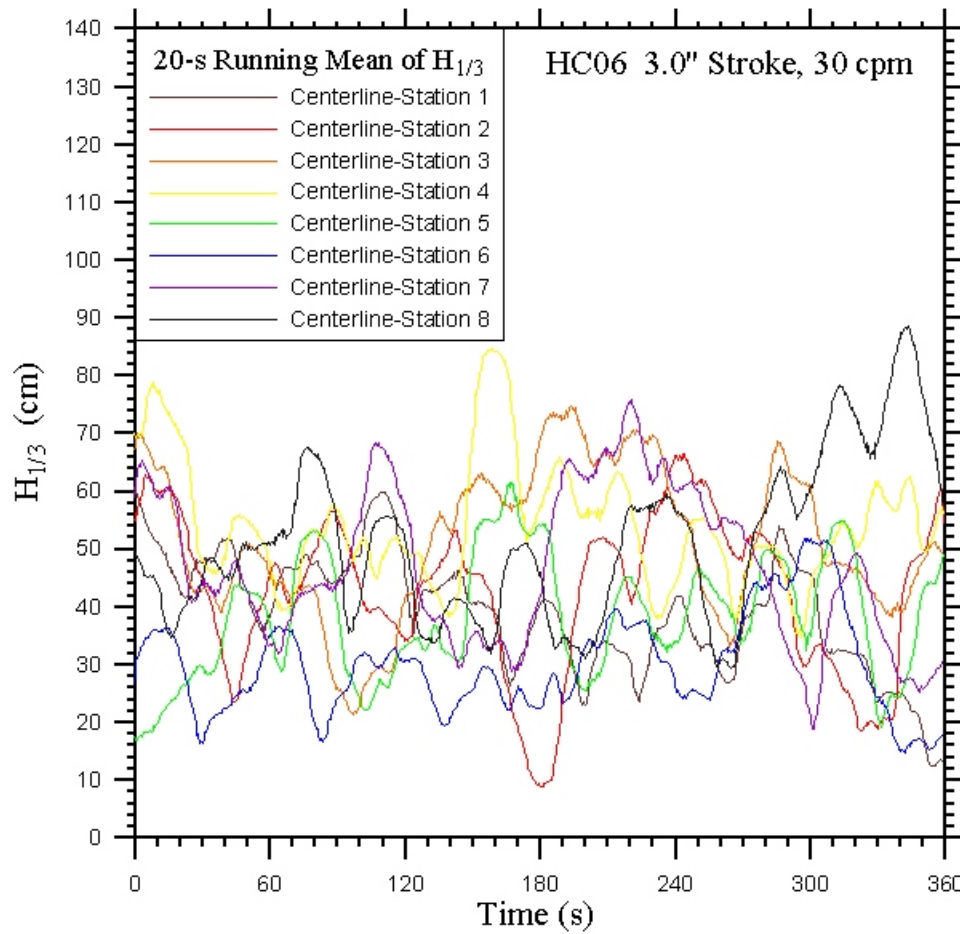


Figure 53: Significant wave height, $H_{1/3}$, calculated as a 20 s moving averaged along the centerline of the wave basin at the eight sampling stations plotted versus time. Paddle conditions for this run correspond to HC06, 3.0" stroke, 30 cpm speed.

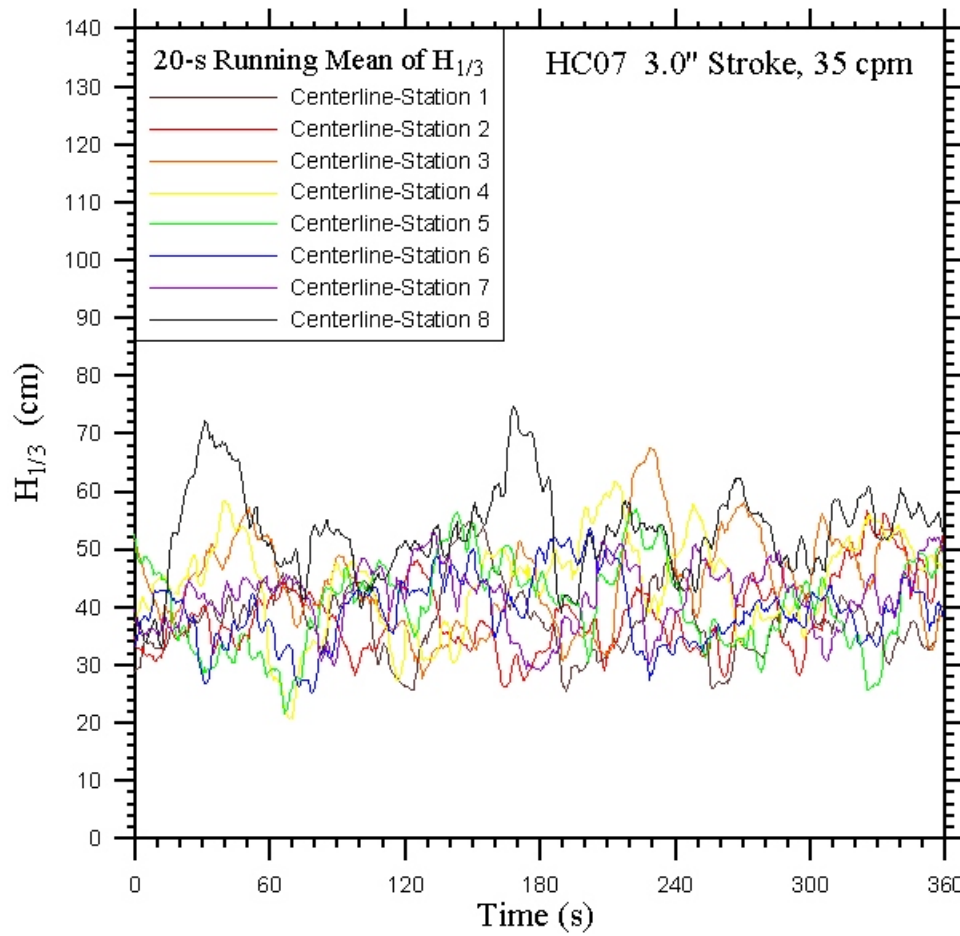


Figure 54: Significant wave height, $H_{1/3}$, calculated as a 20 s moving averaged along the centerline of the wave basin at the eight sampling stations plotted versus time. Paddle conditions for this run correspond to HC07, 4.5" stroke, 35 cpm speed.

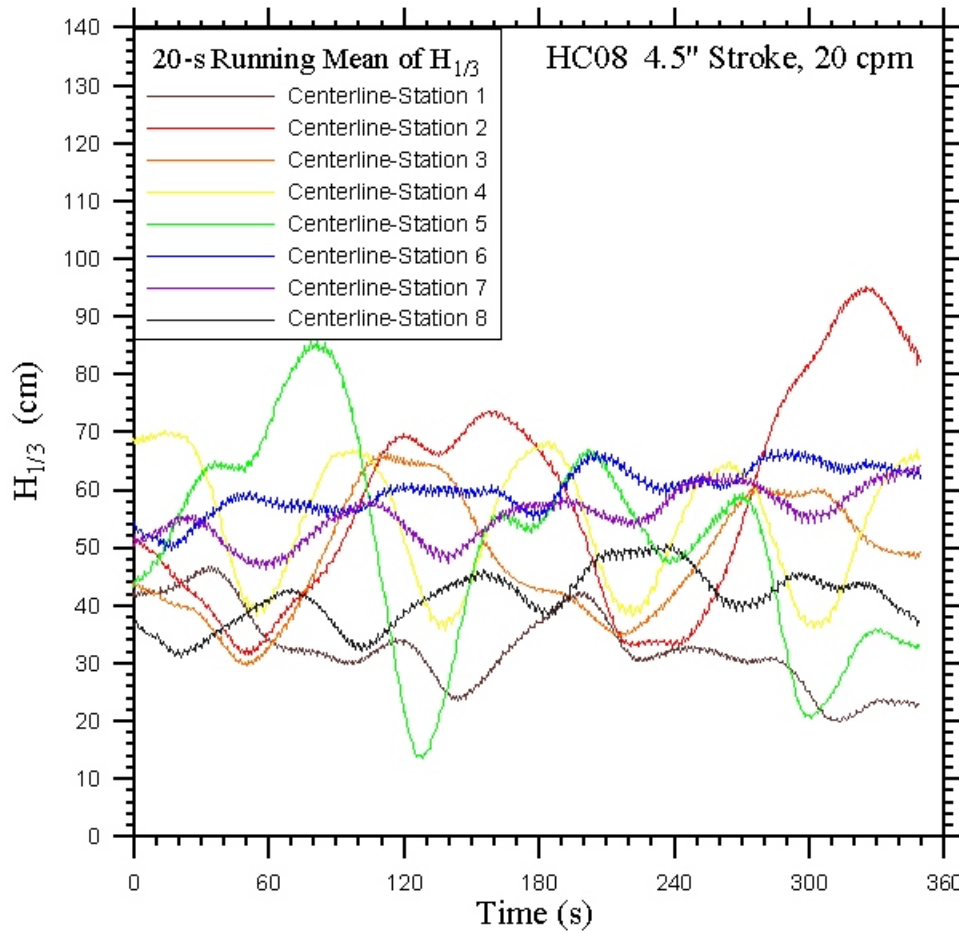


Figure 55: Significant wave height, $H_{1/3}$, calculated as a 20 s moving averaged along the centerline of the wave basin at the eight sampling stations plotted versus time. Paddle conditions for this run correspond to HC08, 4.5" stroke, 20 cpm speed.

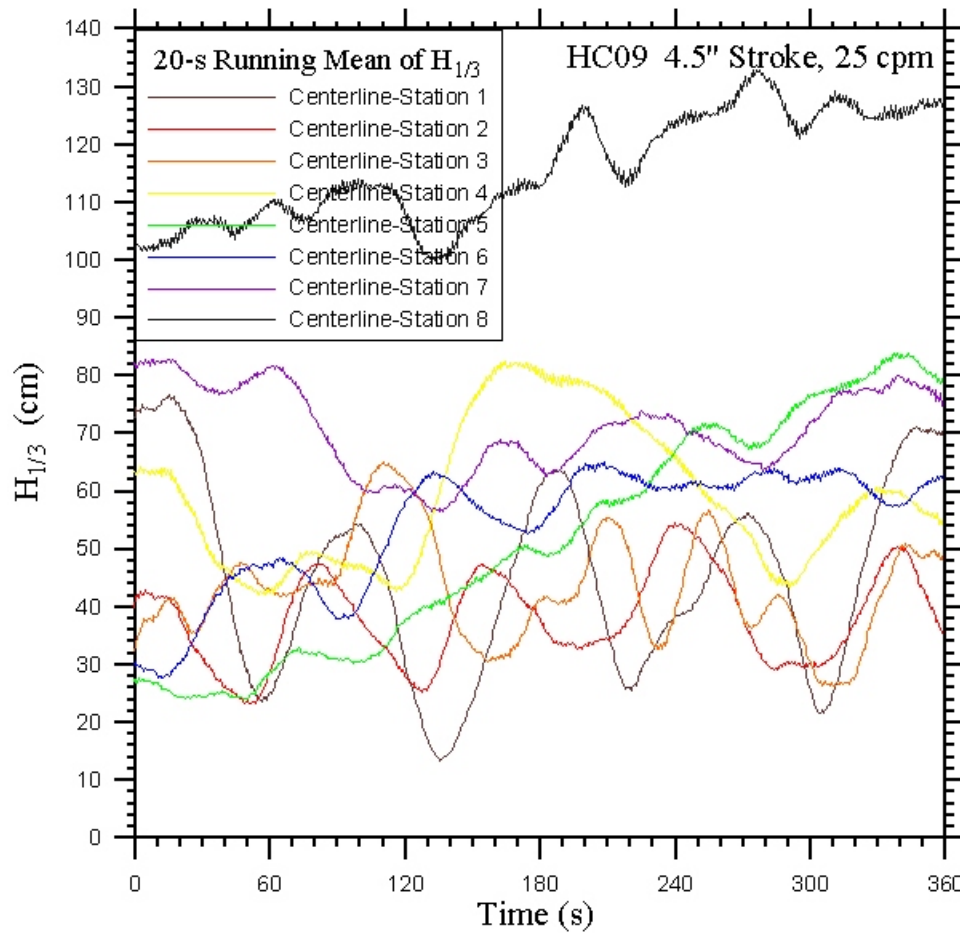


Figure 56: Significant wave height, $H_{1/3}$, calculated as a 20 s moving averaged along the centerline of the wave basin at the eight sampling stations plotted versus time. Paddle conditions for this run correspond to HC09, 4.5" stroke, 25 cpm speed.

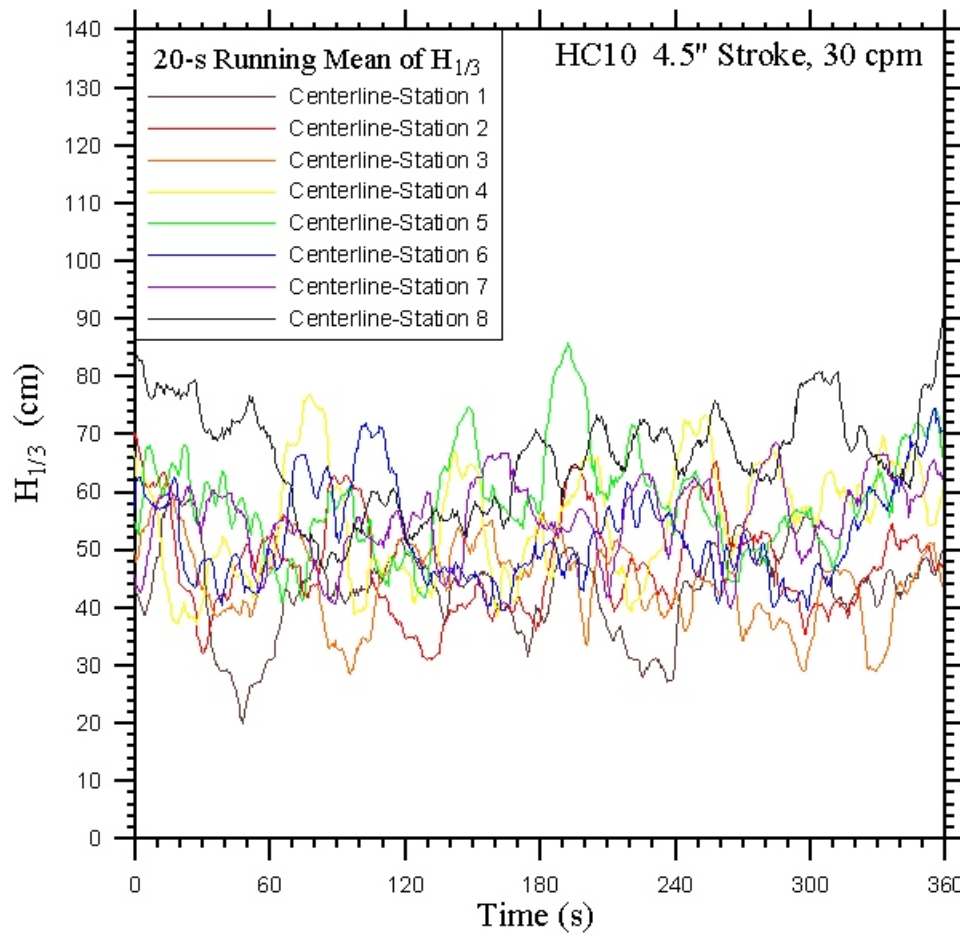


Figure 57: Significant wave height, $H_{1/3}$, calculated as a 20 s moving averaged along the centerline of the wave basin at the eight sampling stations plotted versus time. Paddle conditions for this run correspond to HC10, 4.5" stroke, 30 cpm speed.

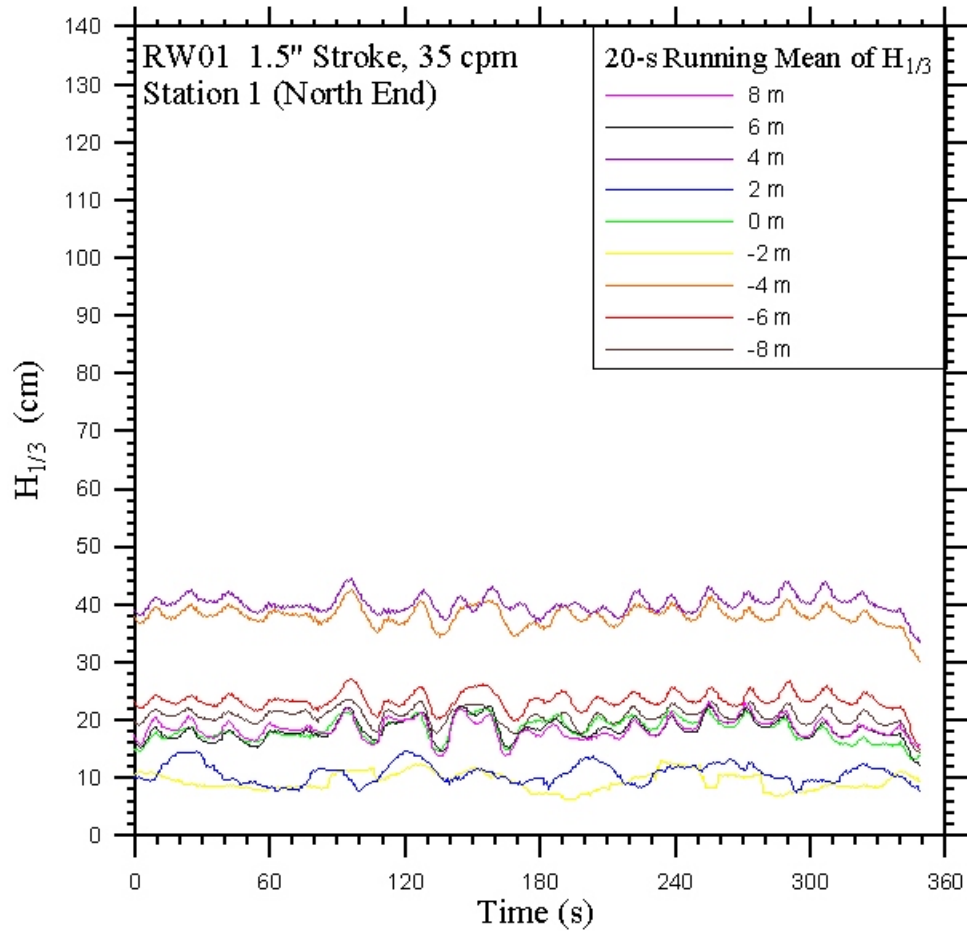


Figure 58: Time series of 20 s moving averaged of significant wave height, $H_{1/3}$, as a function of time for all nine wave probes in the main array at station 1, north end of tank. Paddle conditions for this run correspond to RW01, 1.5" stroke, 35 cpm speed.

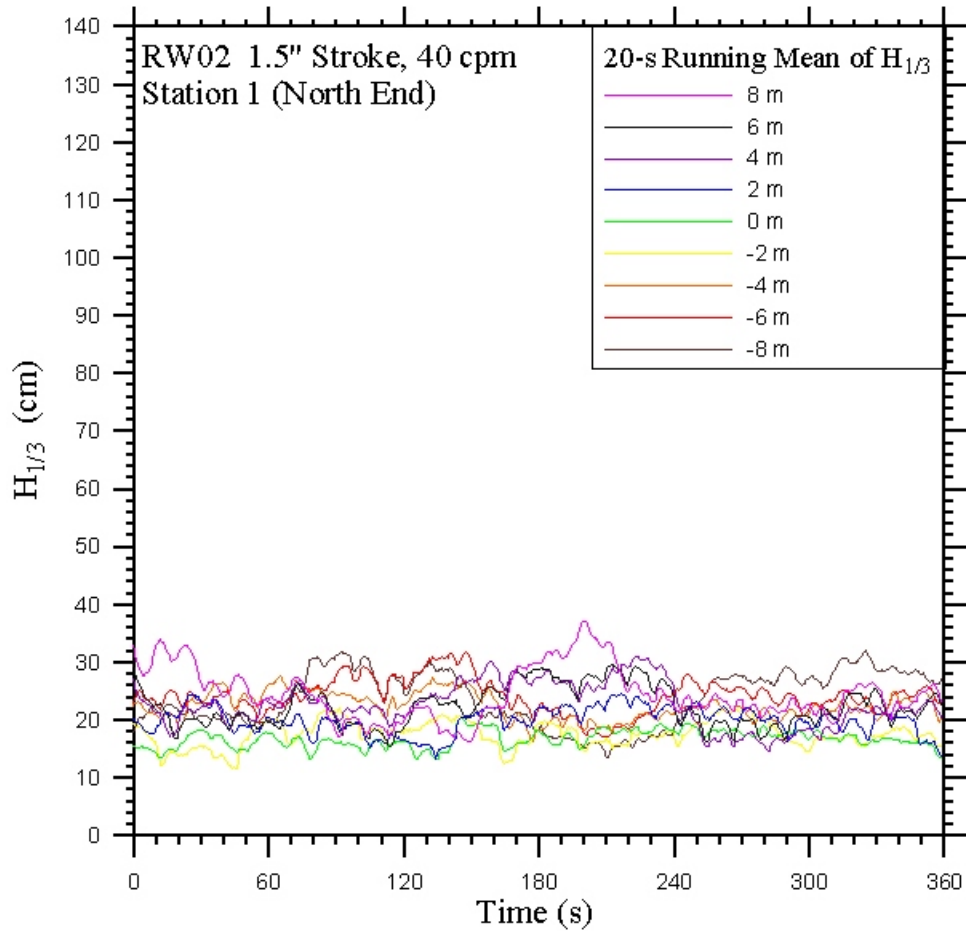


Figure 59: Time series of 20 s moving averaged of significant wave height, $H_{1/3}$, as a function of time for all nine wave probes in the main array at station 1, north end of tank. Paddle conditions for this run correspond to RW02, 1.5" stroke, 40 cpm speed.

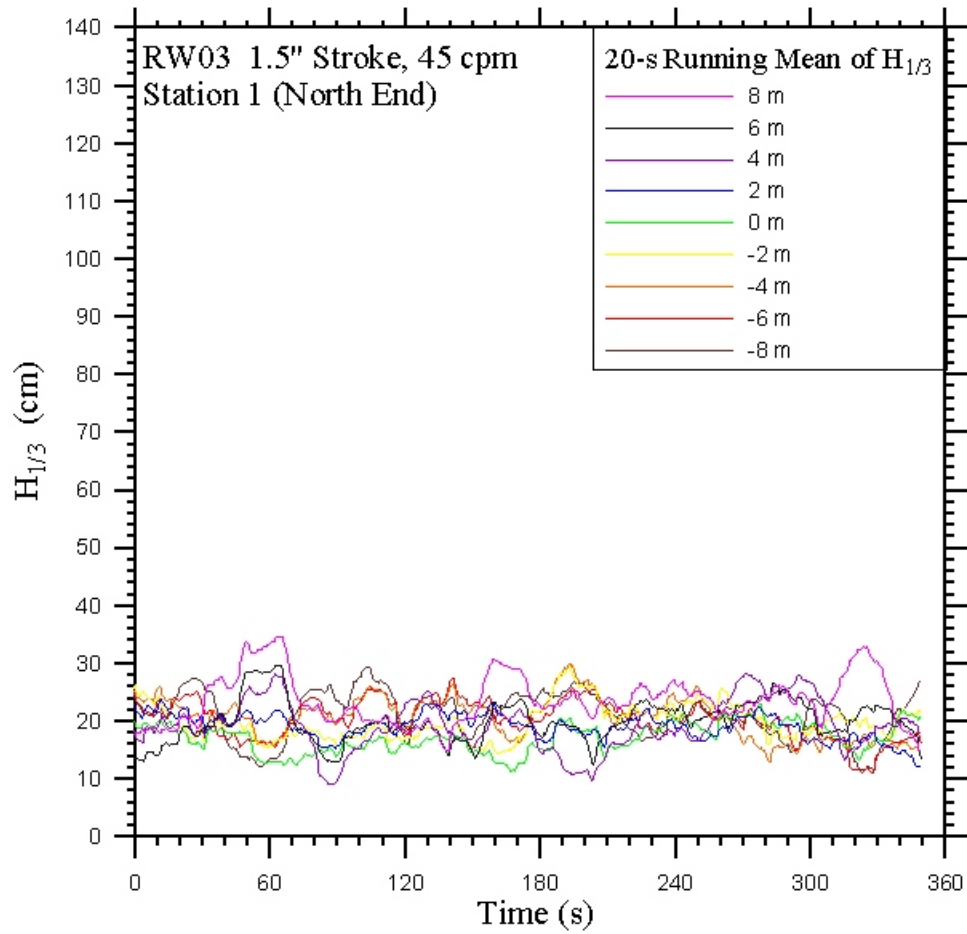


Figure 60: Time series of 20 s moving averaged of significant wave height, $H_{1/3}$, as a function of time for all nine wave probes in the main array at station 1, north end of tank. Paddle conditions for this run correspond to RW03, 1.5" stroke, 45 cpm speed.

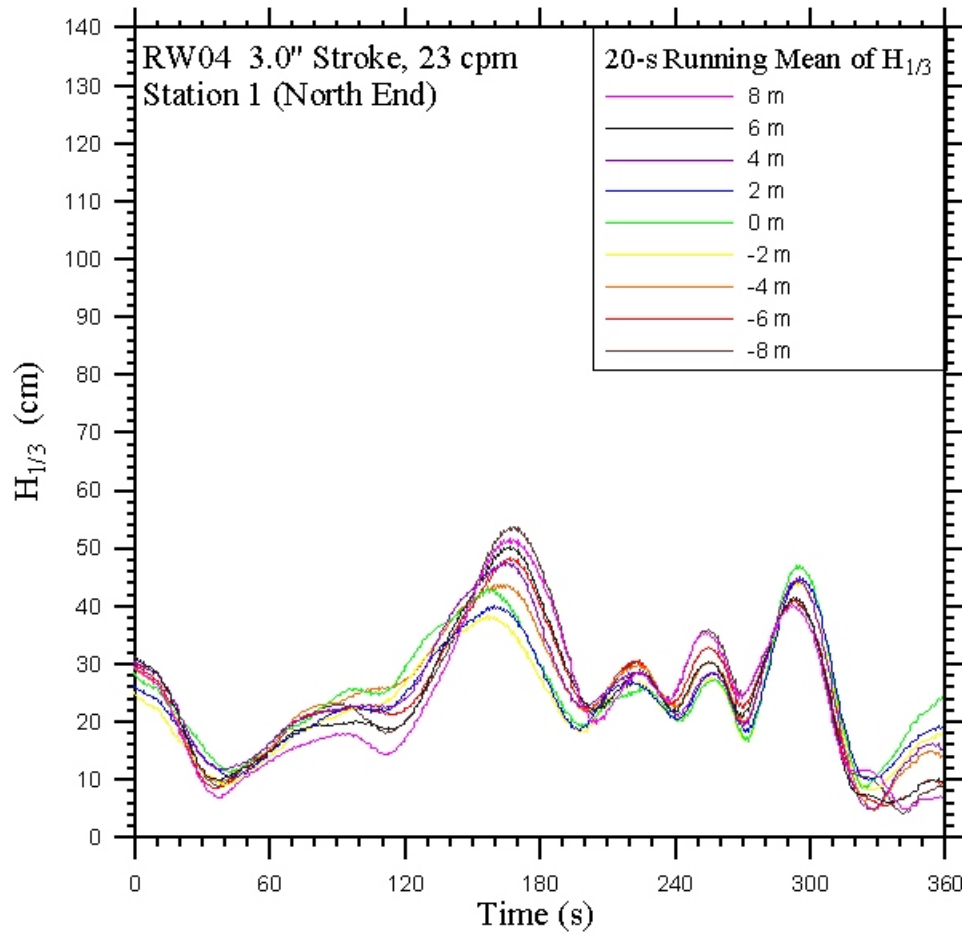


Figure 61: Time series of 20 s moving averaged of significant wave height, $H_{1/3}$, as a function of time for all nine wave probes in the main array at station 1, north end of tank. Paddle conditions for this run correspond to RW04, 3.0" stroke, 21 cpm speed.

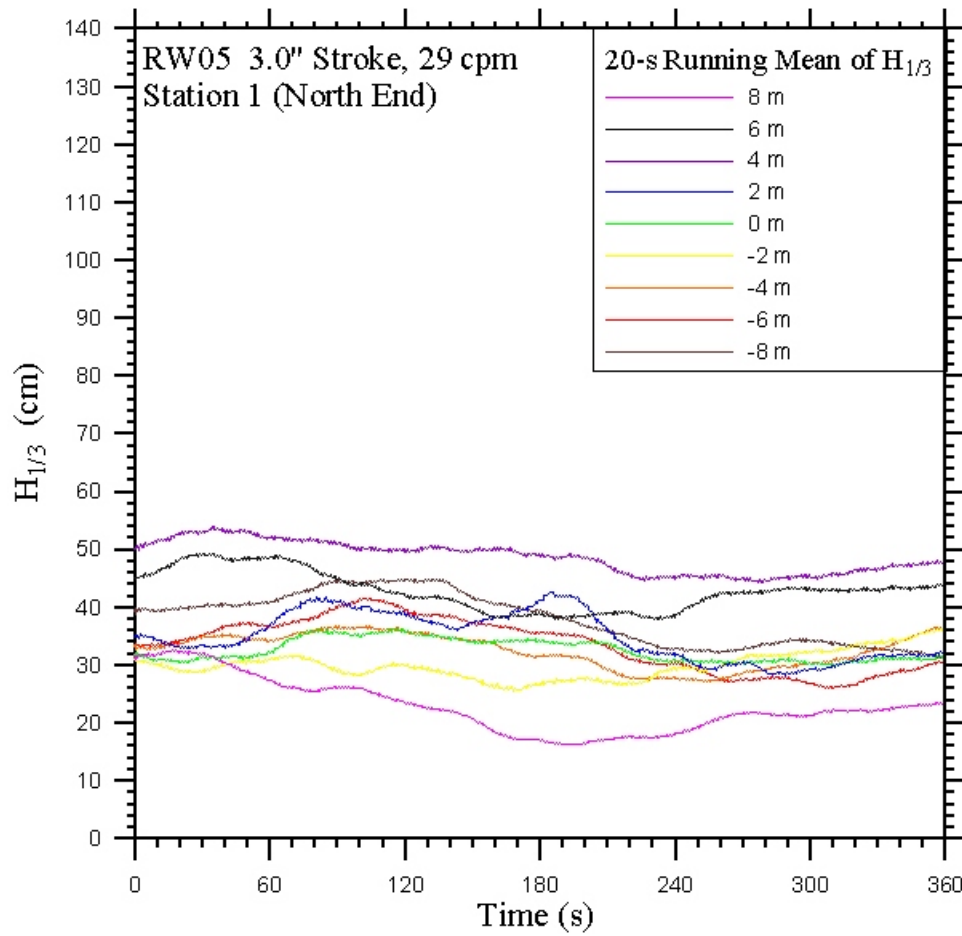


Figure 62: Time series of 20 s moving averaged of significant wave height, $H_{1/3}$, as a function of time for all nine wave probes in the main array at station 1, north end of tank. Paddle conditions for this run correspond to RW05, 3.0" stroke, 37 cpm speed.

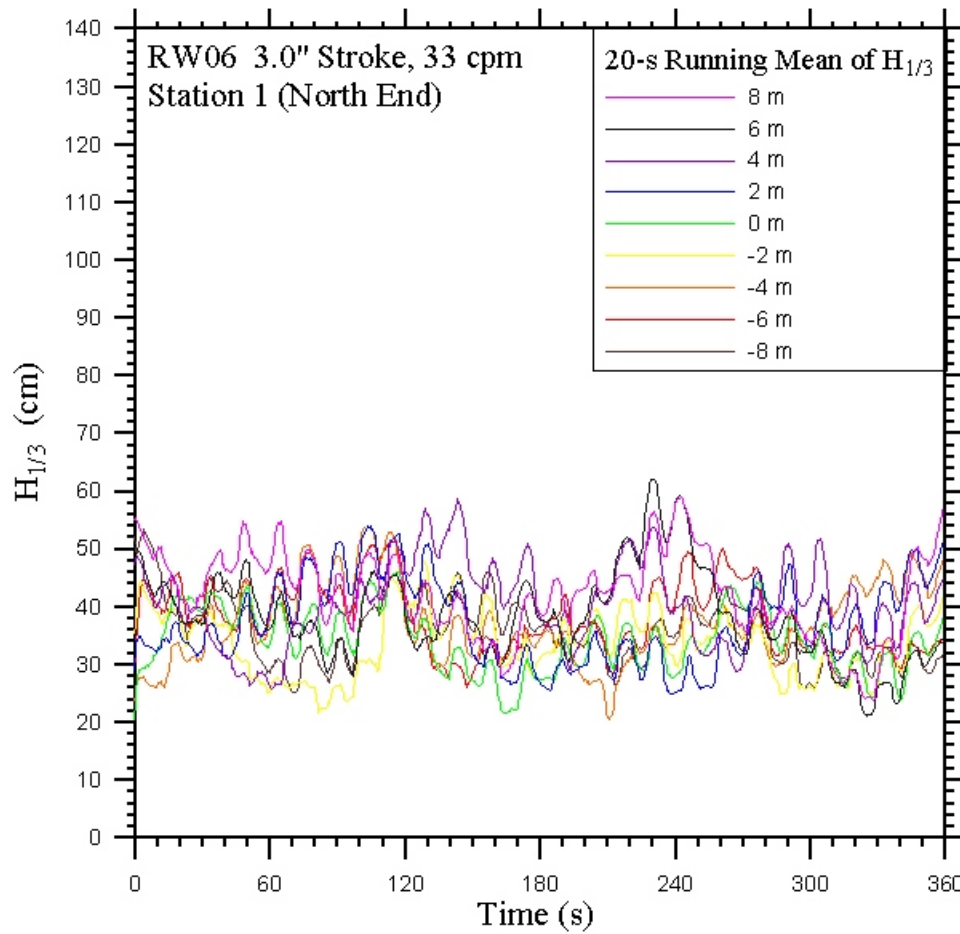


Figure 63: Time series of 20 s moving averaged of significant wave height, $H_{1/3}$, as a function of time for all nine wave probes in the main array at station 1, north end of tank. Paddle conditions for this run correspond to RW06, 3.0" stroke, 33 cpm speed.

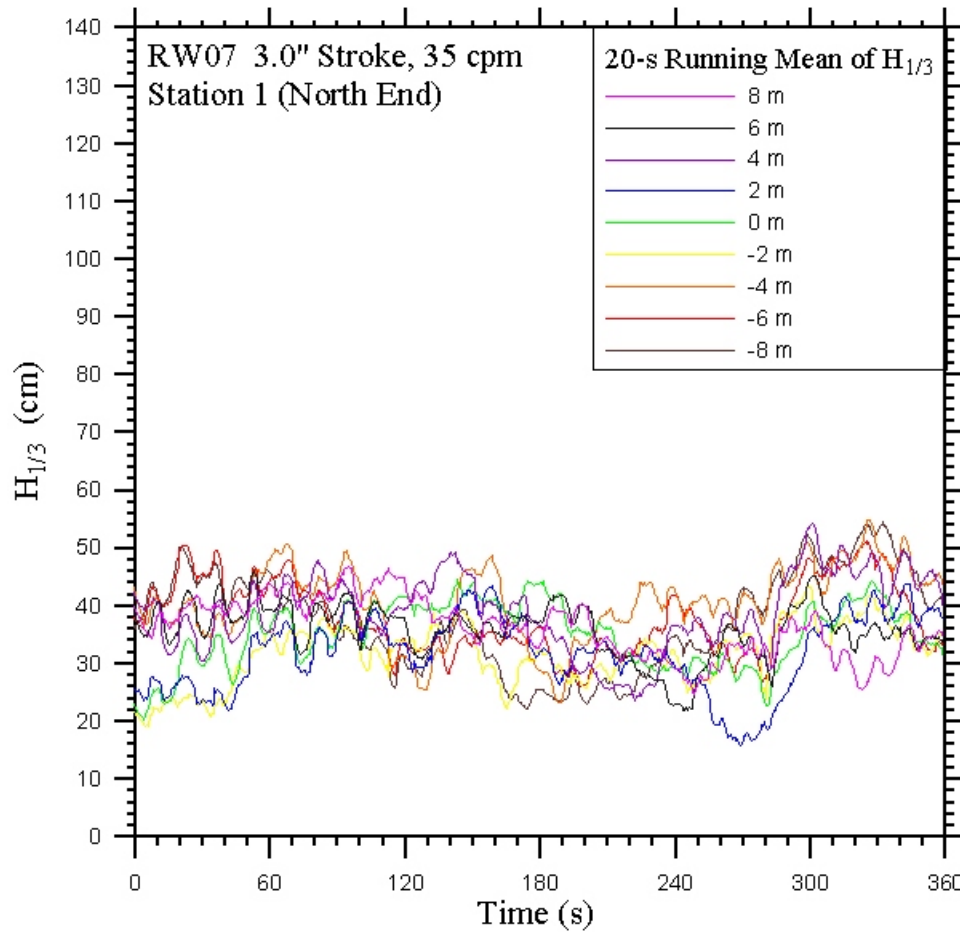


Figure 64: Time series of 20 s moving averaged of significant wave height, $H_{1/3}$, as a function of time for all nine wave probes in the main array at station 1, north end of tank. Paddle conditions for this run correspond to RW07, 3.0" stroke, 35 cpm speed.

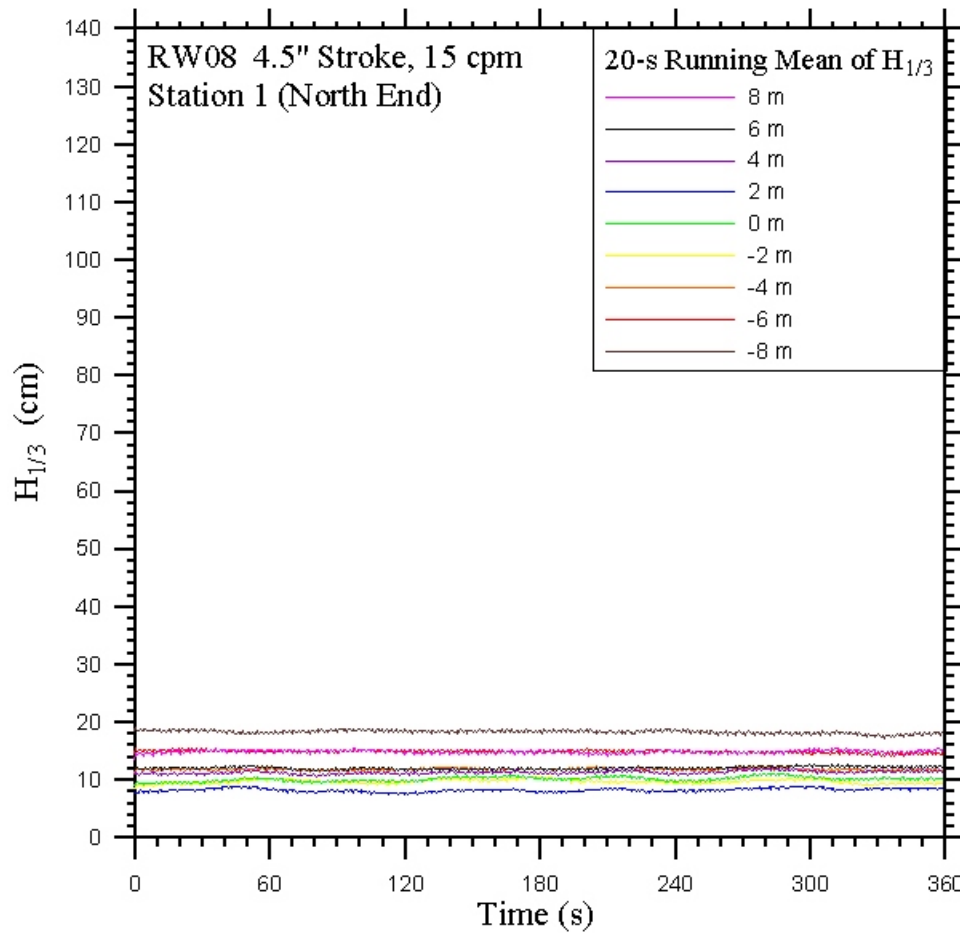


Figure 65: Time series of 20 s moving averaged of significant wave height, $H_{1/3}$, as a function of time for all nine wave probes in the main array at station 1, north end of tank. Paddle conditions for this run correspond to RW08, 4.5" stroke, 15 cpm speed.

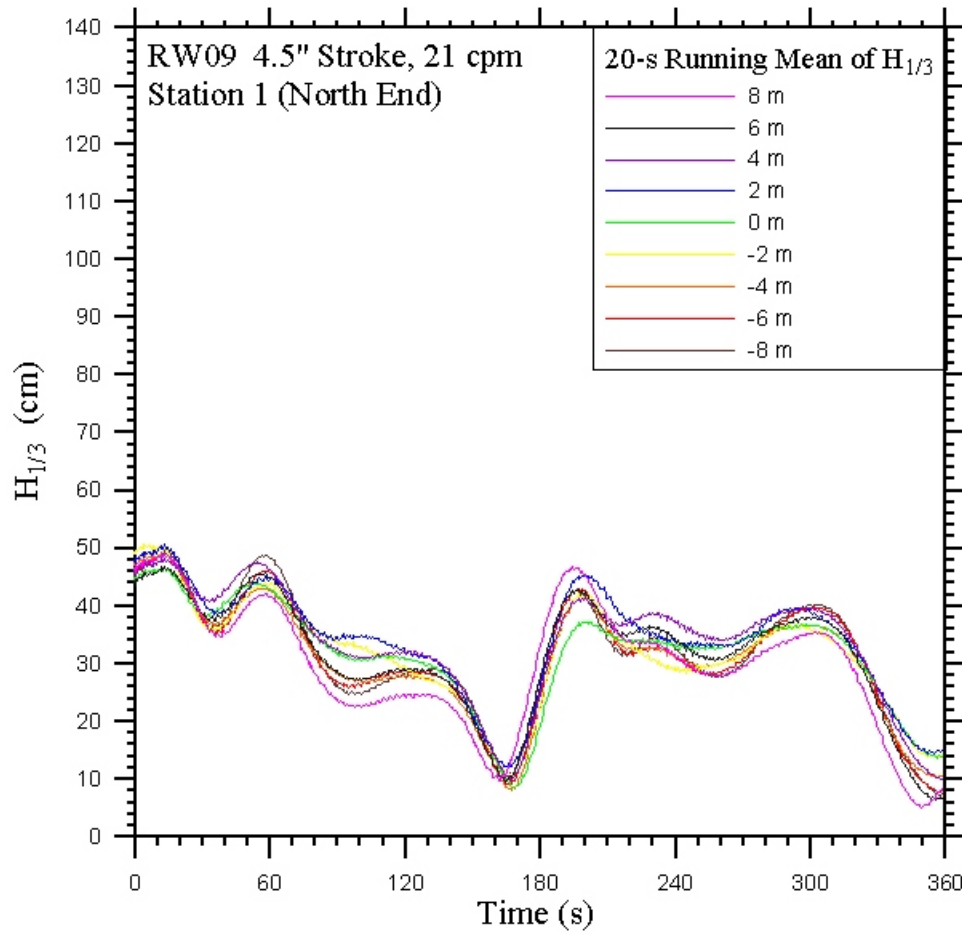


Figure 66: Time series of 20 s moving averaged of significant wave height, $H_{1/3}$, as a function of time for all nine wave probes in the main array at station 1, north end of tank. Paddle conditions for this run correspond to RW09, 4.5" stroke, 21 cpm speed.

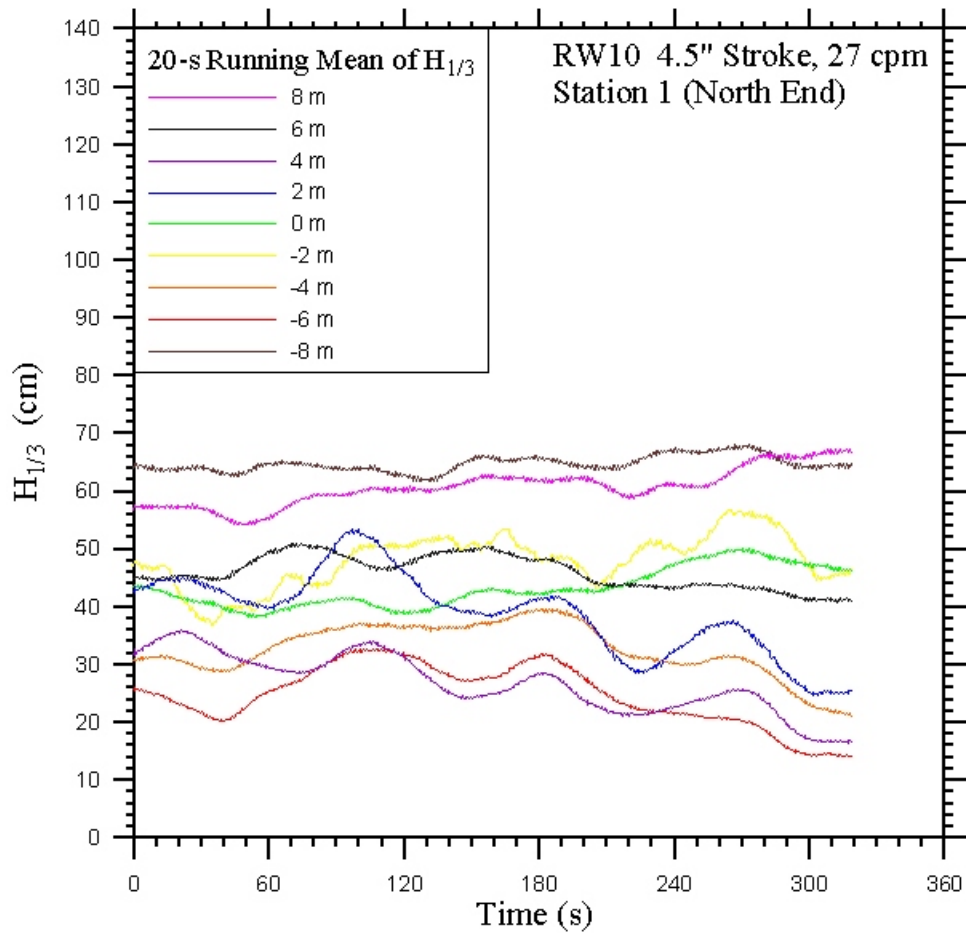


Figure 67: Time series of 20 s moving averaged of significant wave height, $H_{1/3}$, as a function of time for all nine wave probes in the main array at station 1, north end of tank. Paddle conditions for this run correspond to RW10, 4.5" stroke, 27 cpm speed.

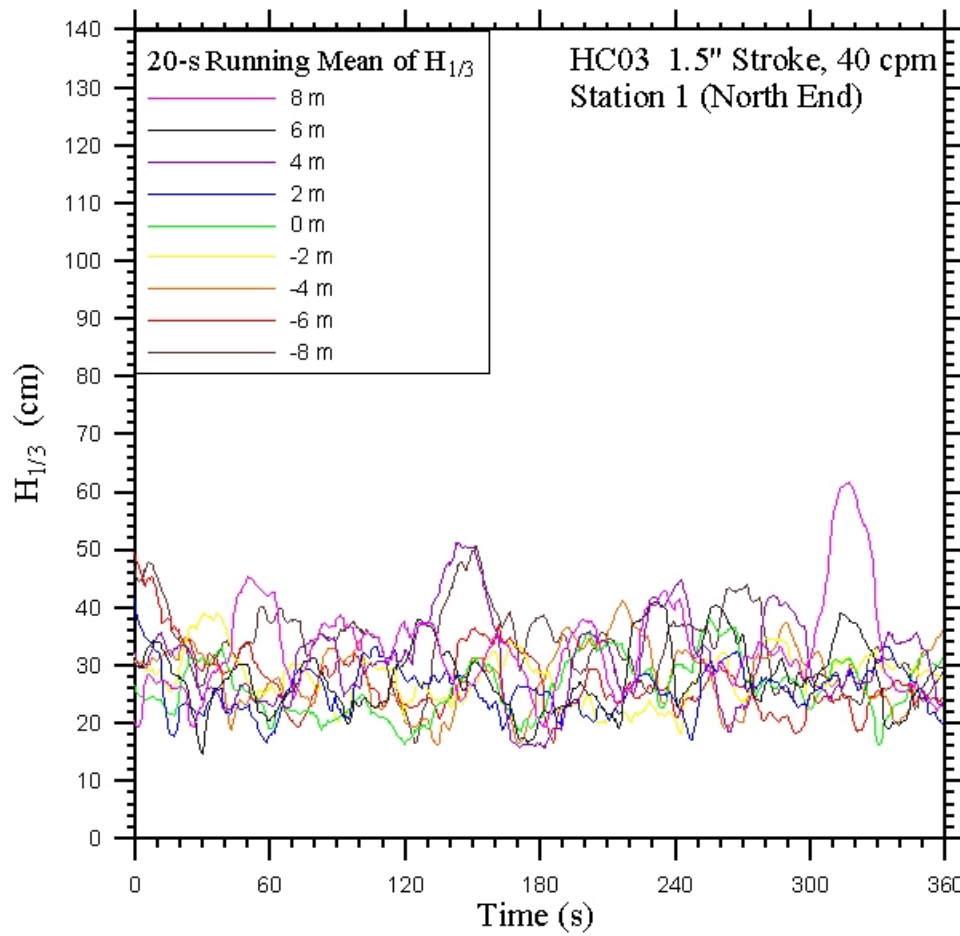


Figure 68: Time series of 20 s moving averaged of significant wave height, $H_{1/3}$, as a function of time for all nine wave probes in the main array at station 1, north end of tank. Paddle conditions for this run correspond to HC03, 1.5" stroke, 40 cpm speed.

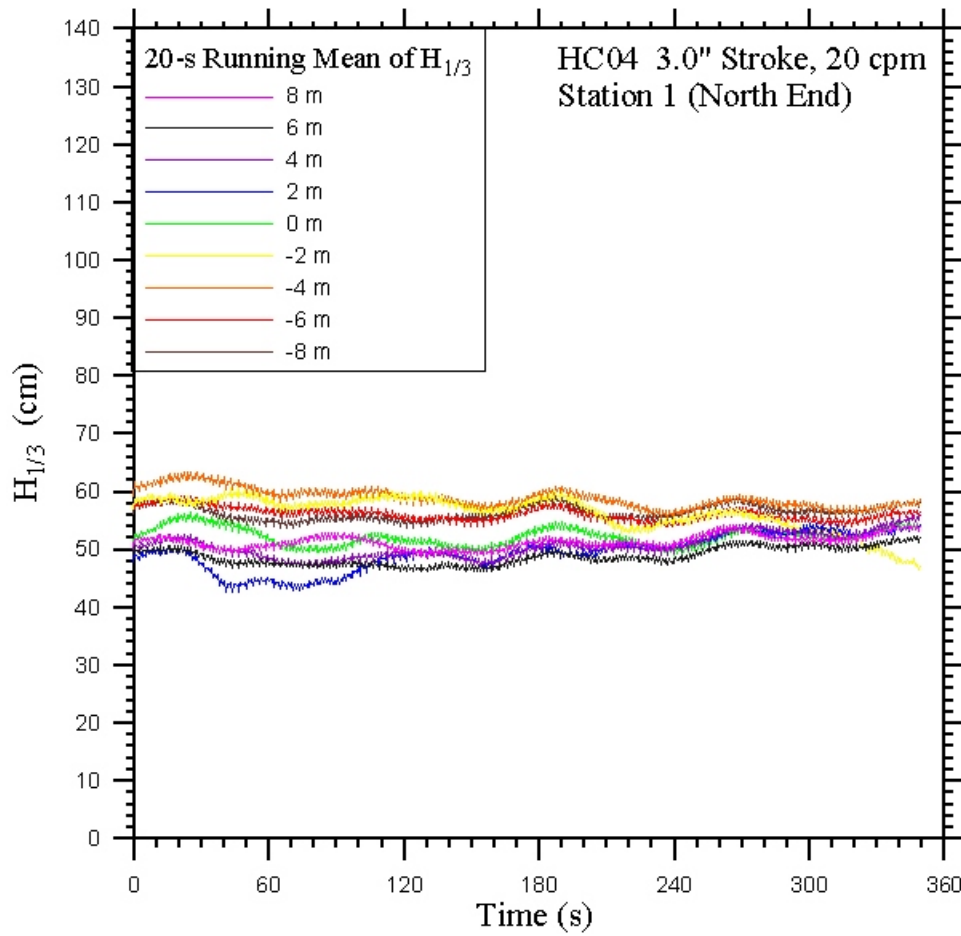


Figure 69: Time series of 20 s moving averaged of significant wave height, $H_{1/3}$, as a function of time for all nine wave probes in the main array at station 1, north end of tank. Paddle conditions for this run correspond to HC04, 3.0" stroke, 20 cpm speed.

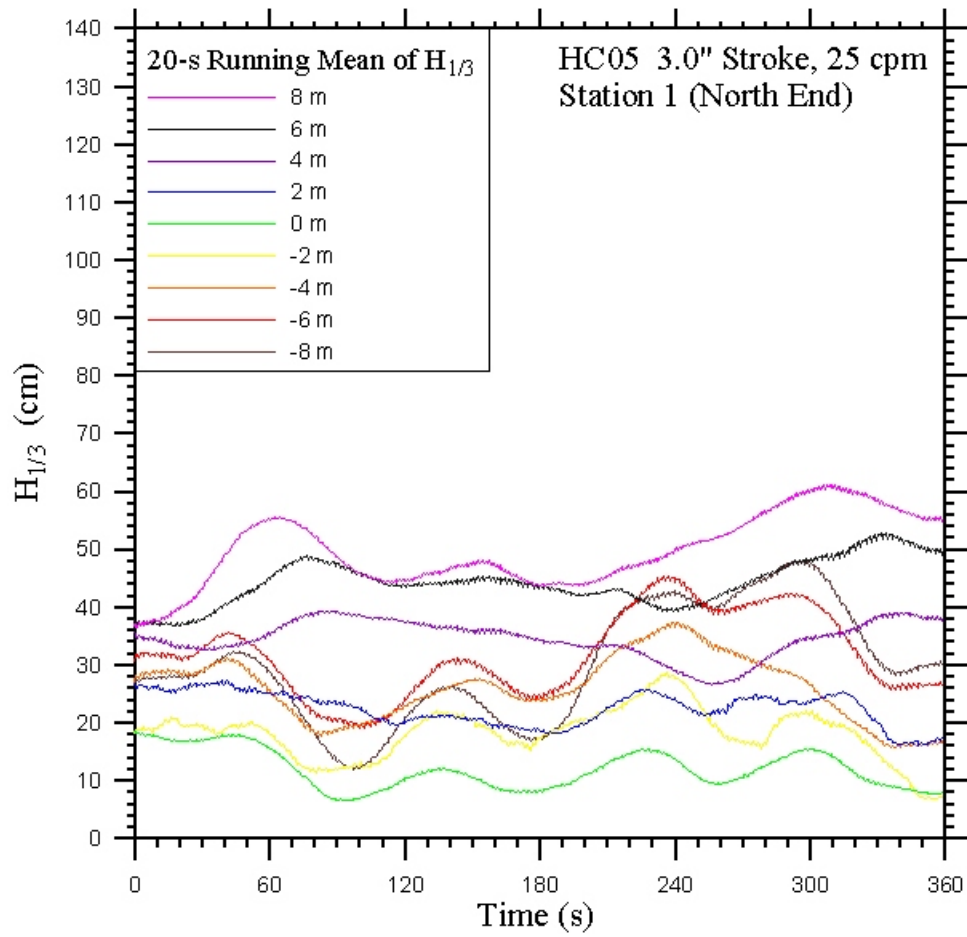


Figure 70: Time series of 20 s moving averaged of significant wave height, $H_{1/3}$, as a function of time for all nine wave probes in the main array at station 1, north end of tank. Paddle conditions for this run correspond to HC05, 3.0" stroke, 25 cpm speed.

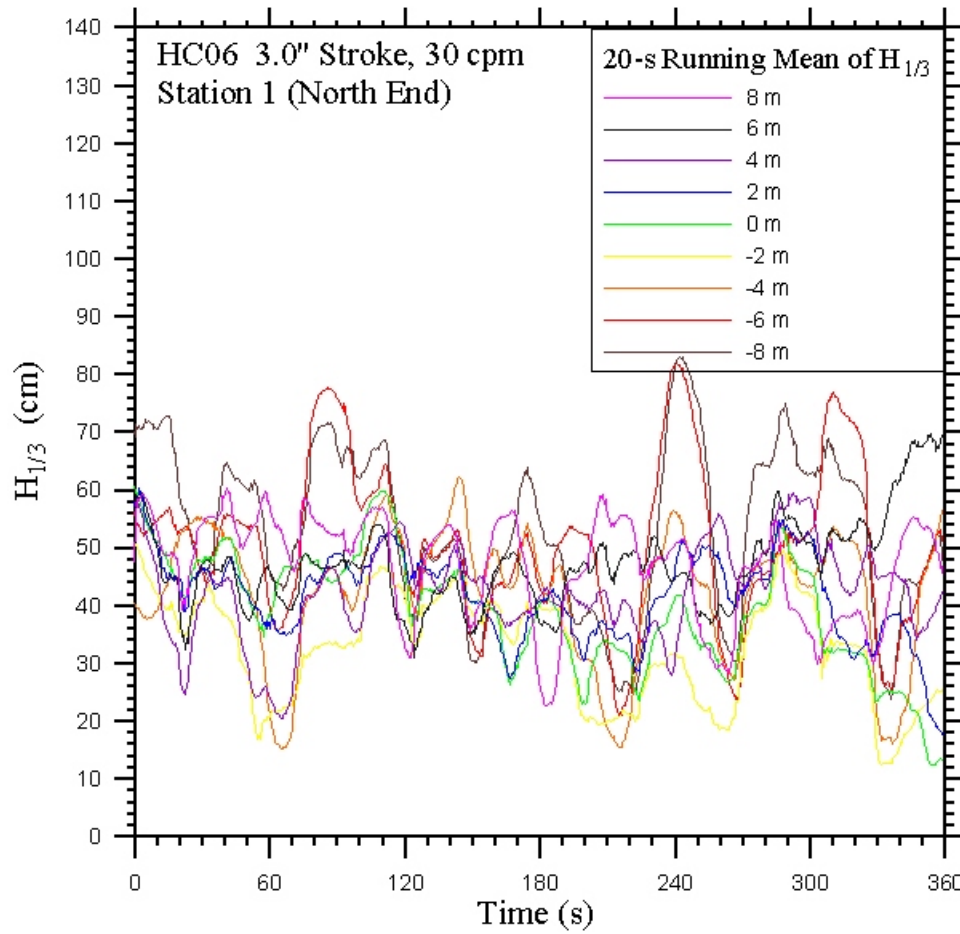


Figure 71: Time series of 20 s moving averaged of significant wave height, $H_{1/3}$, as a function of time for all nine wave probes in the main array at station 1, north end of tank. Paddle conditions for this run correspond to HC06, 3.0" stroke, 30 cpm speed.

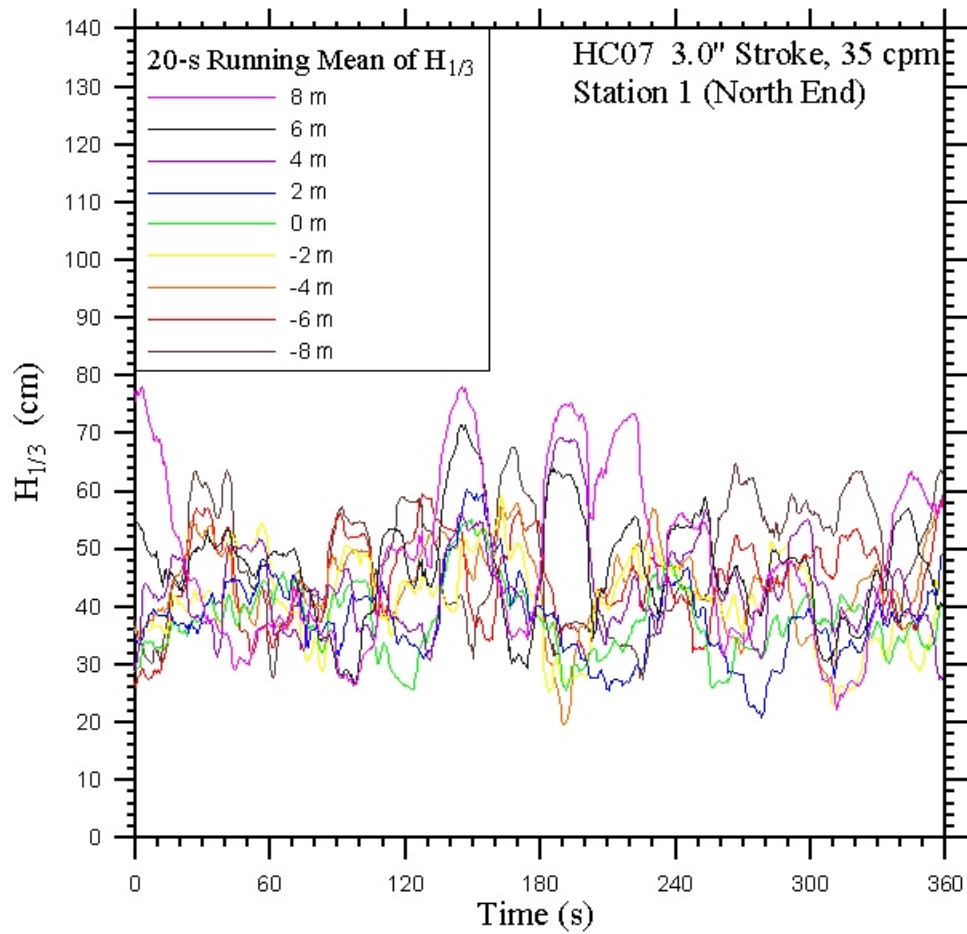


Figure 72: Time series of 20 s moving averaged of significant wave height, $H_{1/3}$, as a function of time for all nine wave probes in the main array at station 1, north end of tank. Paddle conditions for this run correspond to HC07, 4.5" stroke, 35 cpm speed.

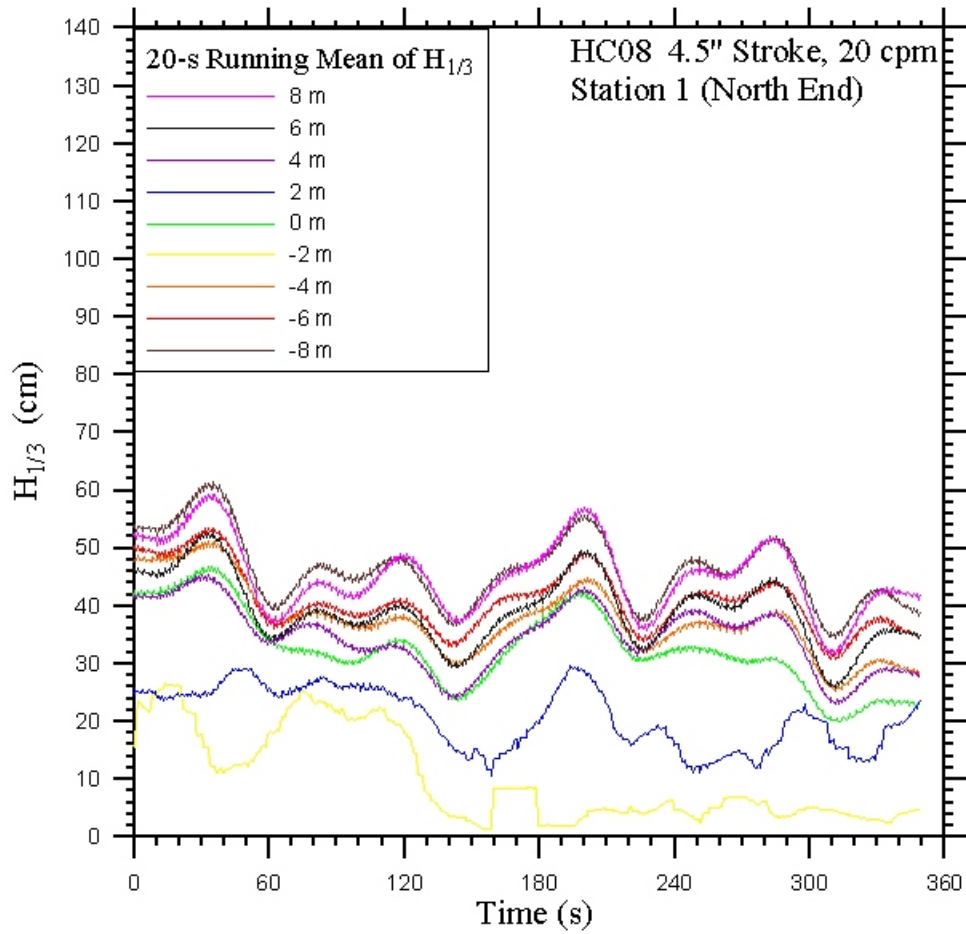


Figure 73: Time series of 20 s moving averaged of significant wave height, $H_{1/3}$, as a function of time for all nine wave probes in the main array at station 1, north end of tank. Paddle conditions for this run correspond to HC08, 4.5" stroke, 20 cpm speed.

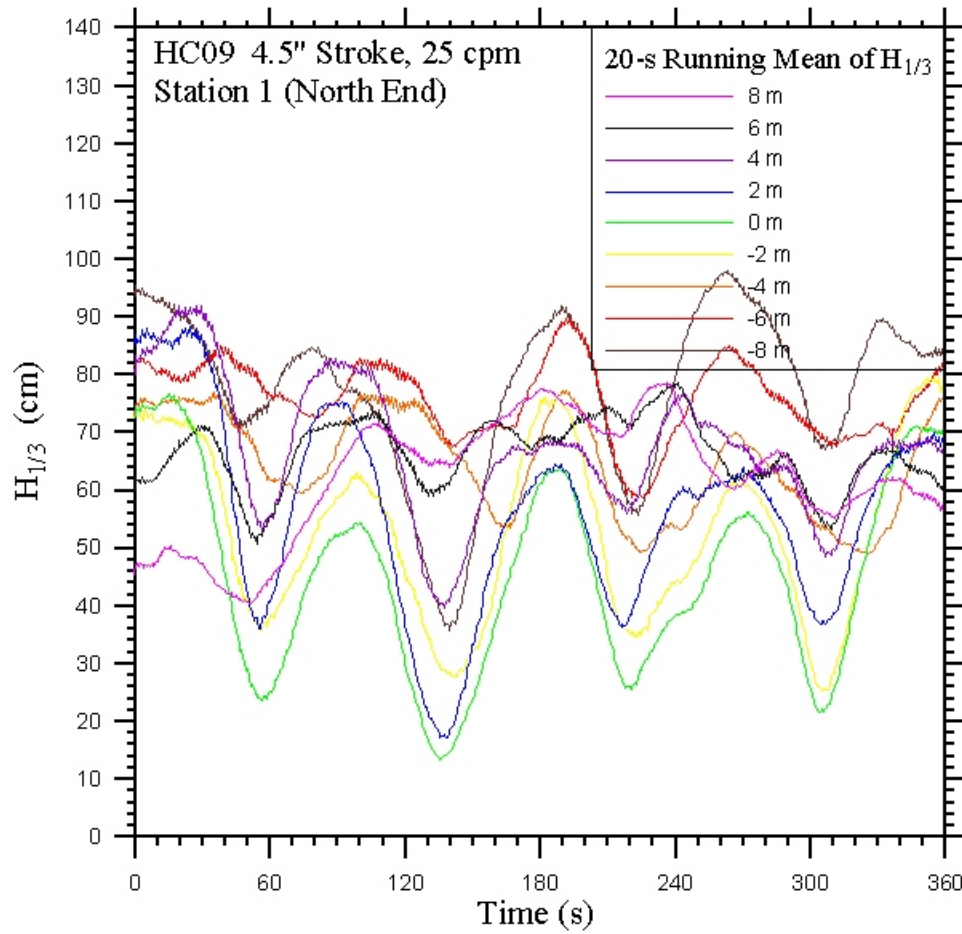


Figure 74: Time series of 20 s moving averaged of significant wave height, $H_{1/3}$, as a function of time for all nine wave probes in the main array at station 1, north end of tank. Paddle conditions for this run correspond to HC09, 4.5" stroke, 25 cpm speed.

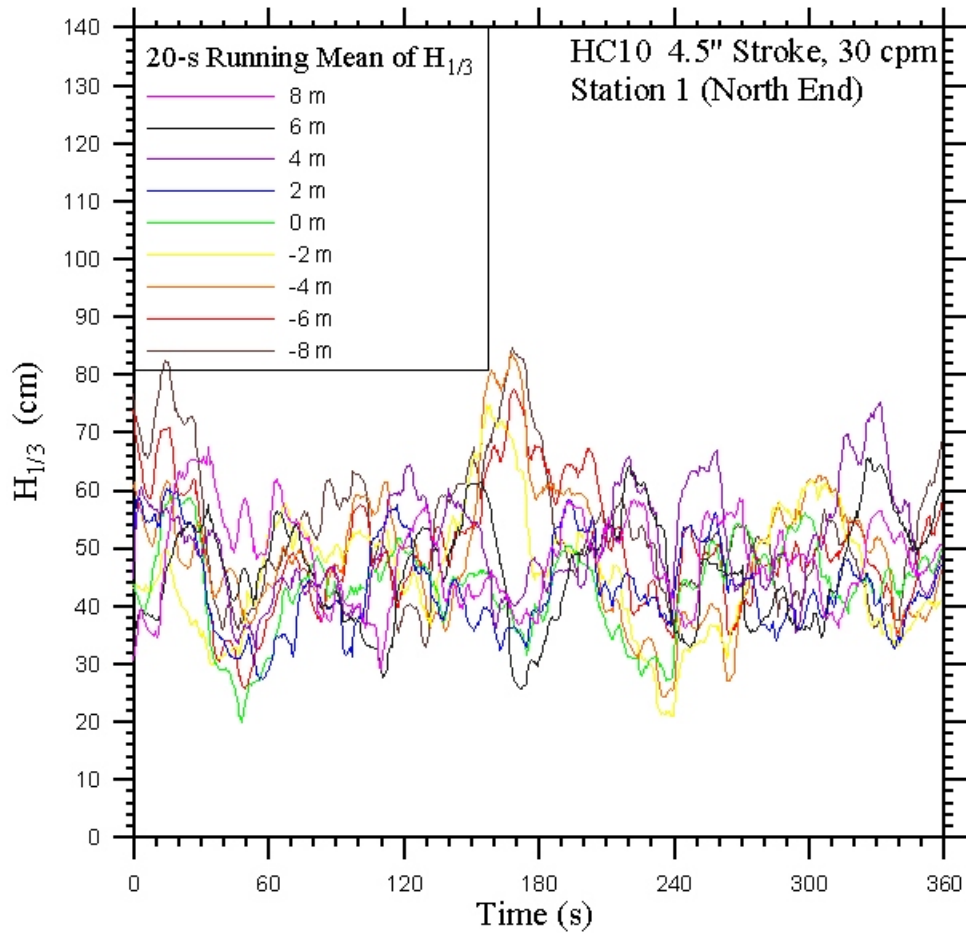


Figure 75: Time series of 20 s moving averaged of significant wave height, $H_{1/3}$, as a function of time for all nine wave probes in the main array at station 1, north end of tank. Paddle conditions for this run correspond to HC10, 4.5" stroke, 30 cpm speed.

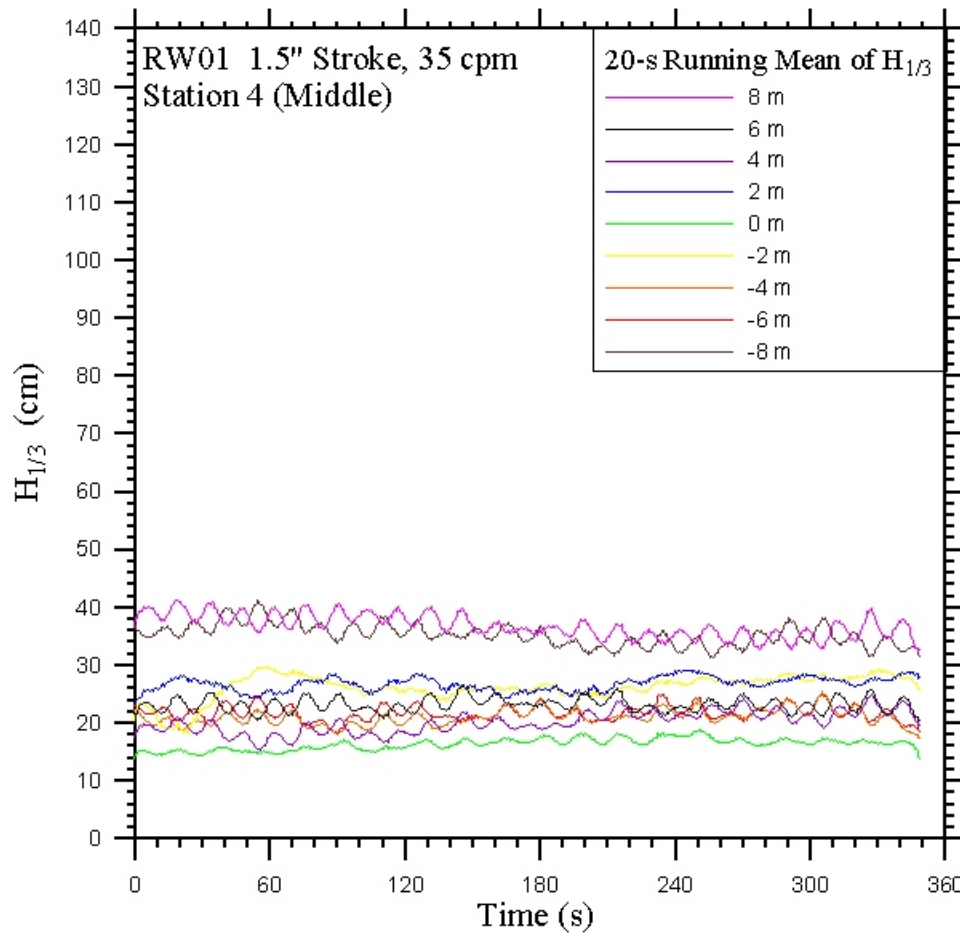


Figure 76: Time series of 20 s moving averaged of significant wave height, $H_{1/3}$, as a function of time for all nine wave probes in the main array at station 4, middle of tank. Paddle conditions for this run correspond to RW01, 1.5" stroke, 35 cpm speed.

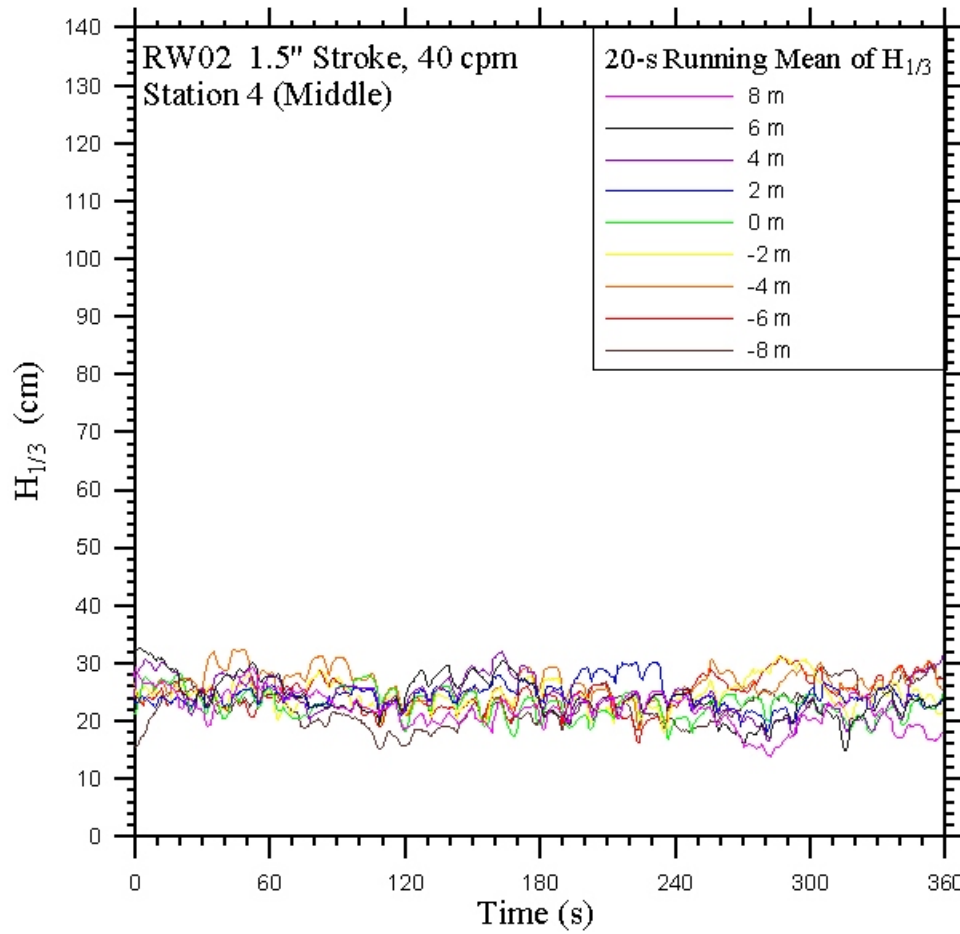


Figure 77: Time series of 20 s moving averaged of significant wave height, $H_{1/3}$, as a function of time for all nine wave probes in the main array at station 4, middle of tank. Paddle conditions for this run correspond to RW02, 1.5" stroke, 40 cpm speed.

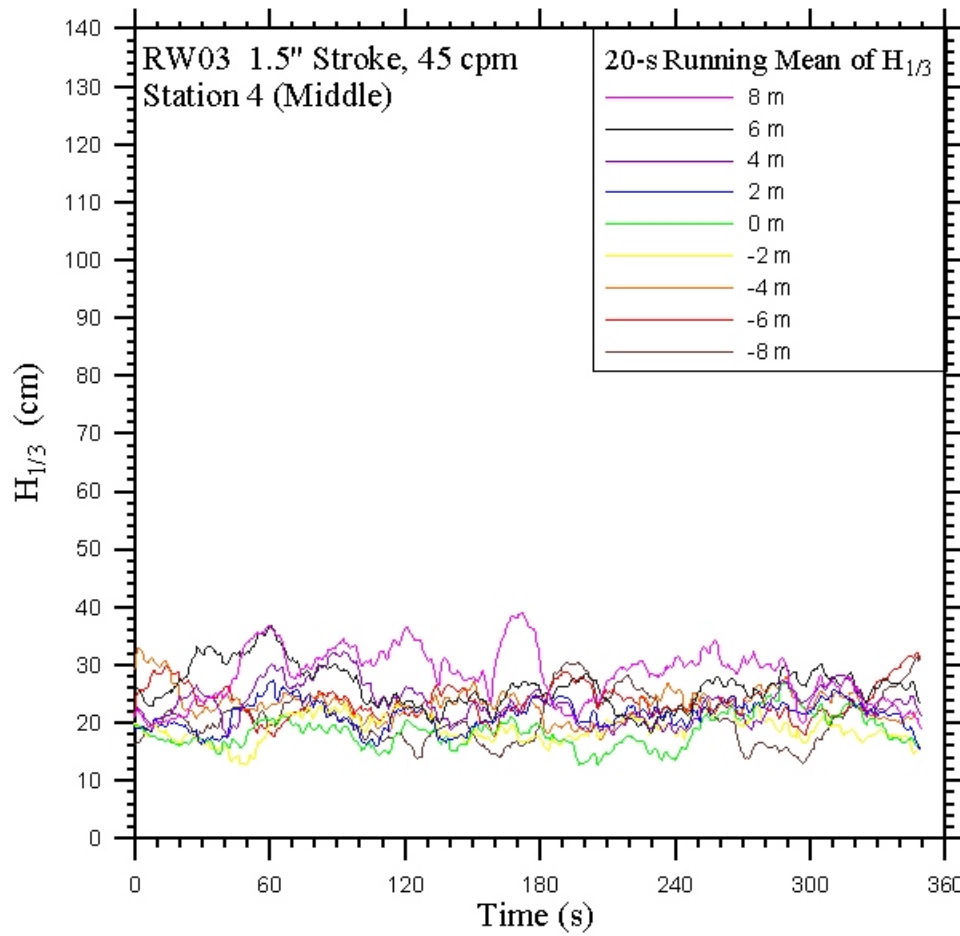


Figure 78: Time series of 20 s moving averaged of significant wave height, $H_{1/3}$, as a function of time for all nine wave probes in the main array at station 4, middle of tank. Paddle conditions for this run correspond to RW03, 1.5" stroke, 45 cpm speed.

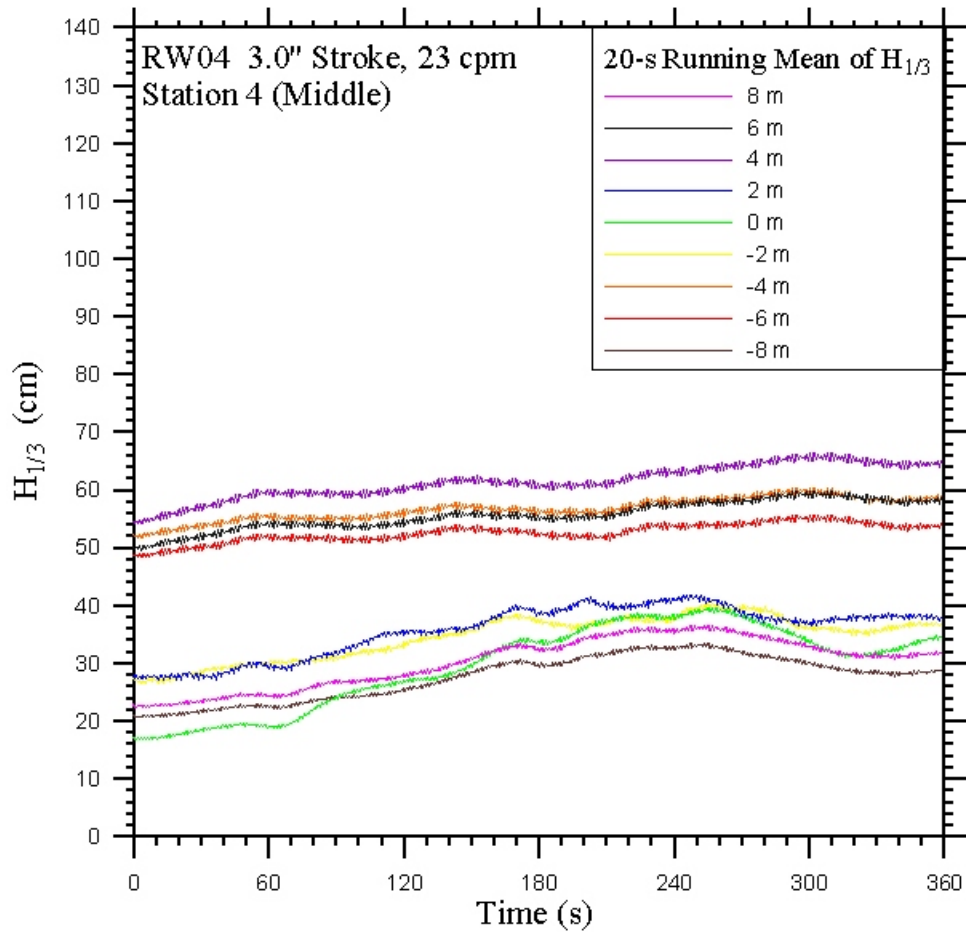


Figure 79: Time series of 20 s moving averaged of significant wave height, $H_{1/3}$, as a function of time for all nine wave probes in the main array at station 4, middle of tank. Paddle conditions for this run correspond to RW04, 3.0" stroke, 21 cpm speed.

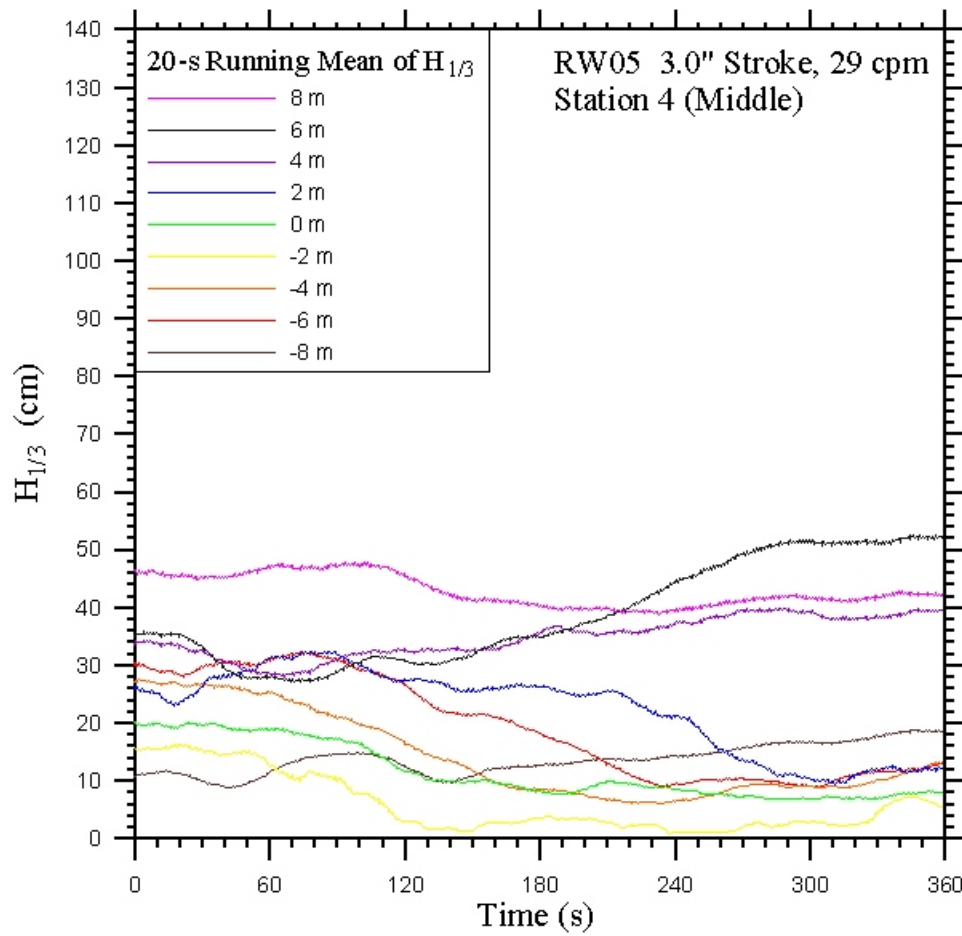


Figure 80: Time series of 20 s moving averaged of significant wave height, $H_{1/3}$, as a function of time for all nine wave probes in the main array at station 4, middle of tank. Paddle conditions for this run correspond to RW05, 3.0" stroke, 37 cpm speed.

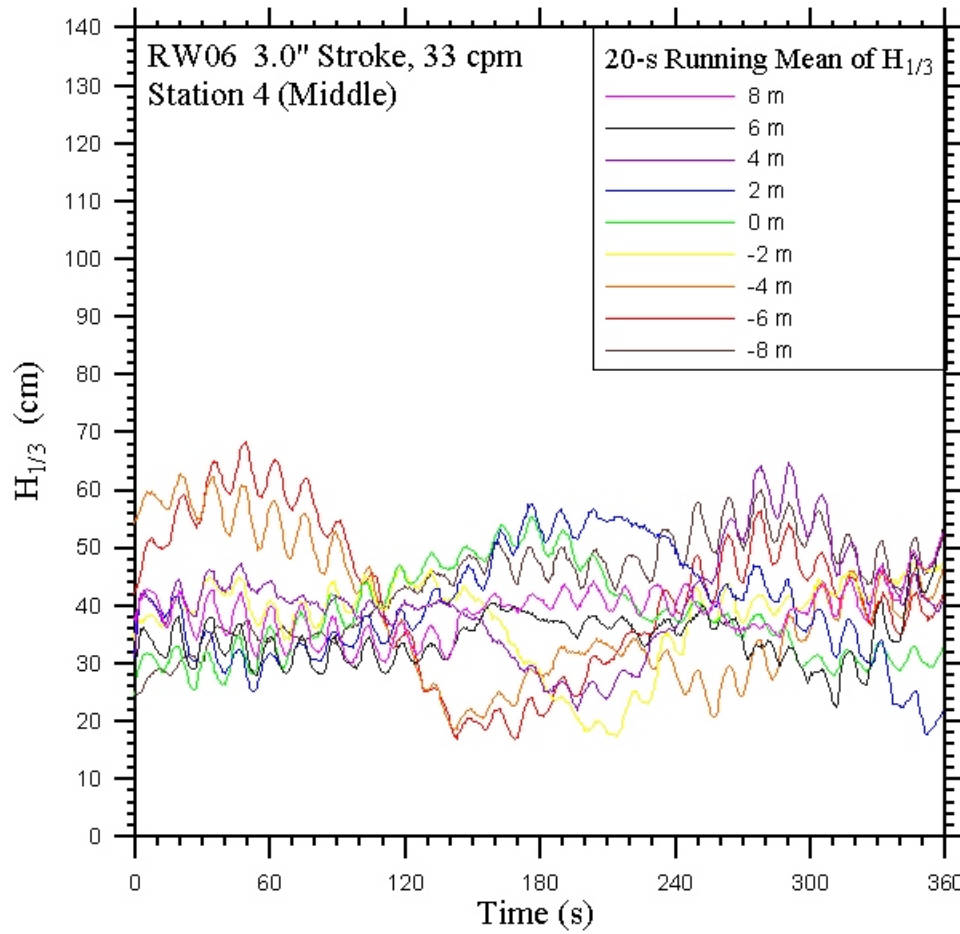


Figure 81: Time series of 20 s moving averaged of significant wave height, $H_{1/3}$, as a function of time for all nine wave probes in the main array at station 4, middle of tank. Paddle conditions for this run correspond to RW06, 3.0" stroke, 33 cpm speed.

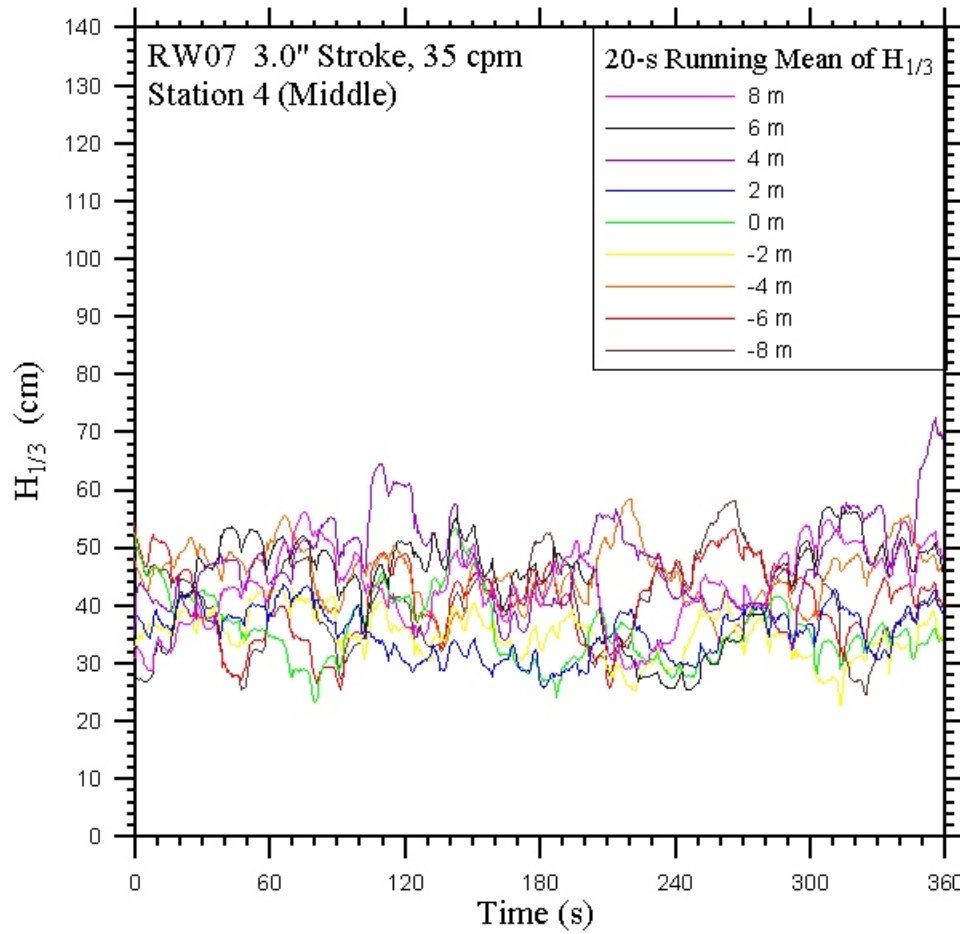


Figure 82: Time series of 20 s moving averaged of significant wave height, $H_{1/3}$, as a function of time for all nine wave probes in the main array at station 4, middle of tank. Paddle conditions for this run correspond to RW07, 3.0" stroke, 35 cpm speed.

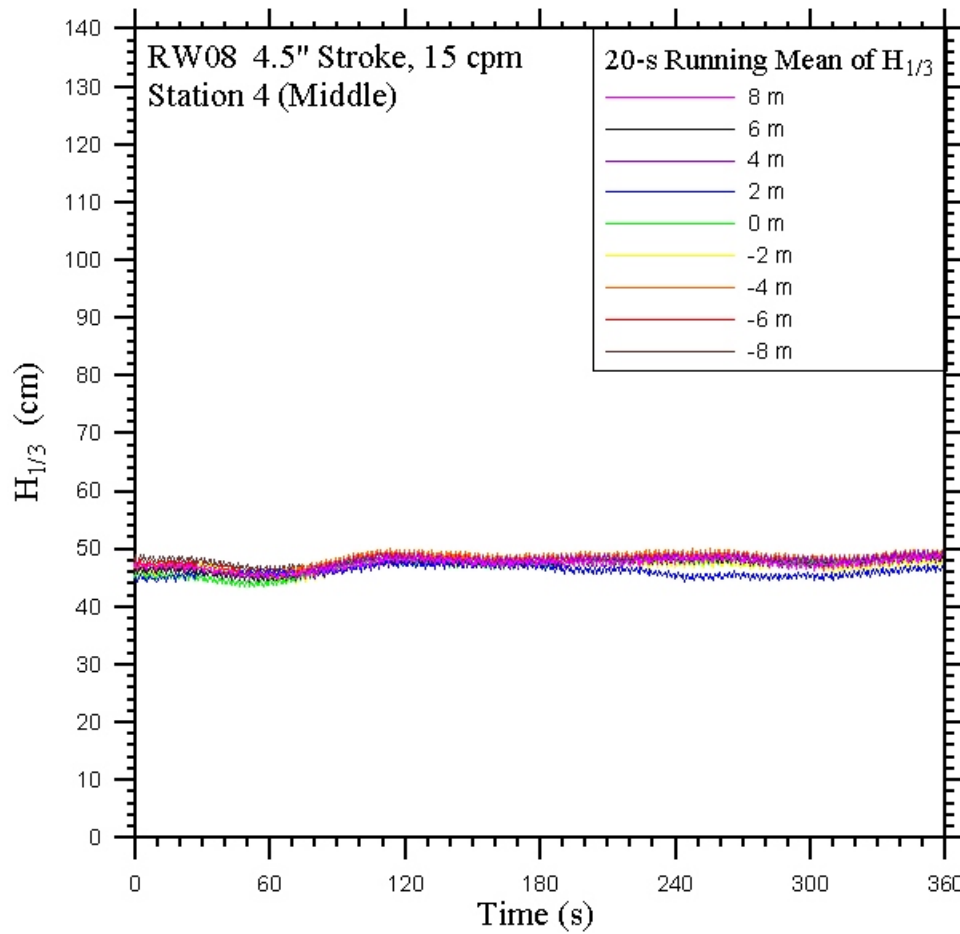


Figure 83: Time series of 20 s moving averaged of significant wave height, $H_{1/3}$, as a function of time for all nine wave probes in the main array at station 4, middle of tank. Paddle conditions for this run correspond to RW08, 4.5" stroke, 15 cpm speed.

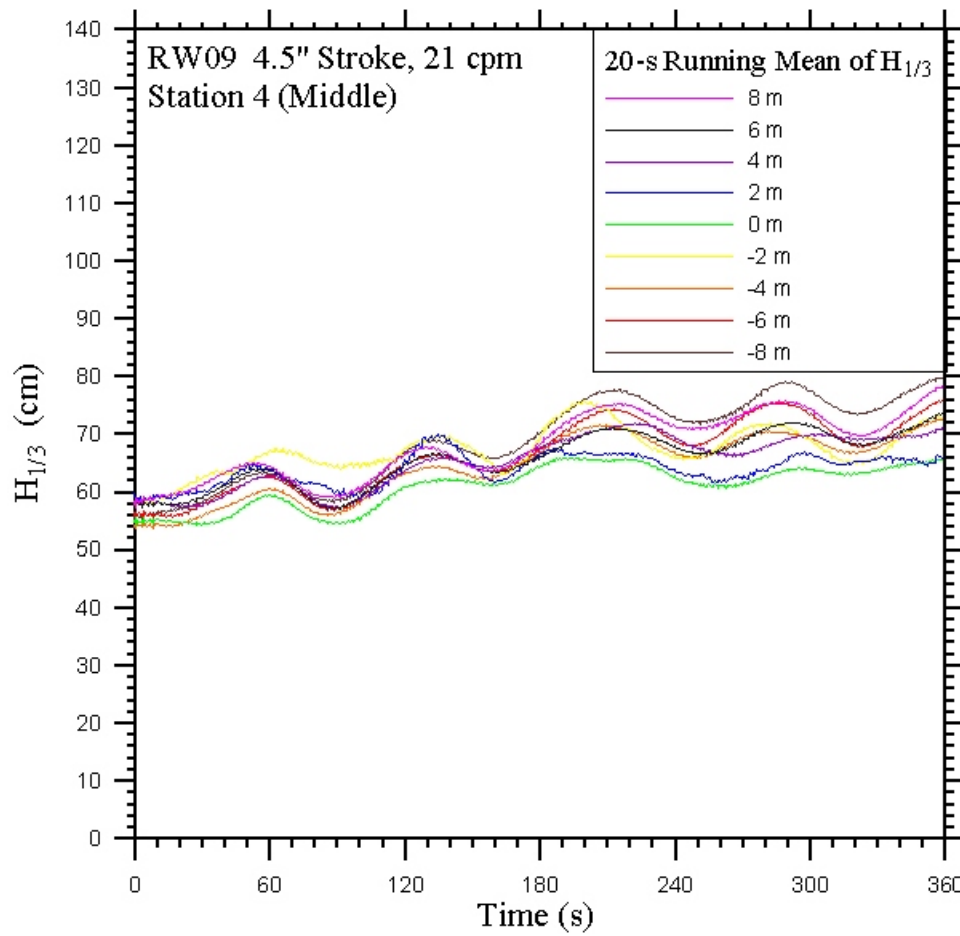


Figure 84: Time series of 20 s moving averaged of significant wave height, $H_{1/3}$, as a function of time for all nine wave probes in the main array at station 4, middle of tank. Paddle conditions for this run correspond to RW09, 4.5" stroke, 21 cpm speed.

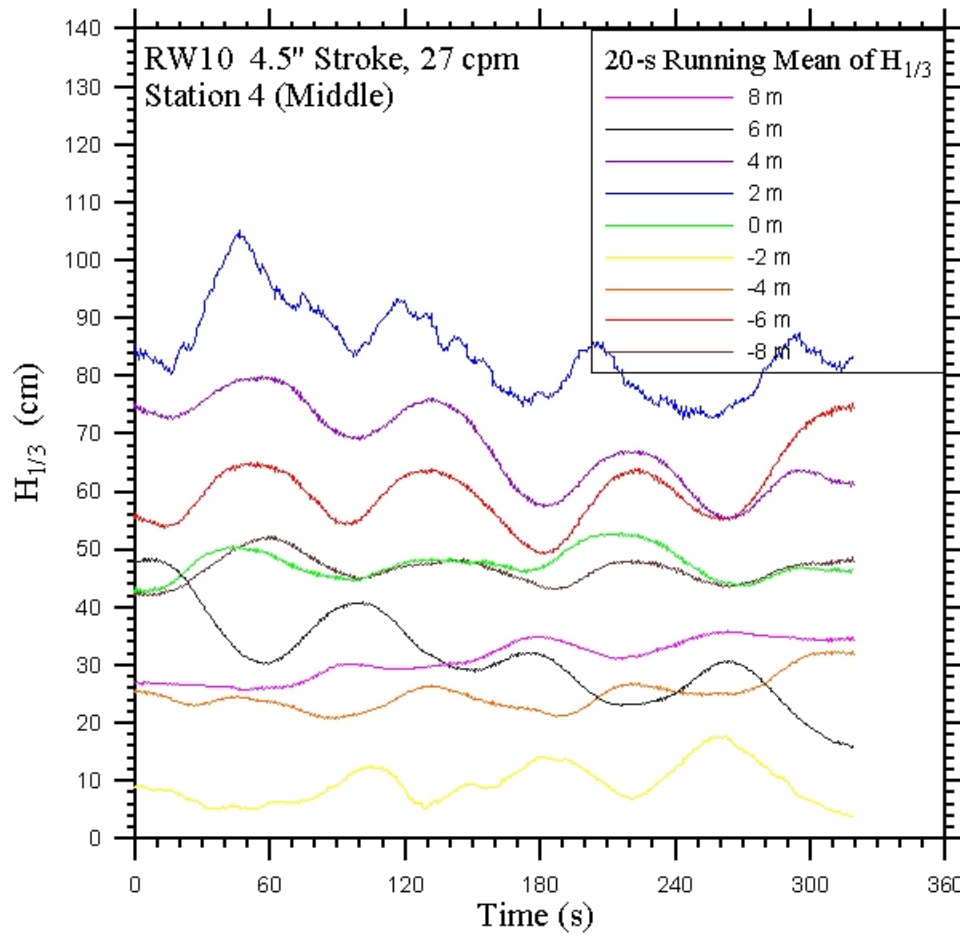


Figure 85: Time series of 20 s moving averaged of significant wave height, $H_{1/3}$, as a function of time for all nine wave probes in the main array at station 4, middle of tank. Paddle conditions for this run correspond to RW10, 4.5" stroke, 27 cpm speed.

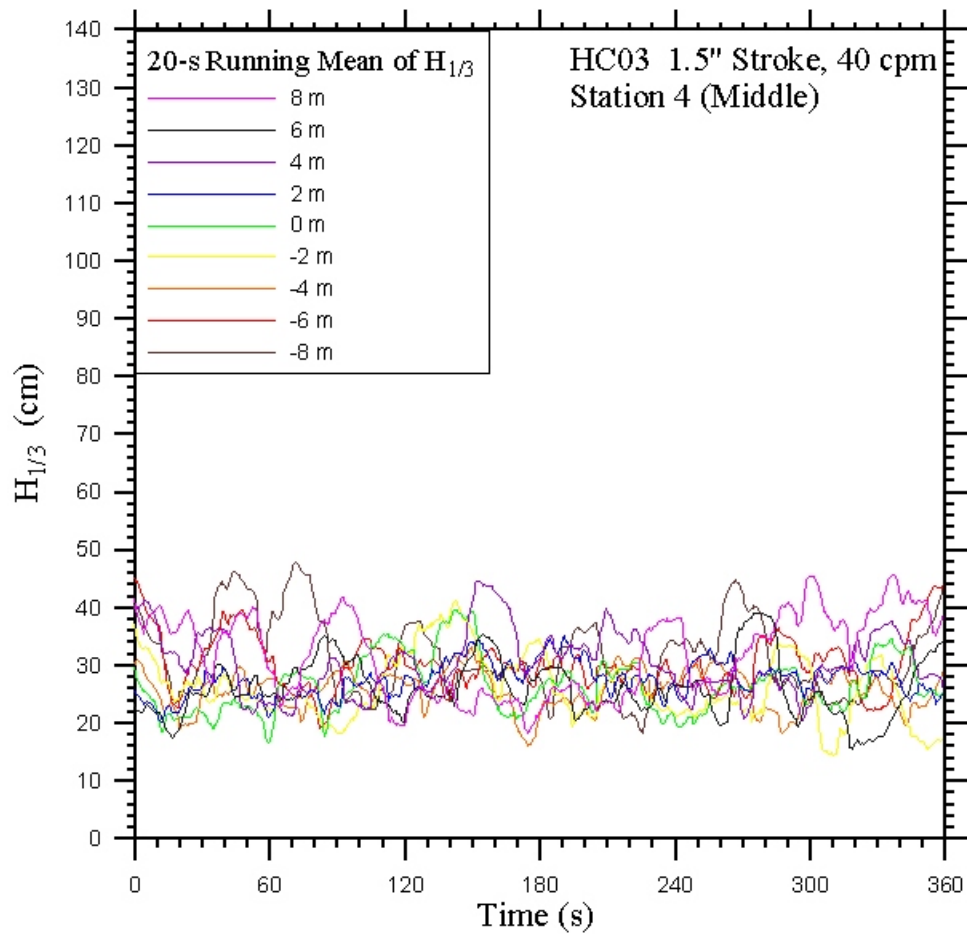


Figure 86: Time series of 20 s moving averaged of significant wave height, $H_{1/3}$, as a function of time for all nine wave probes in the main array at station 4, middle of tank. Paddle conditions for this run correspond to HC03, 1.5" stroke, 40 cpm speed.

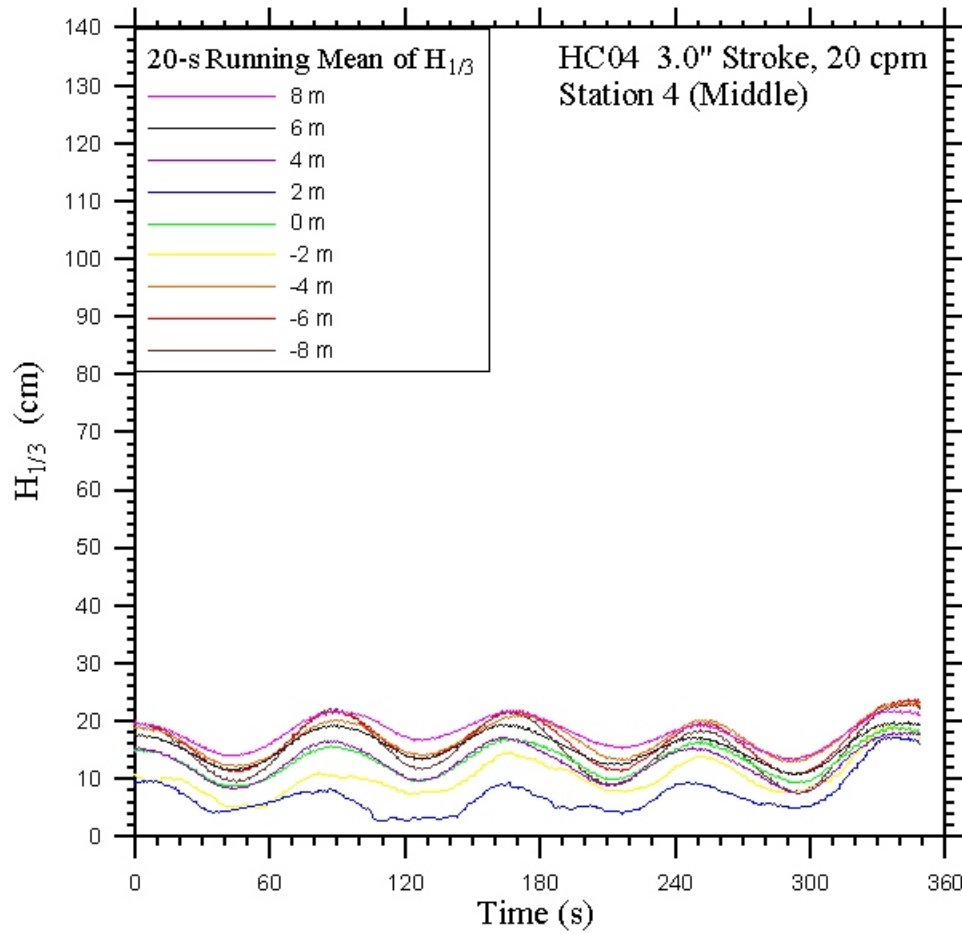


Figure 87: Time series of 20 s moving averaged of significant wave height, $H_{1/3}$, as a function of time for all nine wave probes in the main array at station 4, middle of tank. Paddle conditions for this run correspond to HC04, 3.0" stroke, 20 cpm speed.

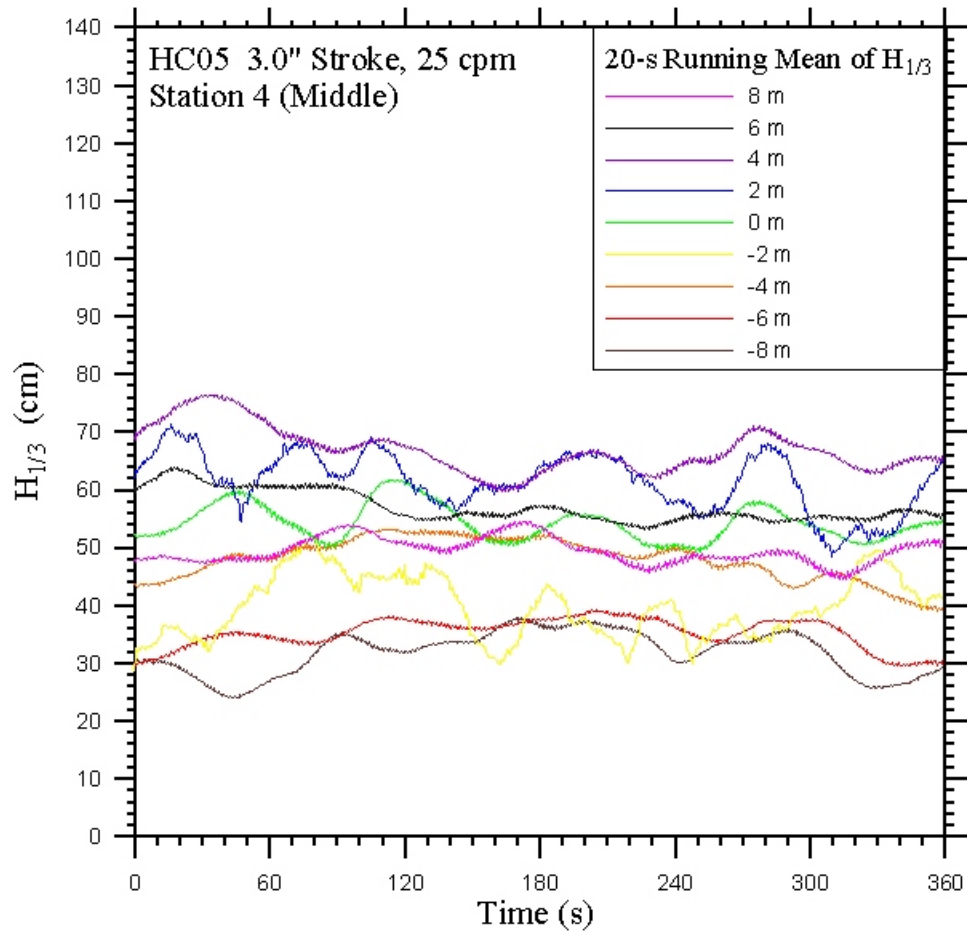


Figure 88: Time series of 20 s moving averaged of significant wave height, $H_{1/3}$, as a function of time for all nine wave probes in the main array at station 4, middle of tank. Paddle conditions for this run correspond to HC05, 3.0" stroke, 25 cpm speed.

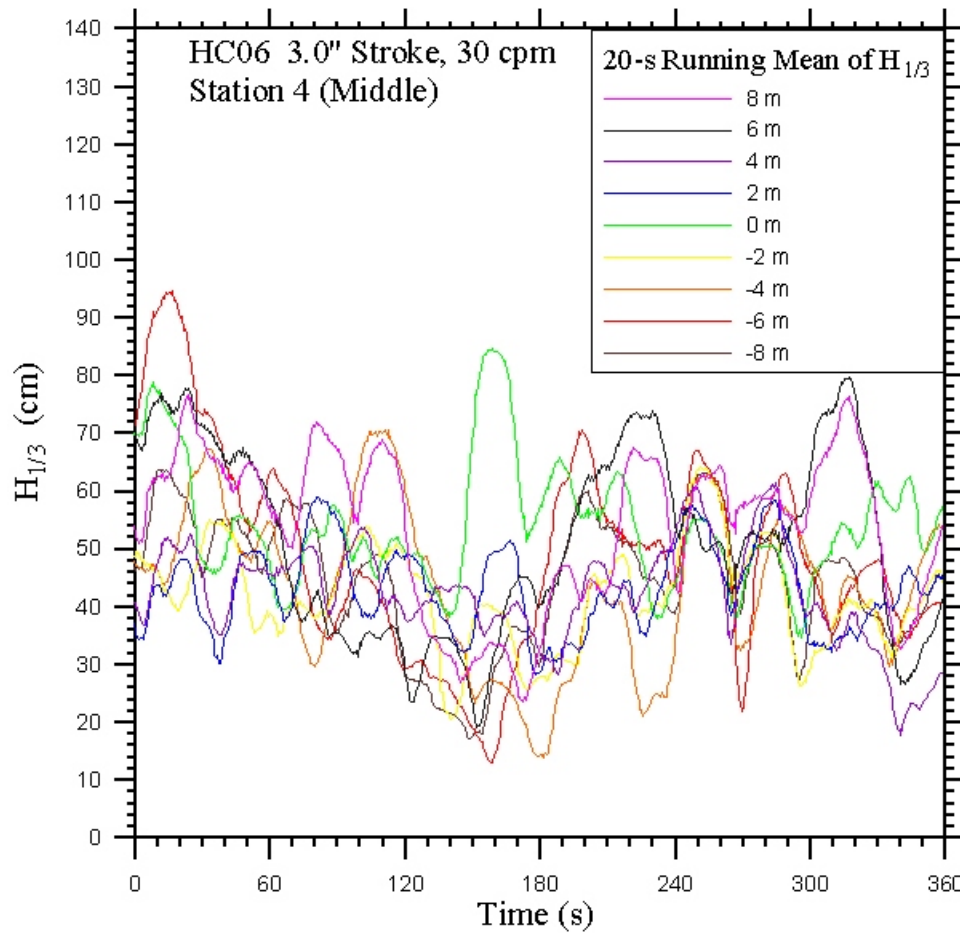


Figure 89: Time series of 20 s moving averaged of significant wave height, $H_{1/3}$, as a function of time for all nine wave probes in the main array at station 4, middle of tank. Paddle conditions for this run correspond to HC06, 3.0" stroke, 30 cpm speed.

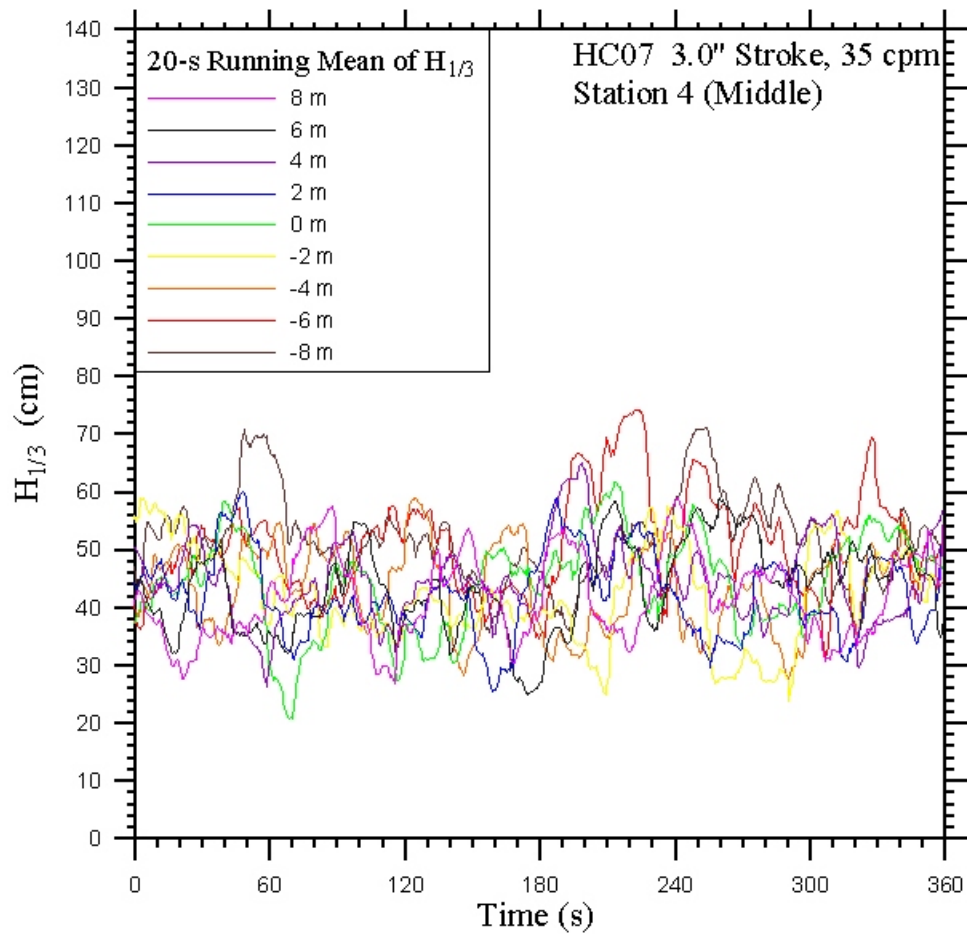


Figure 90: Time series of 20 s moving averaged of significant wave height, $H_{1/3}$, as a function of time for all nine wave probes in the main array at station 4, middle of tank. Paddle conditions for this run correspond to HC07, 4.5" stroke, 35 cpm speed.

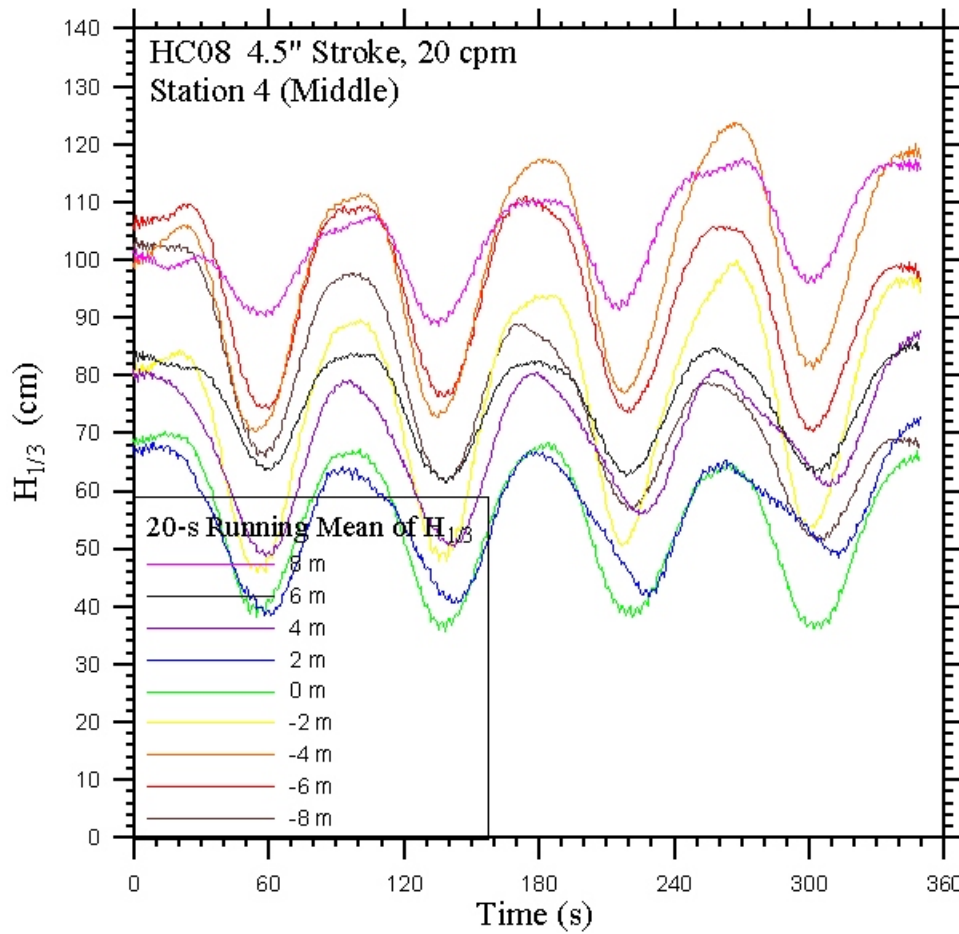


Figure 91: Time series of 20 s moving averaged of significant wave height, $H_{1/3}$, as a function of time for all nine wave probes in the main array at station 4, middle of tank. Paddle conditions for this run correspond to HC08, 4.5" stroke, 20 cpm speed.

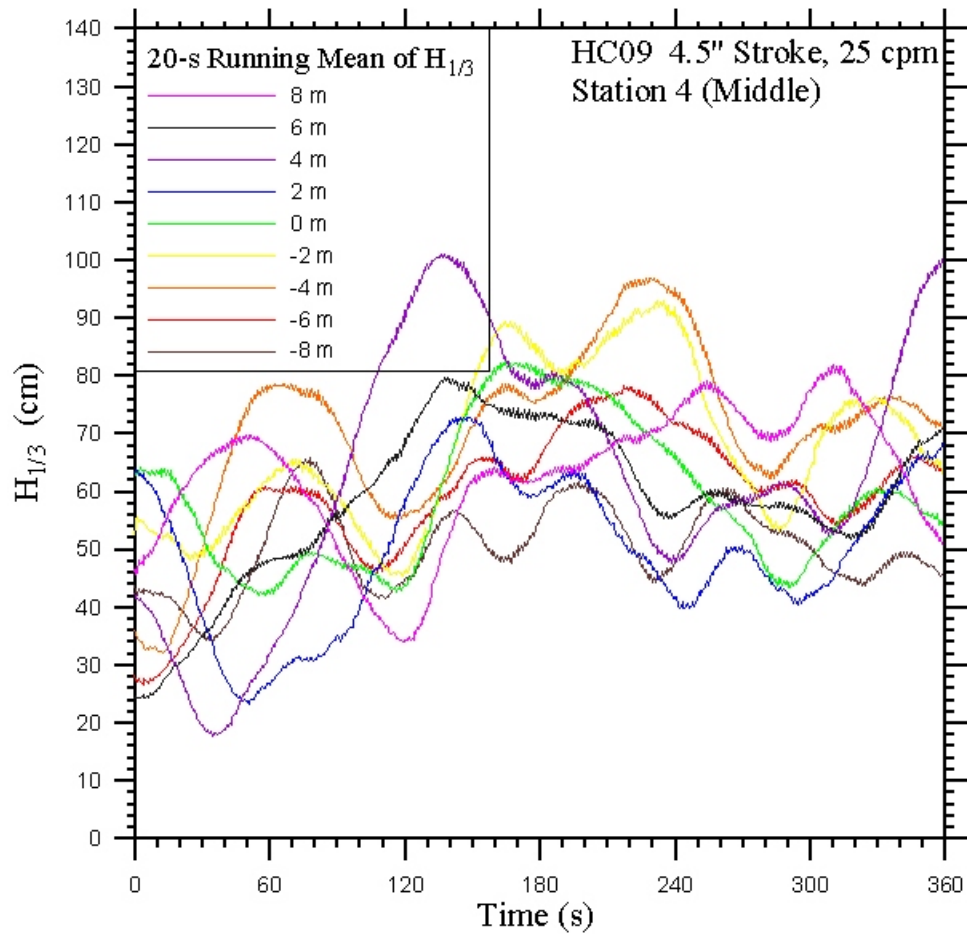


Figure 92: Time series of 20 s moving averaged of significant wave height, $H_{1/3}$, as a function of time for all nine wave probes in the main array at station 4, middle of tank. Paddle conditions for this run correspond to HC09, 4.5" stroke, 25 cpm speed.

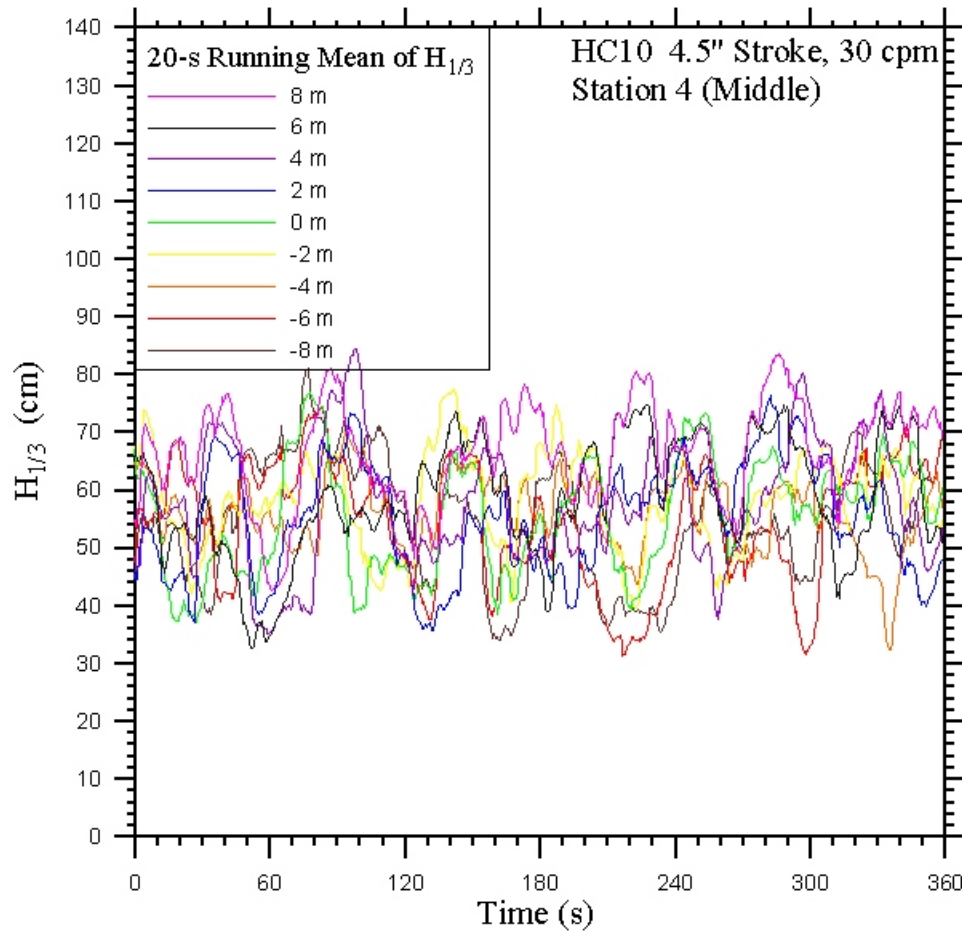


Figure 93: Time series of 20 s moving averaged of significant wave height, $H_{1/3}$, as a function of time for all nine wave probes in the main array at station 4, middle of tank. Paddle conditions for this run correspond to HC10, 4.5" stroke, 30 cpm speed.

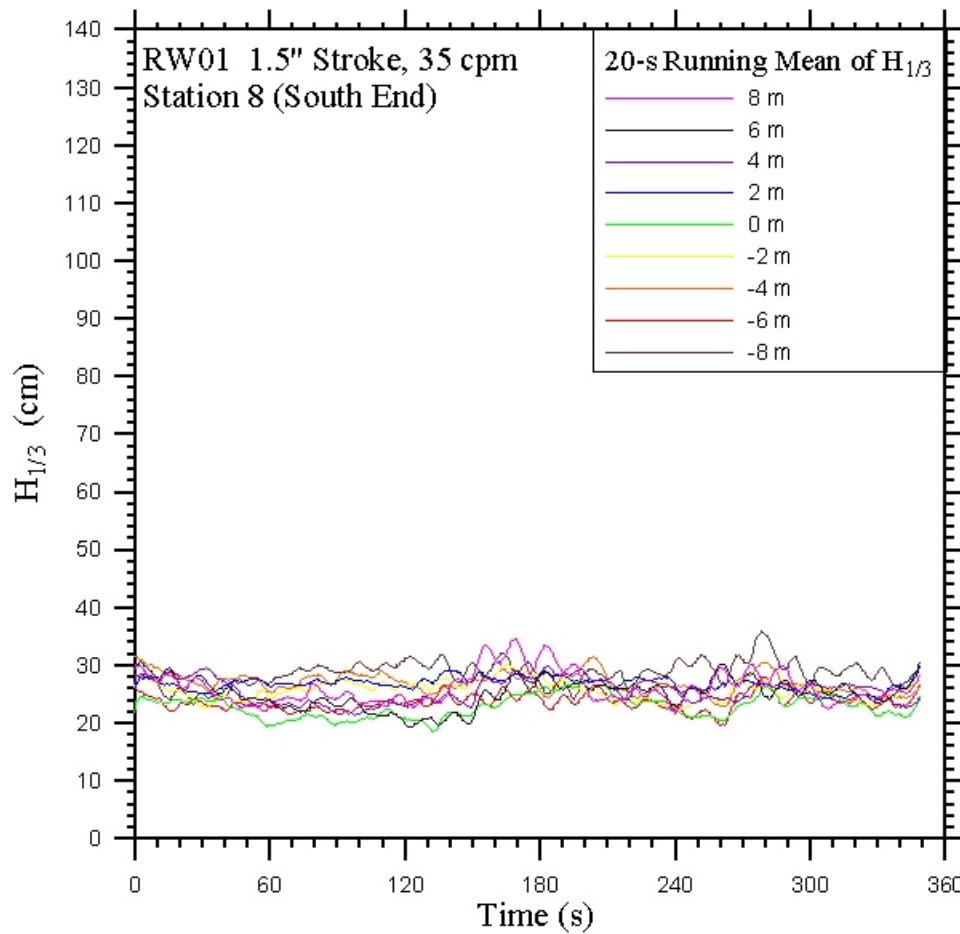


Figure 94: Time series of 20 s moving averaged of significant wave height, $H_{1/3}$, as a function of time for all nine wave probes in the main array at station 8, south end of tank. Paddle conditions for this run correspond to RW01, 1.5" stroke, 35 cpm speed.

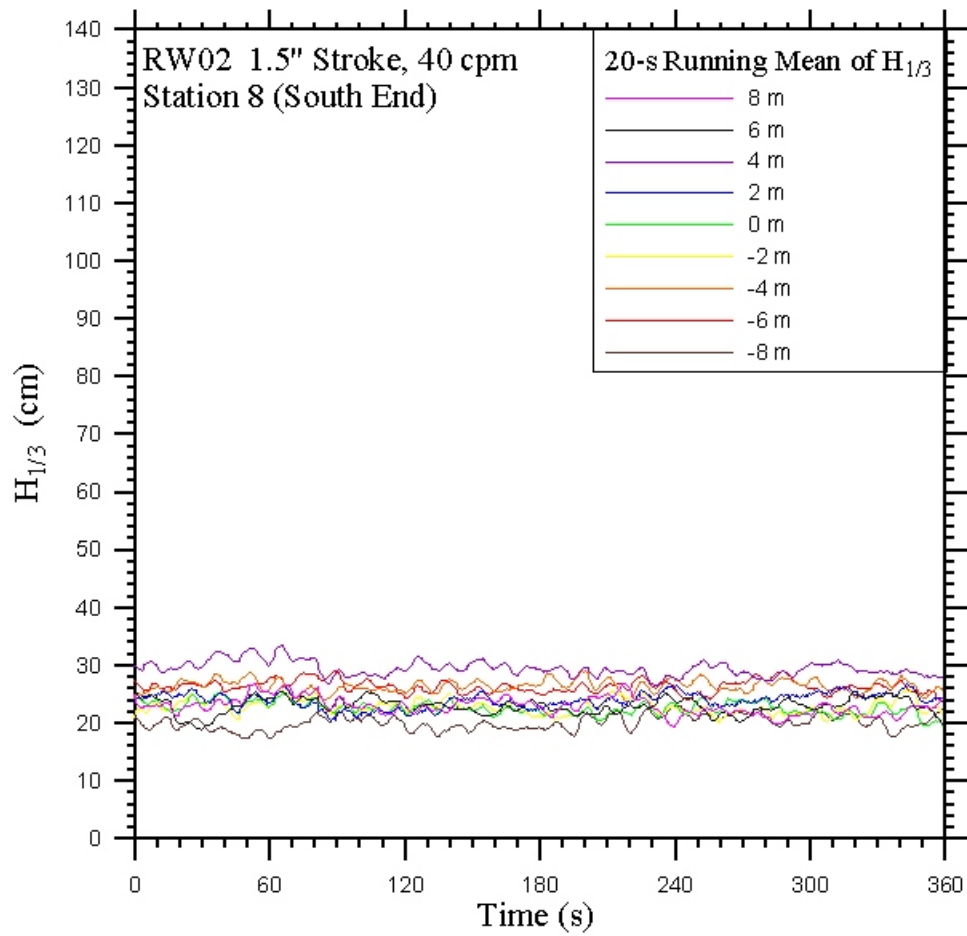


Figure 95: Time series of 20 s moving averaged of significant wave height, $H_{1/3}$, as a function of time for all nine wave probes in the main array at station 8, south end of tank. Paddle conditions for this run correspond to RW02, 1.5" stroke, 40 cpm speed.

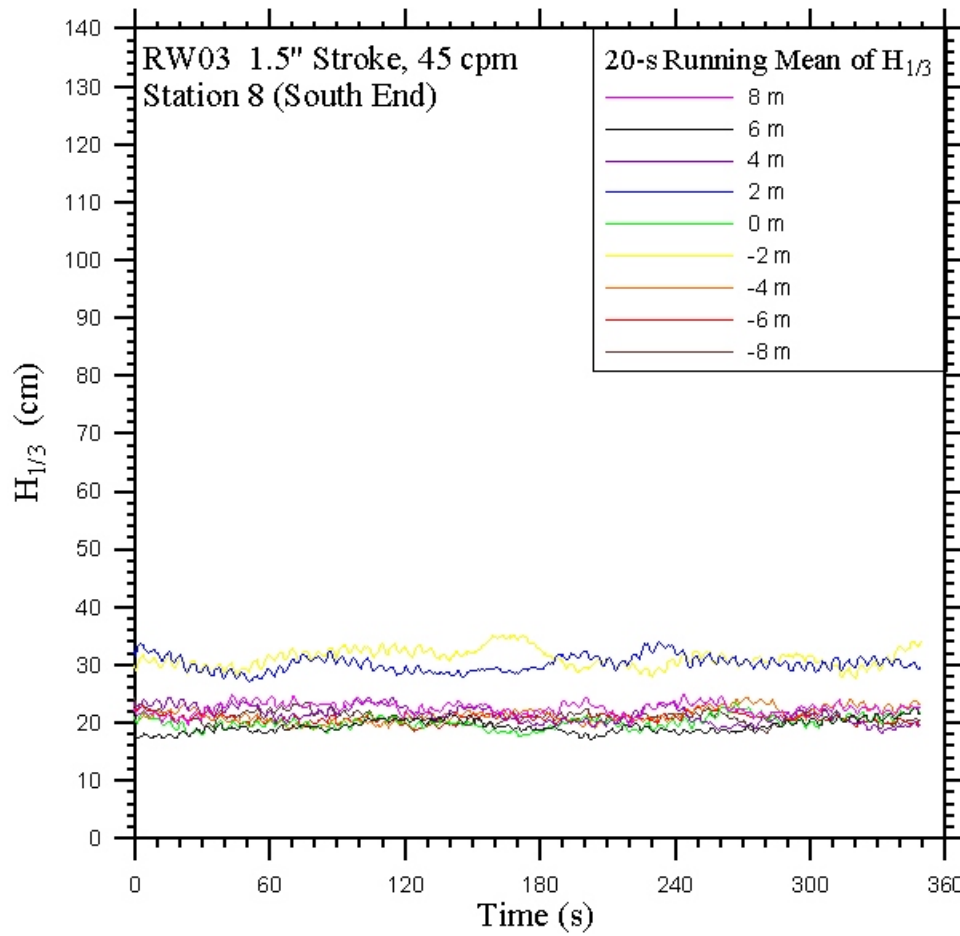


Figure 96: Time series of 20 s moving averaged of significant wave height, $H_{1/3}$, as a function of time for all nine wave probes in the main array at station 8, south end of tank. Paddle conditions for this run correspond to RW03, 1.5" stroke, 45 cpm speed.

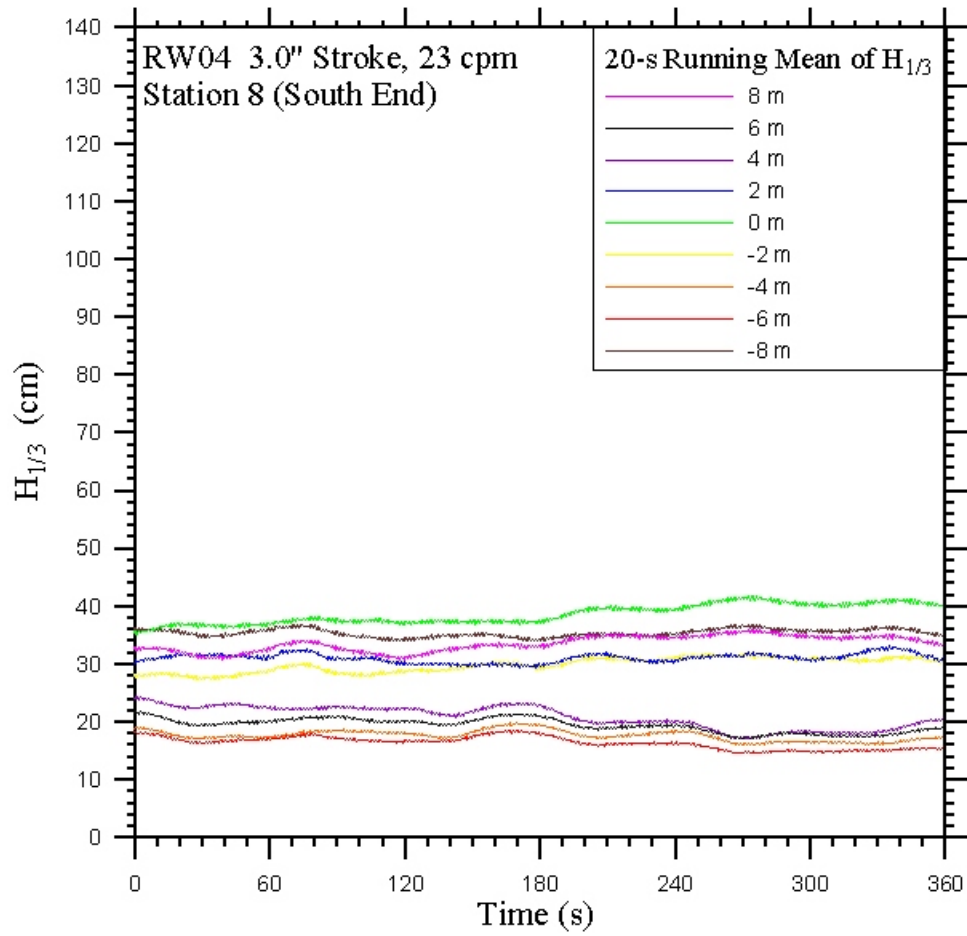


Figure 97: Time series of 20 s moving averaged of significant wave height, $H_{1/3}$, as a function of time for all nine wave probes in the main array at station 8, south end of tank. Paddle conditions for this run correspond to RW04, 3.0" stroke, 21 cpm speed.

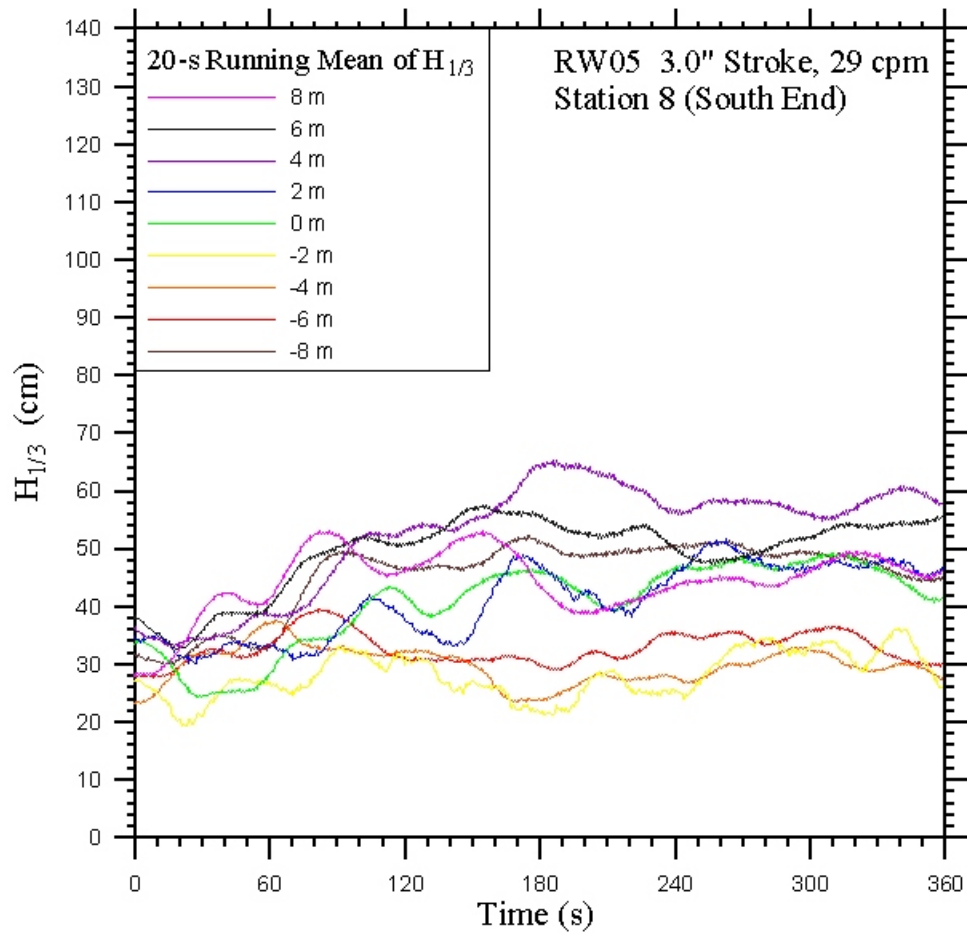


Figure 98: Time series of 20 s moving averaged of significant wave height, $H_{1/3}$, as a function of time for all nine wave probes in the main array at station 8, south end of tank. Paddle conditions for this run correspond to RW05, 3.0" stroke, 37 cpm speed.

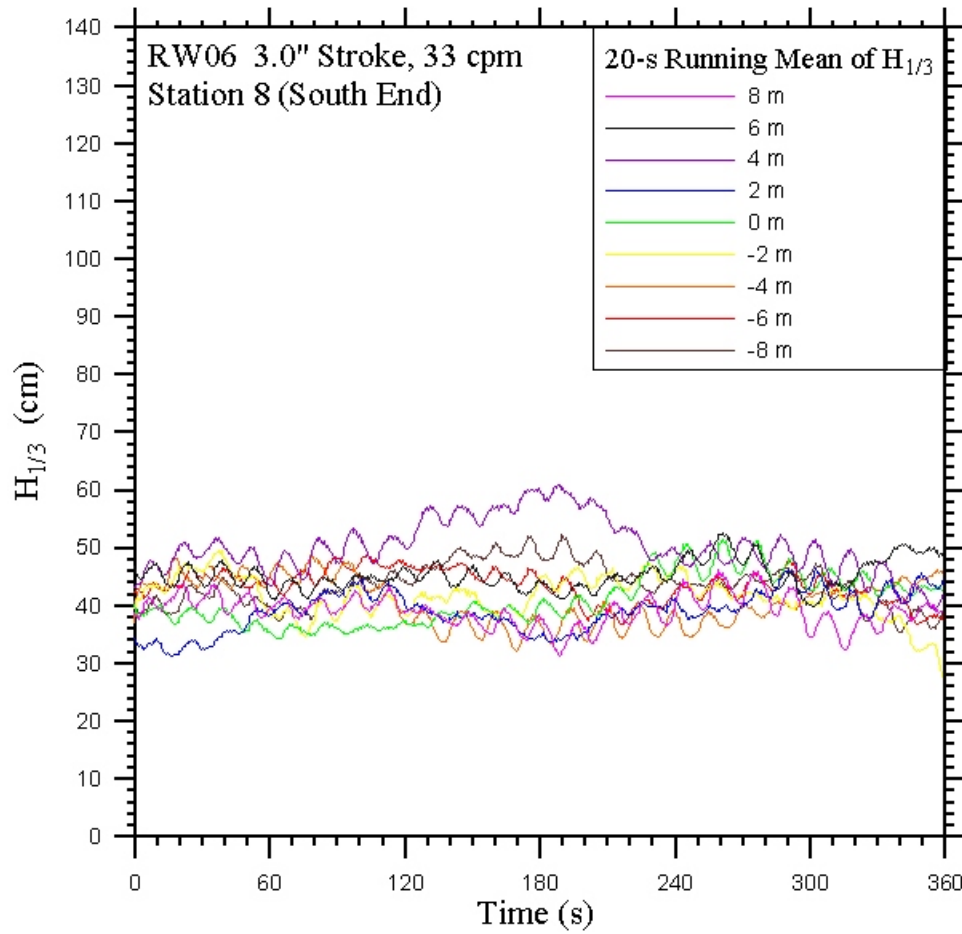


Figure 99: Time series of 20 s moving averaged of significant wave height, $H_{1/3}$, as a function of time for all nine wave probes in the main array at station 8, south end of tank. Paddle conditions for this run correspond to RW06, 3.0" stroke, 33 cpm speed.

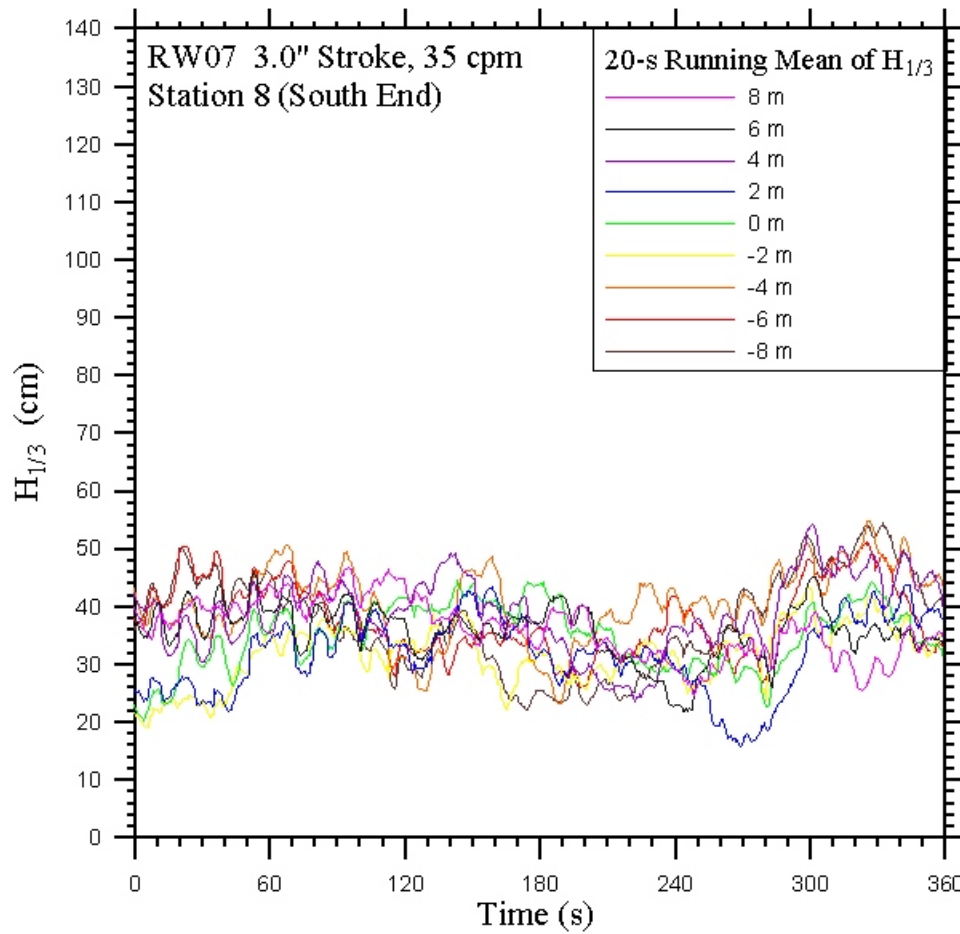


Figure 100: Time series of 20 s moving averaged of significant wave height, $H_{1/3}$, as a function of time for all nine wave probes in the main array at station 8, south end of tank. Paddle conditions for this run correspond to RW07, 3.0" stroke, 35 cpm speed.

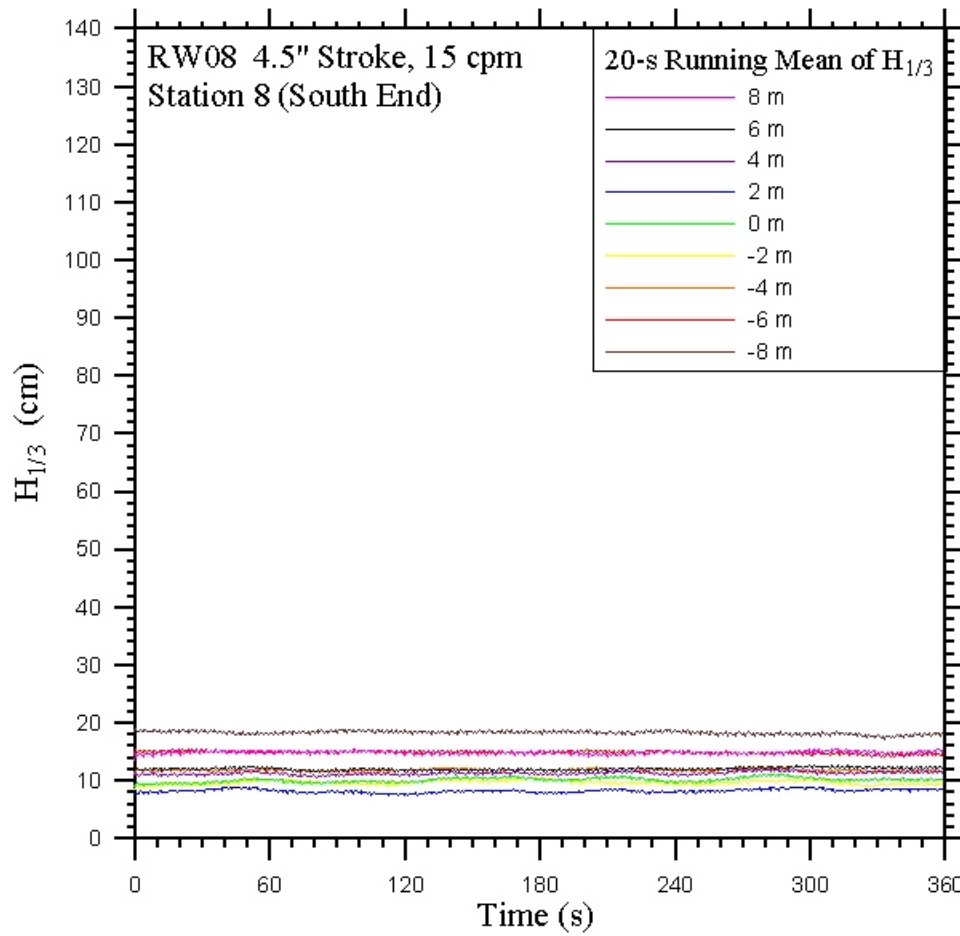


Figure 101: Time series of 20 s moving averaged of significant wave height, $H_{1/3}$, as a function of time for all nine wave probes in the main array at station 8, south end of tank. Paddle conditions for this run correspond to RW08, 4.5" stroke, 15 cpm speed.

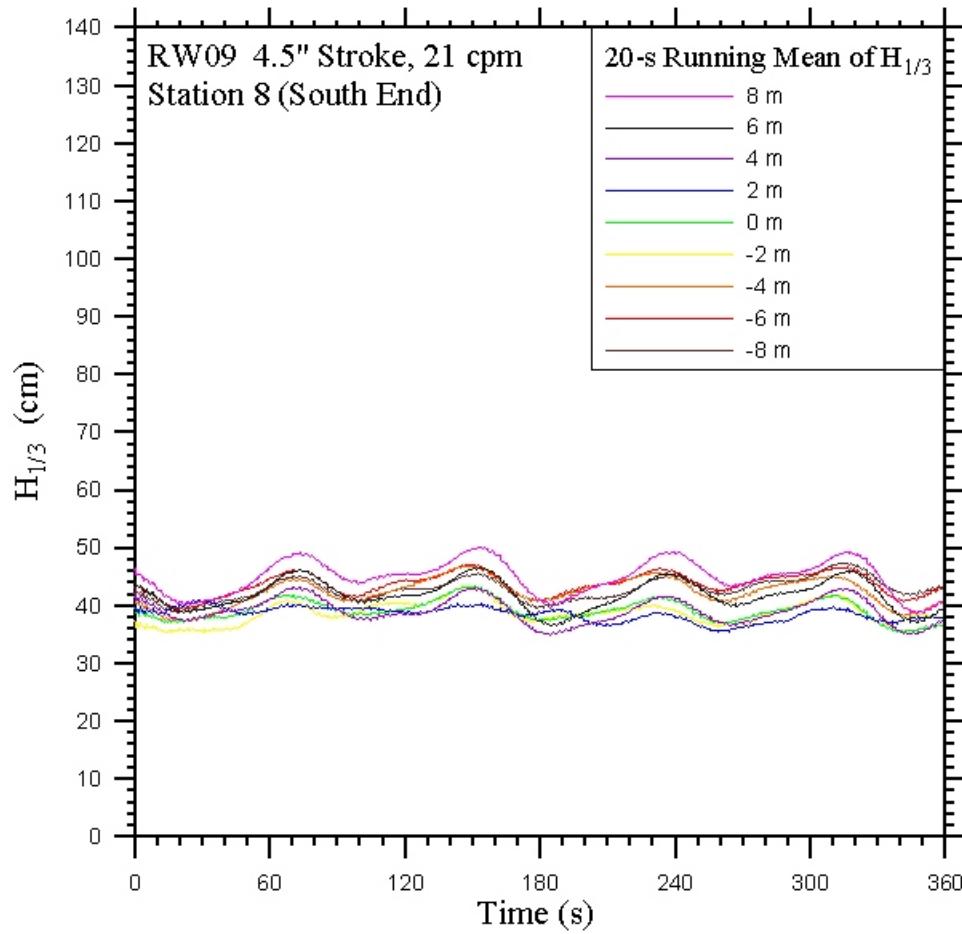


Figure 102: Time series of 20 s moving averaged of significant wave height, $H_{1/3}$, as a function of time for all nine wave probes in the main array at station 8, south end of tank. Paddle conditions for this run correspond to RW09, 4.5" stroke, 21 cpm speed.

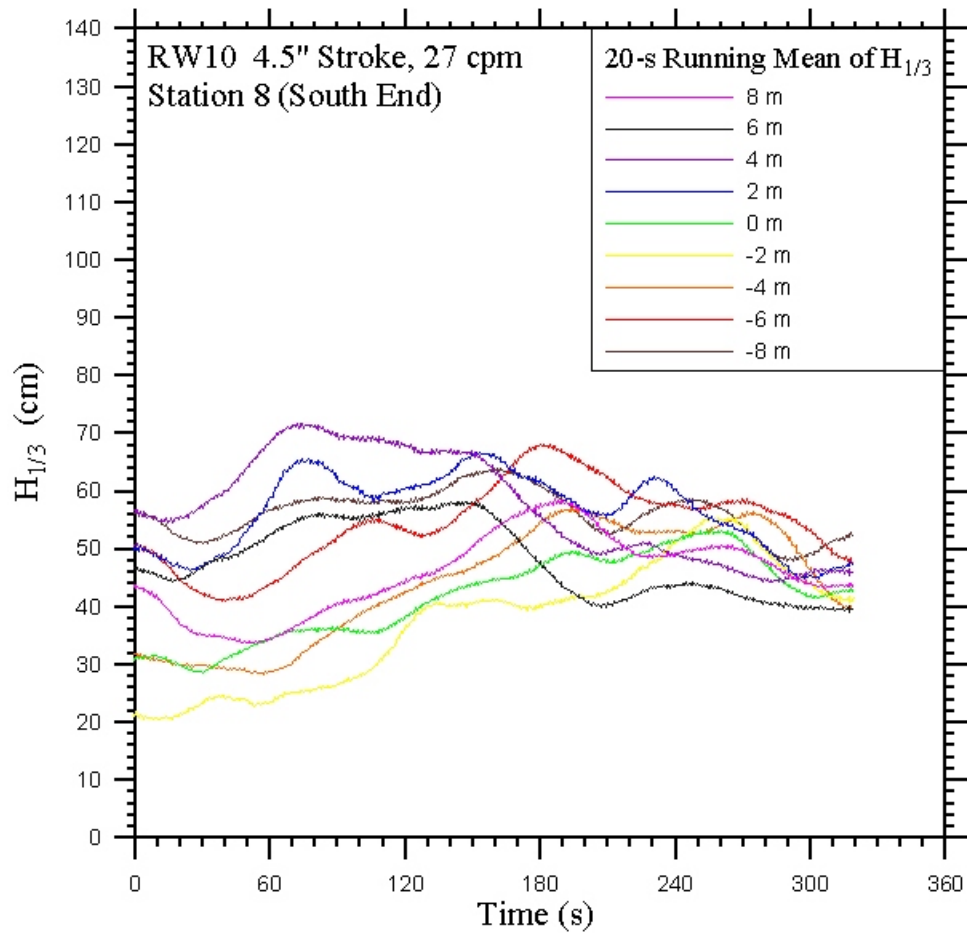


Figure 103: Time series of 20 s moving averaged of significant wave height, $H_{1/3}$, as a function of time for all nine wave probes in the main array at station 8, south end of tank. Paddle conditions for this run correspond to RW10, 4.5" stroke, 27 cpm speed.

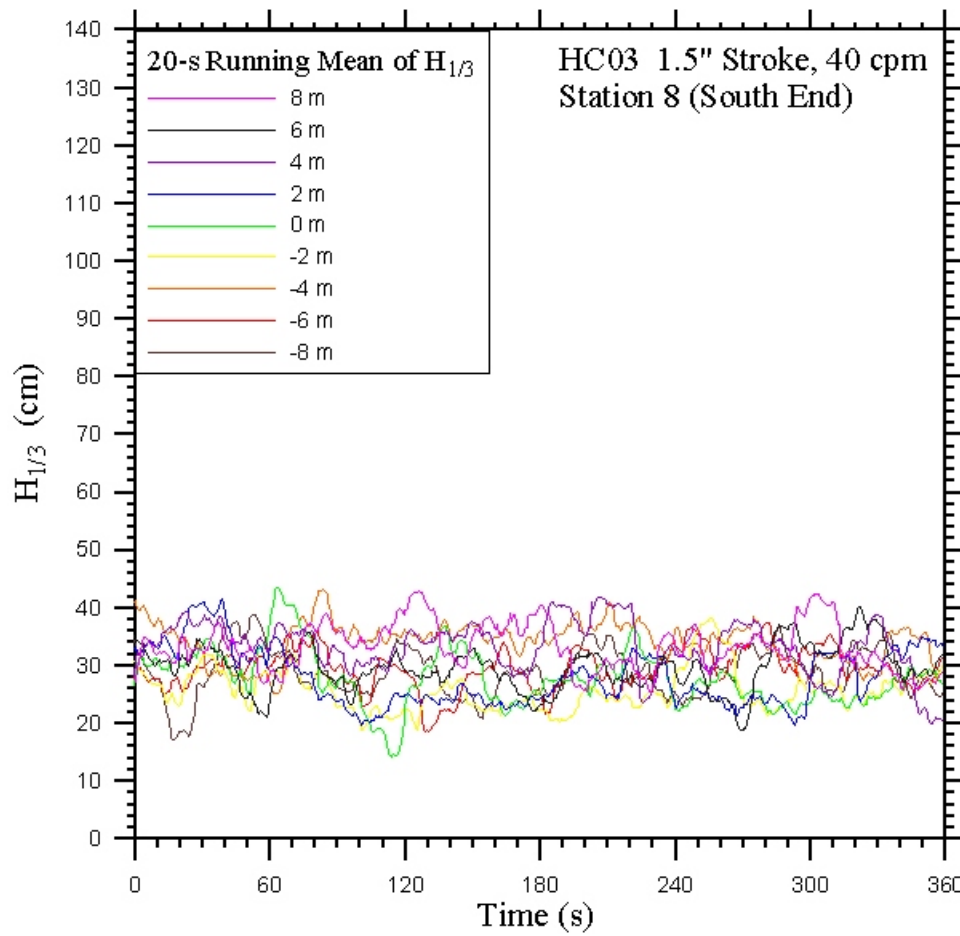


Figure 104: Time series of 20 s moving averaged of significant wave height, $H_{1/3}$, as a function of time for all nine wave probes in the main array at station 8, south end of tank. Paddle conditions for this run correspond to HC03, 1.5" stroke, 40 cpm speed.

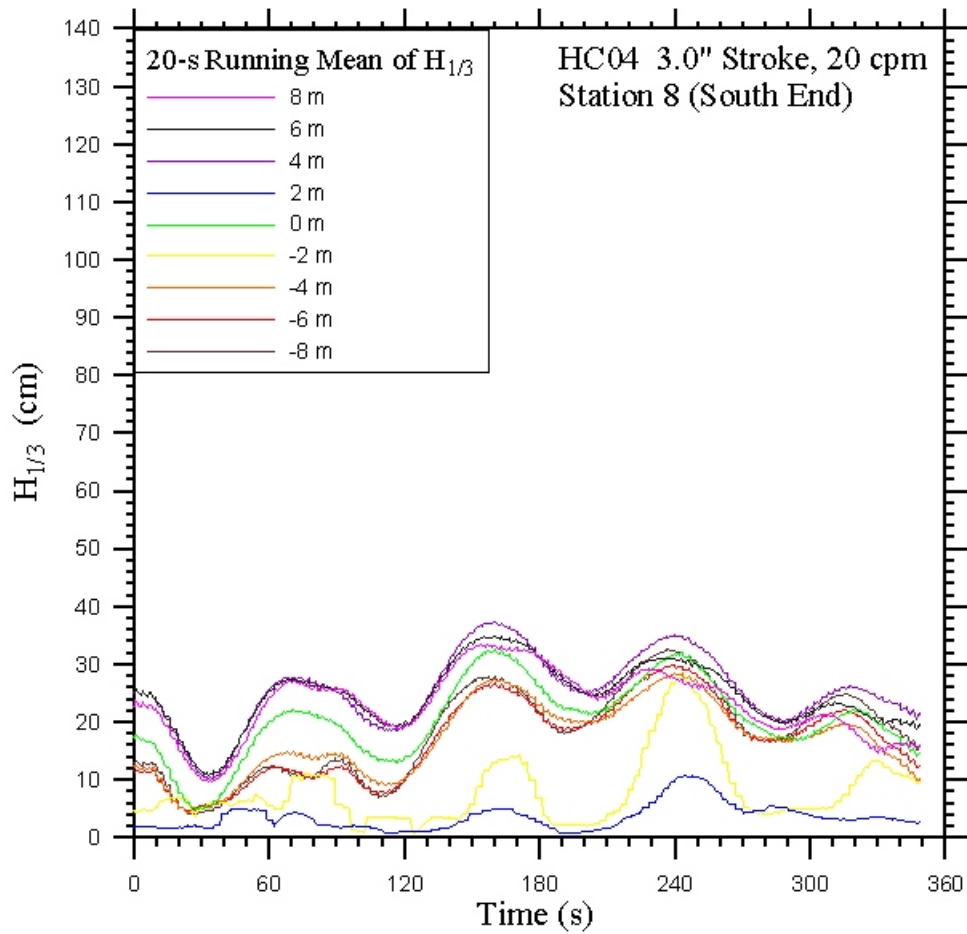


Figure 105: Time series of 20 s moving averaged of significant wave height, $H_{1/3}$, as a function of time for all nine wave probes in the main array at station 8, south end of tank. Paddle conditions for this run correspond to HC04, 3.0" stroke, 20 cpm speed.

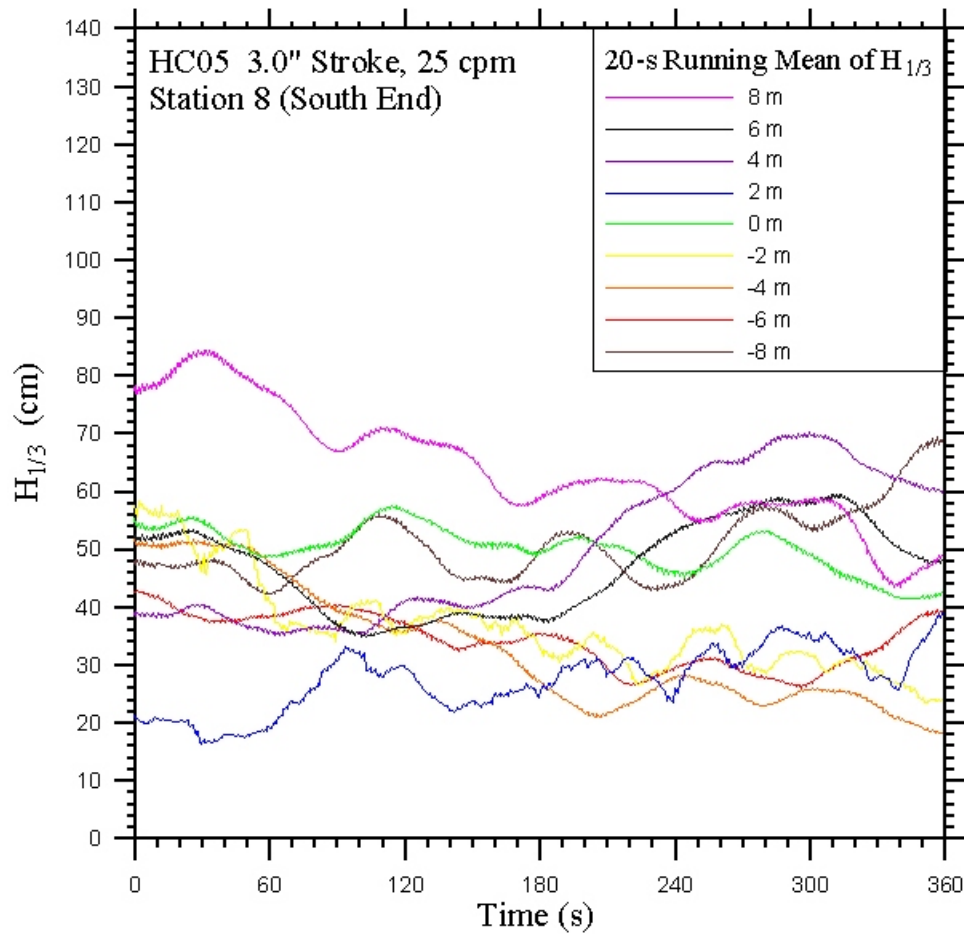


Figure 106: Time series of 20 s moving averaged of significant wave height, $H_{1/3}$, as a function of time for all nine wave probes in the main array at station 8, south end of tank. Paddle conditions for this run correspond to HC05, 3.0" stroke, 25 cpm speed.

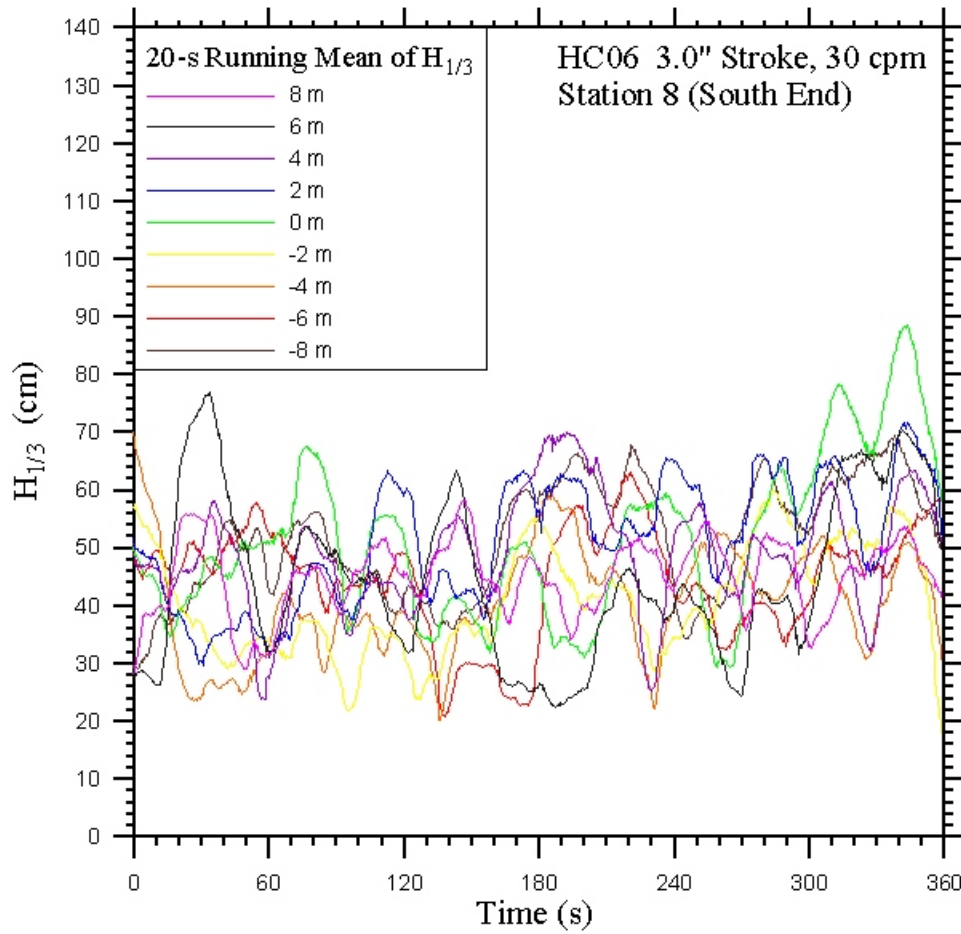


Figure 107: Time series of 20 s moving averaged of significant wave height, $H_{1/3}$, as a function of time for all nine wave probes in the main array at station 8, south end of tank. Paddle conditions for this run correspond to HC06, 3.0" stroke, 30 cpm speed.

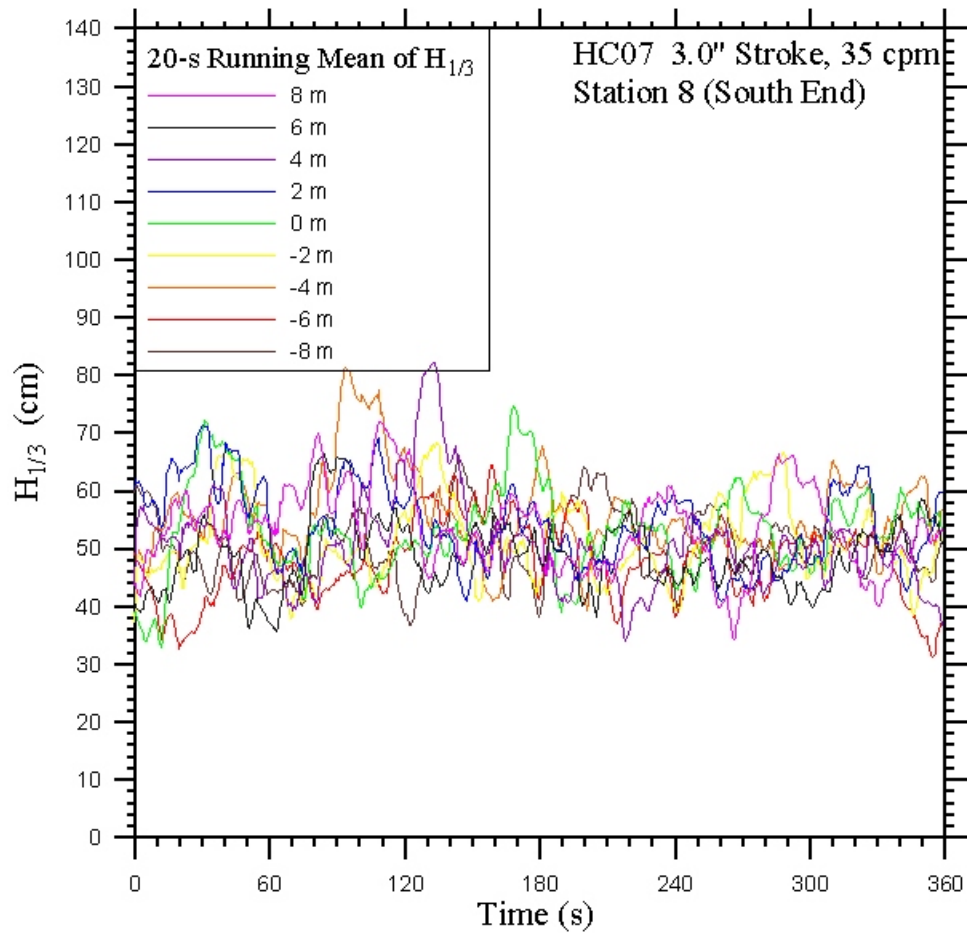


Figure 108: Time series of 20 s moving averaged of significant wave height, $H_{1/3}$, as a function of time for all nine wave probes in the main array at station 8, south end of tank. Paddle conditions for this run correspond to HC07, 4.5" stroke, 35 cpm speed.

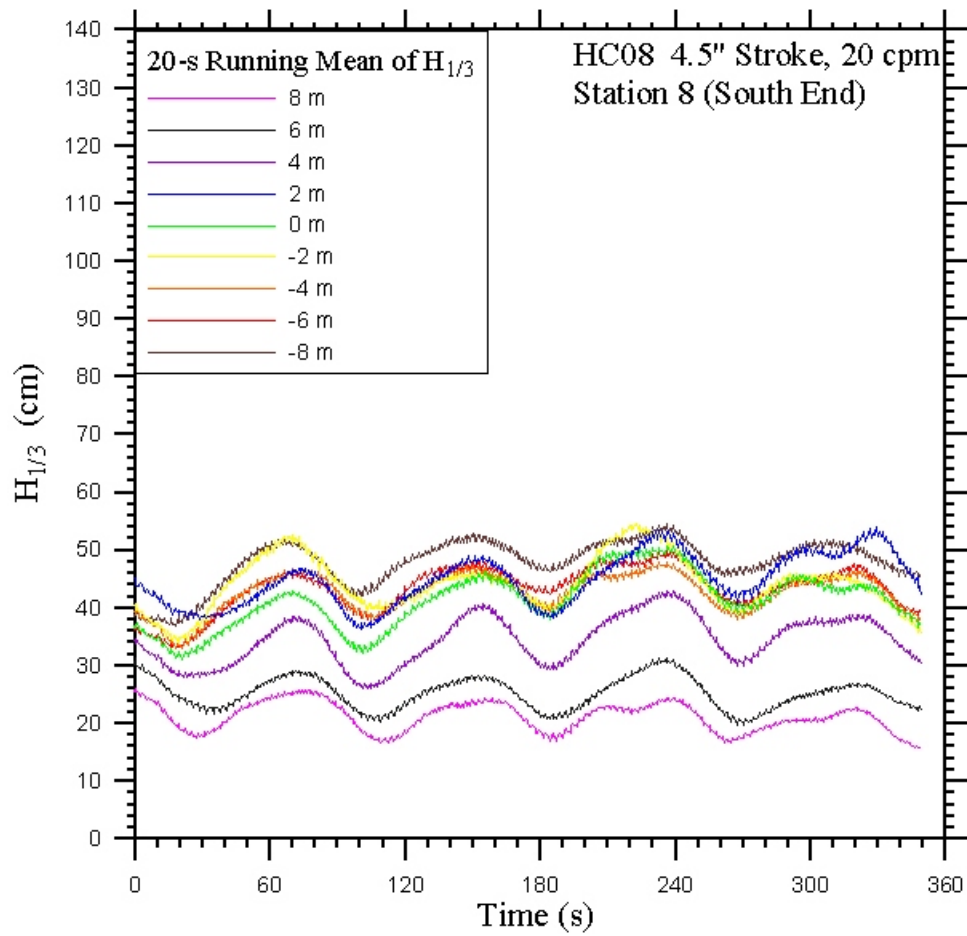


Figure 109: Time series of 20 s moving averaged of significant wave height, $H_{1/3}$, as a function of time for all nine wave probes in the main array at station 8, south end of tank. Paddle conditions for this run correspond to HC08, 4.5" stroke, 20 cpm speed.

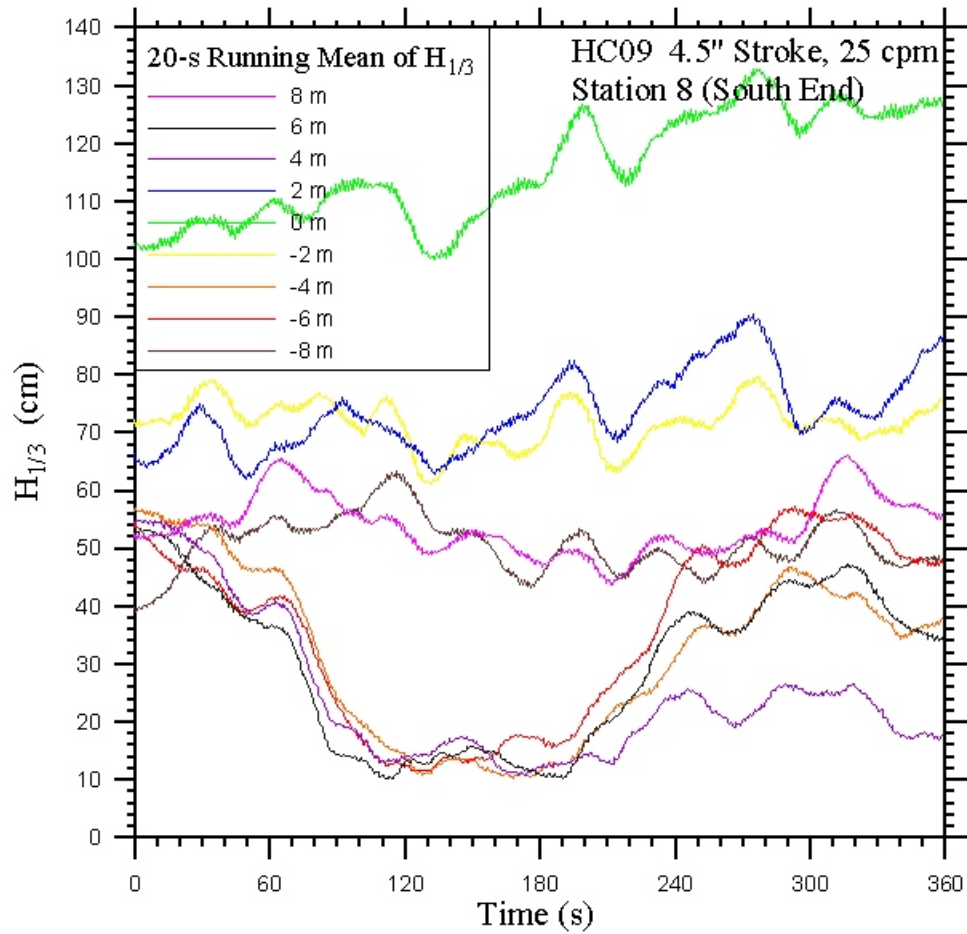


Figure 110: Time series of 20 s moving averaged of significant wave height, $H_{1/3}$, as a function of time for all nine wave probes in the main array at station 8, south end of tank. Paddle conditions for this run correspond to HC09, 4.5" stroke, 25 cpm speed.

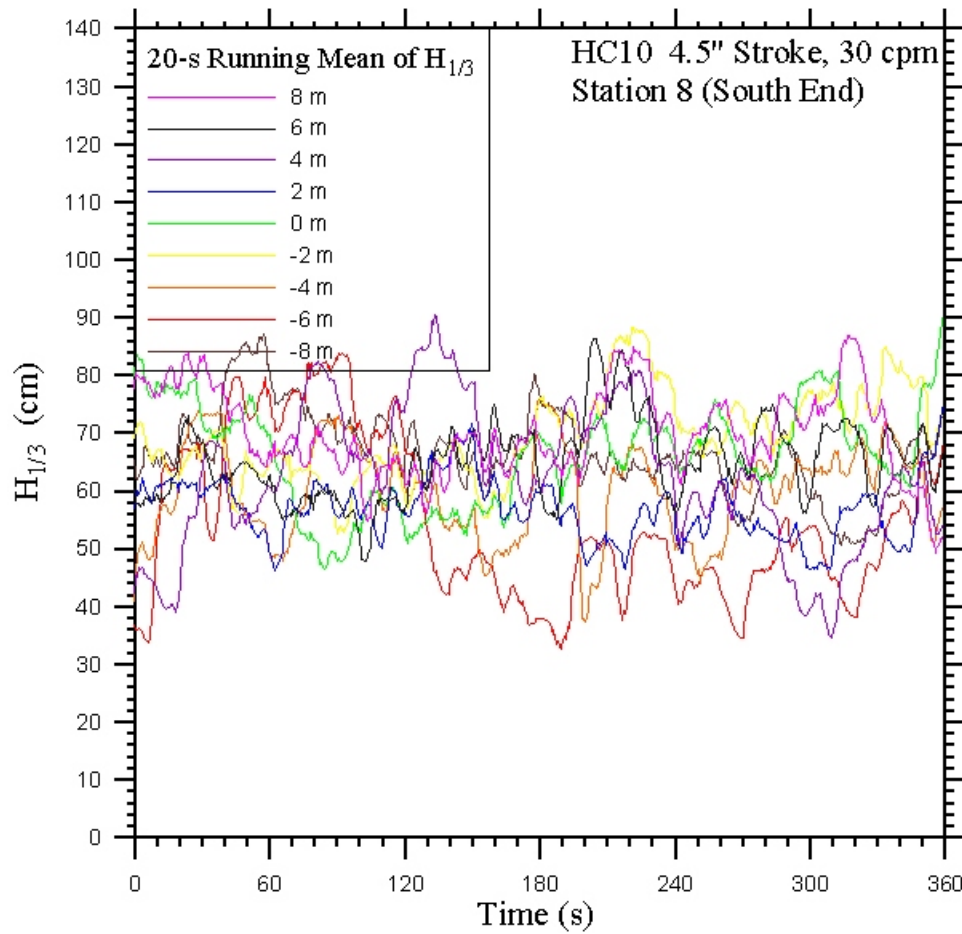


Figure 111: Time series of 20 s moving averaged of significant wave height, $H_{1/3}$, as a function of time for all nine wave probes in the main array at station 8, south end of tank. Paddle conditions for this run correspond to HC10, 4.5" stroke, 30 cpm speed.

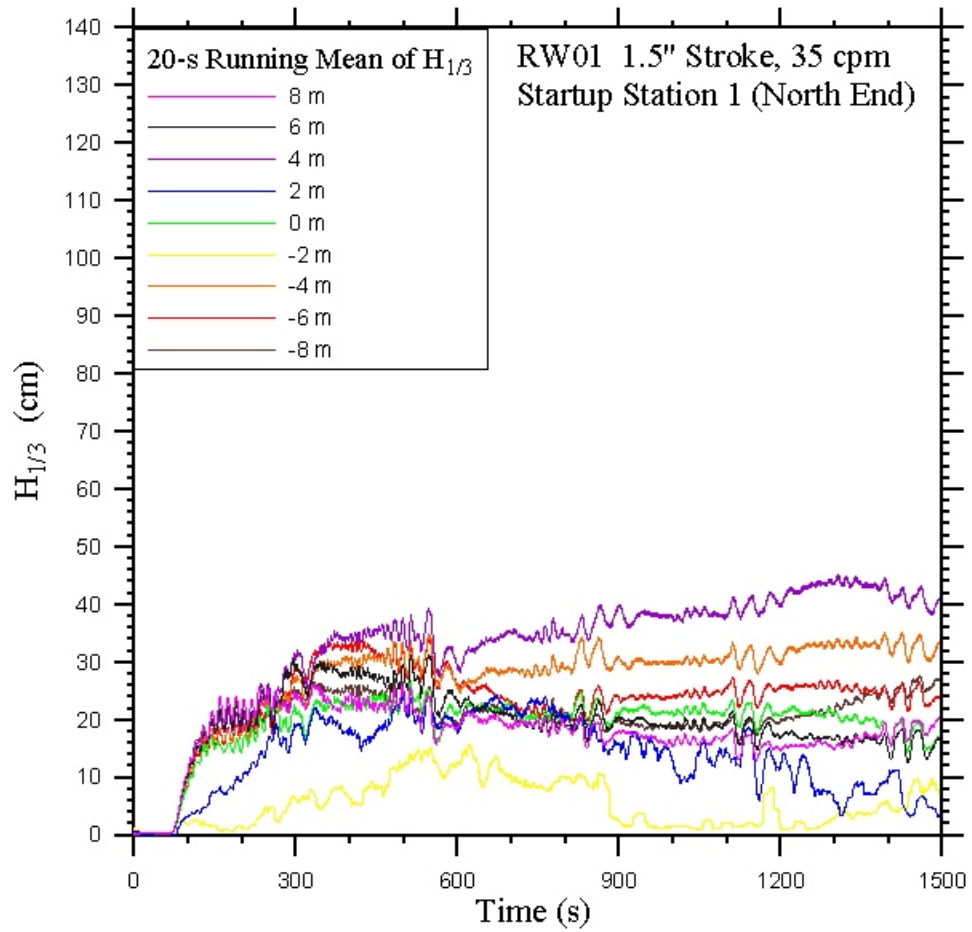


Figure 112: Time series of 20 s moving averaged estimation of significant wave height, $H_{1/3}$, as a function of time after initiation of the wave paddle. Paddle conditions for this run correspond to RW01, 1.5" stroke, 35 cpm speed.

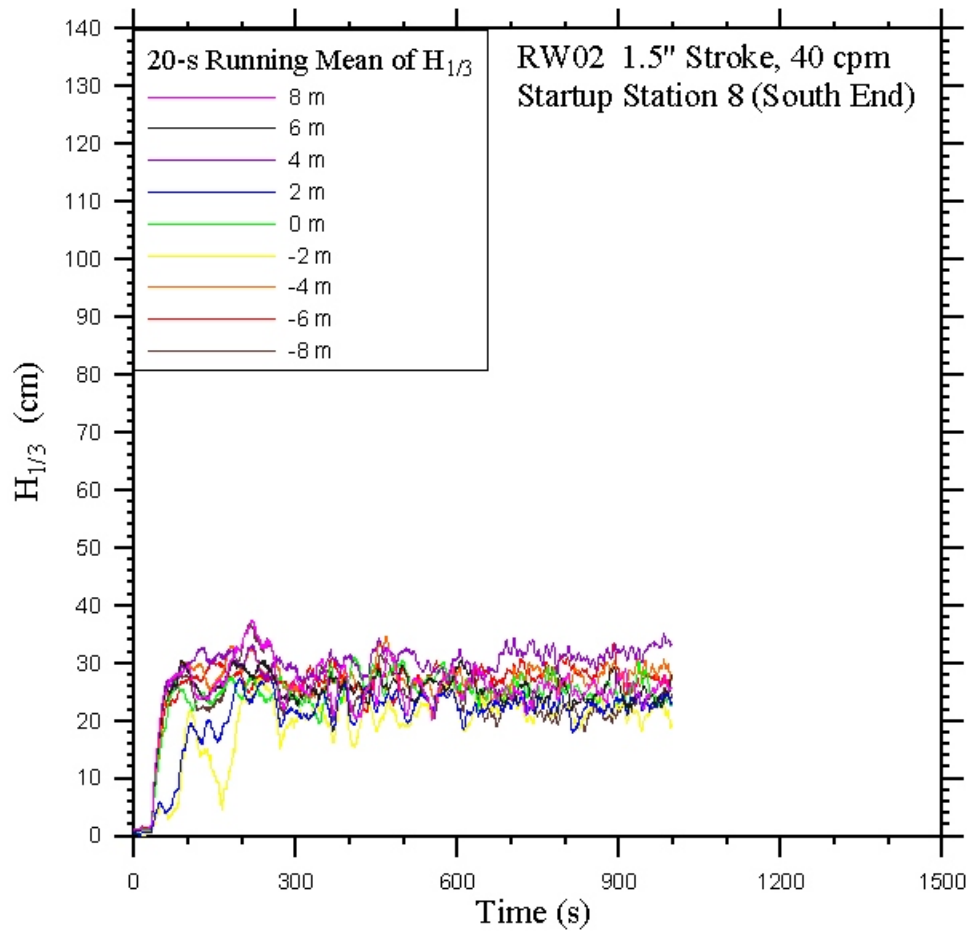


Figure 113: Time series of 20 s moving averaged estimation of significant wave height, $H_{1/3}$, as a function of time after initiation of the wave paddle. Paddle conditions for this run correspond to RW02, 1.5" stroke, 40 cpm speed.

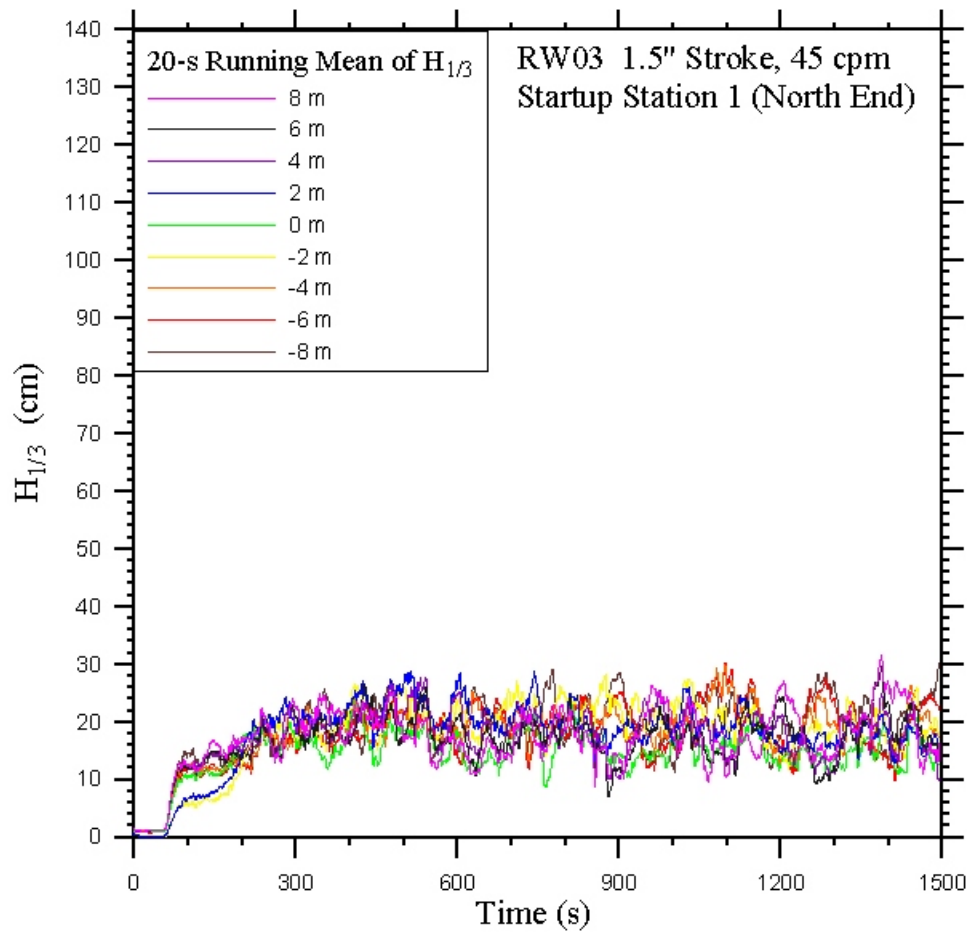


Figure 114: Time series of 20 s moving averaged estimation of significant wave height, $H_{1/3}$, as a function of time after initiation of the wave paddle. Paddle conditions for this run correspond to RW03, 1.5" stroke, 45 cpm speed.

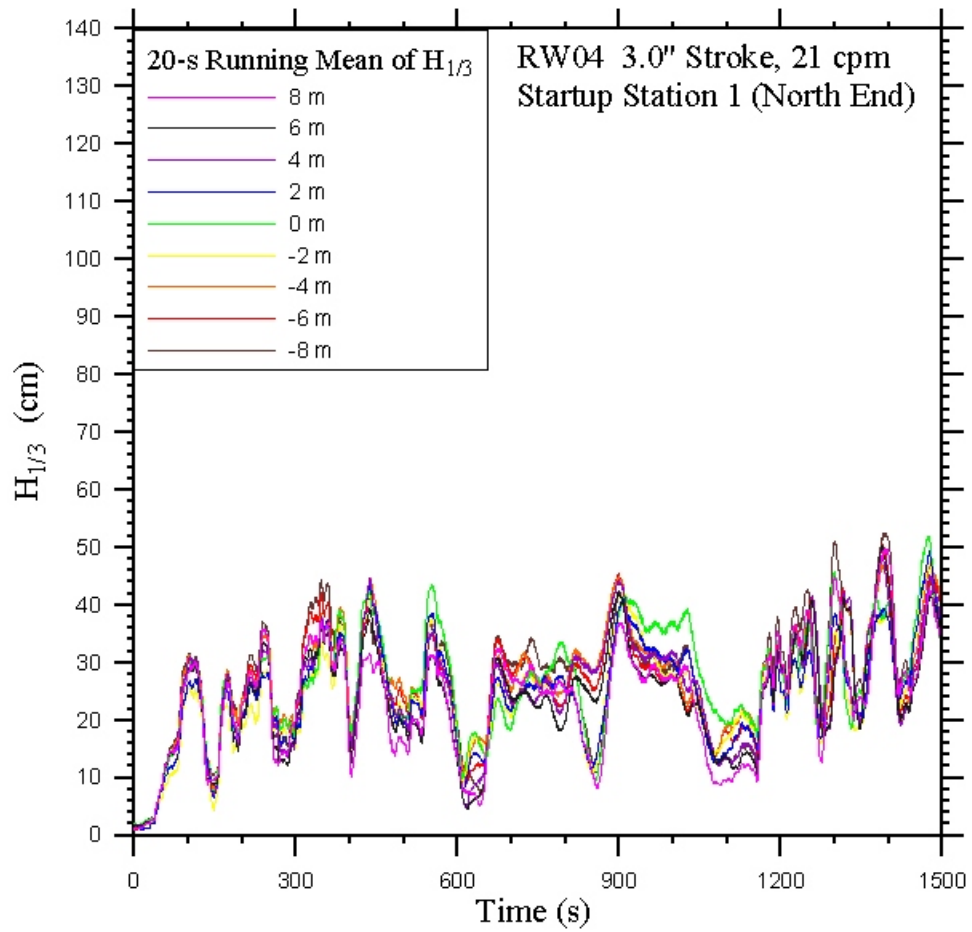


Figure 115: Time series of 20 s moving averaged estimation of significant wave height, $H_{1/3}$, as a function of time after initiation of the wave paddle. Paddle conditions for this run correspond to RW04, 3.0" stroke, 21 cpm speed.

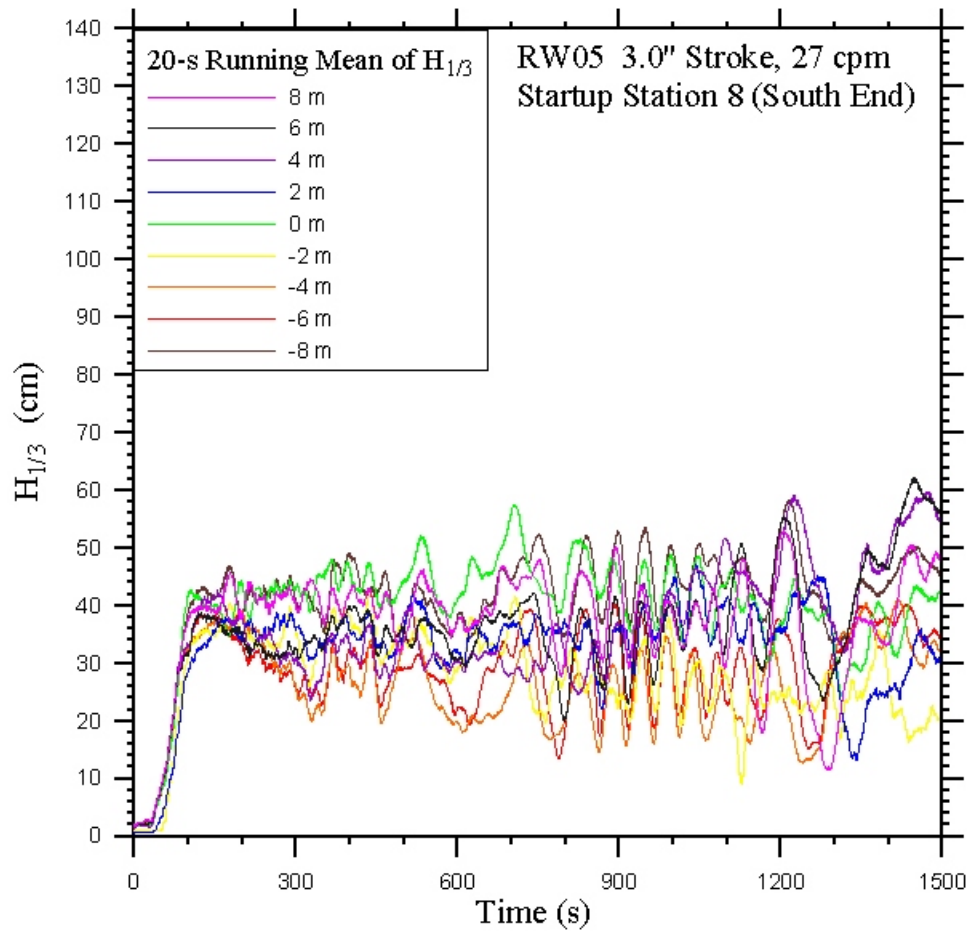


Figure 116: Time series of 20 s moving averaged estimation of significant wave height, $H_{1/3}$, as a function of time after initiation of the wave paddle. Paddle conditions for this run correspond to RW05, 3.0" stroke, 37 cpm speed.

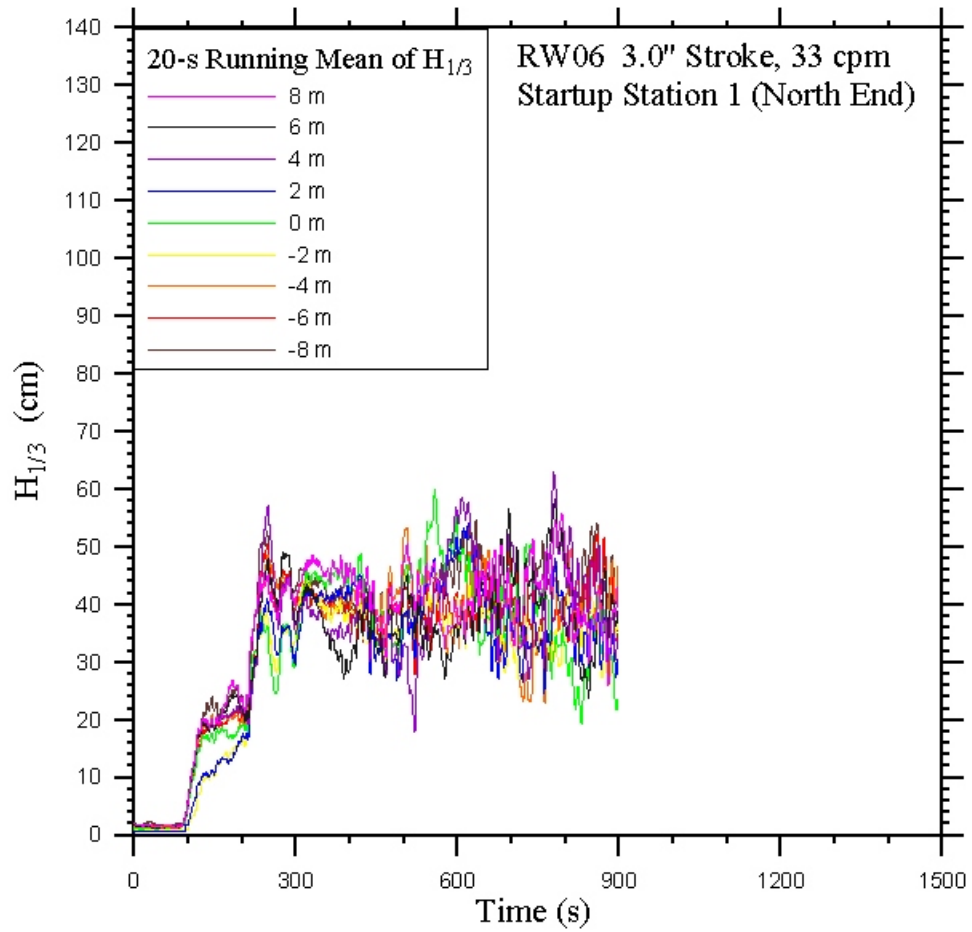


Figure 117: Time series of 20 s moving averaged estimation of significant wave height, $H_{1/3}$, as a function of time after initiation of the wave paddle. Paddle conditions for this run correspond to RW06, 3.0" stroke, 33 cpm speed.

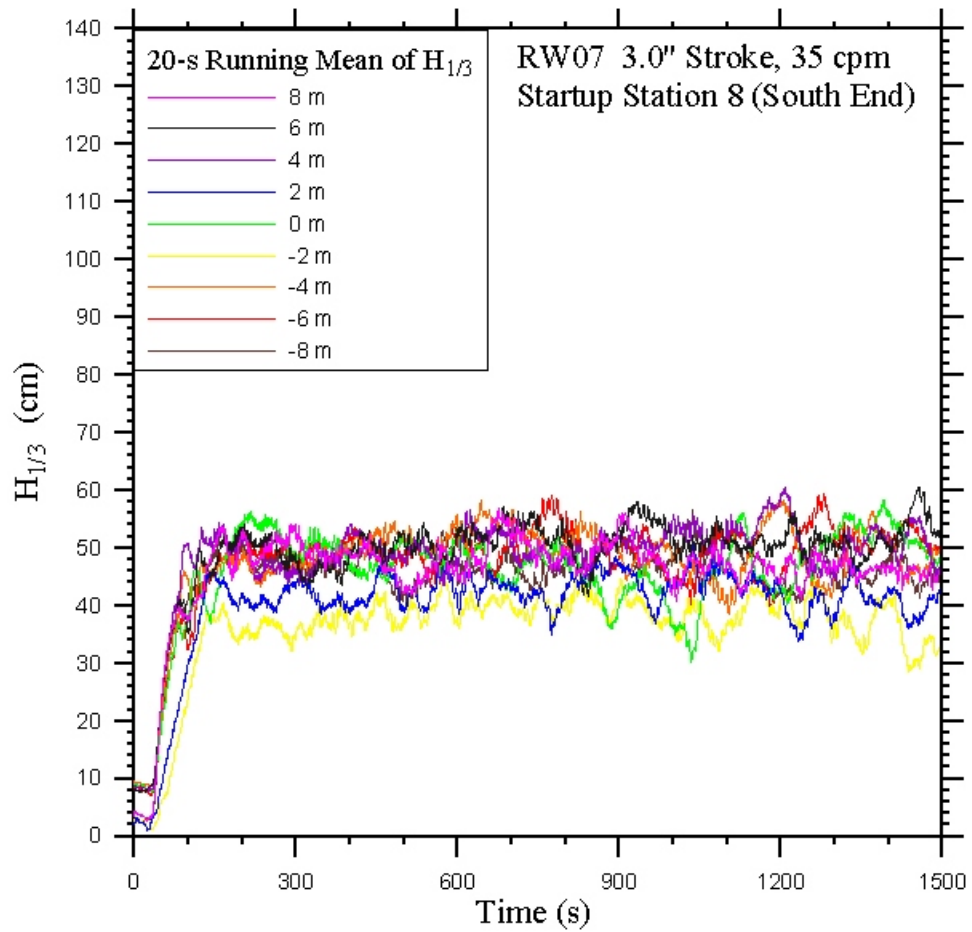


Figure 118: Time series of 20 s moving averaged estimation of significant wave height, $H_{1/3}$, as a function of time after initiation of the wave paddle. Paddle conditions for this run correspond to RW07, 3.0" stroke, 35 cpm speed.

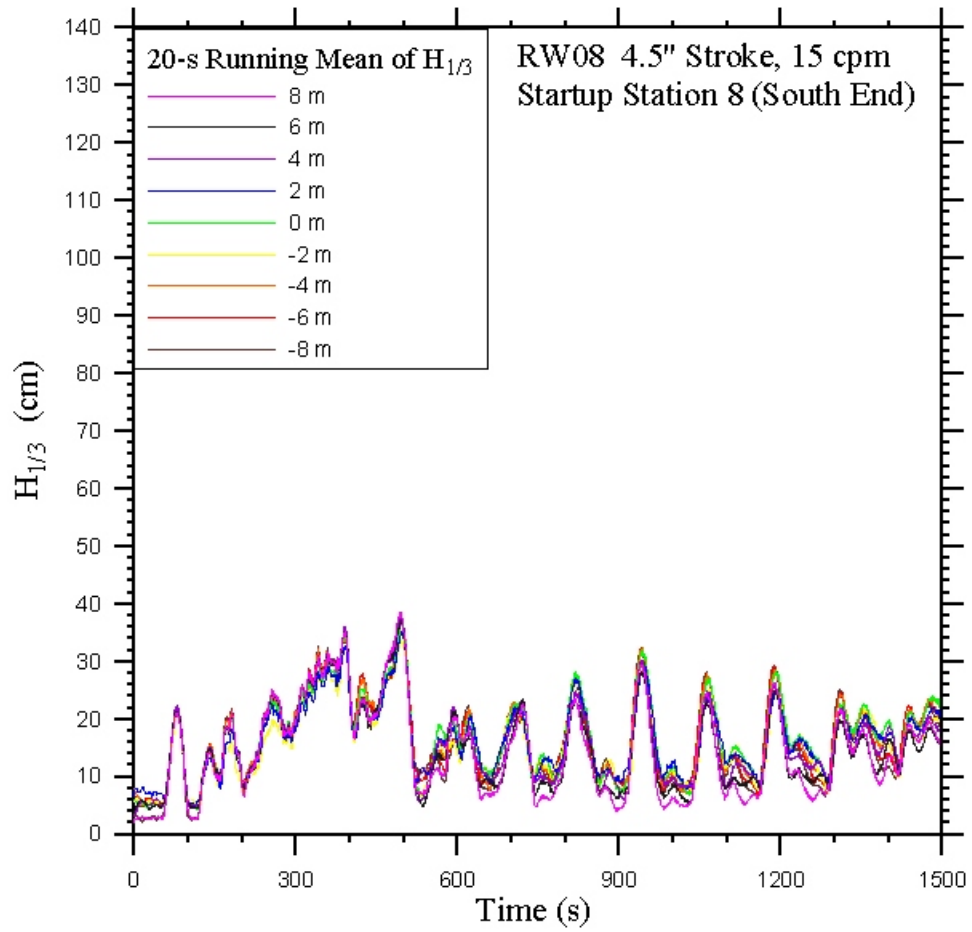


Figure 119: Time series of 20 s moving averaged estimation of significant wave height, $H_{1/3}$, as a function of time after initiation of the wave paddle. Paddle conditions for this run correspond to RW08, 4.5" stroke, 15 cpm speed.

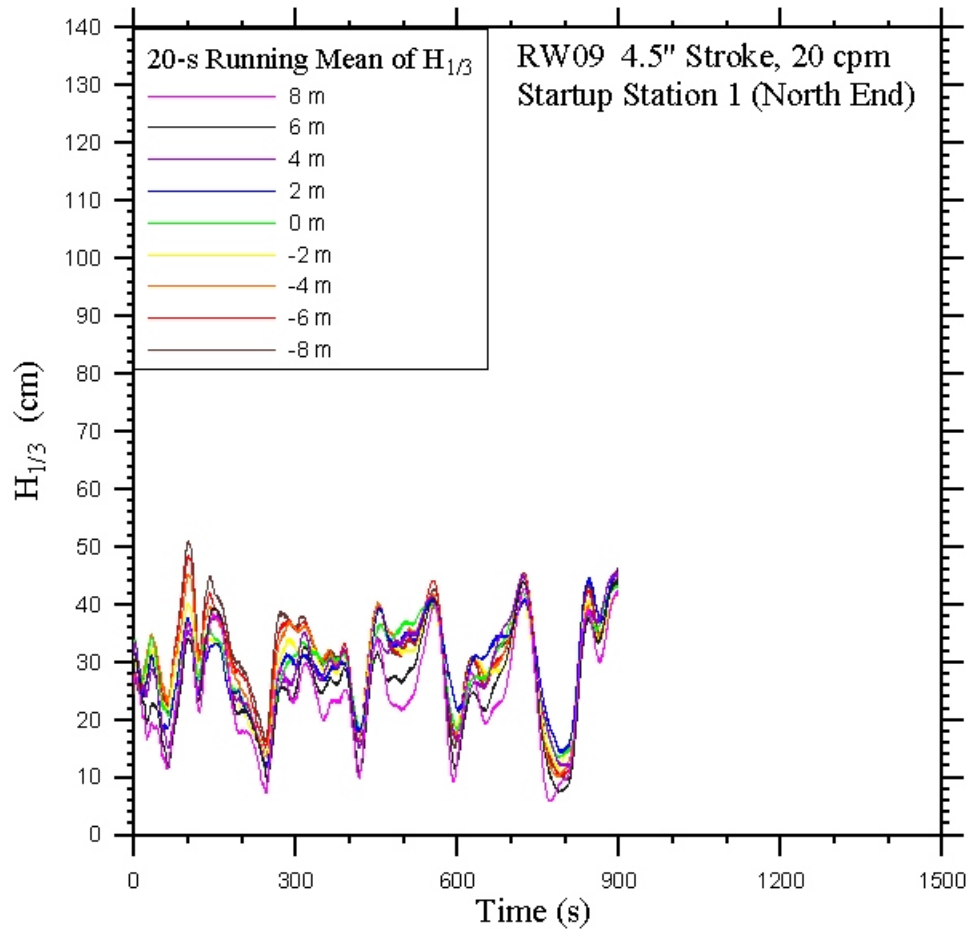


Figure 120: Time series of 20 s moving averaged estimation of significant wave height, $H_{1/3}$, as a function of time after initiation of the wave paddle. Paddle conditions for this run correspond to RW09, 4.5" stroke, 21 cpm speed.

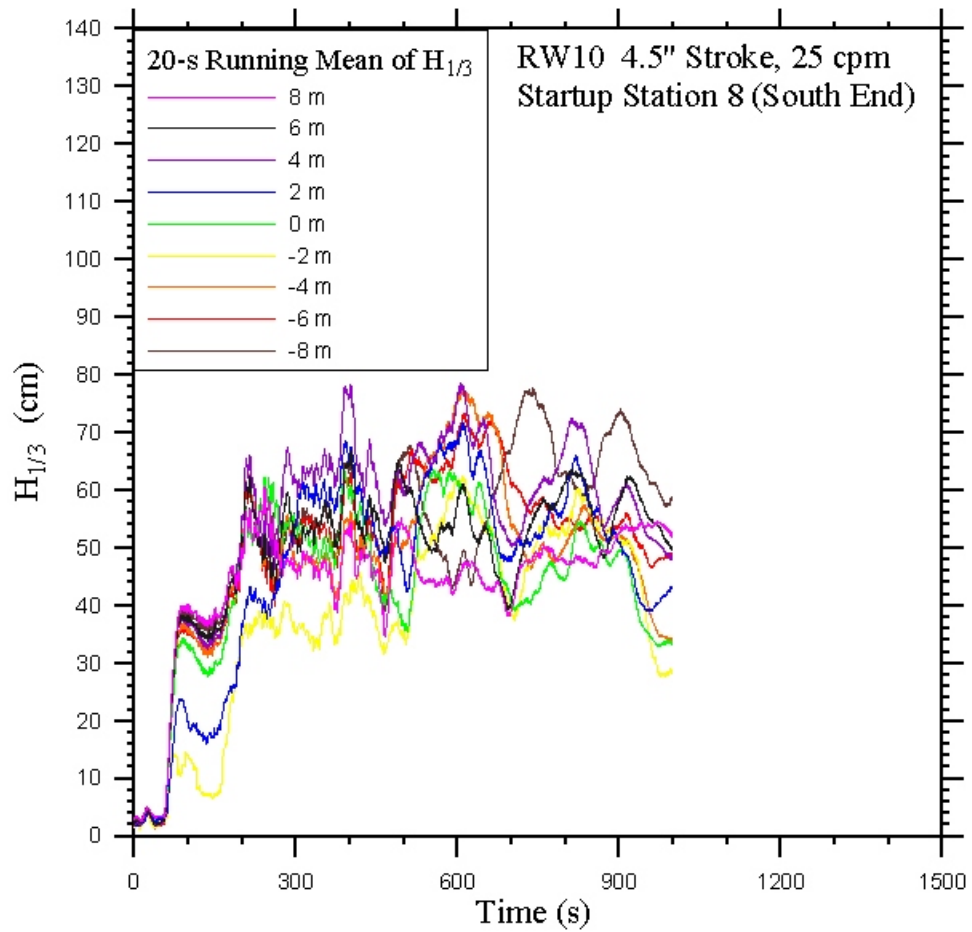


Figure 121: Time series of 20 s moving averaged estimation of significant wave height, $H_{1/3}$, as a function of time after initiation of the wave paddle. Paddle conditions for this run correspond to RW10, 4.5" stroke, 27 cpm speed.

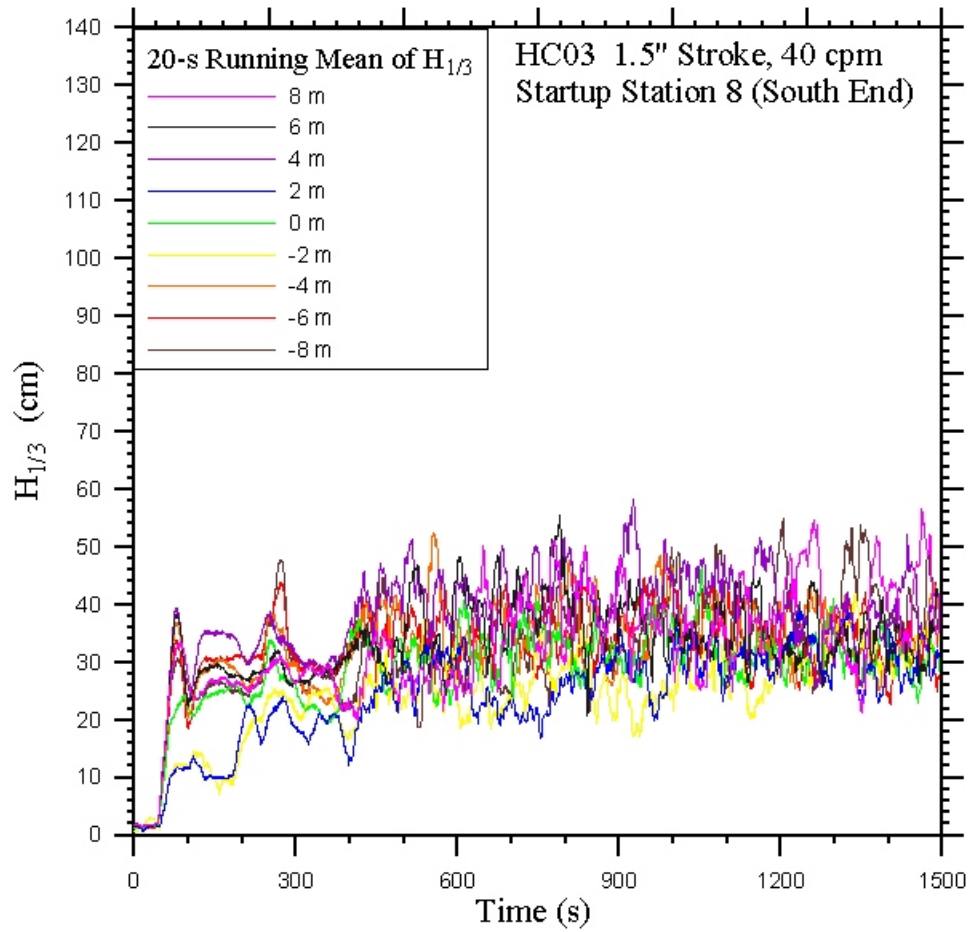


Figure 122: Time series of 20 s moving averaged estimation of significant wave height, $H_{1/3}$, as a function of time after initiation of the wave paddle. Paddle conditions for this run correspond to HC03, 1.5" stroke, 40 cpm speed.

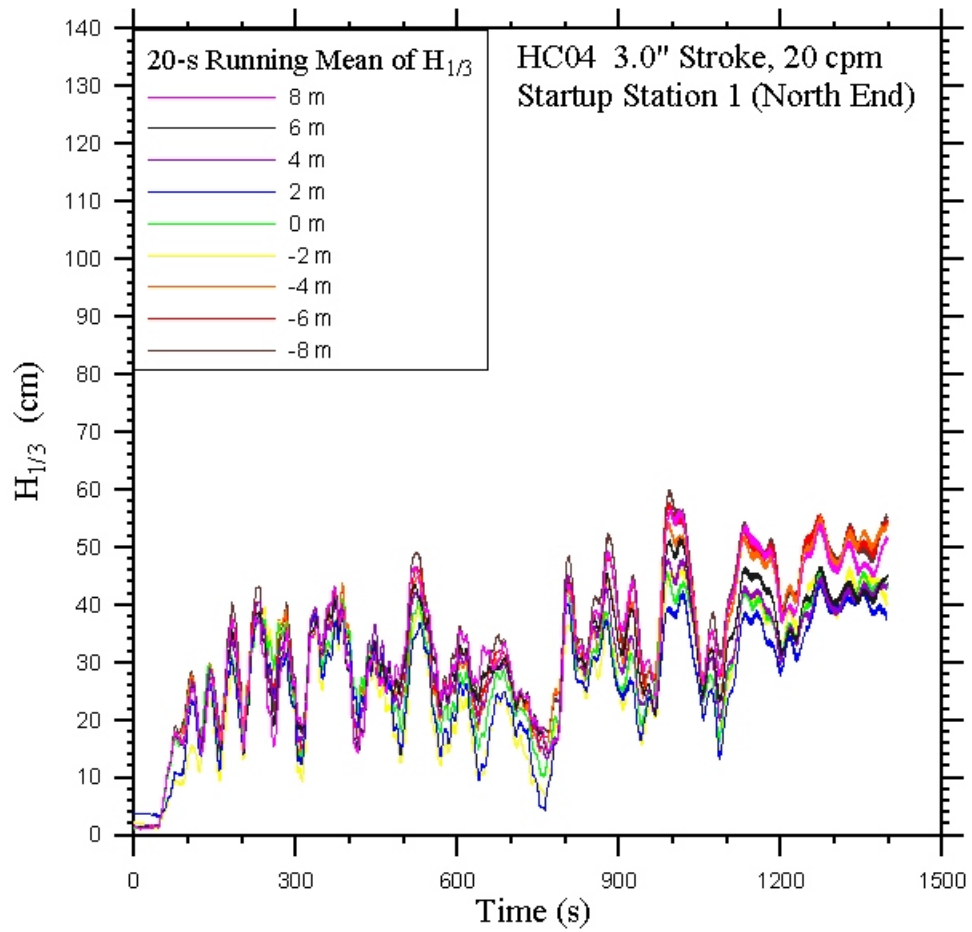


Figure 123: Time series of 20 s moving averaged estimation of significant wave height, $H_{1/3}$, as a function of time after initiation of the wave paddle. Paddle conditions for this run correspond to HC04, 3.0" stroke, 20 cpm speed.

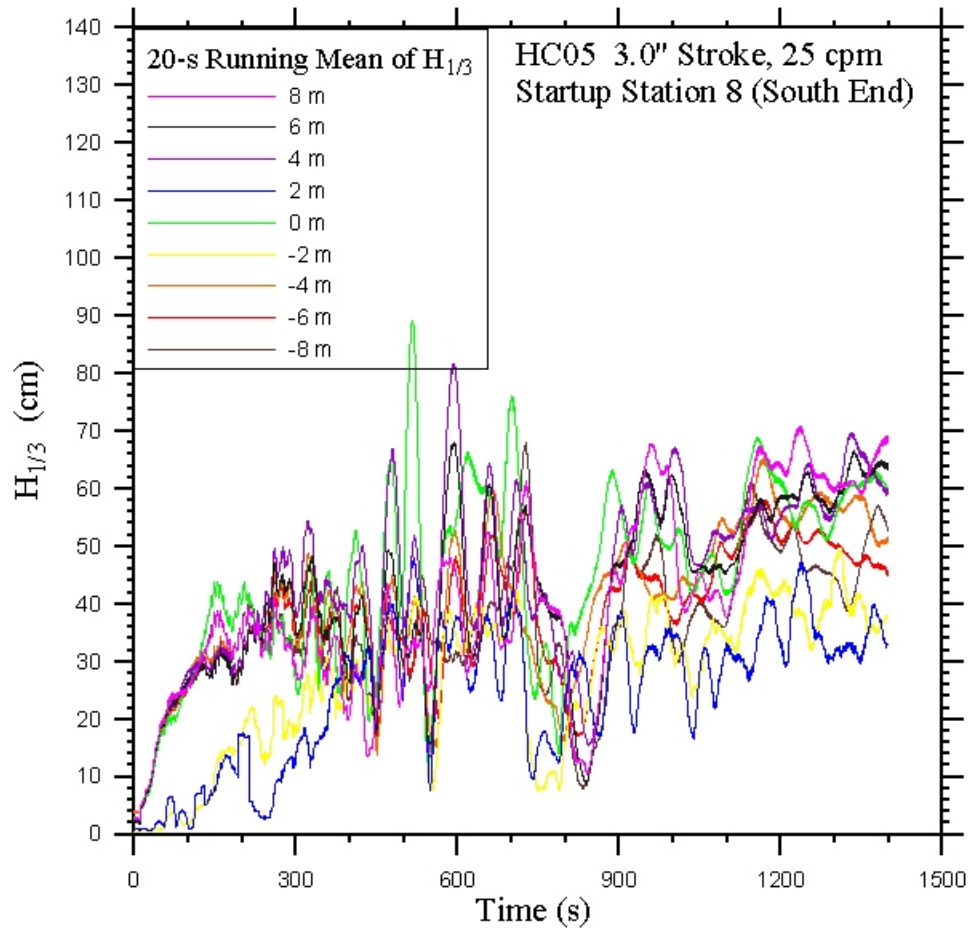


Figure 124: Time series of 20 s moving averaged estimation of significant wave height, $H_{1/3}$, as a function of time after initiation of the wave paddle. Paddle conditions for this run correspond to HC05, 3.0" stroke, 25 cpm speed.

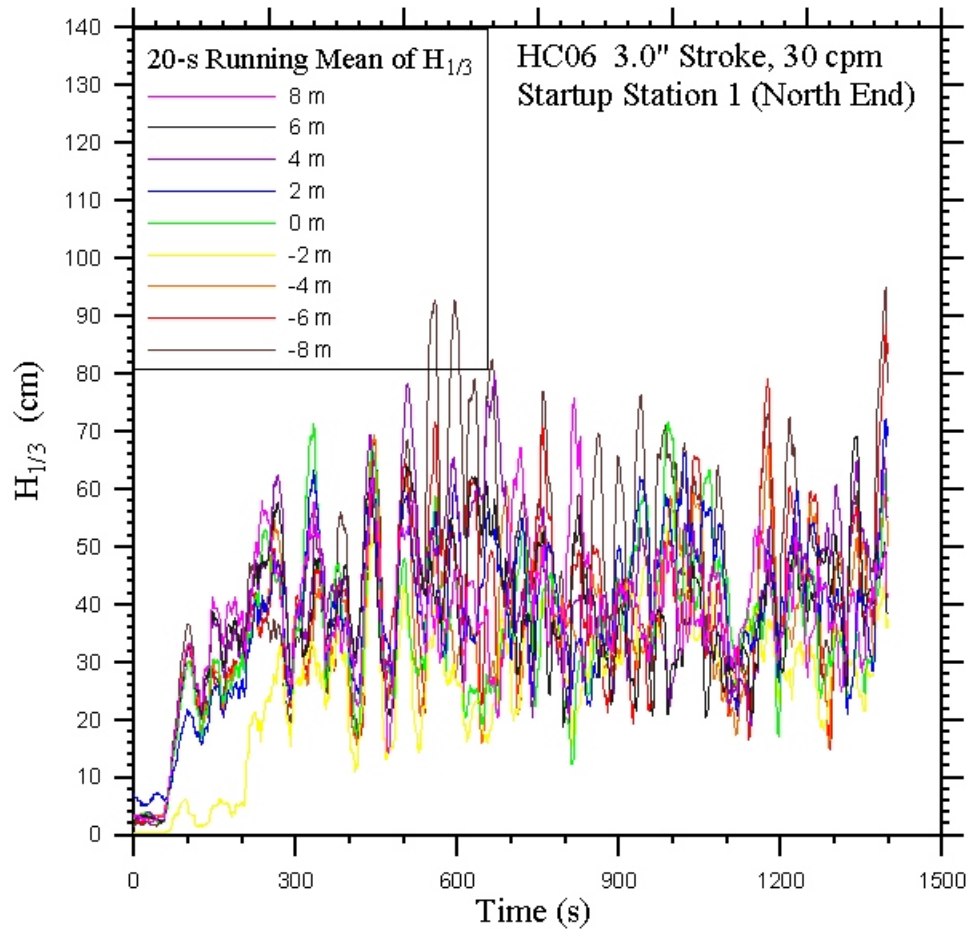


Figure 125: Time series of 20 s moving averaged estimation of significant wave height, $H_{1/3}$, as a function of time after initiation of the wave paddle. Paddle conditions for this run correspond to HC06, 3.0" stroke, 30 cpm speed.

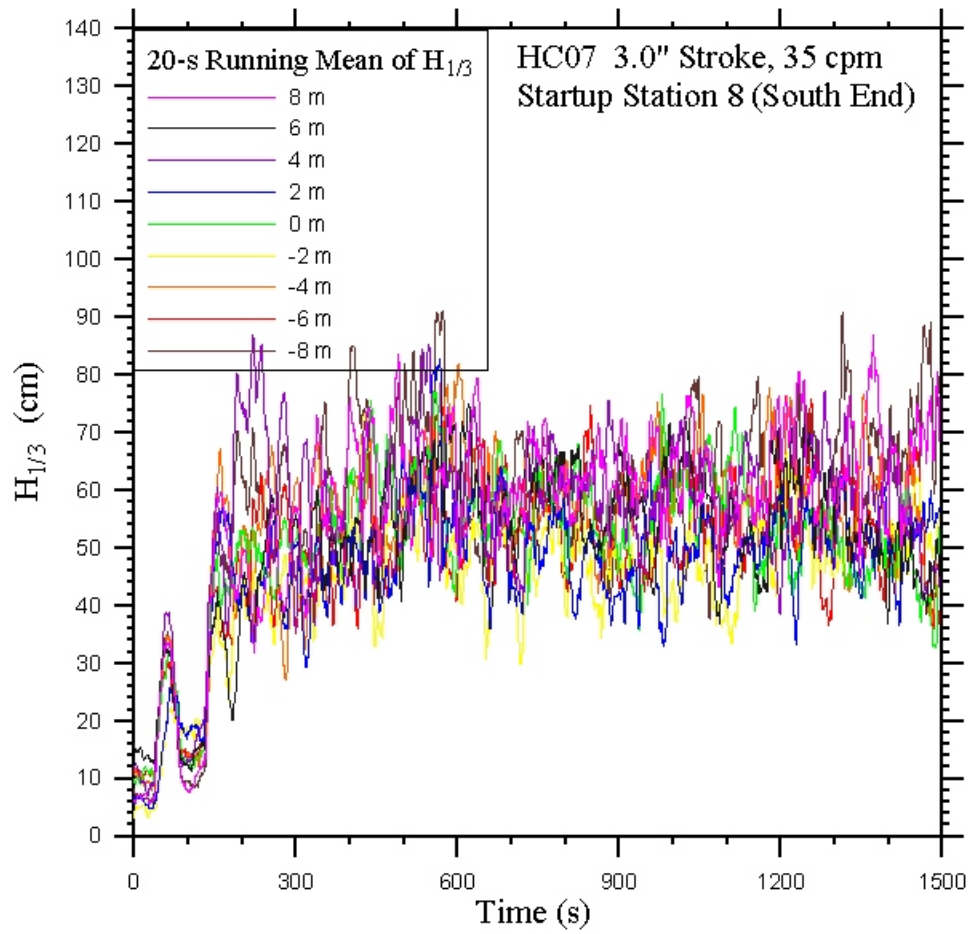


Figure 126: Time series of 20 s moving averaged estimation of significant wave height, $H_{1/3}$, as a function of time after initiation of the wave paddle. Paddle conditions for this run correspond to HC07, 4.5" stroke, 35 cpm speed.

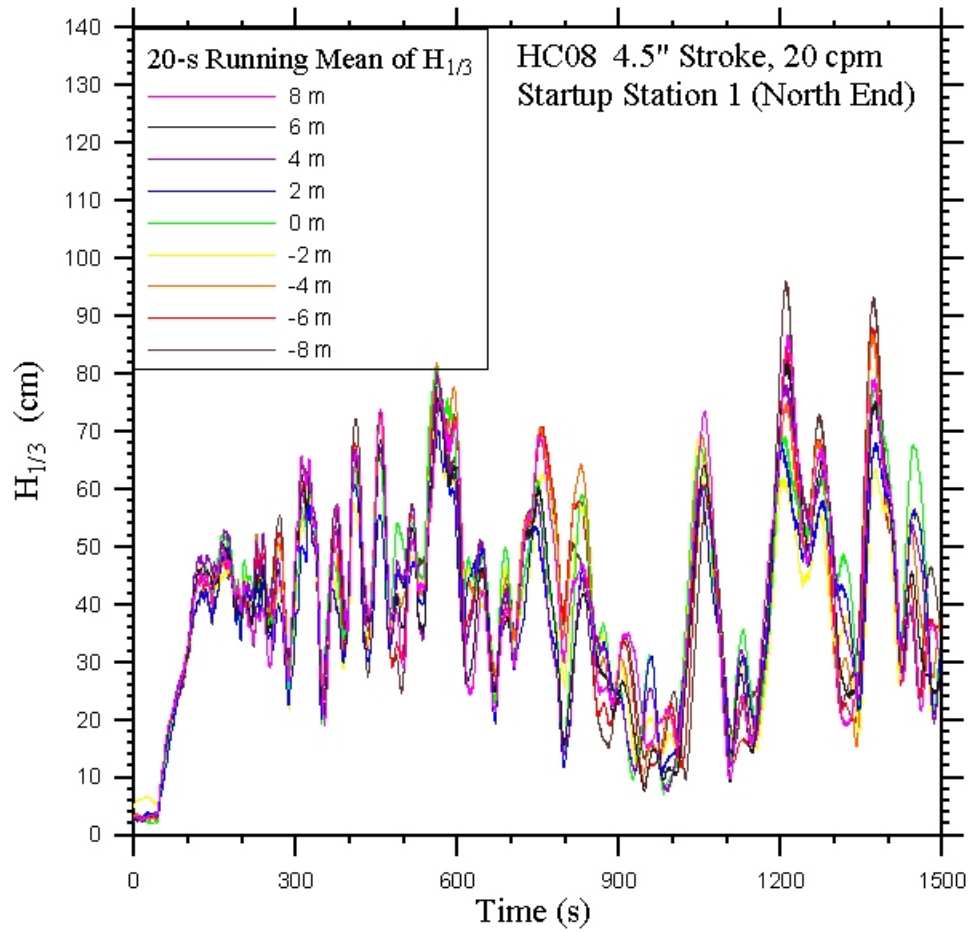


Figure 127: Time series of 20 s moving averaged estimation of significant wave height, $H_{1/3}$, as a function of time after initiation of the wave paddle. Paddle conditions for this run correspond to HC08, 4.5" stroke, 20 cpm speed.

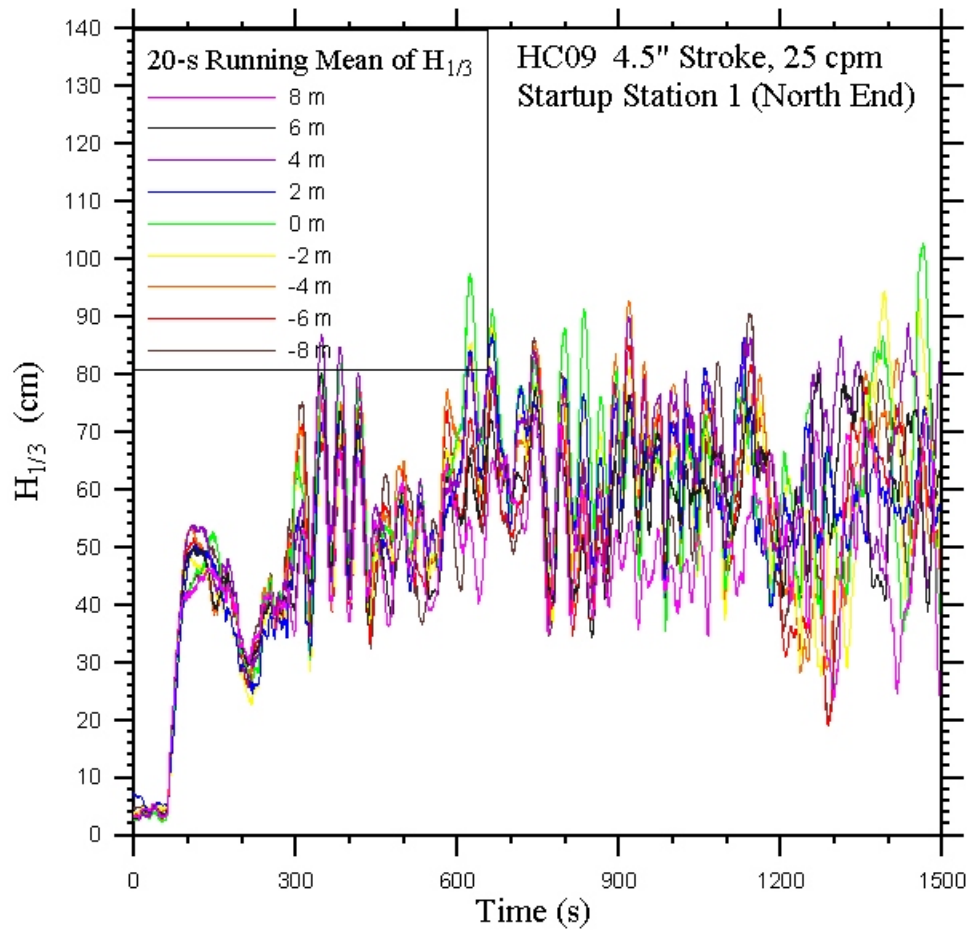


Figure 128: Time series of 20 s moving averaged estimation of significant wave height, $H_{1/3}$, as a function of time after initiation of the wave paddle. Paddle conditions for this run correspond to HC09, 4.5" stroke, 25 cpm speed.

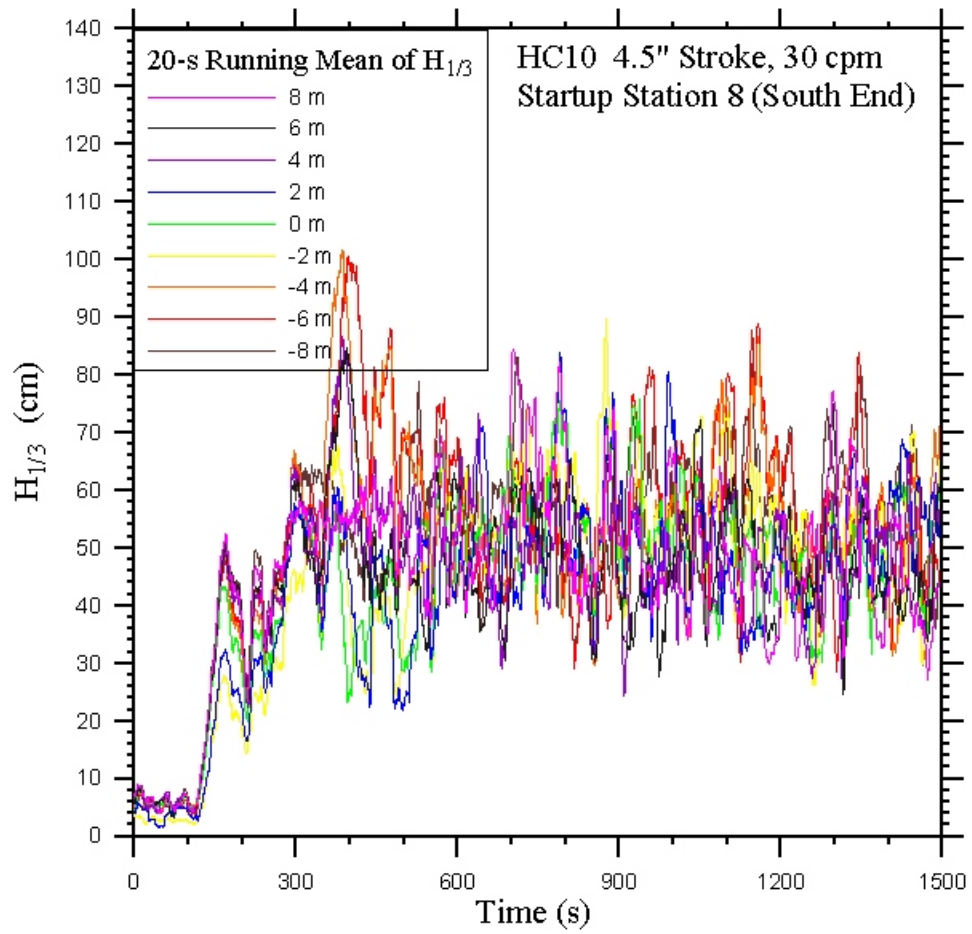


Figure 129: Time series of 20 s moving averaged estimation of significant wave height, $H_{1/3}$, as a function of time after initiation of the wave paddle. Paddle conditions for this run correspond to HC10, 4.5" stroke, 30 cpm speed.

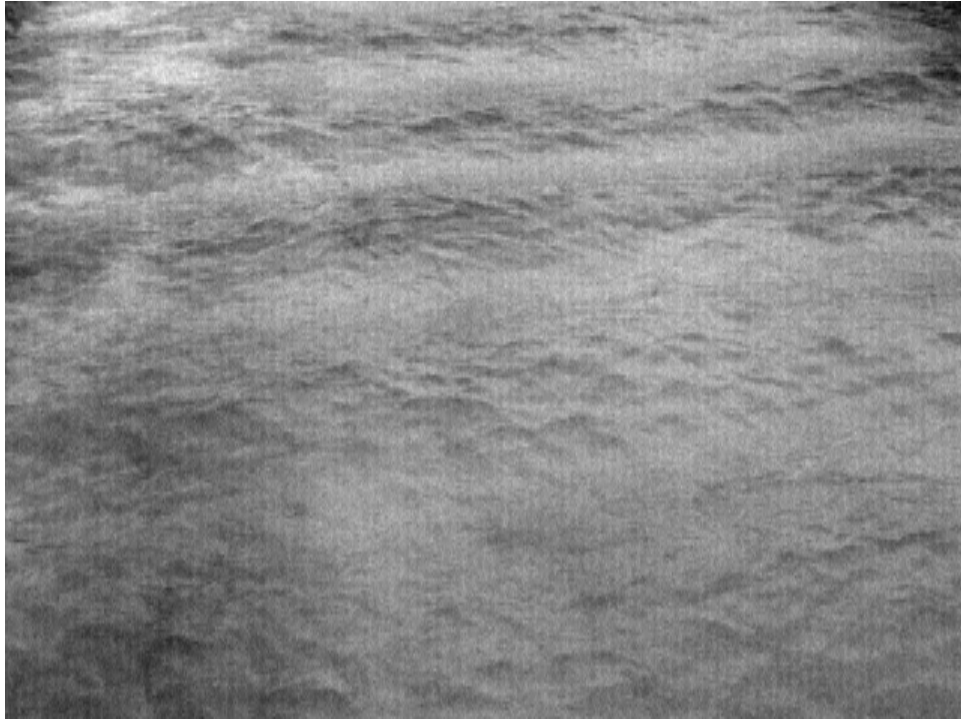


Figure 130: Typical video image available from the wave characterization experiment taken looking southward from Station 4. Paddle conditions for this run correspond to RW06, 3.0" stroke, 33 cpm speed.



Figure 131: Typical video image available from the wave characterization experiment taken looking southward from Station 4. Paddle conditions for this run correspond to RW07, 3.0" stroke, 35 cpm speed.

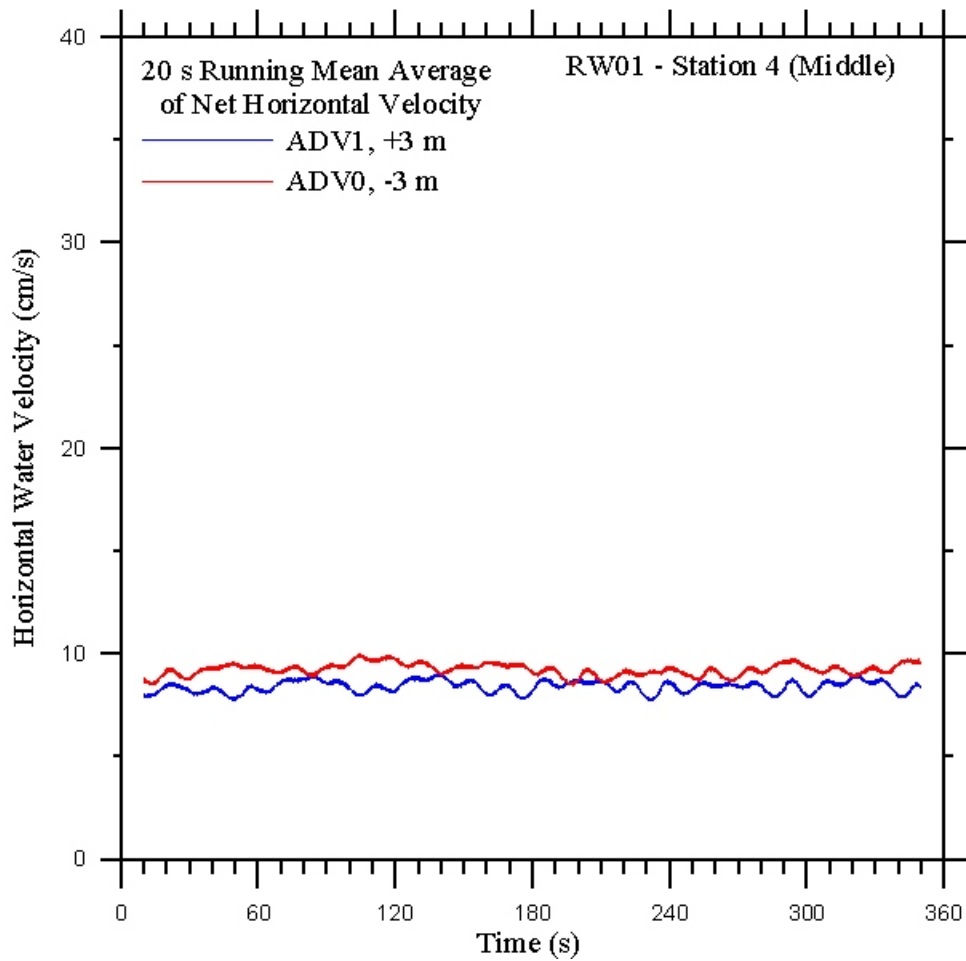


Figure 132: Horizontal surface currents measured by the two acoustic-Doppler velocimeters in the main instrument array at a depth of 50 cm below the mean water level. The data shown are 20-s running mean averages of the horizontal velocities calculated using Eq. 4 at station 4. Paddle conditions for this run correspond to RW01, 1.5" stroke, 35 cpm speed.

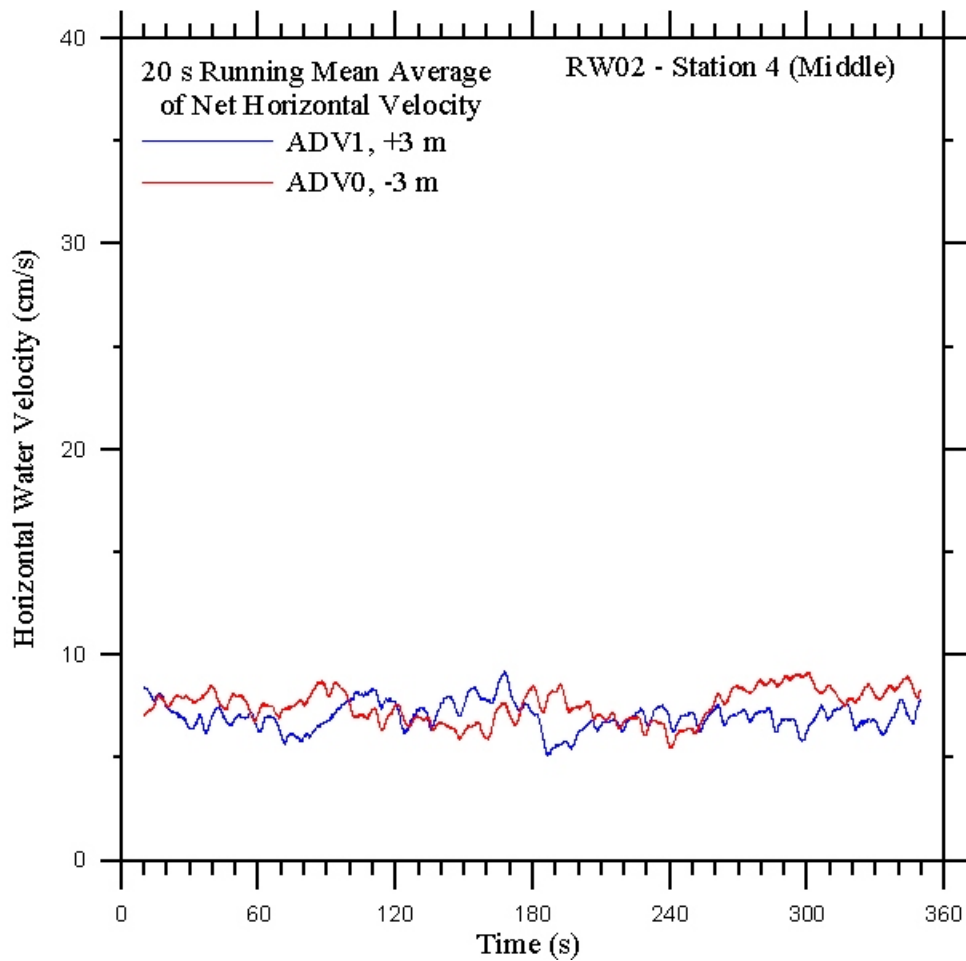


Figure 133: Horizontal surface currents measured by the two acoustic-Doppler velocimeters in the main instrument array at a depth of 50 cm below the mean water level. The data shown are 20-s running mean averages of the horizontal velocities calculated using Eq. 4 at station 4. Paddle conditions for this run correspond to RW02, 1.5" stroke, 40 cpm speed.

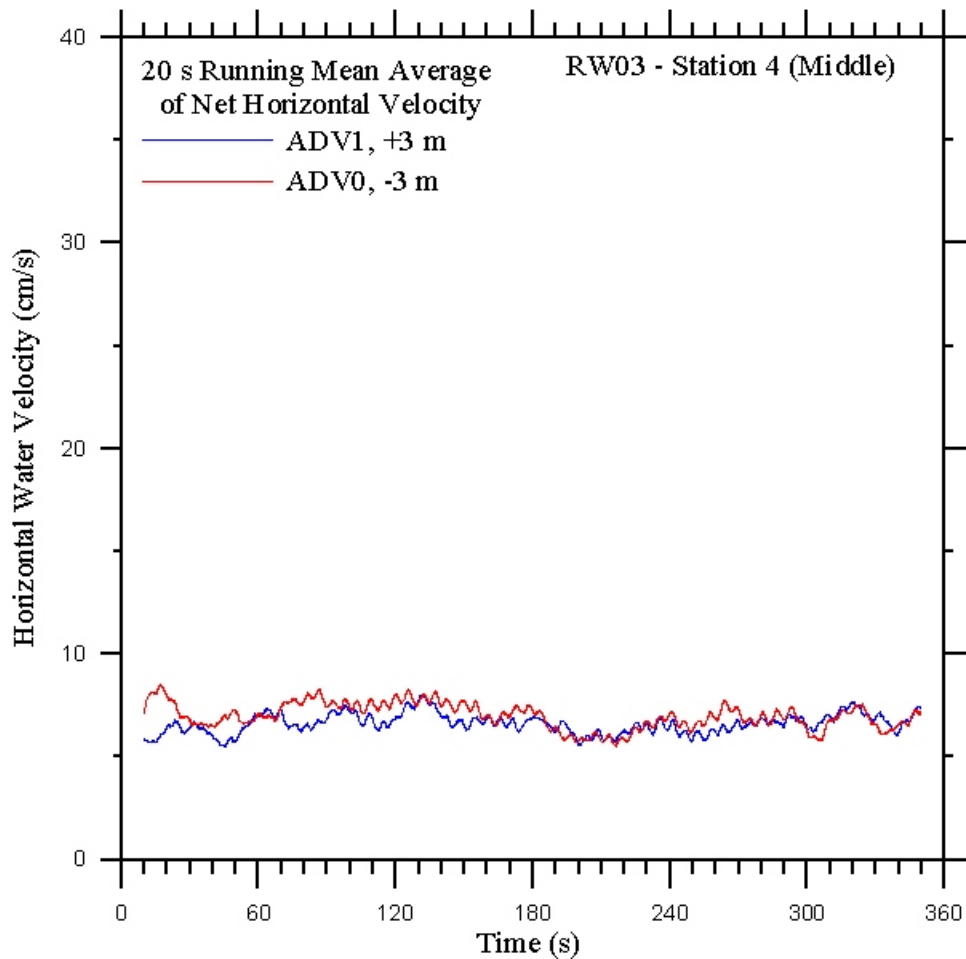


Figure 134: Horizontal surface currents measured by the two acoustic-Doppler velocimeters in the main instrument array at a depth of 50 cm below the mean water level. The data shown are 20-s running mean averages of the horizontal velocities calculated using Eq. 4 at station 4. Paddle conditions for this run correspond to RW03, 1.5" stroke, 45 cpm speed.

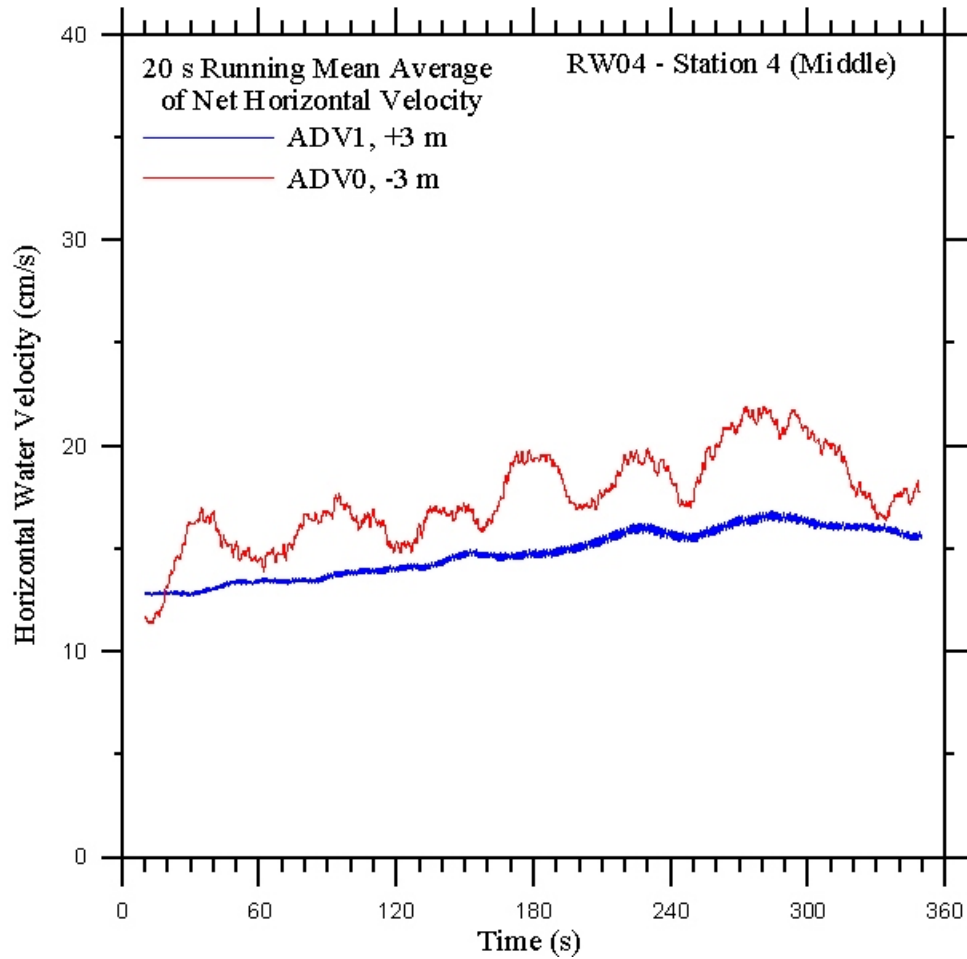


Figure 135: Horizontal surface currents measured by the two acoustic-Doppler velocimeters in the main instrument array at a depth of 50 cm below the mean water level. The data shown are 20-s running mean averages of the horizontal velocities calculated using Eq. 4 at station 4. Paddle conditions for this run correspond to RW04, 3.0" stroke, 21 cpm speed.

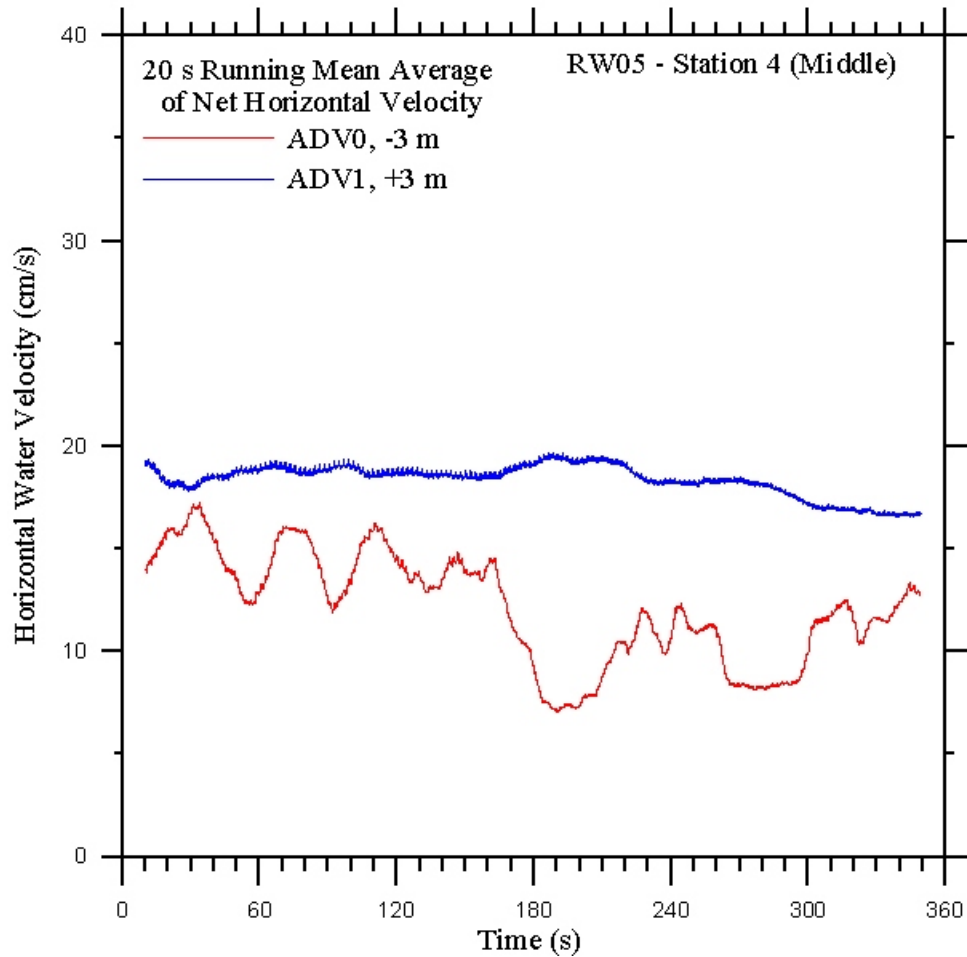


Figure 136: Horizontal surface currents measured by the two acoustic-Doppler velocimeters in the main instrument array at a depth of 50 cm below the mean water level. The data shown are 20-s running mean averages of the horizontal velocities calculated using Eq. 4 at station 4. Paddle conditions for this run correspond to RW05, 3.0" stroke, 27 cpm speed.

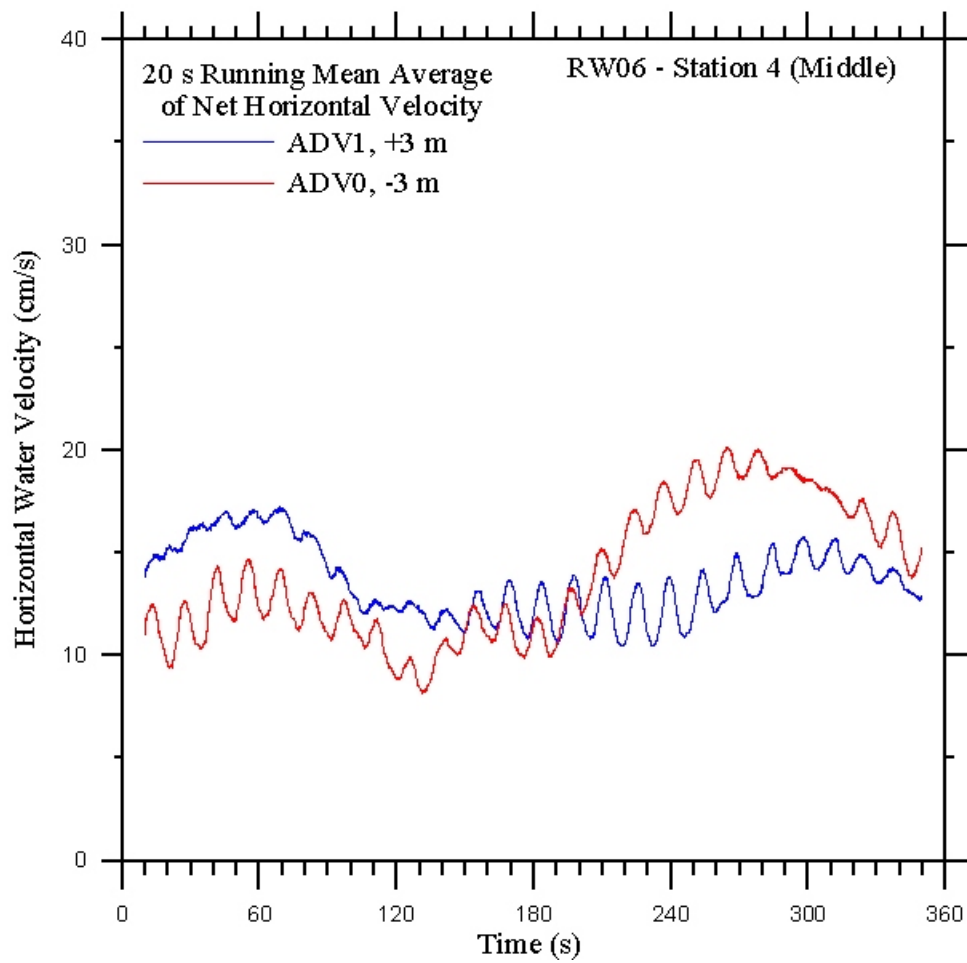


Figure 137: Horizontal surface currents measured by the two acoustic-Doppler velocimeters in the main instrument array at a depth of 50 cm below the mean water level. The data shown are 20-s running mean averages of the horizontal velocities calculated using Eq. 4 at station 4. Paddle conditions for this run correspond to RW06, 3.0" stroke, 33 cpm speed.

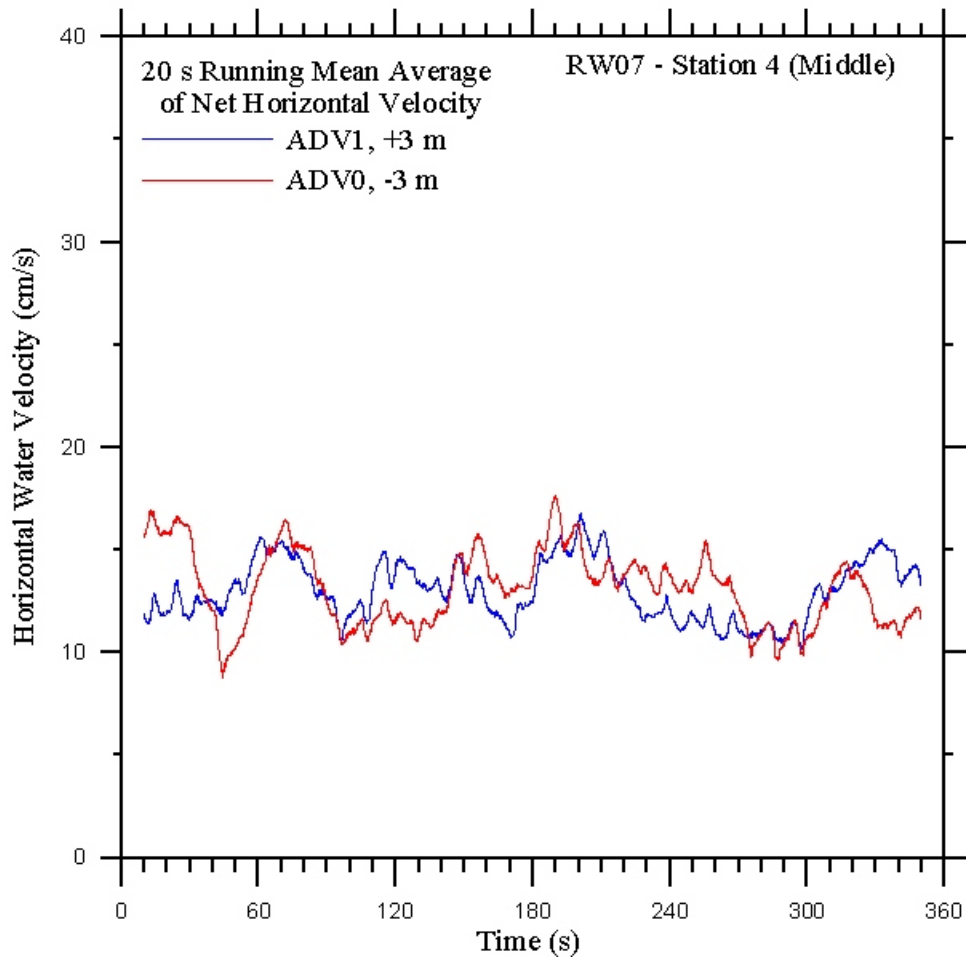


Figure 138: Horizontal surface currents measured by the two acoustic-Doppler velocimeters in the main instrument array at a depth of 50 cm below the mean water level. The data shown are 20-s running mean averages of the horizontal velocities calculated using Eq. 4 at station 4. Paddle conditions for this run correspond to RW07, 3.0" stroke, 35 cpm speed.

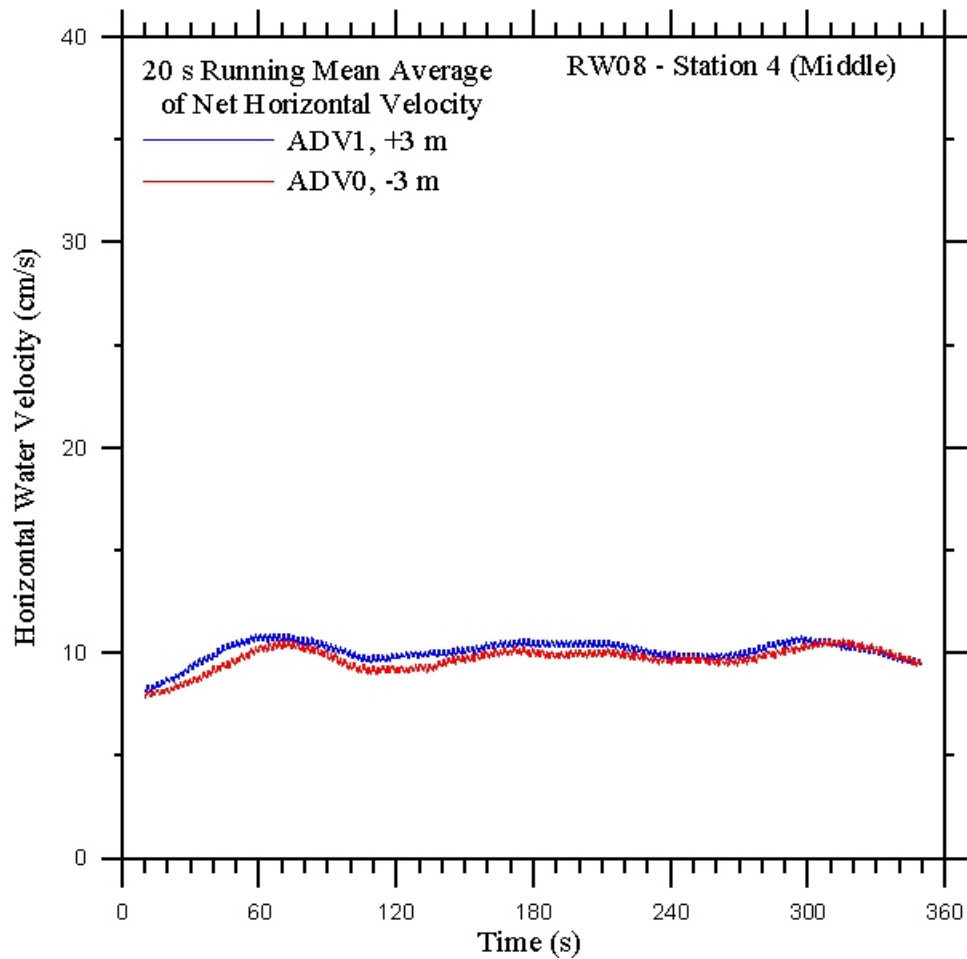


Figure 139: Horizontal surface currents measured by the two acoustic-Doppler velocimeters in the main instrument array at a depth of 50 cm below the mean water level. The data shown are 20-s running mean averages of the horizontal velocities calculated using Eq. 4 at station 4. Paddle conditions for this run correspond to RW08, 4.5" stroke, 15 cpm speed.

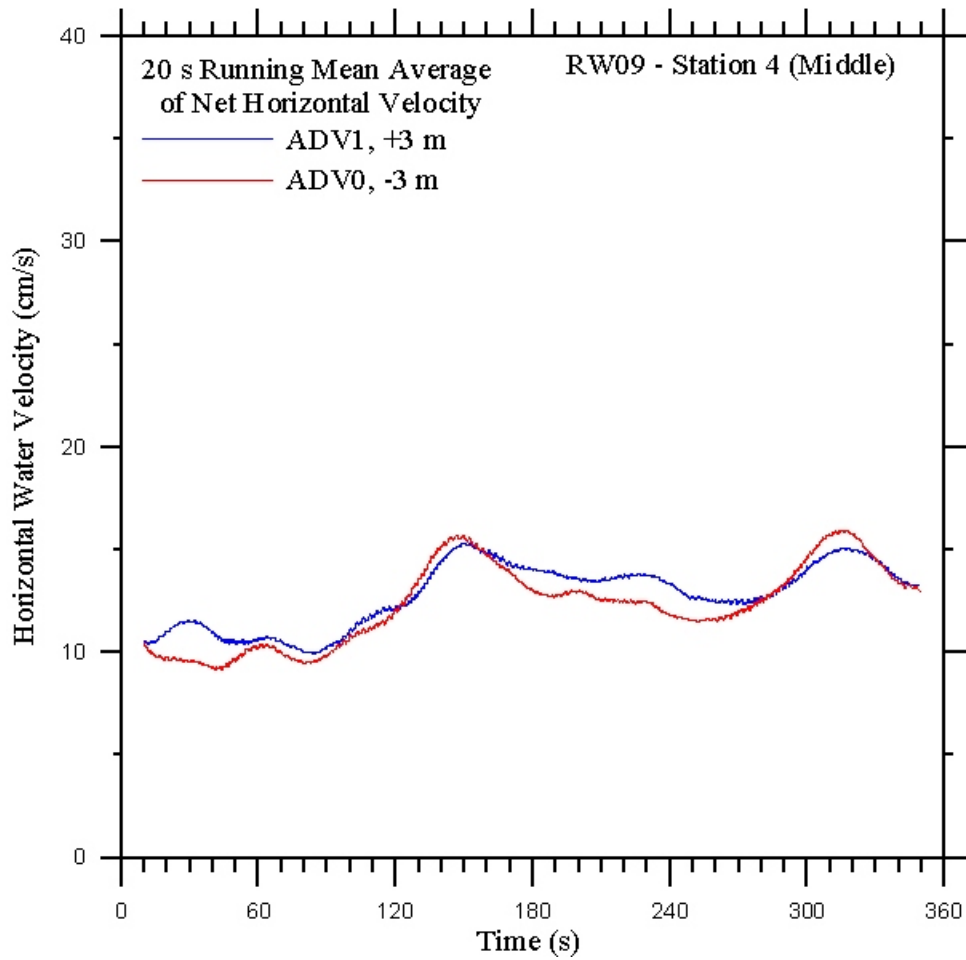


Figure 140: Horizontal surface currents measured by the two acoustic-Doppler velocimeters in the main instrument array at a depth of 50 cm below the mean water level. The data shown are 20-s running mean averages of the horizontal velocities calculated using Eq. 4 at station 4. Paddle conditions for this run correspond to RW09, 4.5" stroke, 21 cpm speed.

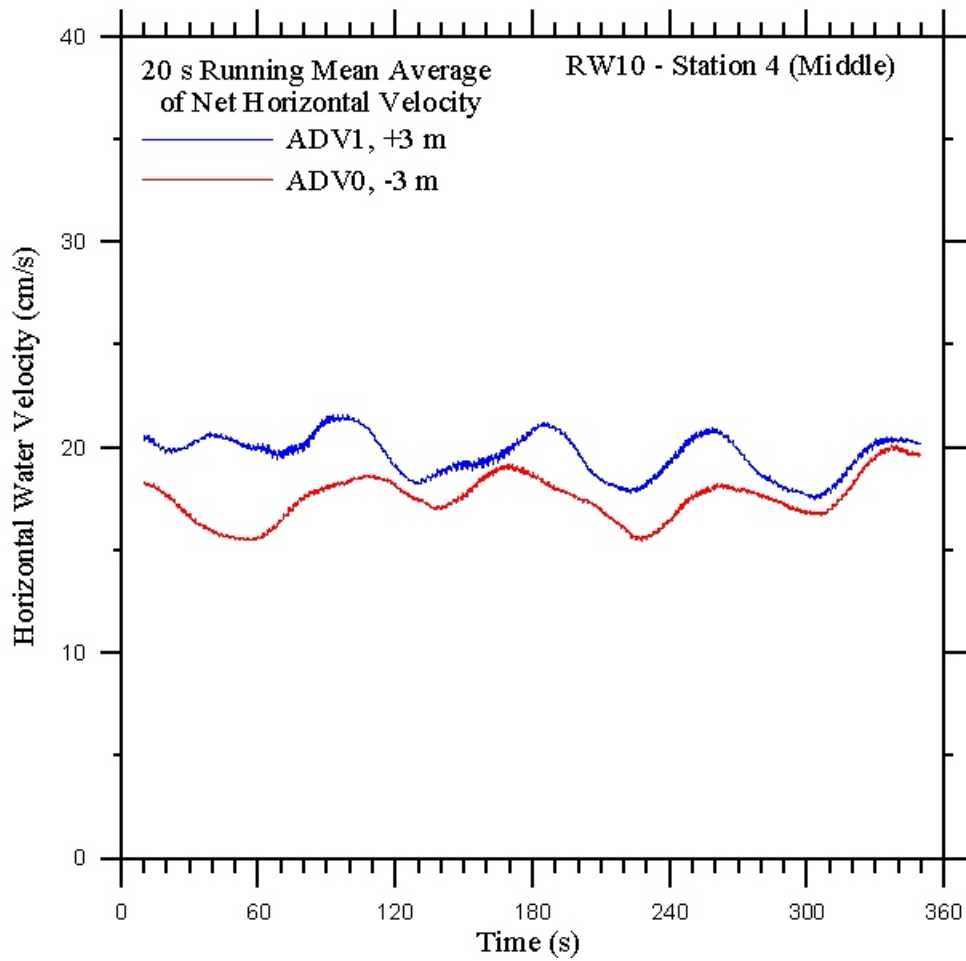


Figure 141: Horizontal surface currents measured by the two acoustic-Doppler velocimeters in the main instrument array at a depth of 50 cm below the mean water level. The data shown are 20-s running mean averages of the horizontal velocities calculated using Eq. 4 at station 4. Paddle conditions for this run correspond to RW10, 4.5" stroke, 27 cpm speed.

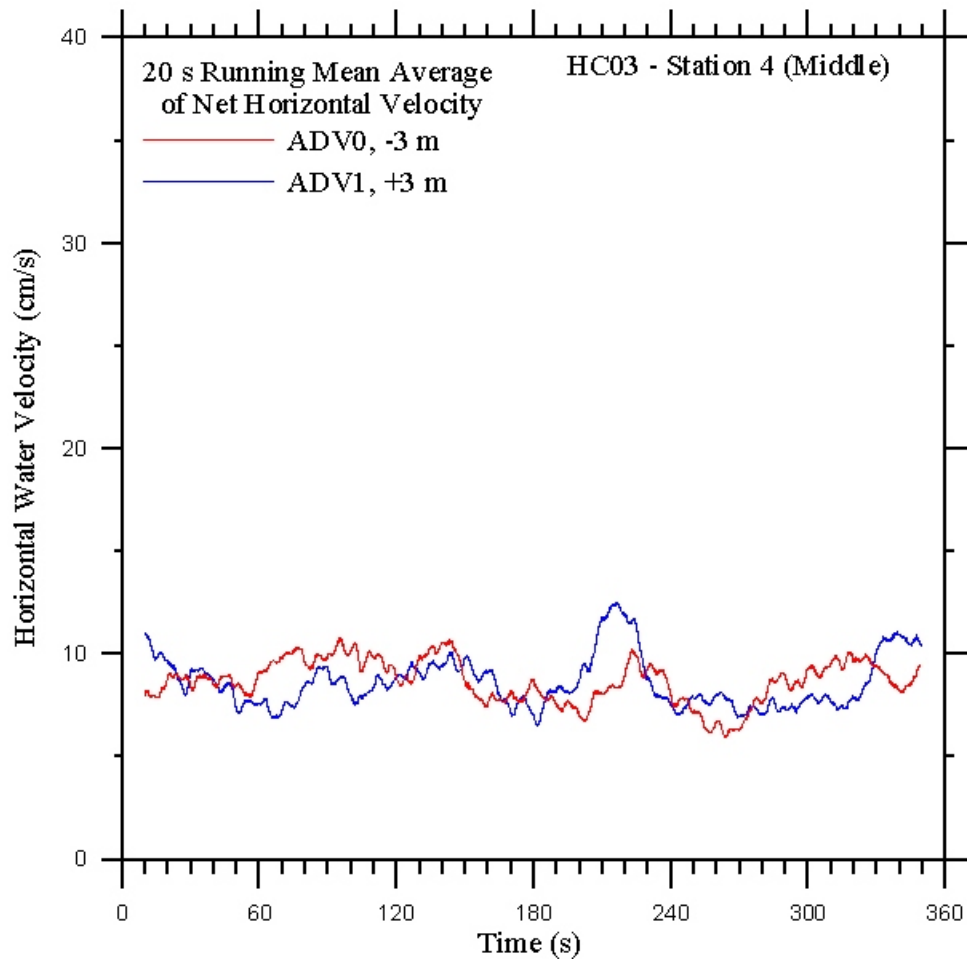


Figure 142: Horizontal surface currents measured by the two acoustic-Doppler velocimeters in the main instrument array at a depth of 50 cm below the mean water level. The data shown are 20-s running mean averages of the horizontal velocities calculated using Eq. 4 at station 4. Paddle conditions for this run correspond to HC03, 1.5" stroke, 40 cpm speed.

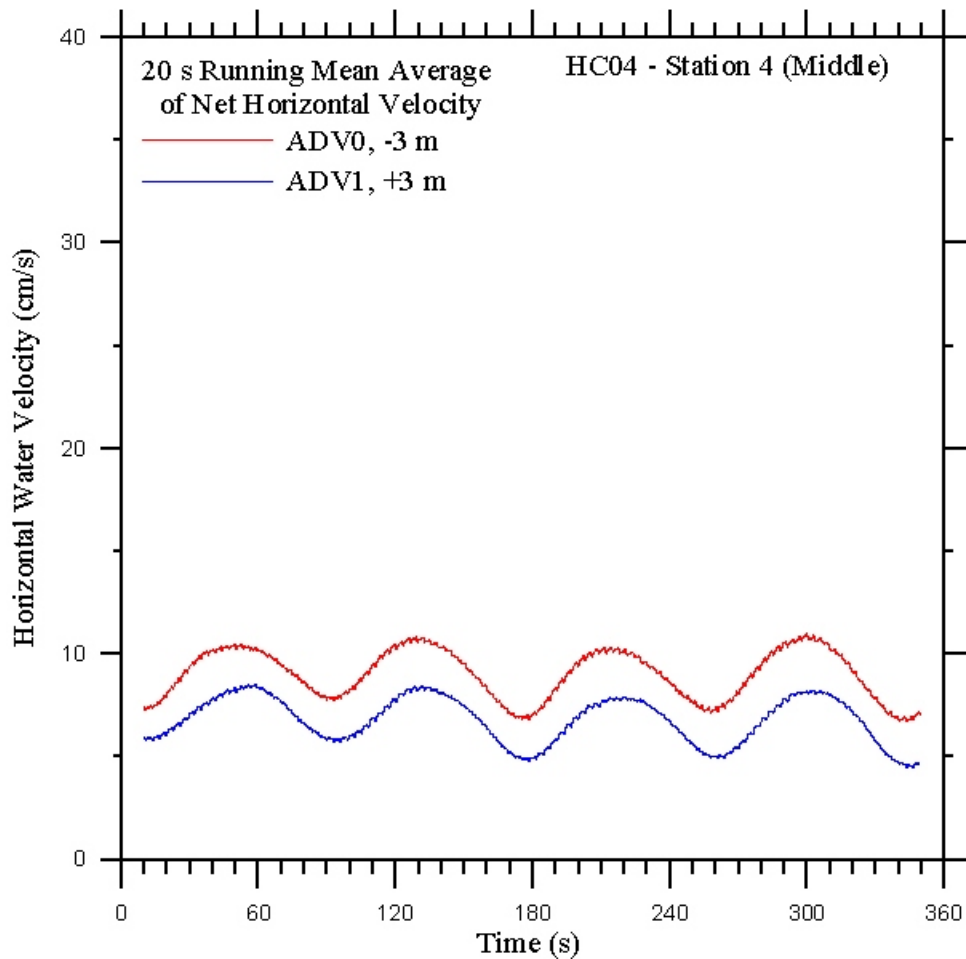


Figure 143: Horizontal surface currents measured by the two acoustic-Doppler velocimeters in the main instrument array at a depth of 50 cm below the mean water level. The data shown are 20-s running mean averages of the horizontal velocities calculated using Eq. 4 at station 4. Paddle conditions for this run correspond to HC04, 3.0" stroke, 20 cpm speed.

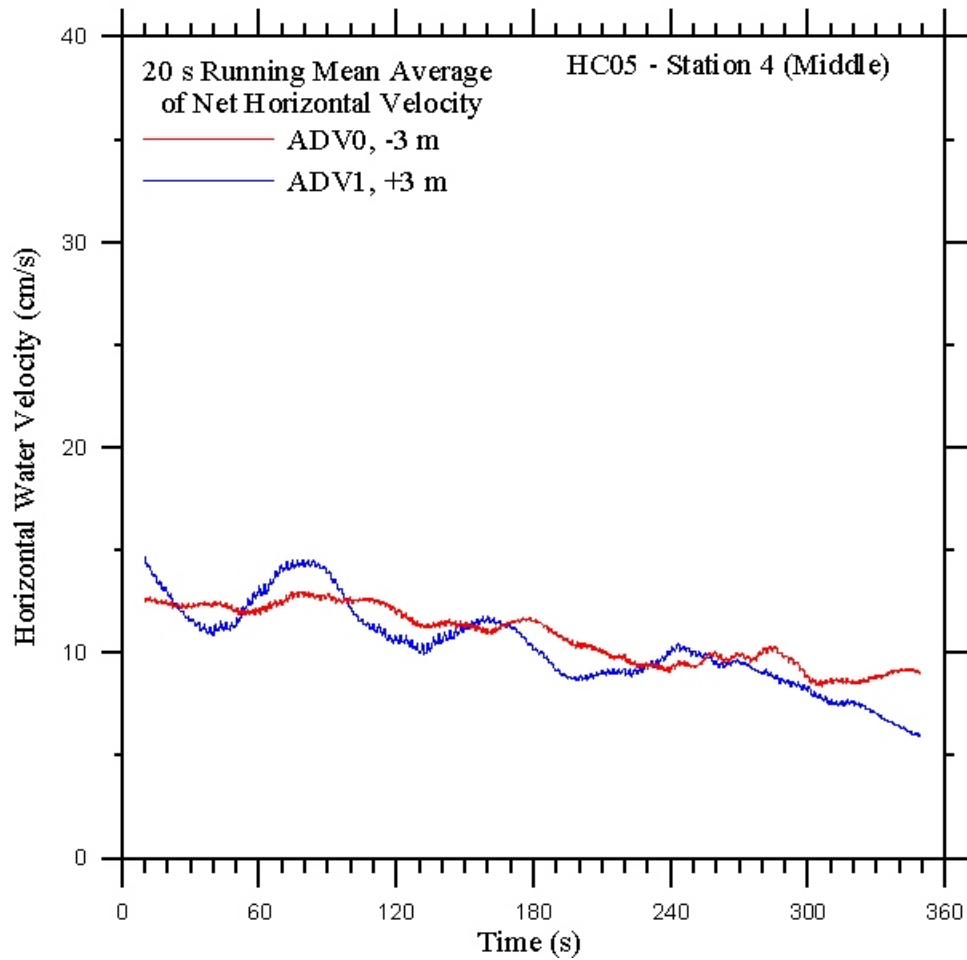


Figure 144: Horizontal surface currents measured by the two acoustic-Doppler velocimeters in the main instrument array at a depth of 50 cm below the mean water level. The data shown are 20-s running mean averages of the horizontal velocities calculated using Eq. 4 at station 4. Paddle conditions for this run correspond to HC05, 3.0" stroke, 25 cpm speed.

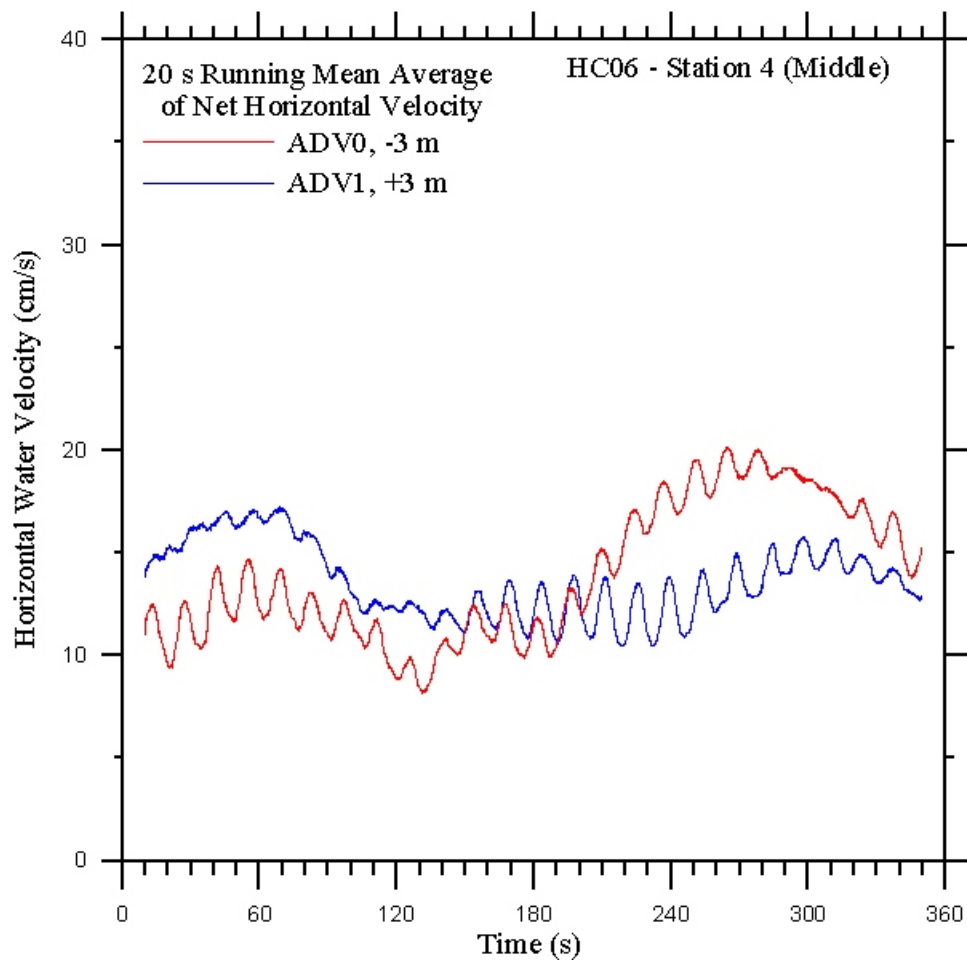


Figure 145: Horizontal surface currents measured by the two acoustic-Doppler velocimeters in the main instrument array at a depth of 50 cm below the mean water level. The data shown are 20-s running mean averages of the horizontal velocities calculated using Eq. 4 at station 4. Paddle conditions for this run correspond to HC06, 3.0" stroke, 30 cpm speed.

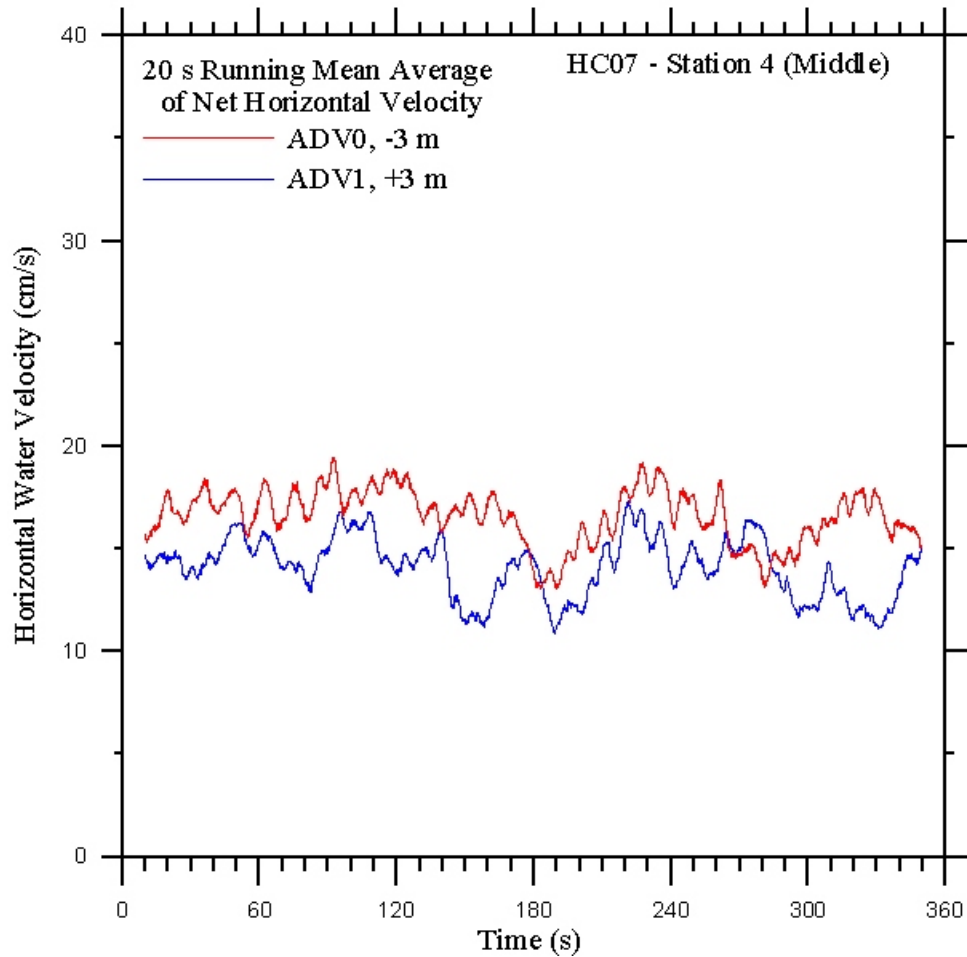


Figure 146: Horizontal surface currents measured by the two acoustic-Doppler velocimeters in the main instrument array at a depth of 50 cm below the mean water level. The data shown are 20-s running mean averages of the horizontal velocities calculated using Eq. 4 at station 4. Paddle conditions for this run correspond to HC07, 3.0" stroke, 35 cpm speed.

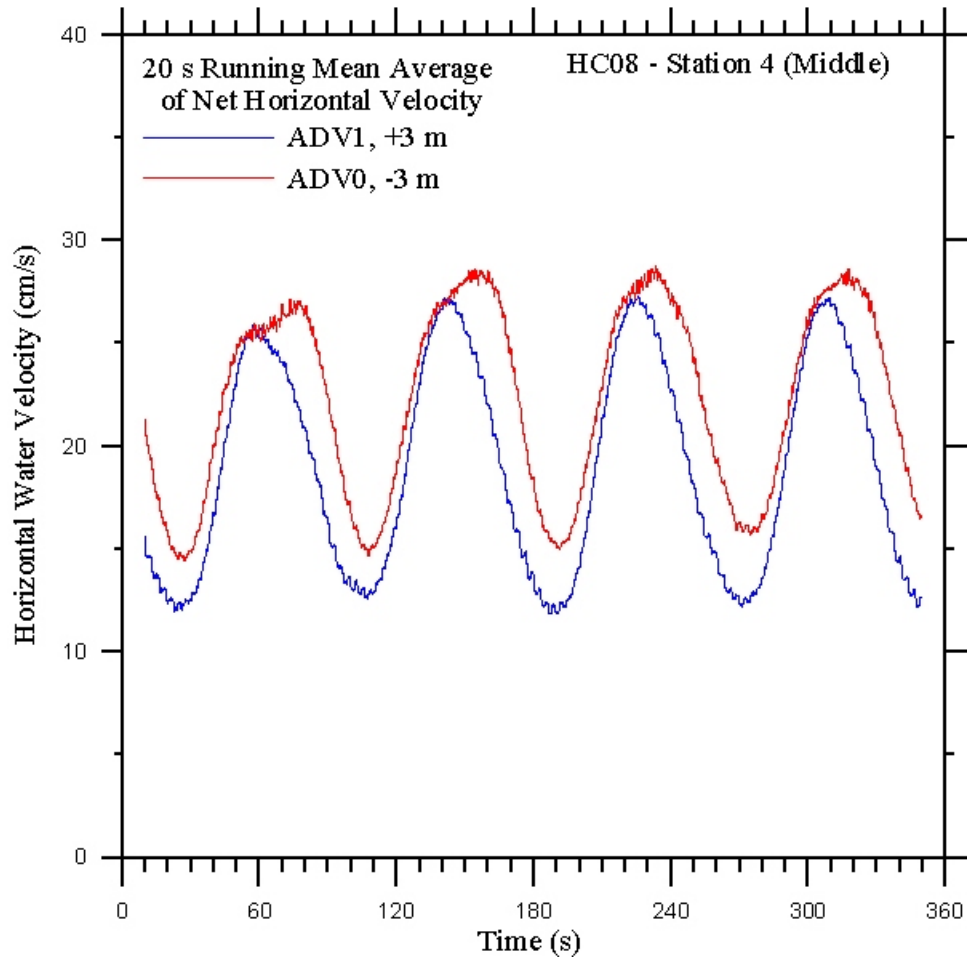


Figure 147: Horizontal surface currents measured by the two acoustic-Doppler velocimeters in the main instrument array at a depth of 50 cm below the mean water level. The data shown are 20-s running mean averages of the horizontal velocities calculated using Eq. 4 at station 4. Paddle conditions for this run correspond to HC08, 4.5" stroke, 20 cpm speed.

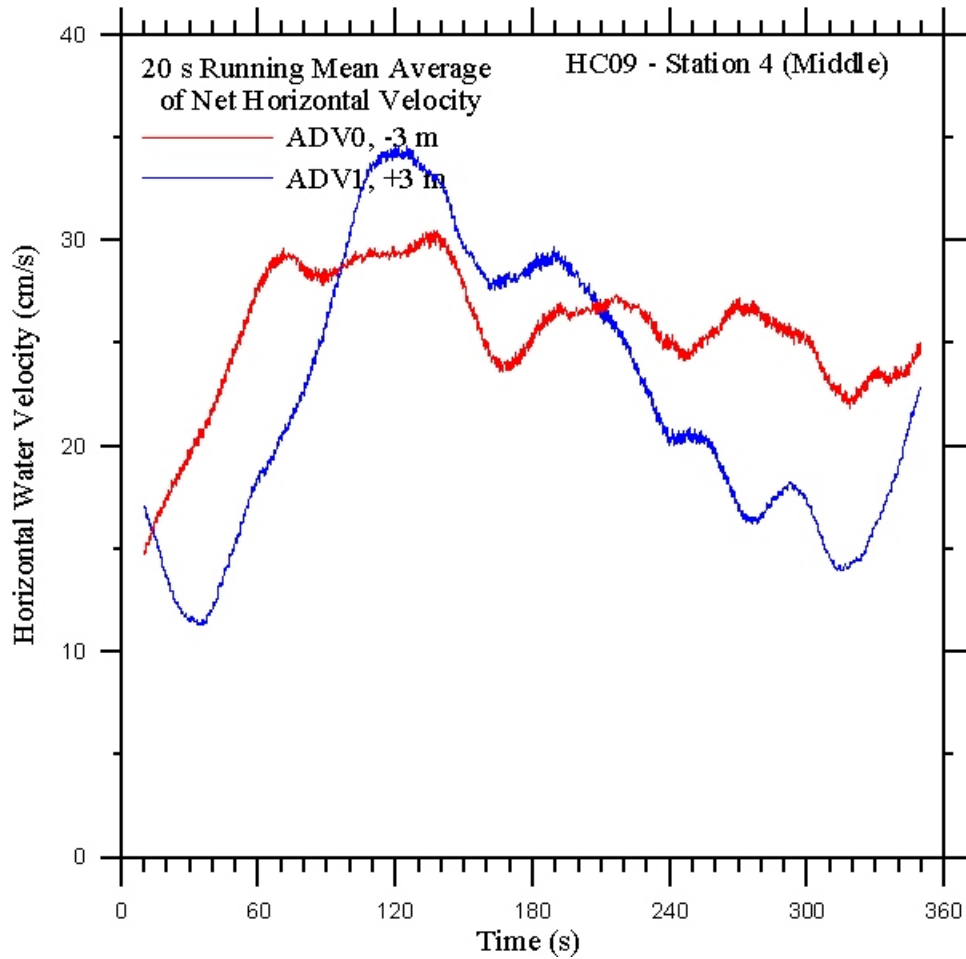


Figure 148: Horizontal surface currents measured by the two acoustic-Doppler velocimeters in the main instrument array at a depth of 50 cm below the mean water level. The data shown are 20-s running mean averages of the horizontal velocities calculated using Eq. 4 at station 4. Paddle conditions for this run correspond to HC09, 4.5" stroke, 25 cpm speed.

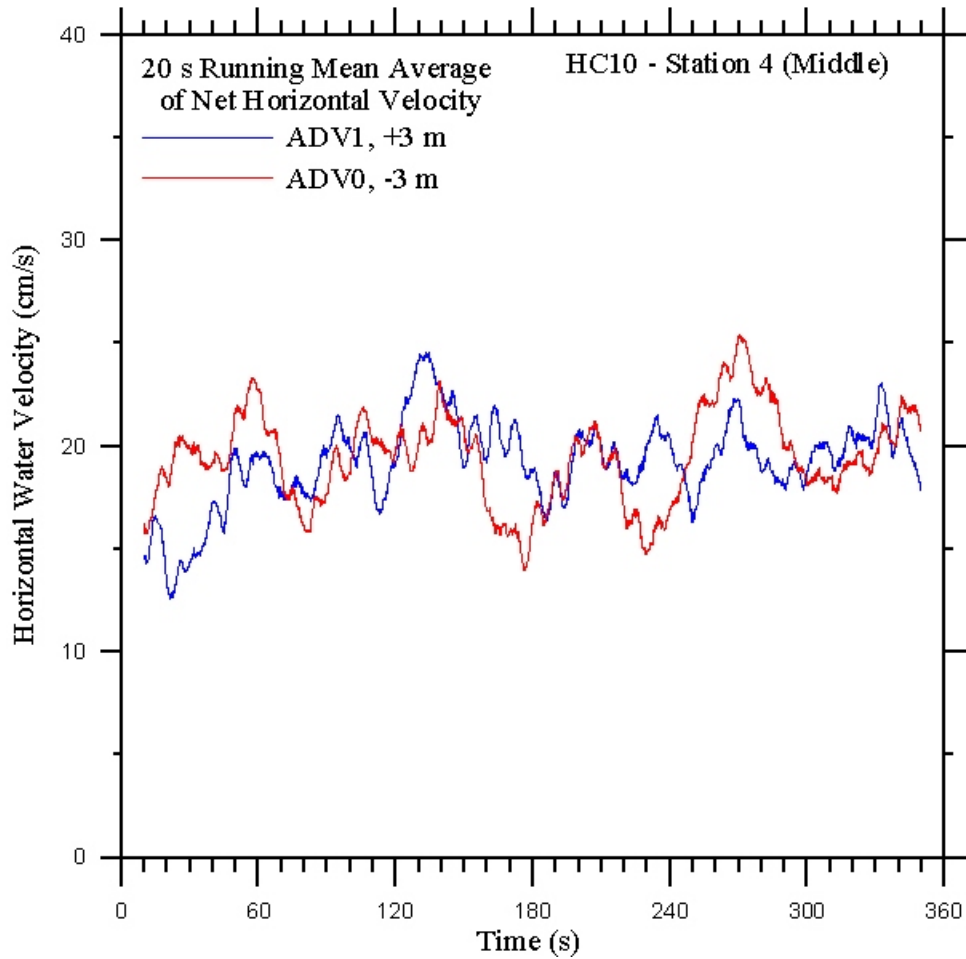


Figure 149: Horizontal surface currents measured by the two acoustic-Doppler velocimeters in the main instrument array at a depth of 50 cm below the mean water level. The data shown are 20-s running mean averages of the horizontal velocities calculated using Eq. 4 at station 4. Paddle conditions for this run correspond to HC10, 4.5" stroke, 30 cpm speed.

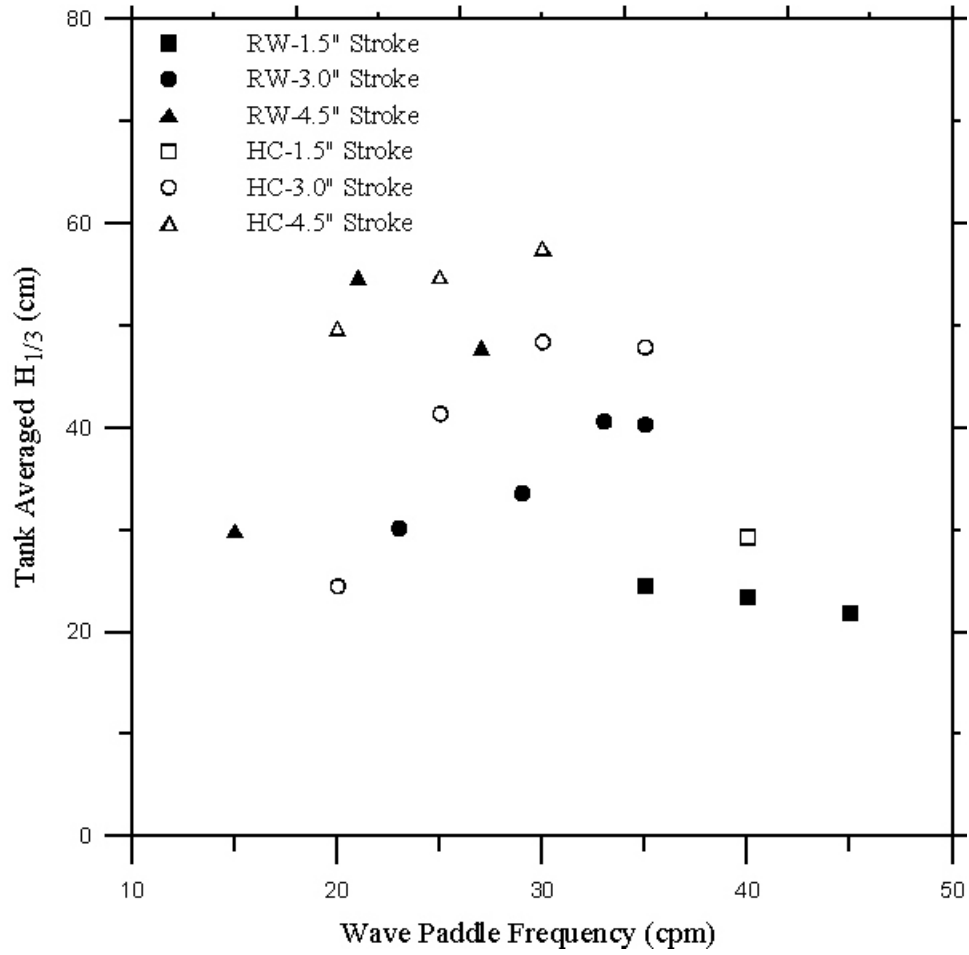


Figure 150: Plot of tank-averaged significant wave heights, $H_{1/3}$, from Table 1 plotted versus the wave paddle oscillation frequency.

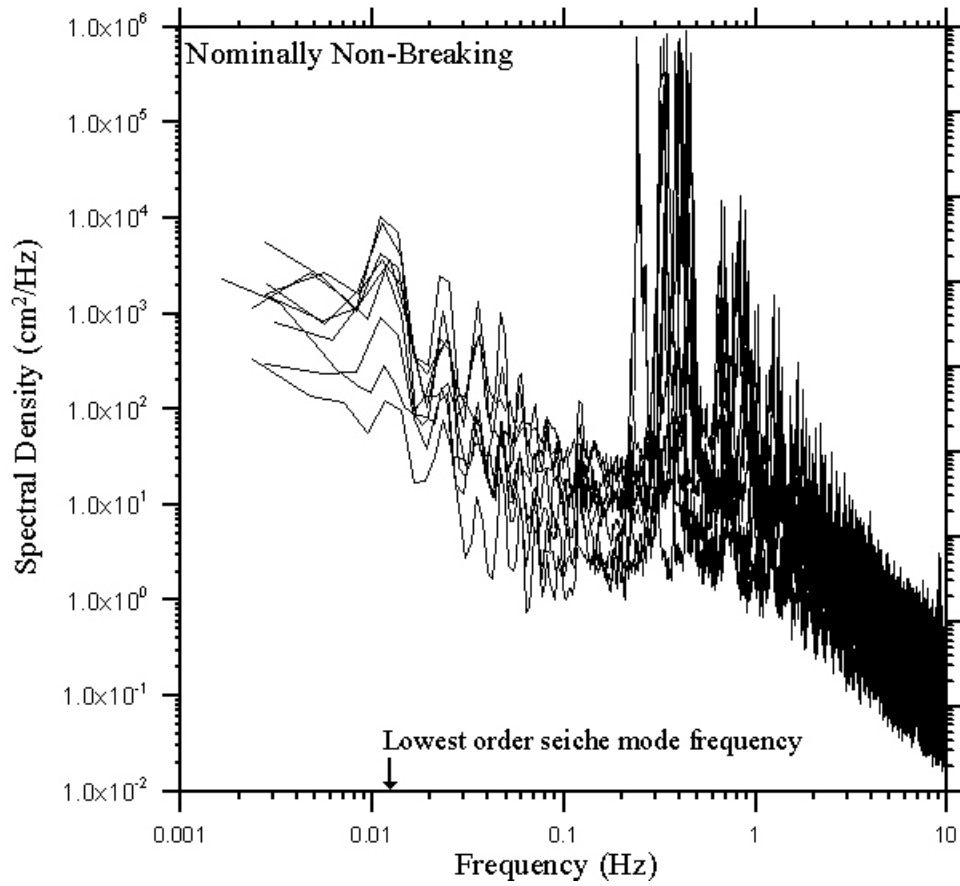


Figure 151: Plot of tank-averaged the tank-average power spectra calculated using 32,000 point record lengths for all conditions found to have wave fields where the waves did not spontaneously break.

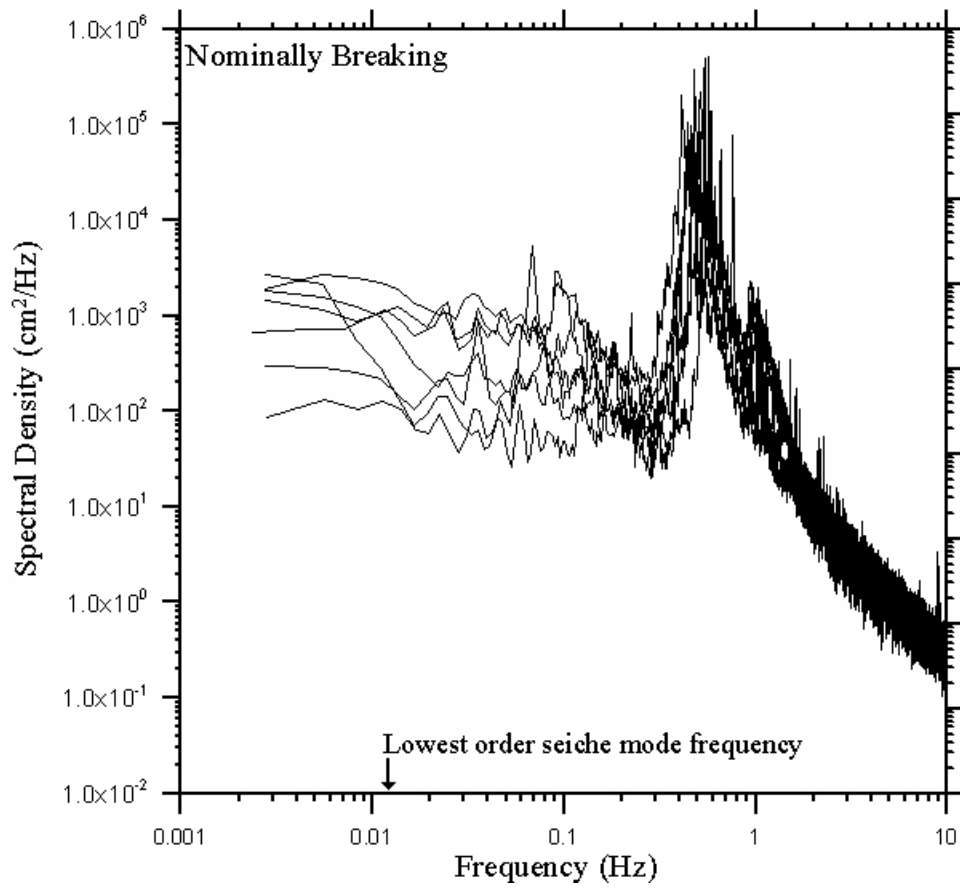


Figure 152: Plot of tank-averaged the tank-average power spectra calculated using 32,000 point record lengths for all conditions found to have wave fields where the waves were spontaneously breaking.

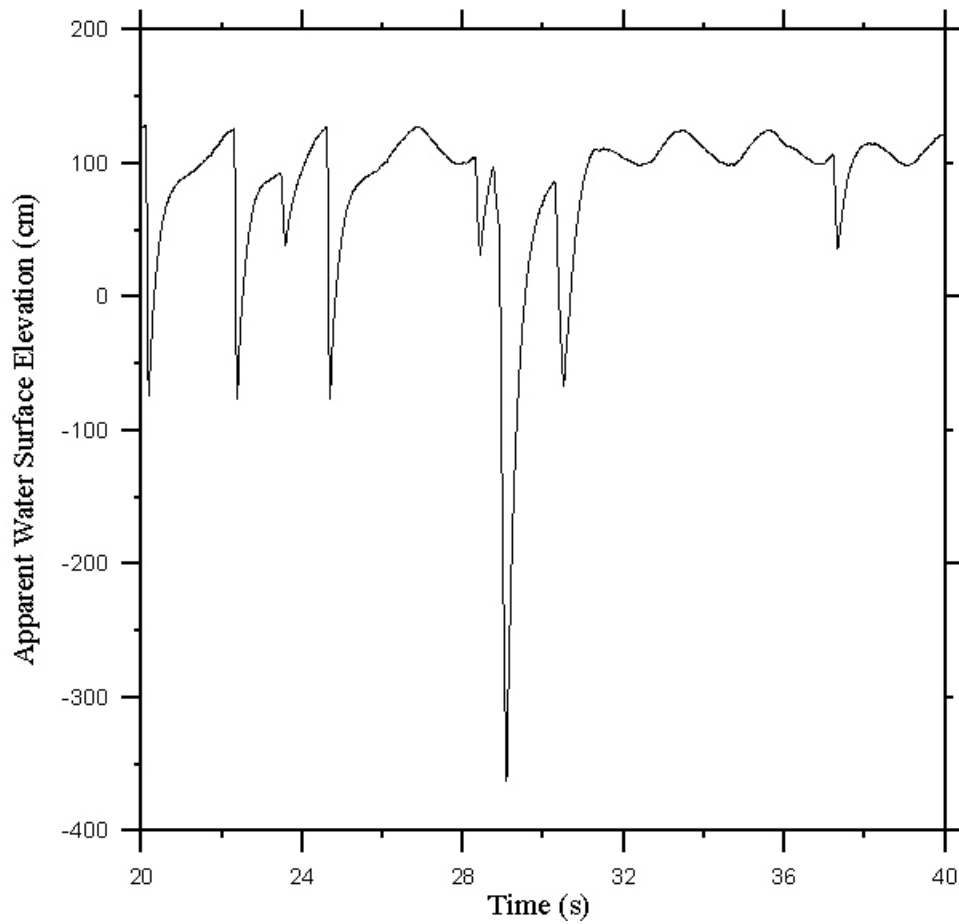


Figure 153: Plot of apparent water surface elevation as measured by the Datasonics PSA-900A for wave condition RW10, station 4. A small subset of the data has been plotted to show details of the noise spikes in the data records for the PSA-900A. It should be noted that these data have already been filtered using a sixth-order Chebyshev digital filter.

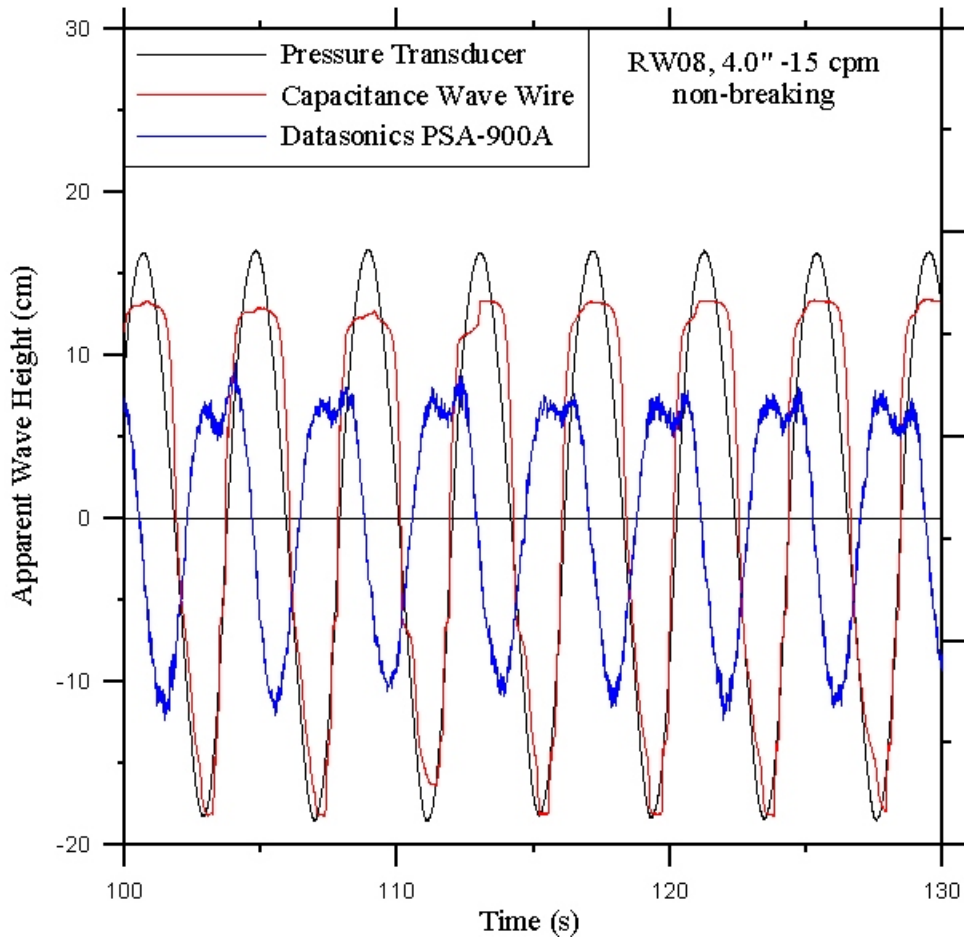


Figure 154: Plot of apparent water surface elevation as measured by the Omega Engineering PX439-002GI pressure transducer, the RBR Ltd. WG-30 capacitance wave wire gauge and the Datasonics PSA-900A acoustic height gauge for wave condition RW08, station 4. A small subset of the data have been shown to provide details of the wave profiles as measured by the three different probes. There is relatively good agreement in the wave profiles between the three probes although the amplitude of the PSA-900A is less than the other two probes due to a calibration problem that was never resolved. The phase lag in the PSA-900A is caused by its being mounted approximately 5 m to the north of the other two probes.

Appendix 1: Matlab Data Analysis Code

Main Analysis Program:

```
close all;
fclose('all');
clear all;
psimax = [2, 5, 2, 2, 2, 2, 2]; % one 5 psi, six 2 psi
gains = [1, 2, 1, 1, 1, 1, 1, 1, 1, 1];
colorval = ['k ', 'r ', 'b ', 'g ', 'm ', 'c ', 'y ', 'k.', 'r-'];
psicon = 70.3089/1.025; % psi to cm of H2O
%pressure transducers calibrated 01/11/05 at APL by L. Couret. Data in
Ohmsett book #2
%calibration data in calibration.xls in OHMSETT_Press directory
press_slope = [0.00622018, 0.00789016, 0.00632399, 0.00634249, 0.00633063, ...
              0.006315203, 0.006303084];
press_int = [-239.99092, -339.87172, -245.58959, -245.55609, -239.21690, ...
            -243.369700, -242.812250];
% wave wires calibrated during POEWEX04 and raw data found in those notebooks
wireslope = [-13.4515, -14.1774]; % from wirecal.xls spreadsheet
wireint = [95.44515, 88.93486]; % from wirecal.xls spreadsheet
tankdepth = 2.43; % in meters (8 feet)
sonicslope = 157.4803; % cal factor from Don Backer
sonicint = 393.7008; % cal factor from Don Backer
handlist = input ('enter filename for list of file handles: ', 's');
fidhand = fopen(handlist, 'r');
dnah = fscanf(fidhand, '%s', [11,18]);
filehand = dnah';
fclose(fidhand);
for i = 1: size(filehand,1)
    filehand(i,1:13) = strcat(filehand(i,1:11), '_0');
end;
ext = 'a_press_ascii.dat';
% now read in the file containing the number of seconds for each data set
timelist = input ('enter filename for number of seconds to process: ', 's');
fid = fopen(timelist, 'r');
timestop = fscanf(fid, '%d');
% figure out how many points are needed based on sampling frequency of 100Hz
istop = 100*timestop;
fclose(fid);
% now read in sample frequency for each data record
freqlist = input ('enter filename containing sample freq. for each set: ',
's');
fid = fopen(freqlist, 'r');
freqs = fscanf(fid, '%d %d %d %d %d %d %d %d');
fclose(fid);
sampfreq = reshape(freqs,8,18);
%now loops over all the data directories
for k = 1: size(filehand,1)
    clear eta etafilt pspec freqs timeswh swseries
% main data processing loop: reads in all transducer data from all stations
    for j = 1:8
        clear h volt rawdata
        filename = filehand(k,1:13);
        filename = strcat(filename, sprintf('%d',j));
        filename = strcat(filename, ext);
        disp(filename);
```

```

rawdata = load(filename);
if (sampfreq(j,k) > 100)
    for i = 1:13
        rawdec(:,i) = decimate(rawdata(:,i), sampfreq(j,k)/100);
    end;
    clear rawdata;
    rawdata = rawdec;
    clear rawdec;
end;
time(1:istop(k),j) = rawdata(1:istop(k),3);
volt = 10*(rawdata(:,4:13)/(2^15) - 1);
for i = 1:1:10,
    volt(:,i) = volt(:,i)/gains(i);
end;
% do the seven pressure transducers
% calculate height directly from calibration, don't use voltage
for i = 1:1:7,
    h(:,i) = rawdata(:,i+3)*press_slope(i) + press_int(i); % h in cm
    hzero(i) = mean(h(:,i)); % mean transducer depth
    eta(1:istop(k),i,j) = h(1:istop(k),i) - hzero(i); % eta in cm
end;
% do the two wave-wire gauges
for i = 8:1:9
    h(:,i) = volt(:,i)*wireslope(i-7)-wireint(i-7);
    hzero(i) = mean(h(:,i));
    eta(1:istop(k),i,j) = h(1:istop(k),i) - hzero(i);
end;
% do the Ohmsett sonic probe, cal factors from Don Backer, 11/30/04
hzero(10) = mean(volt(:,10))*sonicslope - sonicint;
h(:,10) = (volt(:,10)*sonicslope - sonicint) - hzero(10);
% note that the sonic is a height gauge so the measured height gets
% subtracted from the zero level to give water surface elevation
eta(1:istop(k),10,j) = hzero(10) - h(1:istop(k),10);
end;
% for loop for data input
% filter the data
for i = 1 : 1 : 8 % loop over the stations
    filterval = 0.4; % want stop band at 20Hz based on 100Hz sample rate
    [B, A] = cheby2(6, 20, filterval); % 6th order 20 db chebyshev filter
    for j = 1 : 1 : 10 % loop over the wave probes
        filt = filter(B,A,eta(:,j,i));
        [ps, freqs] = spectrum(filt, 4096, 0, 0, 100);
        etafilt(:,j,i) = filt;
        pspec(:,j,i) = ps(:,1);
    end;
end;
%
% now correct pressure transducers, first get dominate wave freq.
%
[fmax,imax] = max(pspec); % maximum in each power spectrum
avgfreq = 0.0; % tank average frequency
icnt = 0;
for i = 1 : 8
    jcnt = 0;
    posfreq(i) = 0.0; % frequency along the tank
    for j = 1 : 9
        avgfreq = avgfreq + freqs(imax(1,j,i));
        posfreq(i) = posfreq(i) + freqs(imax(1,j,i));
    end;
end;

```

```

    icnt = icnt + 1;
    jcnt = jcnt + 1;
end;
posfreq(i) = posfreq(i)/jcnt;
posperiod(i) = 1/posfreq(i);
% calculate the along-tank wavelength from along-tank period
% by solving dispersion relation
[posL(i), dum1, dum2] = fzero('wavelength', [0.1 50], [], posperiod(i));
end;
avgfreq = avgfreq/icnt;
period = 1/avgfreq;
[L, dum1, dum2] = fzero('wavelength', [0.1 50], [], period);
kp = cosh(2*pi*(tankdepth - 0.01*hzero(1:7))/L)./cosh(2*pi*tankdepth/L);
for i = 1 : 8
    for j = 1 : 7 % just do the seven pressure probes
        eta(:,j,i) = eta(:,j,i) / kp(j); % eta already in units of cm
        % do the time series analysis over on the corrected height records
        filt = filter(B,A,eta(:,j,i));
        [ps, freqs] = spectrum(filt, 4096, 1024, 0, 100);
        etafilt(:,j,i) = filt;
        pspec(:,j,i) = ps(:,1);
    end;
end;
%
% end of the height corrections
%
% calculate SWH from the surface elevation time series
for i = 1 : 1 : 8
    ipnt = 1;
    for j = 1 : 60 : istop(k) - 1
        jbeg = j - 1000;
        jend = j + 1000;
        if (jbeg <= 0) jbeg = 1; end;
        if (jend > istop(k)) jend = istop(k); end;
        swhseries(ipnt, :,i) = 4.0 * sqrt((std(etafilt(jbeg:jend,:,i))).^2);
        timeswh(ipnt,i)=0.6*(ipnt-1); % constant = (60/100) (s/sample rate)
        ipnt = ipnt + 1;
    end;
end;
swh = 4.0*sqrt(std(etafilt).^2);
% now we have to reshape SWH so it can be used by CONTOURF
swhsave = swh;
clear swh;
for i = 1:9
    for j = 1:8
        swh(j,i) = swhsave(1,i,j);
    end;
end;
clear swhsave;
% now re-order the probes so they go across the tank
% original positions in array:


|    |                    | ADC Chan | Array Pos |   |
|----|--------------------|----------|-----------|---|
| %1 | probe 1 (press. 1) | = 0 m    | Chan 1    | 2 |
| %2 | probe 2 (press. 2) | = -4 m   | Chan 2    | 3 |
| %3 | probe 3 (press. 3) | = -6 m   | Chan 3    | 4 |
| %4 | probe 4 (press. 4) | = -8 m   | Chan 4    | 5 |
| %5 | probe 5 (press. 5) | = +4 m   | Chan 5    | 6 |
| %6 | probe 6 (press. 6) | = +6 m   | Chan 0    | 1 |
| %7 | probe 7 (press. 7) | = +8 m   | Chan 6    | 7 |


```

```

%8 probe 8 (press. wa) = -2 m           Chan 7           8
%9 probe 9 (press. wb) = +2 m           Chan 8           9
%10 probe 10 (press. os) = -7 m         Chan 9           10 (don't use)
%
% New array:
%
%1 probe 4 (press. 4) = -8 m
% probe 10 (press. os) = -7 m           (note don't use sonic at this point)
%2 probe 3 (press. 3) = -6 m
%3 probe 2 (press. 2) = -4 m
%4 probe 8 (press. wa) = -2 m
%5 probe 1 (press. 1) = 0 m
%6 probe 9 (press. wb) = +2 m
%7 probe 5 (press. 5) = +4 m
%8 probe 6 (press. 6) = +6 m
%9 probe 7 (press. 7) = +8 m
%
swhsave = swh;
sersave = swhseries;
swh(:,1) = swhsave(:,5); % -8 P4
% swh(:,2) = swhsave(:,10); %sonic doesn't make sense at this point
swh(:,2) = swhsave(:,4); % -6 P3
swh(:,3) = swhsave(:,3); % -4 P2
swh(:,4) = swhsave(:,8); % -2 WA
swh(:,5) = swhsave(:,2); % 0 P1
swh(:,6) = swhsave(:,9); % +2 WB
swh(:,7) = swhsave(:,6); % +4 P5
swh(:,8) = swhsave(:,1); % +6 P6
swh(:,9) = swhsave(:,7); % +8 P7
% now reorder the time series of SWH
swhseries(:,1,:) = sersave(:,5,:);
% swhseries(:,2,:) = sersave(:,10,:); %sonic doesn't make sense yet
swhseries(:,2,:) = sersave(:,4,:);
swhseries(:,3,:) = sersave(:,3,:);
swhseries(:,4,:) = sersave(:,8,:);
swhseries(:,5,:) = sersave(:,2,:);
swhseries(:,6,:) = sersave(:,9,:);
swhseries(:,7,:) = sersave(:,6,:);
swhseries(:,8,:) = sersave(:,1,:);
swhseries(:,9,:) = sersave(:,7,:);
% now save the data to some .mat files ...
filename = filehand(k,1:13);
filename = strcat(filename, '_freqs');
save (filename, 'freqs');
filename = filehand(k,1:13);
filename = strcat(filename, '_swh');
save ( filename, 'swh');
filename = strcat(filename, '.jpg');
figure(1);
bridgepos = [40:20:180];
% probepos = [-8, -7, -6, -4, -2, 0, 2, 4, 6, 8];
probepos = [-8, -6, -4, -2, 0, 2, 4, 6, 8]; % without sonic
contourf(probepos, bridgepos, swh, 25);
haxis = gca;
set(get(haxis, 'Xlabel'), 'String', 'Across-Tank Distance (m)');
set(get(haxis, 'Ylabel'), 'String', 'Along-Tank Distance (m)');
colorbar;
haxis = text(12, 120, 'SWH (cm)');

```

```

set(haxis, 'Rotation', 270);
saveas (1, filename, 'jpg');
figure(2);
filename = filehand(k,1:13);
filename = strcat(filename, '_spectra');
save (filename, 'pspec');
filename = strcat(filename, '.jpg');
for i = 1:8
    loglog(freqs(1:200), pspec(1:200, 4, i), colorval(2*i-1)); % wave wire A
    loglog(freqs(1:200), pspec(1:200, 6, i), colorval(2*i-1)); % wave wire B
    hold on;
end;
hold off;
haxis = gca;
set(get(haxis, 'Xlabel'), 'String', 'Frequency (Hz)');
set(get(haxis, 'Ylabel'), 'String', 'Spectral Energy');
saveas (2, filename, 'jpg');
figure(3);
filename = filehand(k,1:13);
filename = strcat(filename, '_etafilt');
save (filename, 'etafilt');
filename = strcat(filename, '_wa.jpg');
for i = 1:8
    plot(time(1:istop(k)/20,i), etafilt(1:istop(k)/20, 4, i), ...
        colorval(2*i-1)); % wave wire A
    hold on;
end;
hold off;
haxis = gca;
set(get(haxis, 'Xlabel'), 'String', 'Time (s)');
set(get(haxis, 'Ylabel'), 'String', 'Eta (cm)');
set(get(haxis, 'Title'), 'String', 'Wave Wire A, Left');
saveas (3, filename, 'jpg');
figure(4);
filename = filehand(k,1:13);
filename = strcat(filename, '_etafilt');
filename = strcat(filename, '_wb.jpg');
for i = 1:8
    plot(time(1:istop(k)/20,i), etafilt(1:istop(k)/20, 6, i), ...
        colorval(2*i-1)); % wave wire B
    hold on;
end;
hold off;
haxis = gca;
set(get(haxis, 'Xlabel'), 'String', 'Time (s)');
set(get(haxis, 'Ylabel'), 'String', 'Eta (cm)');
set(get(haxis, 'Title'), 'String', 'Wave Wire B, Right');
saveas (4, filename, 'jpg');
figure(5);
filename = filehand(k,1:13);
filename = strcat(filename, '_swhseriestime');
save (filename, 'timeswh');
filename = filehand(k,1:13);
filename = strcat(filename, '_swhseries');
save (filename, 'swhseries');
filename = strcat(filename, '.jpg');
for i = 1:9
    plot(timeswh, swhseries(:,i,4), colorval(2*i-1)); %

```

```

hold on;
end;
hold off;
haxis = gca;
set(get(haxis, 'Xlabel'), 'String', 'Time (s)');
set(get(haxis, 'Ylabel'), 'String', 'SWH (cm)');
set(get(haxis, 'Title'), 'String', 'SWH, 2000-pt avg., Position 4')
saveas (5, filename, 'jpg');
% now write out the text format of the analysis results
filename = filehand(k,1:13);
filename = strcat(filename, '_results.txt');
fid = fopen(filename, 'w');
tline = sprintf('%%Tank Averaged Dominant Wave Freq. = %14.5e s\n', ...
    avgfreq);
disp(tline);
fprintf(fid, '%s', tline);
tline = sprintf('%%Tank Averaged Dominant Wave Period = %14.5e s\n', ...
    period);
disp(tline);
fprintf(fid, '%s', tline);
tline = sprintf('%%Tank Averaged Dominant Wavelength (m) = %14.5e s\n', L);
disp(tline);
fprintf(fid, '%s', tline);
tline = sprintf('%%Tank Averaged SWH = %8.3f cm\n', mean(mean(swh)));
disp(tline);
fprintf(fid, '%s', tline);
tline = sprintf('%%Along-tank averaged SWH values (cm)\n');
disp(tline);
fprintf(fid, '%s', tline);
tline = sprintf('%%Station #    Distance (m)                SWH(cm)\n');
disp(tline);
fprintf(fid, '%s', tline);
swhalong = mean(mean(swh,3),2);
for i = 1: 8
    tline = sprintf('%2d        %3d        %8.3f\n',i,bridgepos(i),swhalong(i));
    disp(tline);
    fprintf(fid, '%s', tline);
end;
tline = sprintf('%%SWH values (cm) by station and probe in tank\n');
disp(tline);
fprintf(fid, '%s', tline);
tline = sprintf('%%Sta #    Dist (m)    Probe Pos. (m)\n');
disp(tline);
fprintf(fid, '%s', tline);
tline = sprintf(...'%%                %2d        %2d        %2d        %2d        %2d
    %2d        %2d        %2d        %2d\n',...
    probepos(:));
disp(tline);
fprintf(fid, '%s', tline);
for i = 1: 8
    tline = sprintf(...
        '%2d %3d %8.3f %8.3f %8.3f %8.3f %8.3f %8.3f %8.3f %8.3f %8.3f\n',...
        i, bridgepos(i), swh(i,:));
    disp(tline);
    fprintf(fid, '%s', tline);
end;
tline = sprintf('%%Dominant wavelength along tank\n');
disp(tline);

```

```

fprintf(fid, '%s', tline);
tline = sprintf('%%Station #      Distance (m)          L(m)\n');
disp(tline);
fprintf(fid, '%s', tline);
for i = 1: 8
    tline = sprintf('%2d          %3d          %14.4e\n', i, ...
        bridgepos(i), posL(i));
    disp(tline);
    fprintf(fid, '%s', tline);
end;
fclose(fid);
end; % end loop over k for all the different directories

```

Dispersion Relation Function:

```

function wavelength = dispersion(L, period);
g = 9.8; % m/s2
h = 2.43; % depth of ohmsett in m (8 feet)
wavelength = L - g * period^2 * tanh(2*pi*h/L) / (2*pi);
return;

```